1-1-1986

Free vibration of prestressed continuous composite bridges and skew orthotropic plates.

Nabil Fouad Fanouse Grace
University of Windsor

NOTE TO USERS

This reproduction is the best copy available.

UMI®

FREE VIBRATION OF PRESTRESSED CONTINUOUS COMPOSITE BRIDGES AND SKEW ORTHOTROPIC PLATES

by
Nabil Fouad Fanouse Grace
B.Sc (Honour), M.A.Sc., M.ASCE, P.E.

A Dissertation
submitted to the
Faculty of Graduate Studies
through the Department of
Civil Engineering in Partial Fulfillment
of the Requirements for the Degree
of Doctor of Philosophy in Civil Engineering at
the University of Windsor

Windsor, Ontario, Canada
1986

To my wife, son, parents and parents-in-law
for their sacrifices and moral support

ABSTRACT

FREE VIBRATION OF PRESTRESSED CONTINUOUS
COMPOSITE BRIDGES AND SKEW ORTHOTROPIC PLATES

by

Nabil Fouad Fanouse Grace

This dissertation deals with dynamic response of: (i) continuous composite bridges with prestressed deck; and (ii) skew orthotropic slab bridges. Transverse cracking of the concrete deck, at the intermediate support(s) due to the hogging moment, in continuous composite bridges leads to severe reduction in the bridge stiffness; this reflects on the dynamic characteristics and the fatigue life of the bridge. Furthermore, such cracks increase the susceptibility of the deck steel reinforcing to corrosion, and hence, the maintenance costs are dramatically increased. To solve this problem, the idea of prestressing a portion of the concrete deck around the intermediate support(s) is introduced.

In this research, an experimental study was carried out on two two-span continuous composite bridge models subjected to dynamic, resonance-fatigue and ultimate loads. The effects of prestressing on the dynamic response as well as on the fatigue resistance of different elements of the bridge, such as: longitudinal steel beams, diaphragms, concrete deck, prestressing steel, shear studs and steel reinforcing are determined. The dynamic response of continuous composite bridges, such as natural frequencies and mode shapes, are deduced using the orthotropic plate theory. It is shown that cracking of the concrete deck as well as fatigue cracks can significantly reduce the natural frequencies of the structure.

Furthermore, it is shown that fatigue loading can cause a very rapid increase in the stress range, leading to sudden and sometimes catastrophic failure of the structure. Results show that prestressing a portion of the concrete deck leads to: enhancement in the natural frequencies; improvement in the resonance fatigue life of the structure, as well as its ultimate load-carrying capacity. The influence of aspect ratio and rigidity ratio on the natural frequencies are examined and compared to those obtained from beam theory. The failure of the beam theory to predict the natural frequencies associated with the important torsional mode of the skew bridge is emphasized.

The solution of the free vibration problem of the skew orthotropic slab bridges using orthotropic plate theory is not available in the literature. A solution is developed consisting of mode shapes in the form of Fourier Series satisfying the free vibration governing differential equation in skew coordinates.

The arbitrary constants of the mode shape function are chosen to satisfy the boundary conditions. The computer solution program is written to formulate the transcendental frequency equations for symmetric and anti-symmetric modes of vibration. Such analysis leads to the all-important lower natural frequencies which are compared to the natural frequencies of the applied transient loads in order to avoid the state of resonance; the derived frequencies will be valuable in establishing the dynamic load allowance for use in design practice. The agreement of the deduced results with those obtained from available finite element computer programs as well as from experimental tests on a 45° skew bridge model confirm the validity and accuracy of the developed series solution.

Parametric study is carried out on the effect of aspect ratio and skew angle on the dynamic response of skew orthotropic slab bridge. Furthermore, a comparative study is carried out between skew waffle slabs and skew solid slabs of the same mass and same dimensions, to explore the advantage of waffle slab construction. This study shows that a skew waffle slab possesses higher natural frequencies than a skew solid slab, particularly for large skew angles.

ACKNOWLEDGEMENTS

"The God of heaven will make us prosper, and we his servants will arise and build." (Nehemiah 2:20)

The level of appreciation and respect that I feel towards my advisor, Dr. J. B. Kennedy, of the Civil Engineering Department at the University of Windsor, cannot be expressed in any written form, but will be carried with me for the rest of my life. To him I say "I am really grateful - thank you."

The author wishes to express his sincere gratitude to Dr. G. Abdel-Sayed, of the Civil Engineering Department at the University of Windsor, for his valuable comments and moral support throughout the duration of the author's graduate studies.

The author wishes to thank Dr. G. R. Monforton, of the Civil Engineering Department, for his assistance in preparing the Megadac data acquisition system for the experimental work.

Many thanks are due to Dr. Z. Reif, of the Mechanical Engineering Department, for his valuable comments on the preparation of the experimental models.

The valuable guidance of Dr. H. Aktan, of the Civil Engineering Department at Wayne State University, Detroit, Michigan, throughout his Structural Dynamics Graduate courses is greatly appreciated.

The guidance of Dr. A.C. Smith, of the Department of Mathematics, is greatly acknowledged. The reviewing of the mathematical derivation of the

free vibration problem of the skew orthotropic plate problem by Dr. Kaloni, of the Department of Mathematics, is greatly appreciated.

The author wishes to express his gratitude to Mr. N. Pandya, Director of the Advanced Technology Department, Giffels Associates, Southfield, Michigan, for his encouragement and his assistance in using Giffels' computer facilities to run STRUDL-DYNAL program and for the CPU time used in typing this dissertation.

I would like to express my thanks to Mr. F. Kiss for his continuous help during the experimental work. Thanks are also due to the staff of the computer centre for their assistance and help in producing the computer-trace time histories for each tested model.

The author would like to thank Mr. G. R. Monforton, a student in the Electrical Engineering Department, for his help in interfacing the Megadac data acquisition system and the IBM-PC computer with the main computer of the University of Windsor; also, for his help in developing the computer programs "KOUNT," "AUTO2," and the "Fourier Transform."

The financial assistance given by the National Research Council of Canada under Grant No. A1896, and the scholarship granted by the University of Windsor are sincerely appreciated.

Sincere thanks are due to Ms. Donna Laciak for her tireless effort in typing the manuscript, and for an excellent job.

The author appreciates the assistance of Nelson Stud Company in providing, free of charge, all of the studs and the welding equipments.

Finally, the author is deeply grateful to his wife Nadrine and his son Mina for their great patience and encouragement throughout this research; to them I say "Thanks."

TABLE OF CONTENTS

	PAGE
ABSTRACT	iv
ACKNOWLEDGEMENTS	vii
TABLE OF CONTENTS	ix
LIST OF FIGURES	xiii
LIST OF TABLES	xx
LIST OF APPENDICES	xxii
NOMENCLATURE	xxiii
CHAPTER	
I. INTRODUCTION	1
1.1 General	1
1.1.1 Composite Bridges	1
1.1.2 Waffle Slabs	3
1.2 Motivation and Objectives	5
II. BACKGROUND AND REVIEW OF LITERATURE	11
2.1 General	11
2.2 Free Vibration of Rectangular Orthotropic Plates	11
2.3 Free Vibration of Continuous Rectangular Orthotropic Plates	16
2.4 Free Vibration of Skew Orthotropic Plates	17
2.5 Fatigue of a Continuous Composite Bridge	18
III. THEORETICAL ANALYSIS AND MATHEMATICAL FORMULATION	22
3.1 Introduction	22
3.2 Governing Differential Equation for Rectangular Orthotropic Plate	23
3.2.1 Boundary Conditions	26
3.2.2 Anti-Symmetric Modes About the Intermediate Support	28
3.2.3 Symmetric Modes About Intermediate Support	31
3.2.4 Category I	33
3.2.5 Category II	38
3.2.6 Category III	39

PAGE

3.3 Governing Differential Equation for Skew Orthotropic Plates 40
3.3.1 Boundary Conditions 41
3.3.2 Mode Shape Functions 44

IV. TRANSCENDENTAL FREQUENCY EQUATION FOR SKEW ORTHTROPIC PLATE 51

4.1 Division of the Mode Shapes 51
4.2 Symmetric Mode Shapes 52
4.3 Anti-Symmetric Mode Shapes 58
4.4 Computer Program for the Numerical Solution 61
4.4.1 Flow Diagram 62

V. EXPERIMENTAL INVESTIGATION 67

5.1 Introduction 67
5.2 Scope of Experimental Program 68
5.3 Materials 70
5.3.1 Concrete 70
5.3.2 Grout 71
5.3.3 Sikadur Hi-Mod Epoxy Adhesive 71
5.3.4 Steel Beams 73
5.3.5 Stud Shear Connectors 73
5.3.6 Reinforcing Steel 79
5.3.6.1 Steel for Reinforced Concrete Deck Slab 79
5.3.6.2 High Tensile Steel for the Post-Tensioned Concrete 79
5.3.8 Formwork 79
5.4 Experimental Models 83
5.4.1 Design Procedures and Construction of Bridge Model I 83
5.4.2 Design Procedures and Construction of Bridge Model II 90
5.5 Vibration Excitation System 95
5.5.1 Attached Moving Weights 96
5.5.2 Modified Actuators 96
5.5.3 Gilmore Hydraulic and Electronic Control System 97
5.6 Prestressing Equipment 99
5.7 Instrumentation 99
5.7.1 Introduction 99
5.7.2 Megadac 2000 Data Acquisition System 103
5.7.3 Piezoelectric Accelerometers 110
5.7.4 Accelerometers Power Supply 114
5.7.5 DC Differential Transformer 114
5.7.6 Linear Variable Differential Transformer ... 115

PAGE

5.7.7 Dynamic-Fatigue Strain Gages 115
5.7.7.1 Strain Gages on the Prestressing and Reinforcing Wires..... 115
5.7.7.2 Strain Gages on the Longitudinal Steel Beam..... 116
5.7.7.3 Strain Gages on the Stud Shear Connectors 116
5.7.7.4 Strain Gages on the Concrete 119
5.8 Experimental Set-Up and Test Procedure 119
5.8.1 Static Test 123
5.8.2 Dynamic Test 123
5.8.3 Fatigue Test 125
5.8.4 Ultimate Load Test..... 125
5.9 Push-Out Tests of Stud Shear Connectors 126

VI. DISCUSSION OF RESULTS 131

6.1 Introduction 131
6.2 Finite Element Method..... 132
6.2.1 Structural Analysis Computer Program; SAP IV..... 132
6.2.2 Structural Design Language Computer Program; STRUDL-DYNAL 137
6.3 Confirmation of Earlier Research 139
6.4 Analysis of Dynamic Test Results 150
6.4.1 Sweep-Sine Wave Tests 150
6.4.2 Normal Modes Tests..... 162
6.4.3 Logarithmic Decay Response of Bridge Models I and II 166
6.5 Comparison Between the Natural Frequencies of Bridge Models I and II 177
6.6 Natural Frequencies and Mode Shapes of Rectangular and Skew Waffle Slabs 182
6.6.1 Natural Frequencies of Rectangular Waffle Slabs 182
6.6.2 Natural Frequencies of 45° Skew Waffle Slab 189
6.7 Free Vibration of a Single-Span Orthotropic Plate with Different Boundary Conditions 196
6.7.1 Fixed-Simply Supported Plate 196
6.7.2 Simply-Supported Plate..... 201
6.7.3 Analogy Between a Continuous Composite Bridge and the Single-Span Orthotropic Plate 208
6.8 Fatigue Test Results 212
6.8.1 Bridge Model I..... 213
6.8.2 Bridge Model II and Comparison with Bridge Model I..... 224
6.9 Ultimate Load Test Results 241
6.10 Parametric Study on the Skew Orthotropic Plate 247
6.11 Push-Out Test Results..... 252

PAGE

VII. SUMMARY AND CONCLUSION..... 260

7.1 Summary 260
7.2 Conclusions 261
7.3 Suggestions for Future Research 262

APPENDIX A 263

APPENDIX B 268

APPENDIX C 273

APPENDIX D 275

APPENDIX E 280

APPENDIX F 293

APPENDIX G 319

BIBLIOGRAPHY..... 339

VITA AUCTORIS 345

LIST OF FIGURES

FIGURE		PAGE
1.1	The Gardiner Expressway in Toronto	8
1.2	Spalling and Damage of Concrete at an Expansion Joint of the Gardiner Expressway Bridge	9
1.3	Conestoga River Bridge	10
3.1	Plate Dynamic-Flexural Element	24
3.2	Plan View of Two-Span Continuous Composite Bridge Models I & II	27
3.3	(a) First, (b) Second, (c) Third, and (d) Fourth Mode Shapes of Bridge Models I & II	29
3.4	(a) Fifth, (b) Sixth, (c) Seventh, and (d) Eight Mode Shapes of Bridge Models I & II	30
3.5	Vibration Categories of Orthotropic Plate Structures	34
3.6	Skew Orthotropic Plate	42
4.1	Matrix Equation of (8n+4) Equations for Symmetric Mode Shapes of a 45° Skew Orthotropic Plate	64
4.2	Matrix Equation of (8n+4) Equations for Anti-Symmetric Mode Shape of a 45° Skew Orthotropic Plate	65
4.3	Flow Diagram to Calculate the Natural Frequencies of a 45° Skew Orthotropic Plate for Symmetric and Anti-Symmetric Modes	66
5.1	Small Prestressed Model for Testing the Grout Procedures	72
5.2	Nelson Stud Welding System	78
5.3	Stress-Strain Relationship for 3/16 in. Reinforcing Bar	80
5.4	Typical Stress-Strain Curve for Prestressing Wire of 0.276 inch Diameter	81
5.5	Arrangement of the Form Bracket System	82

FIGURE		PAGE
5.6	Formwork for Prestressed Concrete Portion of Bridge Model II	84
5.7	Close-Up of Formwork for Bridge Model II	85
5.8	Geometry of Two-Span Continuous Composite Bridge Models I and II	86
5.9	Tie-Down System for Bridge Models I and II	88
5.10	Layout of Composite Bridge Model II	89
5.11	Rubber Hoses Used as Conduit for Prestressing Wires and Grout Purpose	91
5.12	Prestressed Concrete Portion of Bridge Model II After Grouting	92
5.13	Instrumented Stud Shear Connectors in the Vicinity of the Prestressed Concrete Portion of Bridge Model II	93
5.14	Support Arrangement for 20 KIP Actuator	98
5.15	20-KIP Hydraulic Actuator Carrying 600 lb. "Moving Mass"	100
5.16	End Bearing System, Bridge Model II	101
5.17	Data Acquisition System Schematic for Dynamic Tests	104
5.18	Schematic Circuit Diagram for Full Bridge Current Energization	107
5.19	Schematic Circuit Diagram for LVDT Energization	108
5.20	Schematic Circuit Diagram for Quarter Bridge 3-Wire Connection	109
5.21	A/D, SCV, SCI-I and SCI-II Terminal Boxes	111
5.22	25g Accelerometers Mounted on Bridge Models I and II	112
5.23	50g Accelerometer on the top of the Moving Mass	113
5.24	Location of Strain Gages at Intermediate Support, Bridge Model I	117
5.25	Location of Longitudinal Strain Gages	118

FIGURE		PAGE
5.26	Location of Longitudinal and Transverse Strain Gages on Bridge Model II	120
5.27	Dynamic and Fatigue Tests Set-Up for Bridge Model I	121
5.28	Dynamic and Fatigue Tests Set-Up for Bridge Model II	122
5.29	Forms for the Push-Out Specimens	127
5.30	Set-Up for Static Push-Out Tests	128
5.31	Set-Up for Fatigue Push-Out Tests	130
6.1	Finite Element Idealization	134
6.2	Quadrilateral Plate Element for SAP IV Analysis	135
6.3	Local and Global Axis for Beam Element Used in Bridge Models I and II Analysis	136
6.4	Typical Cross-Section Waffle Slab	138
6.5	Typical Bottom Plan Layout of Rectangular Waffle Slab	140
6.6	Typical Bottom Plan Layout of Skew Waffle Slab	141
6.7	Finite Element Mesh for a Rectangular Waffle Slab Using Hybrid Plate Element	142
6.8	Finite Element Mesh for a Typical Skew Waffle Slab Bridge	143
6.9	Strain Distribution in Bridge Model I	148
6.10	Strain Distribution on the Diaphragm & Slab in the Transverse Direction	149
6.11	Sinusoidal Forcing Function for Sweep Test	151
6.12	Acceleration Time History at Mid-Span of Bridge Model I	152
6.13	Fourier Transform of Acceleration Time History of Model I	154
6.14	Time History From Accelerometer Mounted on Middle Beam of Bridge Model II	156
6.15	Fourier Transform of the Acceleration Given in Figure 6.14	157

FIGURE		PAGE
6.16	Time History From Accelerometer on the Middle Beam of Model II	158
6.17	Fourier Transform of the Acceleration Time History Given in Figure 6.16	159
6.18	Time History From Accelerometer on the Exterior Girder of Bridge Model II	160
6.19	Fourier Transform of the Acceleration Time History Given in Figure 6.18	161
6.20	First Mode Shape of Bridge Models I & II	163
6.21	Second Mode Shape of Bridge Models I & II	164
6.22	Third Mode Shape of Bridge Models I & II	165
6.23	Fourth Mode Shape of Bridge Models I & II	167
6.24	Fifth Mode Shape of Models I & II	168
6.25	Sixth Mode Shape of Models I & II	169
6.26	Seventh Mode Shape of Models I & II	170
6.27	Eighth Mode Shape of Bridge Models I & II	171
6.28	Acceleration Response for Transient Vibration of Model I	173
6.29	Acceleration Response for Transient Vibration of Bridge Model II	174
6.30	Acceleration Response for Transient Vibration of Bridge Model II	175
6.31	Acceleration Response for Transient Vibration of Bridge Model II	176
6.32	First Mode Shape for the Rectangular Waffle Slab	185
6.33	Second Mode Shape for the Rectangular Waffle Slab	186
6.34	Third Mode Shape for the Rectangular Waffle Slab	187
6.35	Fourth Mode Shape for the Rectangular Waffle Slab	188
6.36	First Mode Shape for the Skew Orthotropic Plate	192

FIGURE		PAGE
6.37	Second Mode Shape for the Skew Orthotropic Plate	193
6.38	Third Mode Shape for the Skew Orthotropic Plate	194
6.39	Fourth Mode Shape for the Skew Orthotrpic Plate	195
6.40	Plan View of Orthotropic Plate with End Conditions	197
6.41	Mode Shapes: (a) First Flexural Mode, i=1; (b) Second Mode (Torsional), i=1; (c) Third Mode (Flexural), i=2; (d) Fourth Mode (Torsional), i=2	200
6.42	Influence of Aspect Ratio (a/b) & Rigidity Ratio (Dx/Dy) on First Mode Frequency	202
6.43	Influence of Aspect Ratio (a/b) & Rigidity Ratio (Dx/Dy) on Second Mode Frequency	203
6.44	Influence of Aspect Ratio (a/b) & Rigidity Ratio (Dx/Dy) on Third Mode Frequency	204
6.45	Influence of Aspect Ratio (a/b) & Rigidity Ratio (Dx/Dy) on Fourth Mode Frequency	205
6.46	Plan View of Orthotropic Plate with Boundary Conditions Shown	206
6.47	Strain Variation at Bottom Flange of Longitudinal Beam at Mid-Span of Model I	214
6.48	Strain Variation at Top of Cracked Flange of Longitudinal Beam at Mid-Span of Model I	215
6.49	Fatigue Crack Propagation in Bridge Model I	216
6.50	Strain Variation at Bottom Flange of Mid-Span Diaphragm of Model I	219
6.51	Strain Variation in Longitudinal Steel Bar at Intermediate Support of Model I	220
6.52	Strain Variation at Top Flange at the Intermediate Support of Model I	221
6.53	Cumulative Resistance of Stud Shear Connectors	222
6.54	Strain Variation in Stud Near End Support of Model I	223
6.55	Repair of Fatigue Cracks in Bridge Model I	225

FIGURE		PAGE
6.56	Strain Distribution due to Prestressing the Deck Near Intermediate Support Section of Model II	227
6.57	Strain Variation at the Bottom Flange of Steel Girder at Mid-Span of Bridge Model II	228
6.58	Strain Variation in the Transverse Direction on the Top of Prestressed Concrete at Intermediate Support	230
6.59	Strain Variation in Shear Connector at Intermediate Support of Bridge Model II	231
6.60	Strain Variation in Prestressed Wire at Intermediate Support of Bridge Model II	232
6.61	Separation Between Prestressed & Non-Prestressed Concrete Portions Along a 45° Plane at 800,000 Cycles....	233
6.62	Transverse Cracks in the Concrete Slab Around the Intermediate Support of Bridge Model I	235
6.63	Transverse Cracks & Spalling of Concrete Cover in the Bottom of the Slab at the Intermediate Support of Bridge Model I	236
6.64	Fatigue Cracks in Top Flanges of Exterior & Middle Girders of Bridge Model II at 840,000 Cycles	237
6.65	Replacing the Stud Shear Connectors by Other Mechanical Connector Near One Side of the Prestressed Concrete Portion	238
6.66	Fatigue Cracks at Mid-Span of Bridge Model II at 1,110,000 Cycles	239
6.67	Ultimate Load Test of Bridge Model I	242
6.68	Close-Up of Mid-span 'Plastic' Hinge of Bridge Model I ..	243
6.69	Load-Deflection of Bridge Model I Under Ultimate Load Test	244
6.70	Strain at Bottom Flange of Steel Beams at the Middle of Unfatigued Span of Bridge Model II	245
6.71	Fatigue Cracks of Bridge Model II Under Ultimate Load Test	246
6.72	Ultimate Load Test of Bridge Model II	248

FIGURE		PAGE
6.73	Close-Up of Negative 'Plastic' Hinge at the Intermediate Support of Bridge Model II	249
6.74	Effect of Skew Angle θ on the Natural Frequencies	250
6.75	Effect of Aspect Ratio (b/a) on Skew Orthotropic Plate	253
6.76	Yielding of Stud Shear Connector Under Static Load	254
6.77	Typical Load-Strain of Push-Out Test	257
6.78	Typical Load-Slip Curve of Push-Out Test	258
6.79	Fatigue Failure of Stud Shear Connectors Under Pulsating Load	259

LIST OF TABLES

TABLE		PAGE
5.1	Properties and Strength of the Grout Mixes	74
5.2	Typical Physical Characteristics for Sikadur Hi-Mod Epoxy Adhesive	74
5.3	Average Mechanical Properties of Steel Beams	75
5.4	Roller Steel Beam Properties	75
5.5	Mechanical Properties of Headed Stud Shear Connector.....	77
6.1	Deflection Distribution at Mid-Span Using Different Methods.....	145
6.2	Longitudinal Bending Moment Distribution at Mid-Span Section Using Different Methods.....	145
6.3	Transverse Bending Moment Distribution at Mid-Span Section Using Different Methods	146
6.4	Longitudinal Bending Moment Distribution at the Intermediate Support Using Different Methods.....	146
6.5	Effect of Own Weight of the Actuators and the Moving Mass on the Natural Frequencies of Bridge Model II	178
6.6	Enhancement of the Natural Frequencies due to Prestressed Concrete in the Negative Moment Region Using Orthotropic Plate Theory.....	180
6.7	Natural Frequencies of Bridge Models I and II Using Different Approaches.....	181
6.8	Natural Frequencies of Rectangular Waffle Slab.....	184
6.9	Natural Frequencies for 45° Skew Waffle Slab.....	190
6.10	Comparison of Frequencies of Fixed-Simply Supported Single-Span Orthotropic Plate	199
6.11	Comparison of Frequencies of Simply-Supported-Free Orthotropic Plate	207
6.12	Frequency Ratio of Two-Span Continuous Bridge to Single-Span Orthotropic Plate Using the Orthotropic Plate Theory.....	209

TABLE		PAGE
6.13	Frequency Ratio of Two-Span Continuous Bridge to Single-Span Orthotropic Plate Using SAP IV (Quadrilateral Plate Elements).....	210
6.14	Frequency Ratio of Two-Span Continuous Bridge to Single-Span Orthotropic Plate Using SAP IV (Isotropic Plate + Three-Dimensional Beam Elements).....	211
6.15	Variation in the First Natural Frequency of Bridge Model II due to Fatigue Loading Using SAP IV.....	240
6.16	Effect of Skew Angle on the Natural Frequencies of the Skew Orthotropic Plate (Aspect Ratio = 1.0).....	251
6.17	Natural Frequencies of the Skew Solid and Skew Waffle Slab Having Same Weight and Same Platform Size.....	255

LIST OF APPENDICES

APPENDIX		PAGE
A	Governing Differential Equation for the Free Vibration of a Skew Orthotropic Plate	263
B	Evaluation of Definite Integrals for Fourier Series ..	268
C	Fast Fourier Transform Computer Program	273
D	Megadac 2000 Data Acquisition System	275
E	List of Computer Program for the Free Vibration of a Skew Orthotropic Plate	280
F	Typical Output of SAP IV for the Natural Frequencies and Associated Mode Shapes of a Skew Orthotropic Plate	293
G	Typical Input and Output of STRUDL-DYNAL for a Skew Orthotropic Plate	319

NOMENCLATURE

In selecting the symbols used in this dissertation, an attempt was made to conform to the list of recommended symbols for structural dynamics adopted in any structural dynamics books. However, some symbols were adopted to avoid confusion. Symbols are defined where they first appear in the text; those which occur several times are listed below.

A_n = shape function's constant, see Equation 3.3.6

$A_{1n} = \cosh R_{1n} \cos R_{r1}$

$A_{2n} = \sinh R_{1n} \sin R_{r1}$

$A_{3n} = \sinh R_{1n} \cos R_{r1}$

$A_{4n} = \cosh R_{1n} \sin R_{r2}$

$A_{5n} = \cosh R_{2n} \cos R_{r2}$

$A_{6n} = \sinh R_{2n} \sin R_{r2}$

$A_{7n} = \sinh R_{2n} \cos R_{r2}$

$A_{8n} = \cosh R_{2n} \sin R_{r2}$

a = skew semi-width of the orthotropic plate.

$\bar{a}$ = span length of continuous composite bridge.

a_{oo}, a_{om}, a_{no}, a_{nm} = Fourier coefficients, see Equation 4.2.2

$a(\omega)$ = real part of Fourier Transform.

B_n = shape function's constant, see Equation 3.3.6

$B_{1n} = \cosh S_{1n} \cos S_{s1}$

$B_{2n} = \sinh S_{1n} \sin S_{s1}$

$B_{3n} = \sinh S_{1n} \cos S_{s1}$

$B_{4n} = \cosh S_{1n} \sin S_{s1}$

$B_{5n} = \cosh R_{2n} \cos S_{s2}$

B_{6n} = sinh R_{2n} sin S_{s2}

B_{7n} = sinh R_{2n} cos S_{s2}

B_{8n} = cosh R_{2n} sin S_{s2}

b = semi span of the skew orthotropic plate.

$\bar{b}$ = width of continuous composite bridge.

b_{om}, b_{nm} = Fourier coefficient, see Equation 4.2.2

$b(\omega)$ = Imaginary part of Fourier Transform.

C_{1n} to C_{16n} = Arbitrary functions dependent on n of the mode shape function.

C_{17} to C_{24} = Arbitrary constants of the polynomial mode shape function.

c = cos θ

C_{rt} = Force in the Longitudinal Reinforcement at mid-span.

C_1, C_2 = constants, see Equation 3.3.8

D_x, D_y = Flexural rigidities of the plate per unit length and unit width for the composite bridge models and per unit width and unit length of the skew orthotropic plate respectively.

D_1, D_2 = Coupling rigidities - contribution of bending to torsional rigidity.

$E_1 = 2K_1K_3$

$E_2 = K_1^2 - K_3^2$

$E_3 = K_1 (K_1^2 - 3K_3^2)$

$E_4 = K_1 (3K_1^2 - K_3^2)$

$E_5 = -EIy_1^4 (E_2^2 - E_1^2)$

$E_6 = 2EI\ y_1^4 E_1E_2$

$E_7 = X_1K_3 - X_2$

$E_8 = y_1 (X_1K_3 + X_2y_1E_2)$

$E_9 = y_1 (X_1K_3 - X_2y_1E_1)$

$E_{10} = X_3E_3 + X_4E_1 - X_5K_1$

$E_{11} = -X_3E_4 + X_4E_2 + X_5K_3 - X_6$

$E_{12} = -y_1 (X_4K_1 - X_5y_1E_1 - X_6y_1^2E_3)$

$E_{13} = -X_3 + X_4y_1K_3 + X_5y_1^2E_2 - X_6y_1^2E_4$

$E_{14} = X_7E_2 + X_8K_5 - X_9$

$E_{15} = -X_7E_1 + X_8K_1$

$E_{16} = -X_{10} + K_3GJ$

$E_{17} = X_9y_1^2E_2 + X_8y_1K_3 - X_7$

$E_{18} = y_1 (X_8K_1 - X_9y_1E_1)$

$E_{19} = y_1^2 (X_{10}y_1E_3 + E_1GJ)$

$E_{20} = y_1^2 (-X_{10}y_1E_4 + E_2GJ)$

$E_{22} = 1/c + (s/c) K_3$

$E_{23} = K_1y_1/c$

$E_{24} = -(s/c) - K_3y_1/c$

$E_{26} = -(s/c) - K_3/c$

$E_{27} = -(s/c) K_1y_1$

$E_{28} = (s/c) K_3y_1 + 1/c$

EI = Flexural rigidity of the edge beam.

E_x, E_y = Modulus of elasticity in x and y directions

$\bar{E}, \bar{\bar{E}}$ = see Equations 6.3 and 6.4

e_x, e_y = distance from the top fiber of the slab to the neutral planes for bending in x and y directions respectively.

$F_1 = 2K_1K_2$

$F_2 = K_1^2 - K_2^2$

$F_3 = K_1 (K_1^2 - 3K_2^2)$

$$F_4 = K_2 (3K_1^2 - K_2^2)$$

$$F_5 = EI (F_1^2 - F_2^2)$$

$$F_6 = 2EIz_1^4 F_1 F_2$$

$$F_7 = -(X_2 + X_1 K_2)$$

$$F_8 = z_1 (X_2 z_1 F_2 - X_1 K_2)$$

$$F_9 = z_1 (X_2 z_1 F_1 - X_1 K_1)$$

$$F_{10} = X_3 F_3 - X_4 F_1 - X_5 K_1$$

$$F_{11} = X_6 + X_5 K_2 - X_4 F_2 - X_3 F_4$$

$$F_{12} = -z_1 (X_4 K_1 + X_5 z_1 F_1 - X_6 z_1^2 F_3)$$

$$F_{13} = -X_6 z_1^3 F_4 - X_5 z_1^2 F_2 + X_4 z_1 K_2 + X_3$$

$$F_{14} = -X_9 - X_9 K_2 + X_7 F_2$$

$$F_{15} = -X_8 K_1 - X_7 F_1$$

$$F_{16} = X_{10} + K_2 GJ$$

$$F_{17} = X_9 z_1^2 F_2 - X_8 z_1 K_2 - X_7$$

$$F_{18} = -z_1 (X_9 z_1 F_1 + X_8 K_1)$$

$$F_{19} = -z_1^2 (F_1 GJ - X_{10} z_1 F_3)$$

$$F_{20} = -z_1^2 (F_2 GJ + X_{10} z_1 F_4)$$

$$F_{21} = -(s/c) K_1$$

$$F_{22} = (s/c) K_2 - 1/c$$

$$F_{23} = K_1 z_1 / c$$

$$F_{24} = (s/c) - K_2 z_1 / c$$

$$F_{25} = K_1 / c$$

$$F_{26} = s/c - K_1 / c$$

$$F_{27} = -K_1 z_1 \, s/c$$

$$F_{28} = -(1/c) + K_2 z_1 \, s/c$$

G_1 to G_4 = Constant coefficients of the governing differential equation for the skew orthotropic plate, see Equation 3.3.2.

G_n = see Equation 4.2.1

H = Effective torsional rigidity of the orthotropic plate.

$H_o(u)$, $H_n(u)$ = Functions in u, see Equation 4.2.1.

h_1 = Equivalent thickness for the skew and rectangular orthotropic plates, respectively.

I = Moment of Inertia of the beam cross-section

I_{k1} to I_{k8} = Definite integral, see Appendix B

I_{j1} to I_{j8} = Definite integral, see Appendix B.

J_{1m} to J_{7m} = Definite integral, see Appendix B.

K_{1m} to K_{8n} = Definite integral, see Appendix B.

K_1, K_2, K_3 = Resulting roots of the satisfaction of the governing equation using the mode shape function for the skew orthotropic plate.

$K_{1m_i n}$, $K_{2m_i n}$ = Resulting roots of the satisfaction of the governing equation using the mode shape function for the continouous composite bridge

M_x, M_y = Bending moment per unit dimension in x and y direction respectively.

M_{xy}, M_{yx} = Twisting moment per unit dimension in x and y directions respectively.

$\bar{m}$ = Mass of beam per unit length or mass per unit volume of the plate

n,m = Integer, number of harmonics for skew plate, and identified whenever used in the text.

n = Integer, number respresents the roots of the transcendental frequency equation for each m_i in the rectangular composite bridges.

N = Number of cycles

m_i = i + 1/4, define the mode shape for rectangular composite bridges.

P = See Equation 3.3.21

P_n = Constant, see Equation 4.2.1

$\bar{Q}_n$, Q_n = Constant, see Equation 3.3.11

Q_x, Q_y = Shear force per unit dimension in x and y directions.

R_{1m_in} to R_{7m_in} = see Equations 3.2.29 to 3.2.42

$R_{r1} = K_2 z_1 \alpha_n b$

$R_{r2} = K_2 \beta_n a$

$R_{1n} = K_1 z_1 \alpha_n b$

$R_{2n} = K_1 \beta_n a$

$S_{s1} = \alpha_n\ b\ y_1 K_3$

$S_{s2} = \beta_n\ a\ K_3$

$S_{xa} = 2/[m^4\pi^4 + \alpha_n^2 b^2 z_1^2\ (2F_2 m^2\pi^2 + \alpha_n^2 b^2)]$

$S_{x1} = (-1)^m\ m\pi S_{xa}$

$S_{x2} = (-1)^m \alpha_n b S_{xa}$

$S_{ya} = 2/[m^4\pi^4 + \alpha_n^2 b^2 y_1^2\ (\ 2E_2 m^2\pi^2 + \alpha_n^2 b^2)]$

$S_{y1} = (-1)^m\ m\pi\ S_{ya}$

$S_{y2} = (-1)^m \alpha_n\ b\ S_{ya}$

$S_{1n} = \alpha_n b z_1 K_1$

s = sin θ

$S_{a1} = \beta_n^2 a^2 F_1$

$S_{a2} = \beta_n^2 a^2 F_2 + m^2\pi^2$

$S_{a3} = K_1\ (m^2\pi^2 + \beta_n^2 a^2/z_1)$

$S_{a4} = K_2\ (-m^2\pi^2 + \beta_n^2 a^2/z_1)$

$S_{b1} = \beta_n^2 a^2 E_1$

$S_{b2} = m^2\pi^2 + \beta_n^2 a^2 E_2$

$S_{b3} = K_1 (m^2\pi^2 + \beta_n{}^2 a^2/y_1)$

$S_{b4} = K_3 (-m^2\pi^2 + \beta_n{}^2 a^2/y_1)$

S_r = Stress range parameter

$T_{aa} = 2/[m^4\pi^4 + \beta_n{}^2 a^2 (2F_2 m^2\pi^2 + \beta_n{}^2 a^2/z_1{}^2)]$

$T_{a1} = (-1)^m m\pi T_{aa}$

$T_{a2} = (-1)^m a\beta_n T_{aa}$

$T_{ba} = 2/[m^4\pi^4 + \beta_n{}^2 a^2 (2E_2 m^2\pi^2 + \beta_n{}^2 a^2/y_1{}^2)]$

$T_{b1} = (-1)^m m\pi T_{ba}$

$T_{b2} = (-1)^m \beta_n a T_{ba}$

$T_n = s/c$

$u_{x1} = \alpha_n{}^2 b^2 z_1{}^2 F_1$

$u_{x2} = m^2\pi^2 + \alpha_n{}^2 b^2 z_1{}^2 F_2$

$u_{x3} = z_1 K_1 (m^2\pi^2 + z_1 \alpha_n{}^2 b^2)$

$u_{x4} = z_1 K_2 (-m^2\pi^2 + z_1 \alpha_n{}^2 b^2)$

$u_{y1} = \alpha_n{}^2 b^2 y_1{}^2 E_1$

$u_{y2} = m^2\pi^2 + \alpha_n{}^2 b^2 y_1{}^2 E_2$

$u_{y3} = K_1 y_1 (m^2\pi^2 + y_1 \alpha_n{}^2 b^2)$

$u_{y4} = K_3 y_1 (m^2\pi^2 + y_1 \alpha_n{}^2 b^2)$

u = Oblique coordinate.

$u_{1n} = K_1 \beta_n u$

$u_{2n} = K_2 \beta_n u$

$u_{3n} = K_3 \beta_n u$

V_x, V_y = Reactive force per unit dimension perpendicular to x and y axis, respectively.

v = oblique coordinate.

w (x,y,t), w (u,v,t) = Mode shape at any time (t).

$W(x,y)$, $W(u,v)$ = Mode shape functions in x,y and u,v directions respectively.

W_1, W_2, W_3 = Shape functions for skew orthotropic plate.

$w_{1n} = \alpha_n z_1 K_1 v$

$\bar{w}_{1n} = \alpha_n y_1 k_1 v$

$w_{2n} = \alpha_n z_1 k_2 v$

$w_{3n} = \alpha_n y_1 k_3 v$

x = Rectangular coordinate.

$\ddot{X}(t)$ = Acceleration time history response in time domain.

$\ddot{X}(\omega)$ = Acceleration resonse in frequency domain (Fourier transform function).

X_1 to X_{10} = Coefficients of derivatives in the boundary conditions.

y = Rectangular coordinate.

y_1 = Basic function of the skew orthotropic plate, see Equation 3.3.19.

z_1 = Basic function of the skew orthotropic plate, see Equation 3.3.19

ν = Poisson's ratio

θ = Skew angle

$\lambda_i, \bar{\lambda}_i$ = Parameter, see Equations 3.3.6 and 3.3.17

ω = Natural frequency in rad./sec. - or - as defined in the figures.

$\alpha_m = m\pi/a$

$\alpha_n = n\pi/a$

$\beta_m = m\pi/b$

$\beta_n = n\pi/b$

ξ = Damping ratio.

σ_r = Stress range.

CHAPTER I

INTRODUCTION

1.1 General

1.1.1 Composite Bridges

Composite construction of concrete-on-steel beams has been used with increasing frequency in both buildings and bridges. Recent design innovation and improvements in construction materials and technologies have combined to achieve significant economies and aesthetically pleasing profiles in bridge structures. These advancements, however, may be accompanied by an increased susceptibility to undesirable vibrations and structural fatigue.

The problem of transverse cracking of concrete decks at intermediate supports of continuous composite bridges, subjected to static, dynamic and fatigue loads, is well known. As a result of such cracking, the advantages of continuity cannot be fully realized in design; the stiffness of the bridge is reduced and hence, its dynamic response is changed; furthermore, the susceptibility of the steel reinforcing to corrosion is increased; and maintenance costs are increased. In addition, the code provisions for the design of the negative moments region of continuous composite bridges with the entire deck prestressed are not as fully developed as provisions for the positive moment region under dynamic and fatigue loads.

In order to avoid the transverse cracking problems in continuous composite bridges, engineers in North America used to design continuous composite bridges as composite in the positive moment regions and non-composite in the negative moment regions. For example, in 1963 the F. G.

Gardiner Expressway in Toronto, was made of 106 simply supported composite units as shown in Figure 1.1. After ten years of construction, spalling and damage of concrete from exposed faces of beams occurred near all expansion joints due to the leakage of salt-laden water at the expansion joints, as shown in Figure 1.2. In 1980, the Ontario Ministry of Transportation and Communications began repairs by removing only the top slab and casting a new slab to be continuous and composite with the existing simply supported girders. However, in the opinion of this author they may solve temporarily the leakage problems, but most probably the transverse cracking problem will recur.

Another recent example is the Conestogo River Bridge, which was designed and built in 1974 as a continuous prestressed composite bridge, shown in Figure 1.3. The deck was prestressed along the entire three spans; this may have eliminated the transverse cracks at the intermediate supports, but it would have increased the compression in the concrete deck as well as the tension in the bottom flanges of the longitudinal steel girders at the midspan sections.

Some codes of practice, such as the OHBDC (53), specify values of a dynamic load allowance (DLA) related to the fundamental natural frequency of the structures; this allowance represents the amount by which the static live loads should be increased to simulate the dynamic effects of the live loads, assuming beam-type mode shapes. However, in a wide rectangular and/or skew bridge with significant transverse rigidities, such an assumption may lead to unacceptable errors in the estimation of the natural frequencies of the bridge. For example, the Tacoma Narrows Bridge, which collapsed due to wind effects, failed at the second mode shape which was

anti-symmetrical in the transverse direction due to weakness in the torsional rigidity of the bridge. Such a second mode shape cannot be reliably predicted by the beam-theory; it can only be accurately predicted by a theory such as the orthotropic plate theory, which takes into account two-way action.

The current design codes are unduly conservative in the design of composite bridges with transverse diaphragms. In such designs, the contribution of the transverse diaphragms to the load distribution in the bridge is minimized. When transverse steel diaphragms of I-Section are connected rigidly to the longitudinal girders, a rigid gridwork is formed. Such a rigid gridwork, together with the composite concrete deck, distribute the wheel loads on the bridge essentially in an "orthotropic" manner. The use of a prestressed deck around the intermediate supports in continuous composite bridges, and taking into account the effectiveness of the diaphragms (21), (36), (37), can have the following advantages:

1. Uniform rigidity along the entire length of the continuous composite bridge.
2. Crack control in the negative moment regions, thus avoiding steel corrosion and concrete deterioration.
3. Reduction of maintenance costs.
4. Enhancement of load distribution leading to a more economical design.
5. Increased effectiveness of the orthotropic plate theory in predicting the elastic response of a continuous composite bridge.

1.1.2 Waffle Slabs

For a number of years, reinforced and prestressed concrete waffle

slabs, rectangular and skew, have been extensively and successfully used in buildings and many other structures, such as Montreal's Olympic Stadium, Houston's International Airport terminals, and the process floor in IBM Computer Building in East Fishkill, New York. Besides the aesthetic beauty and the attractive appearance of a waffle slab, it affords (38): (1) excellent access for inspection and maintenance of salt damage to the reinforcing or prestressing steel, (2) small depth of construction to span ratios leading to dead load reduction and substantial economics, (3) high durability and less maintenance cost, and (4) reduction in the secondary stresses and deflection due to the reduction in the dead load moment.

In spite of these advantages, waffle slabs are rarely employed in bridges. The only example of the use of waffle construction in bridges seems to be that reported by Lin et. al. (1969). However, in 1977 a feasibility study was undertaken at the University of Windsor (17, 18, 38), to investigate and study the suitability and resulting economy thereof of employing prestressed waffle slabs, rectangular or skew, for short and medium span bridges under distributed and concentrated static loads. The results showed that (38): (i) Waffle slab construction for bridges has the potential of being a more economical alternative to solid slab and slab-on-girder bridges, and (ii) when there are large twisting moments in a bridge, the orthogonal rib system in a waffle slab provides an efficient means of incorporating the required large moments in two orthogonal directions.

The feasibility study was continued by El-Sabakhy, et al. (19) to investigate and examine the behavior of prestressed rectangular and skew waffle slabs under dynamic and fatigue loadings. The study, was directed to find the dynamic characteristics and fatigue life of such structures.

This additional information will enable the designer to achieve more improvements in the design, since it is a fact that the understanding of any structure is incomplete unless its structural dynamic and fatigue characteristics are known and can be accurately predicted.

1.2 Motivation and Objectives

As an extension to previous work, it became essential to investigate the effect of dynamic and fatigue loadings on continuous composite bridges with prestressed decks, and in skew waffle slabs. Before embarking on this task, some questions had arisen, such as (1) What is the effect of prestressing a deck on the dynamic characteristics of continuous composite bridge ?; (2) What is the structural response of the bonded prestressed bars and the shear connectors in the vicinity of the negative moment region in a continuous composite bridge subjected to fatigue loading?; (3) If a continuous composite bridge is fatigued, is it possible to repair? If yes, what would be: (a) the ultimate load carrying capacity of the repaired fatigued bridge, and (b) the changes in its dynamic characteristics? and (4) Referring to waffle slab construction, what is the advantage, if any, in using waffle slab construction in bridge design compared to a regular skew solid slab construction with regard to the Dynamic Load Allowance?

In order to answer these questions, dynamics, fatigue and ultimate load tests were carried out on two continuous composite bridge models, as well as on two waffle slab bridge models (19). Although a variety of techniques have been proposed to study the vibration of stiffened plate systems, none is completely satisfactory. There exists no exact solution for a general system. Exact theoretical analysis of the natural

frequencies of the above bridges involves cumbersome mathematical procedures. Several simplifying assumptions are made herein so that the obtained theoretical results are sufficiently reliable and accurate for practical design purposes. The most common method of analysis of plates with parallel stiffeners in both directions has been to replace the stiffened plate system by an equivalent orthotropic plate having different elastic properties in two orthogonal directions.

The objectives of this research are to:

1. Develop a reliable theoretical solution for the problem of the free vibration of continuous two-span composite bridges, and of rectangular or skew waffle slabs, using orthotropic plate theory, and verify the solution by experimental results and by available finite element computer programs.
2. Examine the effect of prestressing a portion of the concrete deck in the vicinity of an intermediate support on the serviceability limit states (cracking) of a composite bridge under dynamic and fatigue loadings.
3. Examine the stress range, due to resonance-fatigue loading, in the: prestressed steel, top flanges of the steel girders, and the shear connectors at the intermediate support(s).
4. Study the influence of fatigue, of any of the bridge's elements, such as shear connectors, diaphragms, and the longitudinal steel reinforcement at the intermediate support, on the natural frequencies, mode shapes and ultimate load.

The content of this dissertation is arranged as follows:

In Chapter II, the background of the theoretical methods used to solve

the free vibration problem in rectangular and skew slabs is provided. Also, a review of the available literature on the fatigue tests of continuous composite bridges is given.

In Chapter III, the mathematical treatment using the orthotropic plate theory in solving the free vibration problem of continuous composite bridges and skew orthotropic slabs is explained.

In Chapter IV, the transcendental frequency equations for symmetric and anti-symmetric modes of vibration for the skew orthotropic slab are derived.

In Chapter V, the experimental work and test procedures for the dynamic, fatigue and ultimate loads are presented.

In Chapter VI, the experimental and theoretical results are discussed, and a parametric study is given.

Conclusions and recommendations for future work are presented in Chapter VII.

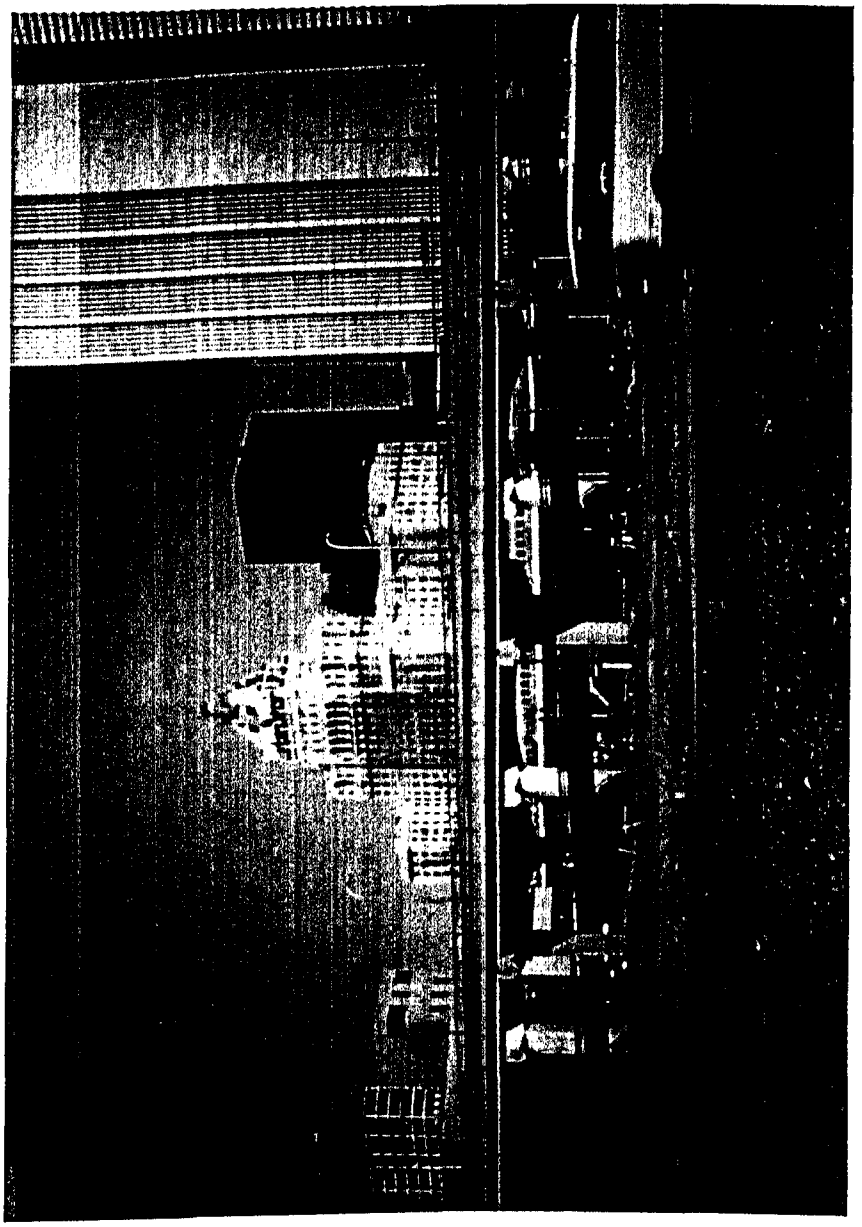

FIGURE 1.1 THE GARDINER EXPRESSWAY IN TORONTO

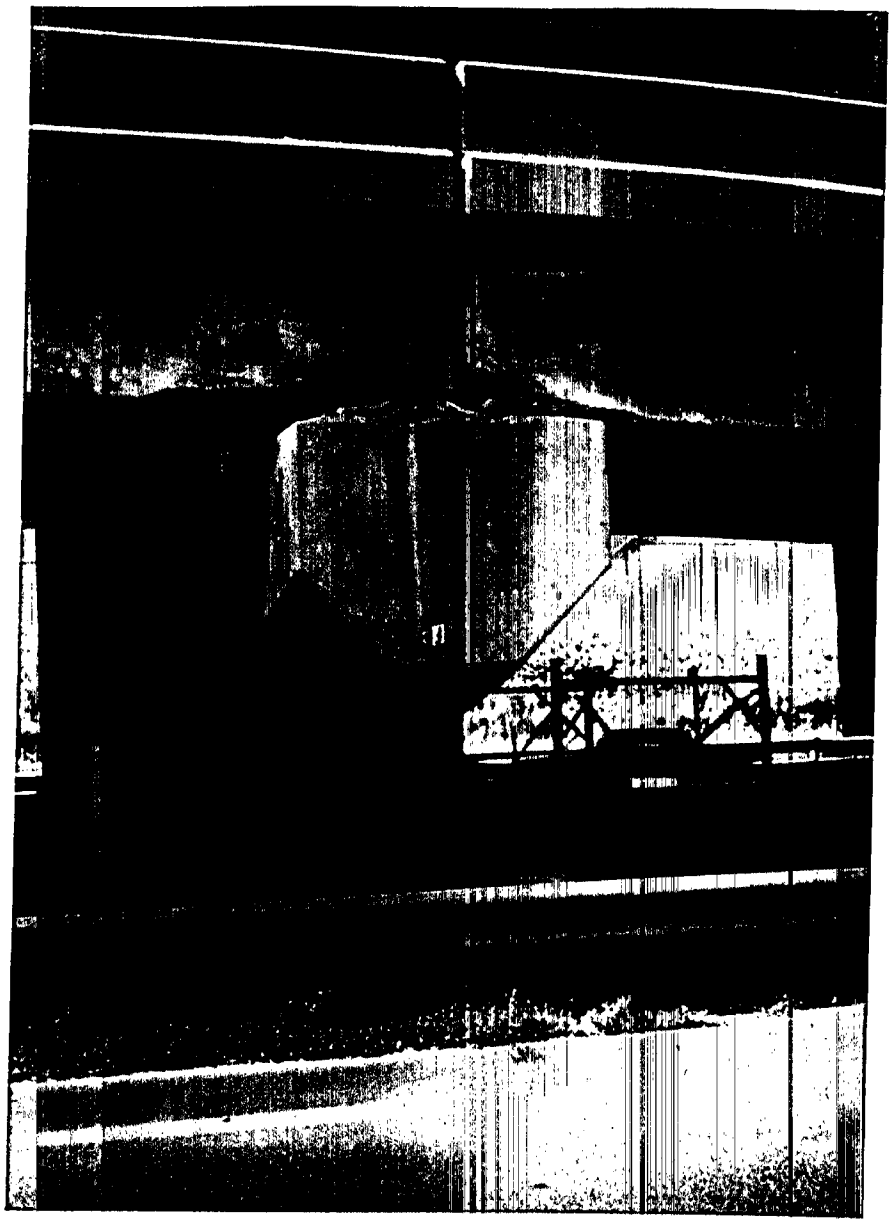

FIGURE 1.2 SPALLING AND DAMAGE OF CONCRETE AT AN EXPANSION JOINT OF THE GARDINER EXPRESSWAY BRIDGE

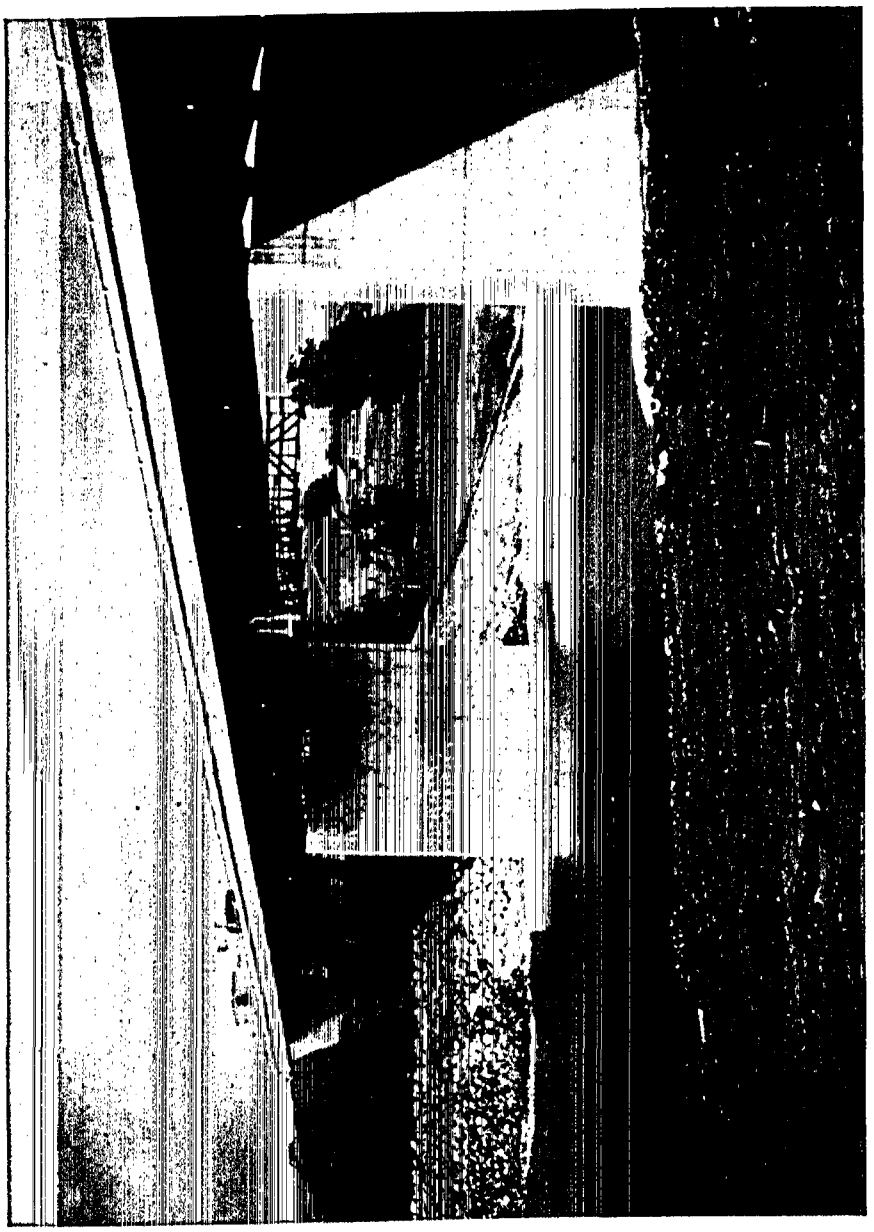

FIGURE 1.3 CONESTOGO RIVER BRIDGE

CHAPTER II

BACKGROUND AND REVIEW OF LITERATURE

2.1 General

The dynamic analysis of a continuous composite bridge or a skew waffle slab bridge commences with the determination of the natural frequencies. The lowest natural frequency of an average deck slab may vary between 2 Hz for long spans to 17 Hz for short spans. On the other hand, the frequency of vibration of a vehicle on its tires and on its combined tire and suspension spring system usually fall in the range of 2-3.5 Hz. The primary purpose of frequency analysis is, therefore, to estimate the frequency range and to avoid the state of resonance under either wind, earthquake, or live load conditions. The literature contains many analyses of specific boundary value problems, in small-deflection thin plate theory, for which transverse vibrations have been investigated.

This chapter presents the background for the present investigation which is divided mainly into three distinct parts. The first part is concerned with the free vibration of rectangular, single and continuous orthotropic plates; the second part with the free vibration of skew orthotropic plates; and, the third is the study of fatigue, and the elimination of undesirable transverse cracks around the intermediate support(s) in continuous composite bridges.

2.2 Free Vibration of Rectangular Orthotropic Plate

The problem of bridge vibration has been of interest ever since the 1847 Chester Rail Bridge collapse in Britain (73). Both vehicles and bridges have changed considerably since that time, and the parameters

affecting vibrations have changed accordingly. Furthermore, the first known observation of nodal patterns on plates was reported by Chladni (8) in 1787 for completely free square plates; this work inspired much subsequent experimental work. However, in 1909 Ritz (54) extended the Rayleigh principle for obtaining upper bounds on vibration frequencies of a completely free plate problem, demonstrating his now-famous direct method of solution.

From the point of the contemporary bridge engineer, the object of an investigation pertaining to bridge vibration is to arrive at the dynamic load allowance (DLA) to be used in the design of highway bridges; this will ascertain the strength of a bridge so that it will not fail as a result of strong wind, severe earthquakes, or the movement of heavy vehicles across it, and also to assure the psychological comfort of people crossing the bridge. The DLA, which represents the amount by which the static live loads should be increased to simulate the dynamic effects of vehicles (53), is related to the fundamental natural frequency of the bridge superstructure. This frequency must be determined at the preliminary design stage in order to assess the dynamic load allowance.

For an easy and comprehensive theoretical analysis, certain simplifying assumptions were made in 1934 by Inglis (34) and Mise (49), in which the bridge is assumed to behave like a beam. But how far the results from such an analysis correspond with the actual behavior is of the utmost importance. The fact is that these assumptions are applicable only for relatively narrow bridges with long and heavy girders as are usual in railway plate girder bridge practice. However, for the calculation of response under earthquake forces or moving loads, a complete and accurate

knowledge of the free vibration characteristics, including both the modal shapes and the natural frequencies, is essential.

The most common method of vibration analysis of bridges or stiffened plates is to replace the structure by a structurally equivalent orthotropic plate. Fundamental to the use of the orthotropic plate technique is the determination of reliable estimates for the orthotropic elastic constants, as shown by Kennedy and Grace (21, 36, 37).

The differential equation for the free vibration of a thin orthotropic plate of constant thickness was established in 1910 by Voigt (71). Significant progress in solving the vibration problem in an orthotropic plate has been made since the early 1950's because of the availability of high-speed computers and suitable measuring equipment. Since that time the problem has been treated in the literature rather extensively.

In 1922 and 1937 Timeshenko published his first two books (63, 64) on the vibration problems in civil engineering and on the forced vibration of bridges. In 1954, Warburton (72) developed an approximate technique for studying the vibration of rectangular plates with any combination of boundary conditions using Rayleigh's method. Warburton obtained his assumed deflected shape by forming the product of the characteristic functions of two beams, each of which has the boundary condition found on one pair of opposite edges of the plate; this method was used also by Mahalingam (48) to study stiffened plates. The frequencies obtained by Mahalingam were compared with those obtained by Kirk (42) in 1960. For shallow stiffeners, Kirk's method is more accurate and for deeper stiffeners, Mahalingam's technique is better. Kirk's frequency results compared favorably with those given by Thorkildsen and Hoffman (61).

Among other methods, Kanazawa and Kawai (35) have analyzed the vibration problem of a rectangular plate with closely spaced stiffeners, for various combinations of clamped and simply-supported boundary conditions; the procedure used is similar to the one used by Timoshenko (62) for the bending of a clamped plate. Hoffman (29) used an experimental approach to determine the elastic compliances of a plate with closely spaced stiffeners. He suggested that the values so obtained can be used for analysis, thus combining experiment with theory. Later in 1959, Huffington and Hoffman (33) solved the differential equation of vibration of an orthotropic rectangular plate with two opposite edges simply supported and the other two having any arbitrary boundary conditions. Frequency equations were given for all combinations of boundary conditions. Furthermore, Thorkildsen and Hoppman (61) modified the classical theory to take into consideration the effect of rotatory inertia forces. By the end of 1959, Hearman (27) had used an approximate procedure first given by Warburton (72) to obtain approximate values for the frequencies of orthotropic plates with various combinations of simply supported and clamped boundary conditions.

Narouka and Yonezawa (50) utilized the theory of orthotropic plate for the analysis of the free vibration of bridge decks made up of interconnected beam systems. Similar studies were reported on a simple I-beam bridge by Yamada and Veletsos (74).

Sundara and Tagadish (60) used the theory of orthotropic plate for the vibration analysis of a rectangular plate with various combinations of simply supported and clamped boundary conditions. They employed the characteristic functions generated by the vibrating beam problem. Further,

a Fourier Series expansion in terms of these functions was used to yield an infinite set of homogeneous equations.

A sine series solution, previously used for the study of the flexural vibration of rectangular isotropic plates by Dill and Pister (15) was modified and extended by Dickinson (13) to apply to the free vibration of orthotropic plates. In his paper, three particular plates with different conditions were given along with two numerical examples.

In 1968, Laura and Smith (43) introduced a solution for the vibration of a clamped and simply supported plate stiffened in two perpendicular directions. The solution satisfied the boundary conditions, but not the governing differential equation of the system. Their assumed solution, in the form of a polynomial with n terms, led to a set of n homogeneous algebraic equations from which the plate frequencies were obtained.

Ng and Kilkarni (51) studied the transverse free vibration of beam-slab type highway bridges. A modified approach based on the orthotropic plate theory for computing the natural frequencies was presented through a set of empirical relations between the plate parameters; their results were in good agreement with those from other methods of solution. Later, in 1973, Leissa (45) presented comprehensive and accurate analytical results for the free vibration of rectangular plate for 21 cases which involved different combinations of support conditions. However, the solution for these 21 cases was limited to isotropic plates.

In 1985, Grace and Kennedy (22) investigated the dynamic response of orthotropic plate structures having fixed-simply supported and free-free boundary conditions, which had not been considered before due to perhaps the mathematical difficulty in satisfying such boundary conditions. The

orthotropic plate theory was used. It is interesting to note that the dynamic response of the aforementioned orthotropic plate was shown to be related to that of a continuous orthotropic bridge with two equal spans.

2.3 Free Vibration of Continuous Rectangular Orthotropic Plates

With the continuing trend towards lighter and more flexible continuous composite bridges, potential problems of dynamic vibration are becoming increasingly prevalent. In addition, with the increasing use of continuous bridges, and in the case of prestressed composite structures, there is considerable evidence that the inherent damping of modern bridges is less than that of older ones which were generally sufficiently stiff and massive to avoid vibration and resonance dynamic problems.

Rectangular orthotropic plates free at the edges and continuous over rigid supports perpendicular to the edges have received less attention in the literature. On the other hand, continuous rectangular isotropic plates simply supported at two opposite edges, were treated by Veletsos and Newmark (69) in 1956 using Holzer's method for torsional vibration of shafts.

In 1950, Ayre, Ford and Jacobsen (1) solved the free and transient vibration problems of a symmetrical, continuous, simply supported two-span beam. In 1979, Elishakoff and Sternberg (16) solved the eigenfrequency problem of continuous plates with arbitrary number of equal spans. The technique consisted in solving two auxiliary problems of the Voigt-Levy type in conjunction with the postulated eigenfrequency/wave-number relationship. However, this approach was applicable to the isotropic plate type only. More recently, in 1984, Grace and Kennedy (23) studied the free

vibration response of continuous composite bridges using the orthotropic plate theory. The obtained experimental and theoretical results were in good agreement. The frequencies were also compared to the results obtained by using a finite element computer program such as SAP IV.

2.4 Free Vibration of Skew Orthotropic Plates

Quite often skewed plates or slabs are used in modern structures such as parts of aeroplane-swept wings, building floor systems and missiles. Recently, the author was involved in the promotion of using waffle slabs (orthotropic plates) as process floors in computer buildings in the United States and France, as a result of the advantages mentioned in Chapter 1.

Exact solution of the differential equation of a vibrating orthotropic plate are known for the case of a rectangular plate with different combinations of different supporting conditions. On the other hand, few works have been published outlining theoretical solutions to the governing free vibration differential equation of skew orthotropic plates. However, a method for predicting the natural frequencies of skew orthotropic plates using the classical approach is not available in the literature. In 1951, Barton (3) used the Ritz method (54) to solve the vibration problem of skewed cantilever plates. The aspect ratio was equal to one and the skew angle took values of 15°, 30° and 45°; the amount of computation depended upon the type of functions used to represent the plate deflection; these functions were combinations of the characteristic functions defining the normal modes of vibration of a beam with one end fixed and other end free, and for a beam with both ends free. It should be mentioned that the inadequacy of the analytical methods at that time led to extensive use of

numerical methods such as finite element and finite difference methods for the analysis of the free vibration of skewed plates.

Thirty years later, Campbell and Siu (7) introduced the equivalent rectangular slab concept. They showed that the natural frequencies of a skew slab could be related to those of the corresponding rectangular slab. Although the results were in good agreement with the results obtained by using the finite element computer program SAP IV, it was only applicable to isotropic skewed bridges which rarely exist in practice. Recently El-Sebakhy, et. al. (19) compared results using the author's theory of the free vibration of skewed orthotropic plates to those from tests on a 45° skewed waffle slab bridge model. Good correspondence was found.

2.5 Fatigue of a Continuous Composite Bridges

A fairly extensive body of laboratory data is available on the fatigue life of composite bridge members. Daniels and Fisher (12) performed tests on four 2-span, full-size continuous composite beams under static and fatigue loadings. In their report, they concluded that: 1) shear connectors are required in the negative moment regions, and 2) an increased amount of longitudinal reinforcement is also required in the negative moment regions, beyond what AASHTO Specifications require, to improve interaction and control cracking of the concrete slab. However, at the end of their report, and because of the divergence in views between this report and other studies, it was concluded that additional study should be done to investigate the fatigue behavior of continuous composite beams. King, et al. (41) obtained helpful information concerning fatigue failure of connectors and effect of connector failure on the performance of a

composite beam by performing several fatigue tests on composite beams containing 1/2-inch diameter stud connectors. This study showed that the fatigue failure of connectors began at the connectors near the span-ends. This fatigue failure was detected by using electric strain gages mounted near connectors on the bottom of the top flange. Toprac (65) tested seven steel-concrete composite beams; he concluded that the fatigue life of the beams with 3/4-inch studs was shorter than that of the beams with 1/2-inch diameter studs used by King, et al. (41); it was reported that the differences were of the order of 3 ksi in the stress range.

In 1972, Maeda, et al. (47) carried out flat plate fatigue tests by using a cyclic extension applied to a plate in order to answer a question in connection with fatigue resistance of the tension flange in the regions of a bridge near an interior support and subjected to repeated negative moments. Maeda concluded that "fatigue strength of plate with a stud shear connector was influenced mainly by the stress concentration caused by a geometrical discontinuity at the root of the stud."

To explore the subject of the fatigue life of highway bridges, to answer the question of how to apply the results from laboratory research to practical design problems, and to ascertain the need for fatigue consideration in the design of highway composite bridges, the American Association of State Highway Officials undertook tests of eighteen composite (steel and concrete) bridges under repeated overstress. These tests were reported by Fisher and Viest (20). This information afforded a rare opportunity to compare the analysis and the results from the prototypes with the laboratory experiments. Fisher's comparison showed that the results of the bridge tests were in excellent agreement with the

results from the simple laboratory fatigue tests. This comparison cleared any doubts on the laboratory fatigue tests and encouraged other researchers to conduct more fatigue tests on models, enabling engineers to reasonably predict the fatigue life and stress range of composite bridges.

Furthermore, fatigue cracking can be a serious problem in a bridge when subjected to several thousands of resonance cycles over its life. It is necessary to assess resonance fatigue as part of the design process. Salane, et al. (55) conducted a steady-state resonance fatigue test and a subsequent ultimate load test on a three-span continuous composite highway bridge in Butler County, Missouri. The fatigue life of the prototype was estimated by Fisher's formula given by

$$\log N = 8.9754 - 2.8768 \log S_r$$

where N is the number of cycles to failure, and S_r is the stress range in ksi. The current AASHTO (58) and OHBDC (53) specifications are based on tests which indicated that only the stress range was the main dominant and important parameter in fatigue design. However, the results reported by Salane indicated that the maximum stress (in the algebraic sense) and toughness were also important and significant variables. Furthermore, they pointed out that design of composite action in the negative moment regions should be given serious consideration to achieve considerable economy in the steel section at the intermediate supports. This last recommendation was important since the tested bridge was designed as composite in the positive moment regions (mid-spans) and non-composite, without shear connectors, at the negative moment regions (intermediate-supports). It was

observed that considerable changes in the natural frequency and damping ratio occurred due to the cumulative fatigue cracks in the bridge elements. The test arrangement adopted by Salane, et al. was very helpful in the experimental work reported herein.

Recently, Grace and Kennedy (23) performed similar tests, but with special treatment for the negative moment region in a continuous composite bridge model. Their study showed that fatigue cracks in the steel beam substantially reduced the natural frequencies while fatigue-induced hair cracks in the secondary members (diaphragms) have no significant effect on the dynamic characteristics nor on the ultimate load-carrying capacity of the bridge.

CHAPTER III

THEORETICAL ANALYSIS AND MATHEMATICAL FORMULATION

3.1 INTRODUCTION

Quite often the engineer is required to design skew or rectangular plate structures of relatively wide planforms, such as those in buildings, marine structures and bridges. To accurately predict the structural response, it becomes necessary to study, among other aspects, the dynamic behavior of the structure. Such a study will lead to the all-important lower natural frequencies which are then compared to the natural frequencies of the applied transient loads in order to avoid the state of resonance; as a consequence the derived frequencies will be valuable in establishing the dynamic load allowance for orthotropic bridges.

In addition to the usual assumptions made in the small deflection theory of thin orthotropic plates, the analysis is based on the following assumptions:

1. The dynamic effects of vertical motion only are considered. Only the lateral inertia forces are taken into account, while the effects of rotatory inertia and shear forces are sensibly small and therefore ignored. The displacement functions are separable in time and space.
2. The rigidities of both the longitudinal and transverse members are uniformly distributed throughout the bridge deck.
3. The actual structure of the bridge is represented by an idealized substitute orthotropic plate of uniform thickness reflecting the characteristic properties of the actual system.

4. The neutral plane in each of the two orthogonal directions coincides with the center of gravity of the total section in the corresponding direction.
5. The area of the deck slab is magnified by the factor $1/(1-\nu^2)$ to allow for the influence of Poisson's ratio (ν).

Past experiences (21, 26, 36, 37) have shown that the above assumptions are valid in practice.

The following mathematical approach attempts to present comprehensive and accurate analytical treatment for the free vibration of two-equal span continuous rectangular composite bridges and the single-span skew orthotropic plates.

3.2 GOVERNING DIFFERENTIAL EQUATION FOR RECTANGULAR ORTHOTROPIC PLATE

A general relation between the forces and displacement resulting from free vibration, considering bending and twisting forces about each of the in-plane axes and the normal shearing forces, is derived as follows (Fig. 3.1):

Summing forces in the z direction gives

$$Q_{x,x} + Q_{y,y} - \bar{m}h_1 w_{,tt} = 0 \qquad (3.2.1)$$

in which

$\bar{m}$ = mass per unit volume of the plate,

h_1 = thickness of an equivalent orthotropic plate

$w(x,y,t)$ = transverse displacement of the plate, a function of time as well as position.

Summing moments about the x and y axes will yield, respectively:

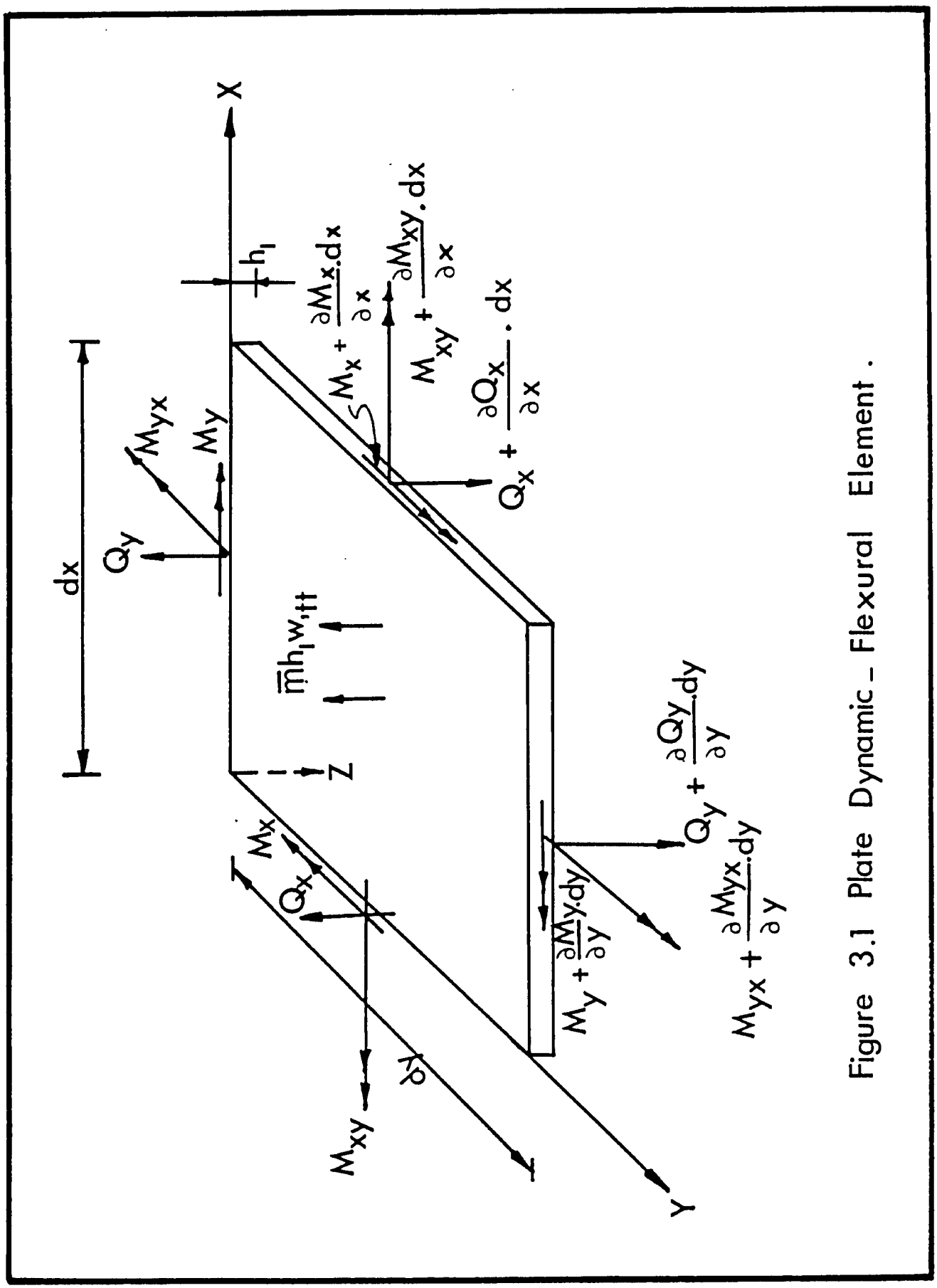

Figure 3.1 Plate Dynamic_ Flexural Element .

$$Q_y + M_{xy,x} - M_{y,y} = 0 \qquad (3.2.2)$$

and

$$Q_x - M_{yx,y} - M_{x,x} = 0 \qquad (3.2.3)$$

Combining the above three equations gives, in the absence of the body couples, the equation of the equilibrium of the plate as

$$M_{x,xx} - 2\,M_{xy,xy} + M_{y,yy} = \bar{m}h_1 w_{,tt} \qquad (3.2.4)$$

The relation between moments and derivatives of the displacement function, w(x,y,t), are obtained from the theory of pure bending of plates in the form (62):

$$\begin{aligned} M_x &= -(D_x\, w_{,xx} + D_1\, w_{,yy}) \\ M_y &= -(D_y\, w_{,yy} + D_2\, w_{,xx}) \\ M_{xy} &= D_{xy}\, w_{,xy} \end{aligned} \qquad (3.2.5)$$

where

D_x, D_y = flexural rigidities of the plate per unit width in x and y directions respectively, (21,36,37).

D_1, D_2 = coupling rigidities - contribution of bending to torsional rigidities of the bridge arising from Poisson's ratio effect (21,36,37).

D_{xy}, D_{yx} = longitudinal and transverse torsional rigidities of the plate (21,36,37).

Substituting equations (3.2.5) into equation (3.2.4), the governing equation for the free vibration of a rectangular orthotropic plate becomes

$$D_x w_{,xxxx} + 2Hw_{,xxyy} + D_y w_{,yyyy} = -\bar{m}h_1 w_{,tt} \qquad (3.2.6)$$

where

H = Effective torsional rigidity of the orthotropic plate.

3.2.1 Boundary Conditions

The continuous bridge under consideration has two end roller supports, one intermediate hinged support and the two sides are free or elastically supported as shown in Figure 3.2. The deflections and the moments at the end supports (x=0 or x=$2\bar{a}$) must be zero, which yield the following two equations:

(i) $w=0$

@

$x=0$ or $x=2\bar{a}$ $\qquad$ for $\frac{-b}{2} \leqslant y \leqslant \frac{-b}{2}$ $\qquad$ (3.2.7)

(ii) $M_x=0$

@

$x=0$ or $x=2\bar{a}$; or

$$M_x = D_x w_{,xx} + D_1 w_{,yy} = 0 \qquad \text{for } \frac{-b}{2} \leqslant y \leqslant \frac{-b}{2} \qquad (3.2.8)$$

(iii) Combining the forces replaced by the twisting couples with the shear force along the edge and equating the same to the pressure transmitted from the plate to the edge beam, at $y = \pm$, the following equation is obtained:

$$- V_y = - (Q_y - M_{xy,x}) = EIw_{,xxxx}$$

or,

$$(D_{xy} + D_{yx} + D_2)\, w_{,xxy} + D_y w_{,yyy} = EIw_{,xxxx} \qquad (3.2.9)$$

where EI is the flexural rigidity of the edge beam.

(iv) To obtain the second boundary condition at $y = \pm \frac{-b}{2}$, the

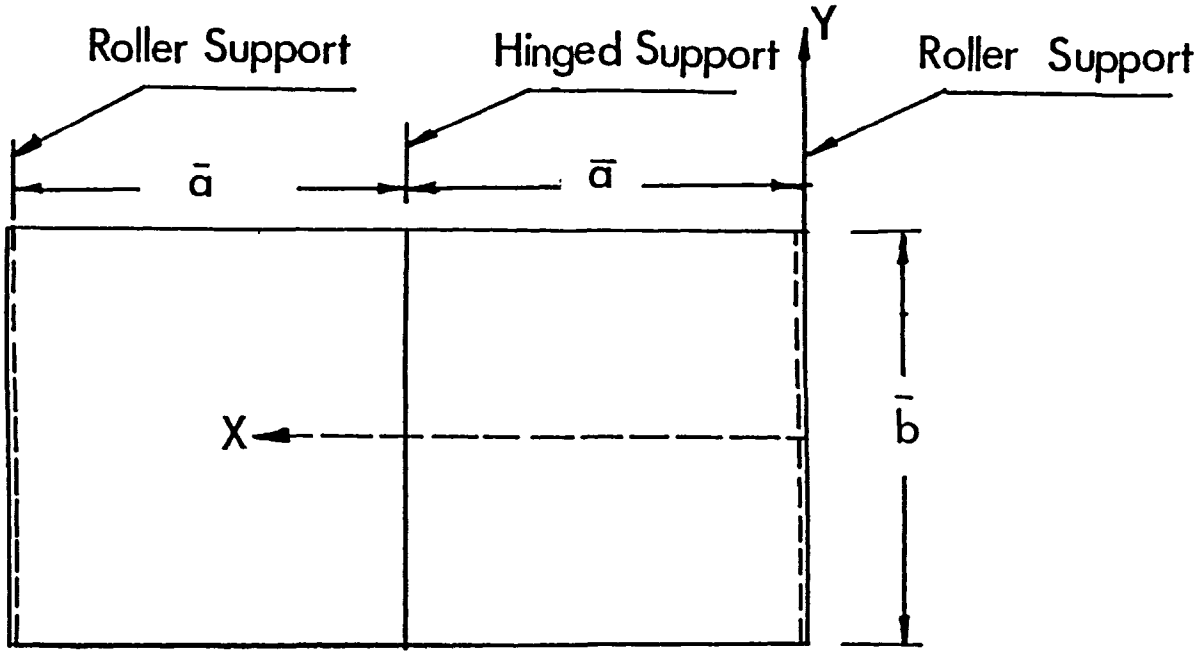

Figure 3.2 Plan View of Two_Span Continuos Composite Bridge Models I & II .

twisting moment of the beam is related to the transverse bending moment in the plate yielding the following equation:

$$D_y w_{,yy} + D_2 w_{,xx} = GJ\ w_{,xxy} \tag{3.2.10}$$

where GJ is the torsional rigidity of the edge beam.

The boundary conditions for the continuous composite bridge having two free edges are obtained by putting (EI) and (GJ) of the edge beam equal to zero in equations (3.2.9) and (3.2.10).

(v) At the pier line (intermediate) support ($x=\bar{a}$): the deflection must be equal to zero,

$$w = 0 \tag{3.2.11}$$

and, either

$$M_x = D_x w_{,xx} + D_1 w_{,yy} = 0 \tag{3.2.12}$$

for anti-symmetrical modes about the intermediate supports, Figures 3.3 (a,b) and 3.4 (a,b); or,

$$w_{,x}=0 \tag{3.2.13}$$

for symmetrical modes about the intermediate support, Figures 3.3 (c,d) and 3.4 (c,d).

Due to the geometric symmetry of the bridge, the vibration modes will be either symmetric or anti-symmetric about the intermediate support; and each of these modes will also be either symmetric or anti-symmetric about the longitudinal x-axis, Figures 3.3 and 3.4.

3.2.2 Antisymmetric Modes About the Intermediate Support

Since the differential governing equation for the free vibration of

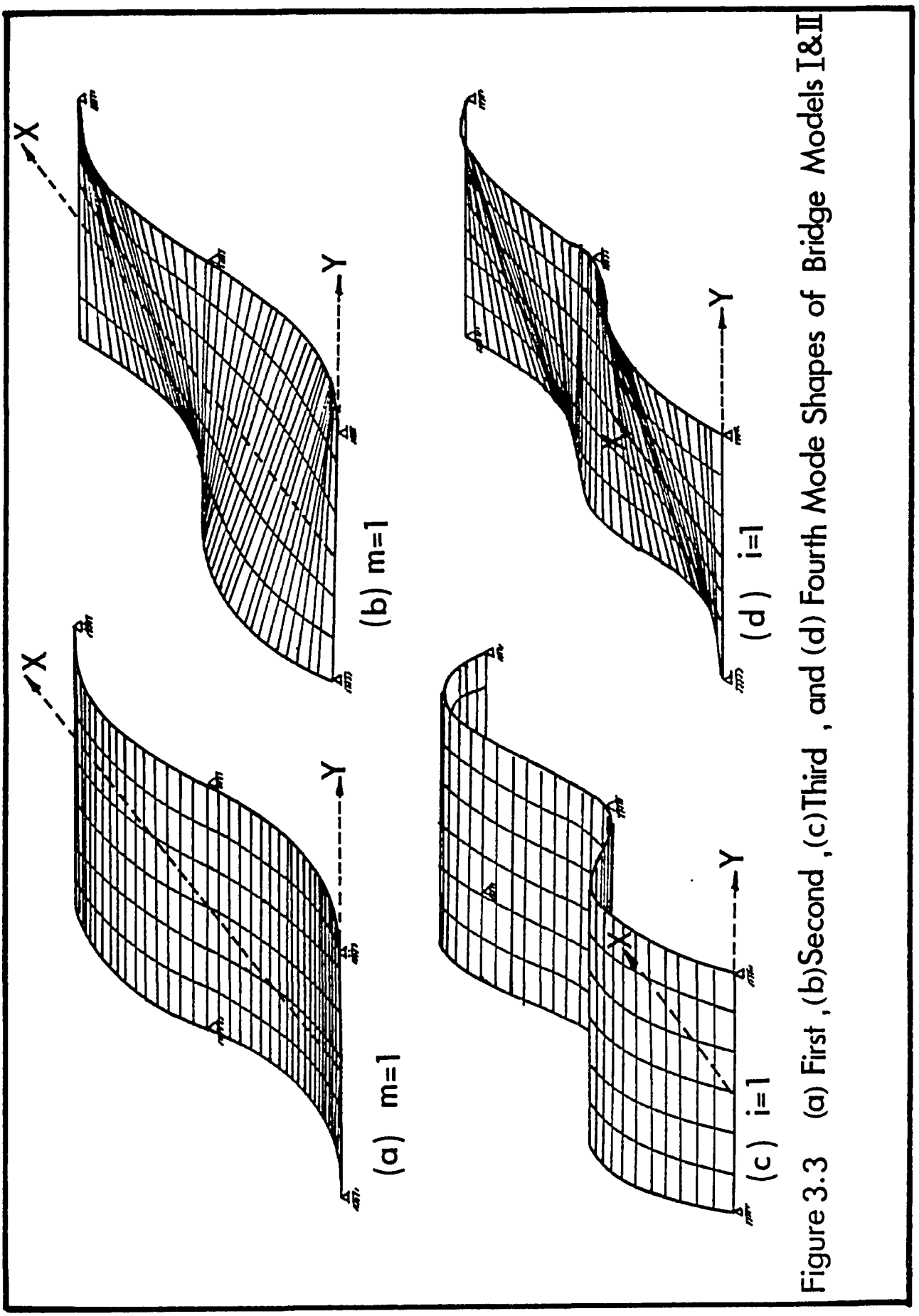

Figure 3.3 (a) First ,(b)Second ,(c)Third , and (d) Fourth Mode Shapes of Bridge Models I&II

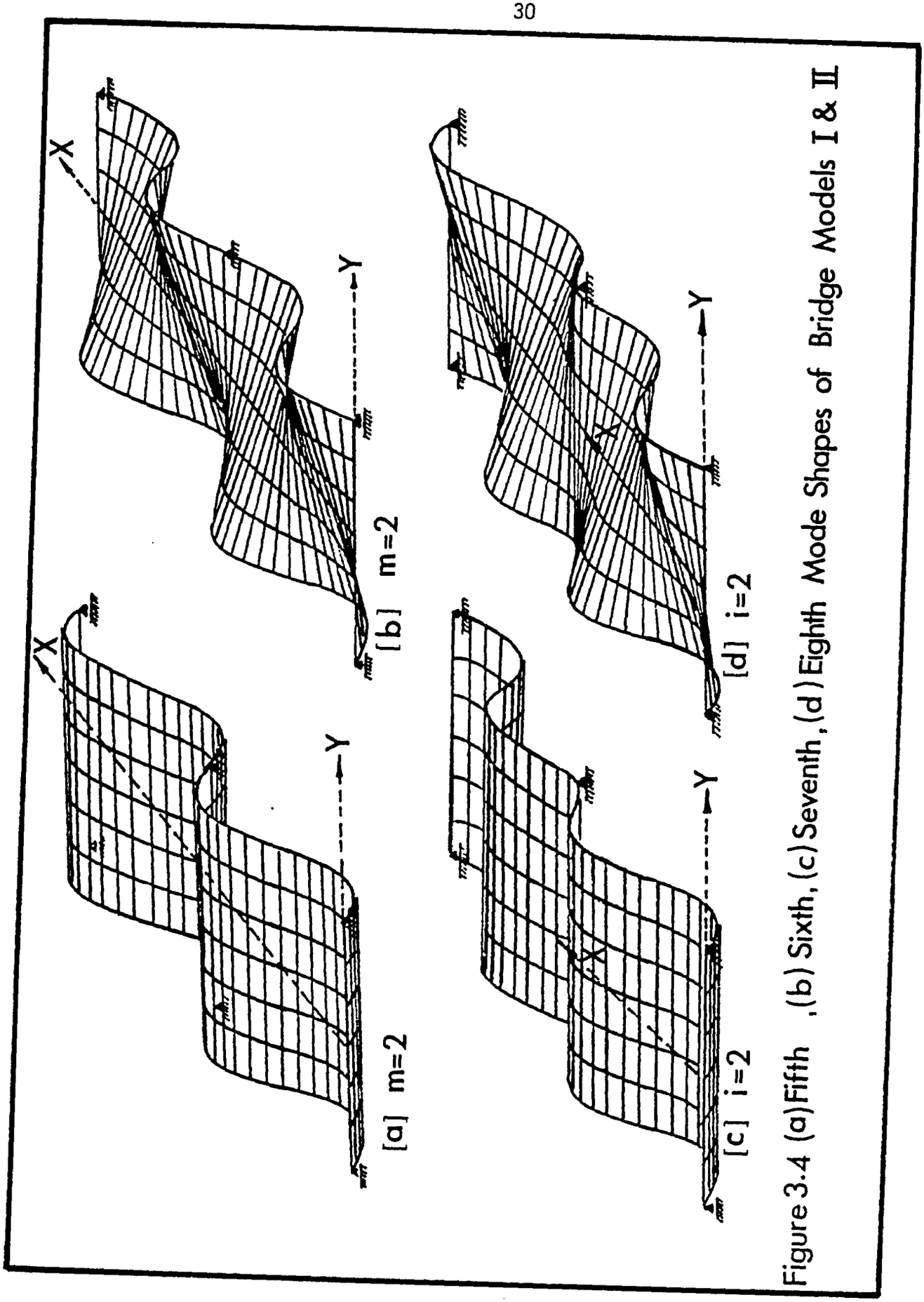

Figure 3.4 (a) Fifth ,(b) Sixth, (c) Seventh, (d) Eighth Mode Shapes of Bridge Models I & II

rectangular orthotropic plates is homogeneous, a solution for equation 3.2.6 can be assumed in the form

$$w(x,y,t) = \Sigma_m \Sigma_n W_{mn}(x,y)\,\theta(t) \qquad (3.2.14)$$

in which

$\theta(t) = \sin \omega_{mn} t$,

t = time,

ω_{mn} = the circular frequency, rad/sec.,

$W_{mn}(x,y)$ = the shape function.

Assuming $W_{mn}(x,y)$ in the form

$$W_{mn}(x,y) = C\, e^{\lambda_{mn} y} \left[\sin \frac{m x}{\bar{a}}\right] \qquad (3.2.15)$$

will satisfy the boundary conditions at $x=0$ and $x=\bar{a}$. Substituting for $\theta(t)$ in terms of ω, and for $W_{mn}(x,y)$ in Eq. 3.2.6 will yield a quadratic equation in λ^2_{mn} with roots

$$\lambda_{mn} = \pm \left[\frac{H \pm \sqrt{H^2 - D_x D_y + \bar{m} h_1 \omega^2_{mn} D_y \dfrac{\bar{a}^4}{m^4 \pi^4}}}{D_y} \right]^{1/2} \frac{m\pi}{\bar{a}} \qquad (3.2.16)$$

in which m is an integer which defines the mode shape.

3.2.3 Symmetric Modes About the Intermediate Support

To satisfy the boundary conditions at $x=0$ and $x=\bar{a}$, the shape function $w_{m_i n}(x,y)$ is assumed as

$$W_{m_i n}(x,y) = C\, e^{\lambda_{m_i n} y} \left[\sin \frac{m_i \pi x}{\bar{a}} - \frac{\sin m_i \pi}{\sinh m_i \pi} \sinh \frac{m_i \pi x}{\bar{a}} \right]$$

for $0 \leqslant x \leqslant \bar{a}$, (3.2.17)

where

$m_i = i + 1/4$, and

$i = 1, 2, 3, \ldots$

The satisfaction of Eq. 3.2.6 is made possible due to the fact that the term in the square brackets in Eq. 3.2.17 is almost equal to the term

$$\left[\sin \frac{m_i \pi x}{\bar{a}} + \frac{\sin m_i \pi}{\sinh m_i \pi} \sinh \frac{m_i \pi x}{\bar{a}} \right]$$

very close to the boundaries x=0 and $x=\bar{a}$. It should be noted that the expression for $m_i \pi$ is quite accurate even for small values of i; e.g., when i = 1, 2, and 3, $m_i \pi = 3.92699$, $m_2 \pi = 7.06858$ and $m_3 \pi = 10.21018$, respectively; the corresponding values, based on the frequency equation $\tan m_i \pi = \tanh m_i \pi$, (13), are 3.9266, 7.0686 and 10.2102. Thus, using Eq. 3.2.17 in Eq. 3.2.6 leads to the following roots for $\lambda_{m_i n}$:

$$\lambda_{m_i n} = \pm \left[\frac{H \pm \sqrt{H^2 - D_x D_y + \Omega_{m_i n}}}{D_y} \right]^{1/2} \frac{m_i \pi}{\bar{a}} \qquad (3.2.18)$$

in which

n = 1, 2, 3, ... and equal to the number of roots of the transcendental frequency equation for each m_i , and,

$\Omega_{m_i n} = \bar{m} h_1 \omega^2_{m_i n} D_y (\bar{a}^4 / m_i^4 \pi^4)$.

Inspection of equation 3.2.16 or 3.2.18 reveals that there are three orthotropic plate categories as shown in Figure 3.5. The term $Ce^{\lambda_{m_i n} y}$ in Equation 3.2.17 can be completely determined for each category by satisfying the boundary conditions at $y=\pm b/2$.

3.2.4 Category I

This describes a torsionally soft and flexurally stiff plate where $H^2 < D_x D_y$. It includes the more common type of open rib plate, waffle slab, T-beam slabs, as well as concrete slab-on-steel beams construction. As shown in Figure 3.5, this category is subdivided into:

Subcategory I(a) in which $(H^2 - D_x D_y) < \Omega_{m_i n}$. This leads to two alternatives, namely:

$$H > \sqrt{H^2 - D_x D_y + \Omega_{m_i n}} \quad \text{or,} \quad H < \sqrt{H^2 - D_x D_y + \Omega_{m_i n}}$$

For the former, the only possible modes are those that are symmetrical about the x-axis. Thus, from the transcendental frequency equation, obtained by satisfying the boundary conditions along $y = \pm \bar{b}/2$ and equating the determinant to zero, it can be shown that the term $Ce^{\lambda_{m_i n} y}$ in equation 3.2.17 becomes

$$Ce^{\lambda_{m_i n} y} = \left[\frac{\cosh K_{1m_i n} \frac{y}{\bar{a}}}{\cosh \frac{R}{2} K_{1m_i n}} - \frac{(K_{1m_i n}^2 D_y - m_i^2 \pi^2 D_2) \cosh K_{2m_i n} \frac{y}{\bar{a}}}{(K_{2m_i n}^2 D_y - m_i^2 \pi^2 D_2) \cosh \frac{R}{2} K_{2m_i n}} \right] \tag{3.2.19}$$

in which $R = \bar{b}/\bar{a}$; and the eigen values

$$K_{1m_i n} = \pm \left[\frac{H + \sqrt{H^2 - D_x D_y + \Omega_{m_i n}}}{D_y} \right]^{1/2} m_i \pi \tag{3.2.20}$$

$$K_{2m_i n} = \pm \left[\frac{H - \sqrt{H_y^2 - D_x D_y + \Omega_{m_i n}}}{D_y} \right]^{1/2} m_i \pi \tag{3.2.21}$$

; these eigen values are not independent but are related by

$$K_{1m_i n}^2 + K_{2m_i n}^2 = 2 m_i^2 \pi^2 \frac{H}{D_y} \tag{3.2.22}$$

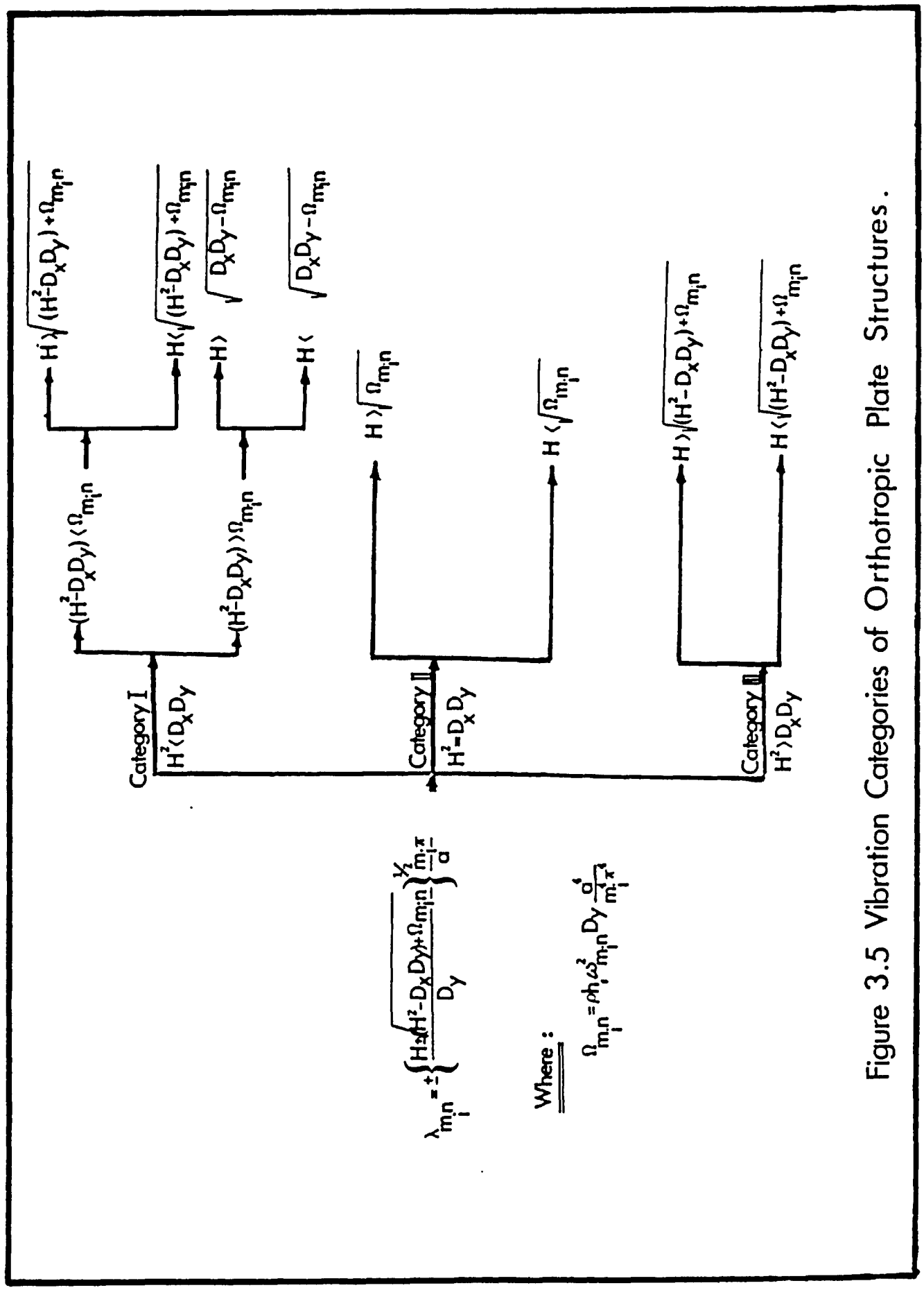

Figure 3.5 Vibration Categories of Orthotropic Plate Structures.

As mentioned earlier, the anti-symmetric modes do not exist since the corresponding frequency equation has no real roots.

For the case $H < \sqrt{H^2 - D_x D_y + \Omega_{m_i n}}$, it can be shown, by following the same procedure, that for symmetrical modes

$$Ce^{\lambda_{m_i n} y} = \left[\frac{\cosh K_{1m_i n} \frac{y}{\bar{a}}}{\cosh \frac{R}{2} K_{1m_i n}} + \frac{(K^2_{1m_i n} D_y - m_i^2 \pi^2 D_2) \cos K_{2m_i n} \frac{y}{\bar{a}}}{(K^2_{2m_i n} D_y + m_i^2 \pi^2 D_2) \cos \frac{R}{2} K_{2m_i n}} \right] \quad (3.2.23)$$

and, for anti-symmetrical modes

$$Ce^{\lambda_{m_i n} y} = \left[\frac{\sinh K_{1m_i n} \frac{y}{\bar{a}}}{\sinh \frac{R}{2} K_{1m_i n}} + \frac{(K^2_{1m_i n} D_y - m_i^2 \pi^2 D_2) \sin K_{2m_i n} \frac{y}{\bar{a}}}{(K^2_{2m_i n} D_y + m_i^2 \pi^2 D_2) \sin \frac{R}{2} K_{2m_i n}} \right] \quad (3.2.24)$$

in which

$$K_{1m_i n} = \pm \left[\frac{\sqrt{(H^2 - D_x D_y) + \Omega_{m_i n}} + H}{D_y} \right]^{1/2} m_i \pi \quad (3.2.25)$$

$$K_{2m_i n} = \pm \left[\frac{\sqrt{(H^2 - D_x D_y) + \Omega_{m_i n}} - H}{D_y} \right]^{1/2} m_i \pi \quad (3.2.26)$$

; these eigen values are related by

$$K^2_{1m_i n} - K^2_{2m_i n} = 2 m_i^2 \pi^2 \frac{H}{D_y} \quad (3.2.27)$$

Subcategory I(b) - In which $(H^2 - D_x D_y) > \Omega_{m_i n}$; for this case Eq. 3.2.18 becomes

$$\lambda_{m_i n} = \pm (K_{1m_i n} \pm K_{2m_i n}) \frac{m_i \pi}{\bar{a}} \quad (3.2.28)$$

$$\text{in which } K_{1m_i n} = \left[\frac{H + \sqrt{R_{1m_i n}}}{2D_y} \right]^{1/2} \tag{3.2.29}$$

$$K_{2m_i n} = \left[\frac{H - \sqrt{R_{1m_i n}}}{2D_y} \right]^{1/2} \tag{3.2.30}$$

$$\text{and } R_{1m_i n} = (D_x D_y - \Omega_{m_i n}) \tag{3.2.31}$$

Thus, when $H > \sqrt{R_{1m_i n}}$ only symmetrical modes about the x-axis are possible, with

$$Ce^{\lambda_{m_i n} y} = \frac{1}{R_{2m_i n}} \cosh(\alpha_{m_i} K_{1m_i n} y) \cosh(\alpha_{m_i} K_{2m_i n} y)$$

$$+ \frac{1}{R_{3m_i n}} \sinh(\alpha_{m_i} K_{1m_i n} y) \sinh(\alpha_{m_i} K_{2m_i n} y) \tag{3.2.32}$$

in which $\alpha_{m_i} = m_i \pi / \bar{a}$ and

$$R_{2m_i n} = (H - D_2) \cosh(\alpha_{m_i} K_{1m_i n} \frac{\bar{b}}{2}) \cosh(\alpha_{m_i} K_{2m_i n} \frac{\bar{b}}{2})$$

$$+ (H^2 - R_{1m_i n})^{1/2} \sinh(\alpha_{m_i} K_{1m_i n} \frac{\bar{b}}{2}) \sinh(\alpha_{m_i} K_{2m_i n} \frac{\bar{b}}{2}) \tag{3.2.33}$$

$$R_{3m_i n} = (D_2 - H) \sinh(\alpha_{m_i} K_{1m_i n} \frac{\bar{b}}{2}) \sinh(\alpha_{m_i} K_{2m_i n} \frac{\bar{b}}{2})$$

$$- (H^2 - R_{1m_i n})^{1/2} \cosh(\alpha_{m_i} K_{1m_i n} \frac{\bar{b}}{2}) \cosh(\alpha_{m_i} K_{2m_i n} \frac{\bar{b}}{2}) \tag{3.2.34}$$

When $H < \sqrt{R_{1m_in}}$, it can be shown that for symmetrical modes

$$Ce^{\lambda_{m_in} y} = \frac{1}{R_{4m_in}} \cosh(\alpha_{m_i} K_{1m_in} y) \cosh(\alpha_{m_i} K_{2m_in} y)$$

$$+ \frac{1}{R_{5m_in}} \sinh(\alpha_{m_i} K_{1m_in} y) \sinh(\alpha_{m_i} K_{2m_in} y) \qquad (3.2.35)$$

in which

$$K_{1m_in} = \left[\frac{\sqrt{R_{1m_in}} + H}{2D_y} \right]^{1/2} \qquad (3.2.36)$$

$$K_{2m_in} = \left[\frac{\sqrt{R_{1m_in}} - H}{2D_y} \right]^{1/2} \qquad (3.2.37)$$

$$R_{4m_in} = (D_2 - H) \cosh(\alpha_{m_i} K_{1m\,n} \tfrac{\bar{b}}{2}) \cos(\alpha_{m_i} K_{2m_in} \tfrac{\bar{b}}{2})$$

$$+ (R_{1m_in} - H^2)^{1/2} \sinh(\alpha_{m_i} K_{1m_in} \tfrac{\bar{b}}{2}) \sin(\alpha_{m_i} K_{2m_in} \tfrac{\bar{b}}{2}) \qquad (3.2.38)$$

$$R_{5m_in} = (H - D_2) \sinh(\alpha_{m_i} K_{1m_in} \tfrac{\bar{b}}{2}) \sin(\alpha_{m_i} K_{2m_in} \tfrac{\bar{b}}{2})$$

$$+ (R_{1m_in} - H^2)^{1/2} \cosh(\alpha_{m_i} K_{1m_in} \tfrac{\bar{b}}{2}) \cos(\alpha_{m_i} K_{2m_in} \tfrac{\bar{b}}{2}) \qquad (3.2.39)$$

For anti-symmetrical modes

$$Ce^{\lambda_{m_in} y} = \frac{1}{R_{6m_in}} \sinh(\alpha_{m_i} K_{1m_in} y) \cos(\alpha_{m_i} K_{2m_in} y)$$

$$+ \frac{1}{R_{7m_in}} \cosh(\alpha_{m_i} K_{1m_in} y) \sin(\alpha_{m_i} K_{2m_in} y) \qquad (3.2.40)$$

in which

$$R_{6m_in} = (H - D_2) \sinh (\alpha_{m_i} K_{1m\,n} \tfrac{\bar{b}}{2}) \cos (\alpha_{m_i} K_{2m_in} \tfrac{\bar{b}}{2})$$

$$+ (R_{1m_in} - H^2)^{1/2} \cosh (\alpha_{m_i} K_{1m_in} \tfrac{\bar{b}}{2}) \sin (\alpha_{m_i} K_{2m_in} \tfrac{\bar{b}}{2}) \qquad (3.2.41)$$

$$R_{7m_in} = (H - D_2) \cosh (\alpha_{m_i} K_{1m_in} \tfrac{\bar{b}}{2}) \sin (\alpha_{m_i} K_{2m_in} \tfrac{\bar{b}}{2})$$

$$+ (R_{1m_in} - H^2)^{1/2} \sinh (\alpha_{m_i} K_{1m_in} \tfrac{\bar{b}}{2}) \cos (\alpha_{m_i} K_{2m_in} \tfrac{\bar{b}}{2}) \qquad (3.2.42)$$

3.2.5 Category II

This describes an orthotropic plate structure where $H^2 = D_x D_y$, and would include reinforced or prestressed concrete slabs which may or may not have different amounts of steel in the longitudinal and transverse directions. For this category Eq. 3.2.18 simplifies to

$$\lambda_{m_in} = \pm \left[\frac{H \pm \sqrt{\Omega_{m_in}}}{D_y} \right]^{1/2} m_i \pi \qquad (3.2.43)$$

Thus, when $H > \sqrt{\Omega_{m_in}}$, only symmetric modes about the x-axis exist and the term $Ce^{\lambda_{m_in} y}$ is given by Eq. 3.2.19 with K_{1m_in} and K_{2m_in} defined as

$$K_{1m_in} = \pm \left[\frac{H + \sqrt{\Omega_{m_in}}}{D_y} \right]^{1/2} m_i \pi \qquad (3.2.44)$$

$$K_{2m_in} = \pm \left[\frac{H - \sqrt{\Omega_{m_in}}}{D_y} \right]^{1/2} m_i \pi \qquad (3.2.45)$$

If $H < \sqrt{\Omega_{m_i n}}$, the term $Ce^{\lambda_{m_i n} y}$ for the symmetic and anti-symmetric modes are given by Eqs. 3.2.23 and 3.2.24 respectively, with

$$K_{1m_i n} = \pm\left[\frac{\sqrt{\Omega_{m_i n}} + H}{D_y}\right]^{1/2} m_i \pi \qquad (3.2.46)$$

$$K_{2m_i n} = \pm\left[\frac{\sqrt{\Omega_{m_i n}} - H}{D_y}\right]^{1/2} m_i \pi \qquad (3.2.47)$$

3.2.6 Category III

This category describes torsionally stiff but flexurally weak orthotropic structures in which $H^2 > D_x D_y$; it includes closed rib plates and hollow box girder constructions in which the torsional rigidity is more dominant than the flexural rigidity. The two subcategories are:

When $H > (H^2 - D_x D_y + \Omega_{m_i n})^{1/2}$, the term $Ce^{\lambda_{m_i n} y}$ for a symmetric mode about the x-axis is given by Eq. 3.2.19 with $K_{1m_i n}$ and $K_{2m_i n}$ defined by Eq. 3.2.20. As before, no antisymmetric modes are possible.

When $H < (H^2 - D_x D_y + \Omega_{m_i n})^{1/2}$, then the solutions for the term $Ce^{\lambda_{m_i n} y}$ for symmetric and antisymmetric modes are identical to those given by Eqs. 3.2.23 and 3.2.24, respectively, with $K_{1m_i n}$ and $K_{2m_i n}$ defined by Eqs. 3.2.25 and 3.2.26.

It should be noted that once the term $Ce^{\lambda_{m_i n} y}$ is found, as shown previously, the shape function $W(x,y)$ is determined from Eq. 3.2.17.

By replacing m_i by m in Eqs. 3.2.19 through 3.2.47, one can deduce the shape functions for the anti-symmetric modes about the intermediate support, discussed in Section 3.2.2.

3.3 GOVERNING DIFFERENTIAL EQUATION FOR SKEW ORTHOTROPIC PLATES

The problem associated with skew orthotropic plate structures under dynamic loadings, either from highway traffic, supported machinery, or from any other external sources, has received less attention than that given to rectangular orthotropic plates; it requires special solution dictated by its boundary conditions and dynamic characteristics. This lack of attention could be, perhaps, due to the mathematical difficulties encountered in satisfying the boundary conditions and choosing the proper displacement function. For design purposes, skew orthotropic plates must first satisfy the criteria for static loadings (17,18,38), and then it must be satisfactory for resisting the dynamic condition by knowing its dynamic characteristics; this will enable the designer to avoid resonance, thus enhancing its performance under dynamic loadings.

Many skew slab-type bridges have been built; they have been successfully analyzed as skew orthotropic plate structures; it is desirable to find a solution for the dynamic problem based on the classical orthotropic plate theory also, rather than depend on existing numerical solutions. Therefore, the following mathematical treatment is meant to be a comprehensive solution for the free vibration problem of skew orthotropic plates.

The coordinates of the rectangular (x,y,z) and oblique (u,v,z) systems are related by

$$u = x/\cos\theta$$

$$v = y - x\tan\theta \qquad (3.3.1)$$

where θ = skew angle,

The free vibration governing differential equation for a rectangular plate, Eq. 3.2.6 is transformed into skew coordinates, as explained in Appendix A, yielding

$$D_x w_{,uuuu} + G_1 w_{,uuuv} + G_2 w_{,uuvv} + G_3 w_{,uvvv} + G_4 w_{,vvvv} = -\bar{m}h_1 c^4 w_{,tt} \qquad (3.3.2)$$

where

$$G_1 = -4sD_x$$

$$G_2 = 2(3D_x s^2 + Hc^2)$$

$$G_3 = -4s\,(D_x s^2 + Hc^2)$$

$$G_4 = D_x s^4 + 2Hs^2c^2 + D_y c^4$$

$c = \cos\theta$

$s = \sin\theta$ and

$\bar{m}h_1 c^4 w_{,tt}$ = inertia force due to free vibration

The elastic properties, flexural and torsional rigidities of an orthotropic plate can be found elsewhere in (19,25,39).

3.3.1 Boundary Conditions

A skew orthotropic plate having two opposite ends simply supported and two other sides elastically supported or free is shown in Figure 3.6.

(i) At the simply supported ends $v = \pm b$, the deflection must be zero which yield the same equation as Equation 3.2.7 for $-a \leqslant u \leqslant +a$.

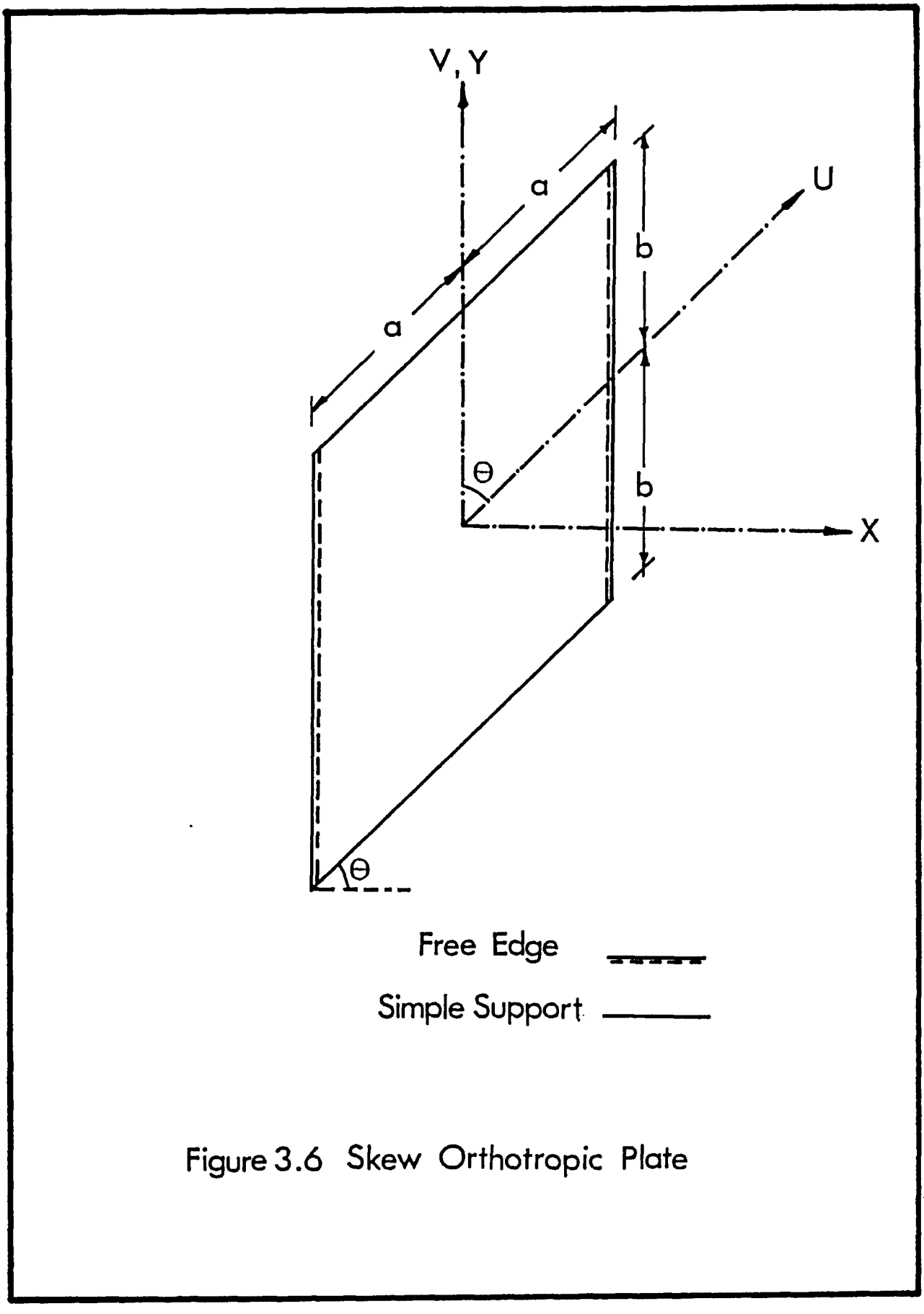

Figure 3.6 Skew Orthotropic Plate

(ii) Also, the moment normal to the support must be zero:

$$M_{n_{@v = \pm b}} = 0, \quad \text{or} \quad M_x s^2 + M_y c^2 + (M_{xy} - M_{yx})sc = 0$$

or

$$X_1 w_{,uv} + X_2 w_{,vv} = 0 \quad \text{at } v = \pm b \qquad \text{for } -a \leqslant u \leqslant a \qquad (3.3.3)$$

where

$$X_1 = s(2D_x s^2/c^2 + 2D_2 + D_{xy} + D_{yx})$$
$$X_2 = -s^2 (D_x s^2/c^2 + 2H) - c^2 D_y$$

(iii) At the elastically supported edge Equations 3.2.9 and 3.2.10 can be transformed into skew coordinates which yields the following two boundary conditions: For equating the transverse shear,

$$X_3 w_{,uuu} + X_4 w_{,uuv} + X_5 w_{,uvv} + X_6 w_{,vvv} = EI w_{,vvvv} \qquad (3.3.4)$$

at $u = +a$ for $-b \leqslant v \leqslant b$

where

$$X_3 = D_x c^3$$
$$X_4 = -3D_x s/c^3$$
$$X_5 = (3D_x s^2/c^2 + D_1 + D_{xy} + D_{yx})/c$$
$$X_6 = -s(D_x s^2 c^2 + D_1 + D_{xy} + D_{yx})/c$$

;for equating the edge plate moment to the twisting moment in the edge beam;

$$X_7 w_{,uu} + X_8 w_{,uv} + X_9 w_{,vv} + GJ w_{,uvv} + X_{10} w_{,vvv} = 0$$

at $u = + a$ for $-b \leqslant v \leqslant b$ (3.3.5)

where

$X_7 = D_x/c$

$X_8 = -2D_x s/c$

$X_9 = (D_x s^2 + D_1 c^2)/c$

$X_{10} = -sGJ$

The above two boundary conditions Eqs. 3.3.4 and 3.3.5 will not be the same at u = -a unless the mode shape function consists either of even or odd terms only.

3.3.2 Mode Shape Functions

The differential equation for the free vibration problem of a skew orthotropic plate is homogeneous and the solution is assumed as:

$$w(u,v,t) = \sum_{n=1}^{\infty} e^{\lambda_i u} (A_n \sin\beta_n v + B_n \cos\beta_n v) \sin\omega t \qquad (3.3.6)$$

where

λ_i = number of the roots resulted from satisfying the governing equation;

n = integer, represents the number of harmonics to be considered for the required accuracy of the resulting frequencies.

$\beta_n = n\pi/b$

λ_i, A_n and B_n are functions of the geometry and the elastic properties of the skew plate.

By substituting Equation 3.3.6 into Equation 3.3.2, then separating and equating the coefficients of $\sin\beta_n v$ and $\cos\beta_n v$, dividing by $\sin\omega t$, yield the following two equations in A_n and B_n.

$$C_1 A_n + C_2 B_n = 0 \qquad (3.3.7)$$

$$-C_2 A_n + C_1 B_n = 0$$

where

$$C_1 = D_x\lambda_i^4 - 2(3D_xs^2 + Hc^2)\lambda_i^2\beta_n^2 + (D_xs^4 + 2Hs^2c^2 + D_yc^4)\beta_n^4 - c^4\bar{m}h_1\omega^2$$

and

$$C_2 = [4sD_x\lambda_i^2 - 4s(D_xs^2 + Hc^2)/\beta_n]\lambda_i\beta_n$$

These two equations have a non-trivial solution; therefore, their determinant must be equal to zero. This determinant yields the following characteristic octic equation in λ_i.

$$C_1^2 + C_2^2 = 0 \tag{3.3.8}$$

which yields the quartic equation,

$$A_n \pm iB_n = 0 \tag{3.3.9}$$

and

$$C_1 = \mp i\,C_2 \tag{3.3.10}$$

where

$$i = \sqrt{-1}$$

In order to solve this quartic equation, another variable is introducted as

$$Q_n = \lambda_i \pm is\beta_n \tag{3.3.11}$$

which yields the following quadratic equation in Q_n^2

$$D_xQ_n^4 - 2Hc^2Q_n^2\beta_n^2 + D_yc^4\beta_n^4 = 0 \tag{3.3.12}$$

whose roots are given by

$$Q_n = \pm\left[\frac{H \pm\sqrt{H^2 - D_xD_y + \bar{m}h_1\omega^2D_x/\beta_n^4}}{D_x}\right]^{1/2}\beta_n c \tag{3.3.13}$$

Using Equation 3.3.11, gives

$$\lambda_i = \pm\left\{\left[\frac{H \pm\sqrt{H^2 - D_xD_y + \bar{m}h_1\omega^2D_x/\beta_n^4}}{D_x}\right]^{1/2} c \mp is\right\} \beta_n \qquad (3.3.14)$$

Inspection of Equation 3.3.14 reveals that there are eight possible combinations of λ_i. Only one case will be considered herein, corresponding to a plate having $H^2<D_xD_y$, which is torsionally soft and flexurally stiff where $(H^2-D_xD_y)$, which has a negative value, is greater than the frequency term of $\bar{m}h_1\omega^2D_x/\beta_n^4$.

Separating the real and imaginary parts under the sign of the square root in expression of λ_i (Equation 3.3.14) and simplifying, yield the following roots

$$\lambda_i = (\pm k_1 + ik_2)\beta_n \quad \text{OR} \quad (\pm k_1 + ik_3)\beta_n \qquad (3.3.15)$$

where

$$k_1 = c\left[\frac{\sqrt{D_xD_y - \bar{m}h_1\omega^2D_x/\beta_n^4} + H}{2D_x}\right]^{1/2}$$

$$k_2 = c\left[\frac{\sqrt{D_xD_y - \bar{m}h_1\omega^2D_x/\beta_n^4} - H}{2D_x}\right]^{1/2} + s$$

$$k_3 = c\left[\frac{\sqrt{D_xD_y - \bar{m}h_1\omega^2D_x/\beta_n^4} - H}{2D_x}\right]^{1/2} - s$$

Substituting Equations 3.3.15 and 3.3.10 into Equation 3.3.6, taking into consideration all of the eight possible combination of all the roots and utilizing the relations between the hyperbolic, trigonometric and exponential functions, a possible mode shape function in u,v and t can be assumed as

$$w_1(u,v,t) = \sum_{n=1}^{\infty} \Big\{ [C_{1n} \cosh k_1\beta_n u + C_{2n} \sinh k_1\beta_n u] \cos (k_2 u+v)\, \beta_n$$
$$+ [C_{3n} \cosh k_1\beta_n u + C_{4n} \sinh k_1\beta_n u] \sin (k_2 u+v)\beta_n$$
$$+ [C_{5n} \cosh k_1\beta_n u + C_{6n} \sinh k_1\beta_n u] \cos (k_2 u-v)\, \beta_n$$
$$+ [C_{7n} \cosh k_1\beta_n u + C_{8n} \sinh k_1\beta_n u] \sin (k_2 u-v)\, \beta_n \Big\}$$
$$x \sin \omega t \qquad (3.3.16)$$

To minimize the CPU time and to improve the efficiency of this mathematical solution, advantage is taken of the quadrant symmetry of the skew plate and its boundaries. As it will be observed later on that the mode shapes of the skew plate are either symmetric or anti-symmetric about the center of the polar coordinates. For that reason, when either even (symmetric modes) or odd terms (anti-symmetric modes) are considered at a time, the boundary conditions at the opposite edges would become identical and the number of boundary conditions would reduce from eight to four for each mode shape.

When the mode shape function w(u,v,t) is used to satisfy the four boundary conditions, it becomes necessary to expand the mode shape function of u and v in a fourier series yielding (2n+1) equations (25,26) for each boundary condition or 4(2n+1) for four boundary conditions. In order to have a more general representation of each mode shape, another mode shape function is introduced by replacing u by v in Equation 3.3.6, giving,

$$w_2(u,v,t) = \sum_{n=1}^{\infty} e^{\bar{\lambda}_i v} [A_n \cos\alpha_n u + B_n \sin\alpha_n u] \sin \frac{\omega \bar{\lambda}_i^{-2}}{\alpha_n^2} t \qquad (3.3.17)$$

where

$\alpha_n = n\pi/a$, and

$\bar{\lambda}_i$ = number of the considered roots resulted from satisfying the governing equation.

Again, substituting Equation 3.3.17 into Equation 3.3.2, separating and then equating the coefficients of $\sin\alpha_n u$ and $\cos\alpha_n u$, and introducng another variable of $\bar{Q}_n$, which is given by

$$\bar{Q}_n = \alpha_n - is\,\bar{\lambda}_i$$

where

$$i = \sqrt{-1}$$

yield the following roots

$$\bar{\lambda}_i = \left\{ \frac{1}{\pm\left[\frac{H \pm \sqrt{H^2 - D_x D_y + \bar{m}h_1\omega^2 D_x/\alpha_n^4}}{D_x}\right]^{1/2} c \pm is} \right\} \alpha_n \qquad (3.3.18)$$

In order to have a relation between $\bar{\lambda}_i$ and λ_i, one can assume that $\alpha_n = \beta_n$ which means that a must be equal to b, i.e., this solution is only applicable to a plate having an aspect ratio equal to one. The values of $\bar{\lambda}_i$ in Eq. 3.3.18 are re-written in a simplified form as shown below.

$$\bar{\lambda}_i = \frac{\alpha_n}{\pm k_1 \pm i\,k_2} \quad \text{OR} \quad \frac{\alpha_n}{\pm k_1 \pm i\,k_3}$$

$$= (\pm k_1 \pm i\,k_2)\, y_1 \alpha_n \quad \text{OR} \quad (\pm k_1 \pm i\,k_3)\, z_1 \alpha_n \qquad (3.3.19)$$

where

$$y_1 = \frac{1}{k_1^2 + k_2^2}$$

$$z_1 = \frac{1}{k_1^2 + k_3^2}$$

Proceeding as before, considering all of the linear combinations of the roots, another shape function, $w_2(u,v,t)$, can be taken as shown below.

$$w_2(u,v,t) = \sum_{n=1}^{\infty}\Big\{ [C_{9n} \cosh (y_1 k_1 \alpha_n)v + C_{10n} \sinh (y_1 k_1 \alpha_n)v] \cos (y_1 k_2 v + u)\alpha_n$$

$$+ [C_{11n} \cosh (y_1 k_1 \alpha_n)v + C_{12n} \sinh (y_1 k_1 \alpha_n)v] \sin (y_1 k_2 v + u)\alpha_n$$

$$+ [C_{13n} \cosh (z_1 k_1 \alpha_n)v + C_{14n} \sinh (z_1 k_1 \alpha_n)v] \cos (z_1 k_3 v - u)\alpha_n$$

$$+ [C_{15n} \cosh (z_1 k_1 \alpha_n)v + C_{16n} \sinh (z_1 k_1 \alpha_n)v] \sin (z_1 k_3 v - u)\alpha_n \Big\}$$

$$\times \sin \frac{\omega \lambda_i^{-2}}{\alpha_n^2} t \qquad (3.3.20)$$

where C_{9n}, C_{10n}, ... C_{16n} are arbitrary constants dependent on n.

Combining the two mode shape functions $w_1(u,v,t)$ and $w_2(u,v,t)$ and considering either symmetric modes (even terms) or anti-symmetric modes (odd terms) yield eight dependent constants for each mode shape. In order to have the same number of arbitrary constants in the mode shape function as there are equations, the following polynomial function of (u,v) only and independent of (t) is added to the other two mode shape functions (26).

$$w_3(u,v) = C_{17} + C_{18}\frac{u}{a} + C_{19}\frac{u}{b} + C_{20}\frac{u^2}{a^2} +$$

$$C_{21}\frac{v^2}{b^2} + C_{22}\frac{u^3}{a^3} + C_{23}\frac{v^3}{b^3}$$

$$+ C_{24}\frac{Pu^4 - v^4}{b^4} \qquad (3.3.21)$$

where C_{17}, C_{18}, ... C_{24} are arbitrary constants.

Substituting equation 3.3.21 in the governing equation 3.3.2 yields expression for the constant (P) given by

$$P = (s^4 D_x + 2s^2 c^2 H + c^4 D)/D_x$$

However, it should also be noted that each function of $w_1(u,v,t)$, $w_2(u,v,t)$ and $w_3(u,v)$ has an equal number of odd and even terms; adding them results in (8n+4) terms, which correspond to either symmetric and/or anti-symmetric mode shapes. The satisfaction of the boundary conditions and formulating the transcendental frequency equation for the skew orthotropic plate will be discussed in more detail in Chapter IV.

CHAPTER IV

TRANSCENDENTAL FREQUENCY EQUATION FOR SKEW ORTHOTROPIC PLATES

4.1 DIVISION OF THE MODE SHAPES

Basically, the vibration modes of skew orthotropic plates are either symmetrical or anti-symmetrical about the center of the polar coordinates. To utilize this observation, the mode shape function given by

$$w(u,v,t) = w_1(u,v,t) + w_2(u,v,t) + w_3(u,v) \tag{4.1.1}$$

is divided into even and odd terms. The even terms represent the symmetric modes and therefore the following arbitrary constants of the odd terms must vanish in order to calculate the symmetric modes:

$$C_{2n}=C_{3n}=C_{6n}=C_{7n}=C_{10n}=C_{11n}=C_{14n}=C_{15n}=C_{18}=C_{19}=C_{22}=C_{23}=0 \tag{4.1.2}$$

(For symmetric modes)

Furthermore, the odd terms represent the anti-symmetric modes and the following arbitrary constants of the even terms in this case must vanish:

$$C_{1n}=C_{4n}=C_{5n}=C_{8n}=C_{9n}=C_{12n}=C_{13n}=C_{16n}=C_{17}=C_{20}=C_{21}=C_{24}=0 \tag{4.1.3}$$

(For anti-symmetric modes)

The transcendental frequency equation for symmetric or anti-symmetric modes is obtained by satisfying the four boundary conditions, at the end and side supports, discussed in Chapter III, and by considering only even or odd terms, respectively. However, to facilitate this mathematical approach, and since the values of $\sin \omega t$ and $\sin \frac{\omega \lambda_i^{-2}}{\alpha_n^2} t$ in Equations 3.3.16 and

3.3.20 are in the range of -1 to +1, it is assumed that

$$\sin \omega t = \sin \frac{\omega \lambda_i^{-2}}{\alpha_n^2} t = 1.0$$

Without this assumption, the satisfaction of the four boundary conditions becomes impossible. However, while the above assumption facilitates the mathematical solution, it limits the applicability of the solution to a skew orthotropic plate having a 45° skew angle.

In this chapter, the satisfaction of the four boundary conditions at u = $\pm$ b for -a $\leqslant$ v $\leqslant$ a and at v = $\pm$ a for -b $\leqslant$ u $\leqslant$ b for either symmetric or anti-symmetric mode shapes of a skew orthotropic plate are discussed.

4.2 SYMMETRIC MODE SHAPES

The boundary condition given by Equation 3.2.7 at v = $\pm$ b, states that the deflection must be equal to zero; thus, by substituting equations 4.1.1 and 4.1.2 in Equation 3.2.7 the following equation is obtained:

$$H_o(u) + \sum_{n=1}^{\infty} [H_n(u) + P_n \cos\alpha_n u + G_n \sin\alpha_n u] = 0 \qquad (4.2.1)$$

where

$$H_o(u) = C_{17} + C_{20} \frac{u^2}{a^2} + C_{21} + C_{24}\left(\frac{Pu^4}{b^4} - 1\right)$$

$$H_n(u) = (-1)^n \; (C_{1n} \cosh u_{1n} \cos u_{2n} + C_{4n} \sinh u_{1n} \sin u_{2n}$$

$$+ C_{5n} \cosh u_{1n} \cos u_{3n} + C_{8n} \sinh u_{1n} \sin u_{3n})$$

$$P_n = C_{9n} A_{1n} + C_{12n} A_{2n} + C_{13n} B_{1n} + C_{16n} B_{2n}$$

$$G_n = - C_{9n} A_{4n} + C_{12n} A_{3n} + C_{13n} B_{4n} - C_{16n} B_{3n}$$

where

A_{1n} to A_{8n}, B_{1n} to B_{8n} and u_{1n}, u_{2n}, u_{3n} are defined in the nomenclature.

To satisfy exactly this boundary condition, it becomes necessary to expand the two function $H_o(u)$ and $H_n(u)$ in Fourier Series over the range $-a \leq u \leq a$. Hence,

$$H_o(u) = a_{oo} + \sum_{m=1} (a_{om} \cos\alpha_m u + b_{om} \sin\alpha_m u) \tag{4.2.2}$$

and

$$H_n(u) = a_{no} + \sum_{m=1} (a_{nm} \cos\alpha_m u + b_{nm} \sin\alpha_m u)$$

where $\alpha_m = \frac{m\pi}{a}$; and, a_{oo}, a_{om}, b_{om}, a_{no}, a_{nm} and b_{nm} are Fourier coefficients; their expressions are derived in Appendix B.

By substituting Equation 4.2.2 into Equation 4.2.1, this boundary condition becomes

$$a_{oo} + \sum_{n=1}^{\infty} a_{no} + \sum_{m=1}^{\infty} [(a_{om} + \sum_{n=1}^{\infty} a_{nm} + P_n) \cos\alpha_m u + (b_{om} + \sum_{n=1}^{\infty} b_{nm} + G_n) \sin\alpha_m u] = 0 \tag{4.2.3}$$

The resulting equation 4.2.3 shows that the coefficients of $\sin\alpha_m u$ and $\cos\alpha_m u$ are linearly independent. Therefore, they must be equal to zero. Thus,

$$a_{oo} + \sum_{n=1}^{\infty} a_{no} = 0$$

$$a_{om} + \sum_{n=1}^{\infty} (a_{nm} + P_n) = 0 \qquad \text{for } m \geq 1$$

$$b_{om} + \sum_{n=1}^{\infty} (b_{nm} + G_n) = 0 \qquad \text{for } m \geq 1 \tag{4.2.4}$$

Substituting the Fourier coefficients and P_n and G_n into Equation 4.2.4, yields the following three equations:

$$C_{17} + \frac{1}{3} C_{20} + C_{21} + C_{24} \frac{(Pa^4}{5b^4} - 1)$$

$$+ \sum_{n=1}^{\infty} (-1)^n (C_{1n} K_{1n} + C_{4n} K_{2n} + C_{5n} K_{3n} + C_{8n} K_{4n}) = 0 \qquad (4.2.5)$$

$$C_{20} J_{1m} + C_{24} PJ_{3m} \frac{a^4}{b^4} + \sum_{n=1}^{\infty} (-1)^n (C_{1n} I_{k1} + C_{4n} I_{k2} + C_{5n} I_{k3} + C_{8n} I_{k4})$$

$$+ C_{9n} A_{1n} + C_{12n} A_{2n} + C_{13n} B_{1n} + C_{16n} B_{2n} = 0 \qquad \text{for } m \geq 1 \quad (4.2.6)$$

$$- C_{9n} A_{4n} + C_{12n} A_{3n} - C_{13n} B_{3n} - C_{16n} B_{4n} = 0 \qquad \text{for } m \geq 1 \quad (4.2.7)$$

If m harmonics of the series are considered, the second and third equations yield 2m equations, and together with the first one yields (2m+1) equations for one boundary condition.

The boundary condition given by Equation 3.3.3 at $v=\pm b$ states that the moment normal to the support must be equal to zero; proceeding in a similar way, as before, another set of three equations are obtained as shown below:

$$2 C_{21} \frac{X_2}{b^2} - 12 C_{24} \frac{X_2}{b^2}$$

$$+ \sum_{n=1} (-1)^n \beta_n^2 [C_{1n} (F_7 K_{1n} - X_1 k_1 k_{2n}) + C_{4n} (X_1 k_1 k_{1n} + F_7 K_{2n})$$

$$+ C_{5n} (E_7 K_{3n} + X_1 k_1 k_{4n}) + C_{8n} (-X_1 k_1 k_{3n} + F_7 K_{4n})] = 0 \qquad (4.2.8)$$

$$\sum_{n=1} (-1)^n \beta_n^2 [C_{1n}(F_7 I_{k1} - X_1 k_1 I_{k2}) + C_{4n} (X_1 k_1 I_{k1} + F_7 I_{k2})$$
$$+ C_{5n} (E_7 I_{k3} + X_1 k_1 I_{k4}) + C_{8n} (-X_1 k_1 I_{k3} + E_7 I_{k4})]$$
$$+\alpha_m^2 [C_{9n} (F_8 A_{1n} + F_9 A_{2n}) + C_{12n} (-F_9 A_{1n} + F_8 A_{2n})$$
$$+ C_{13n} (E_8 B_{1n} + E_9 B_{2n}) + C_{16n} (-E_9 B_{1n} + E_8 B_{2n})] = 0$$

For $m \geq 1$ (4.2.9)

$$\alpha_n^2 [C_{9n} (-F_8 A_{4n} + F_9 A_{3n}) + C_{12n} (F_9 A_{4n} + F_8 A_{3n})$$
$$+ C_{13n} (E_8 B_{4n} - E_9 B_{3n}) + C_{16n} (-E_9 B_{4n} - E_8 B_{3n})] = 0$$

For $n \geq 1$ (4.2.10)

Similarly, the satisfaction of the boundary condition given by Equation 3.3.4, at $u=\pm a$, yields the following three equations,

$$24 C_{24} (X_3 Pa + EI)/b^4 +$$
$$\sum_{n=1}^{\infty}(-1)^n \alpha_n^4 [C_{9n} (F_5 K_{5n} + F_6 K_{6n}) + C_{12n} (-F_6 K_{5n} + F_5 K_{6n})$$
$$+ C_{13n} (E_5 K_{7n} + E_6 K_{8n}) + C_{16n} (-E_6 K_{7n} + E_5 K_{8n})] = 0$$

(4.2.11)

$$\sum_{m=1} (-1)^m \alpha_m^4 [C_{9n} (F_5 I_{k5} + F_6 I_{k6}) + C_{12n} (-F_6 I_{k5} + F_5 I_{k6})$$
$$+ C_{13n} (E_5 I_{k7} + E_6 I_{k8}) + C_{16n} (-E_6 I_{k7} + E_5 I_{k8})]$$
$$+ \beta_n^3 [C_{1n} (-EI\ \beta_n A_{5n} + F_{10} A_{7n} + F_{11} A_{8n})$$
$$+ C_{4n} (-EI\ \beta_n A_{6n} - F_{11} A_{7n} + F_{10} A_{8n})$$
$$+ C_{5n} (-EI\ \beta_n B_{5n} + E_{10} B_{7n} + E_{11} B_{8n})$$
$$+ C_{8n} (-EI\ \beta_n B_{6n} - E_{11} B_{7n} + E_{10} B_{8n})] = 0 \qquad n \geq 1 \quad (4.2.12)$$

$$- 24\, C_{24} X_6 J_{5m}/b^3 +$$

$$\sum_{m=1}^{\infty} (-1)^m \alpha_m^3 [C_{9n} (F_{12} I_{J5} + F_{13} I_{J6})$$

$$+ C_{12n} (-F_{13} I_{J5} + F_{12} I_{J6}) + C_{13n} (E_{12} I_{J7} + E_{13} I_{J8})$$

$$+ C_{16n} (-E_{13} I_{J7} + E_{12} I_{J8})] +$$

$$\beta_n^3 [C_{1n} (F_{11} A_{5n} - F_{10} A_{6n} + EI\, \beta_n A_{8n})$$

$$+ C_{4n} (F_{10} A_{5n} + F_{11} A_{6n} - EI\, \beta_n A_{7n}) + C_{5n} (-E_{11} B_{5n} + E_{10} B_{6n} - EI \beta_n B_{8n})$$

$$+ C_{8n} (-E_{10} B_{5n} - E_{11} B_{6n} + EI\, \beta_n B_{6n})] = 0 \qquad n \geq 1 \quad (4.2.13)$$

The following three equations are obtained from the fourth boundary condition, given by Equation 3.3.5, at $u = \pm a$:

$$2\, C_{20} X_7/a^2 + 2\, C_{21} X_9/b^2 + \frac{1}{b^4} C_{24} (12 X_7 P a^2 - 4 X_9 b^2)$$

$$+ \sum_{n=1}^{\infty} (-1)^n \alpha_n^2 [C_{9n} (F_{17} K_{5n} + F_{19} K_{6n}) + C_{12n} (-F_{18} K_{5n} + F_{17} K_{6n})$$

$$+ C_{13n} (E_{17} K_{7n} + E_{18} K_{8n}) + C_{16n} (-E_{18} K_{7n} + E_{17} K_{8n})] = 0 \quad (4.2.14)$$

$$-12\, C_{24}X_9J_{1m}/b^2$$

$$+ \sum_{m=1} (-1)^m \alpha_m^2 [C_{9n} (F_{17}I_{k5} + F_{18}I_{k6}) + C_{12n} (-F_{18}I_{k5} + F_{17}I_{k6})$$

$$+ C_{13n} (E_{17}I_{k7} + E_{18}I_{k8}) + C_{16n} (-E_{18}I_{k7} + E_{17}I_{k8})]$$

$$+ \beta_n^2 \Big\{ C_{1n} [F_{14}A_{5n} + F_{15}A_{6n} + \beta_n (F_{16}A_{8n} - GJK_1A_{7n})]$$

$$+ C_{4n} [F_{14}A_{6n} - F_{15}A_{5n} - \beta_n (GJK_1A_{8n} + F_{16}A_{7n})]$$

$$+ C_{5n} [E_{14}B_{5n} + E_{15}B_{6n} + \beta_n (E_{16}B_{8n} - GJK_1B_{9n})]$$

$$+ C_{8n} [E_{14}B_{6n} - E_{15}B_{5n} - \beta_n (GJK_1B_{8n} + E_{16}B_{7n})] \Big\} = 0$$

$$n \geq 1 \qquad (4.2.15)$$

$$- 24\, C_{24}X_{10}J_{5m}/b^3$$

$$+ \sum_{m=1} (-1)^m \alpha_m^3 [C_{9n} (F_{19}I_{j5} + F_{20}I_{j6}) + C_{12n} (-F_{20}I_{j5} + F_{20}I_{j6})$$

$$+ C_{13n} (E_{19}I_{j7} + E_{20}I_{j8}) + C_{16n} (E_{19}I_{j8} - E_{20}I_{j7})]$$

$$+ \beta_n^2 \Big\{ C_{1n} [\beta_n (F_{16}A_{5n} + GJK_1A_{6n}) + F_{15}A_{7n} - A_{14}A_{8n}]$$

$$+ C_{4n} [\beta_n (F_{16}A_{6n} - GJK_1A_{5n}) + F_{15}A_{8n} + A_{14}A_{7n}]$$

$$+ C_{5n} [-\beta_n (E_{16}B_{5n} + GJK_1B_{6n}) - E_{15}B_{7n} + E_{14}B_{8n}]$$

$$+ C_{8n} [\beta_n (-E_{16}B_{6n} + GJK_1B_{5n}) - E_{15}B_{8n} - E_{14}B_{7n}] \Big\} = 0$$

$$n \geq 1 \qquad (4.2.16)$$

The satisfaction of the above four boundary conditions yields infinite set of equations, (8n+4), of infinite number of constants, (8n+4), as shown in Figure 4.1. Equating the determinant, which consists of the coefficients of these constants, to zero yields the transcendental frequency equation for symmetric mode shapes. The accuracy of the

resulting frequencies depends on the number of harmonics and on the rate of convergence of the roots of the transcendental frequency equation.

4.3 ANTI-SYMMETRIC MODE SHAPES

Proceeding as discussed before for symmetric mode shapes, another set of 4(2n+1) equations will be obtained for the same four boundary conditions corresponding to the anti-symmetric mode shapes.

Substituting Equations 4.1.1 and 4.1.3 into Equation 3.2.7, the following set of (2n+1) equations are obtained.

$$C_{19} + C_{23} = 0 \qquad (4.3.1.)$$

$$C_{10n} A_{3n} + C_{11n} A_{4n} + C_{14n} B_{3n} + C_{15n} B_{4n} = 0 \qquad n \geq 1 \qquad (4.3.2)$$

$$C_{18} J_{5m}/a + C_{22} J_{7m}/a^3 + \sum_{m=1} (-1)^m (C_{2n} I_{j1} + C_{3n} I_{j2} + C_{6n} I_{j3} + C_{7n} I_{j4}) - C_{10n} A_{2n} + C_{11n} A_{1n} + C_{14n} B_{2n} - C_{15n} B_{1n} = 0 \qquad n \geq 1 \qquad (4.3.3)$$

Proceeding as before, the following three equations are obtained for the boundary condition given by Equation 3.3.3:

$$6\, C_{23} X_2/b^2 = 0 \qquad (4.3.4)$$

$$\alpha_n^2 [C_{10n} (F_8 A_{3n} + F_9 A_{4n}) + C_{11n} (-F_9 A_{3n} + F_8 A_{4n}) + C_{14n} (E_8 B_{3n} + E_9 B_4) + C_{15n} (-E_9 B_{3n} + E_8 B_{4n})] = 0 \qquad n \geq 1 \qquad (4.3.5)$$

$$\sum_{m=1}^{\infty} (-1)^m \beta_m^2 [C_{2n} (F_7 I_{j1} - X_1 K_1 I_{j2}) + C_{3n} (X_1 K_1 I_{j1} + F_7 I_{j2})$$
$$+ C_{6n} (E_7 I_{j3} + X_1 K_1 I_{j4}) - C_{7n} (-X_1 K_1 I_{j3} + E_7 I_{j4})]$$
$$+\alpha_n^2 [C_{10n} (F_9 A_{1n} - F_8 A_{2n}) + C_{11n} (F_8 A_{1n} + F_9 A_{2n})$$
$$+ C_{14n} (-E_9 B_{1n} + E_8 B_{2n}) + C_{15n}(-E_8 B_{1n} - E_9 B_{2n})] = 0 \qquad n \geq 1 \qquad (4.3.6)$$

For the boundary condition at the elastically supported edge given by Equation 3.3.4, the following set of (2n+1) equations are obtained:

$$6 C_{22} X_7/a^3 + 6 C_{23} X_6/b^3$$
$$+ \sum_{n=1}^{\infty} (-1)^n \alpha_n^3 [C_{10n}(F_{12} K_{5n} + F_{13} K_{6n}) + C_{11n} (F_{12} K_{6n} - F_{13} K_{5n})$$
$$+ C_{14n} (E_{12} K_{7n} + E_{13} K_{8n}) + C_{15n}(E_{12} K_{8n} - E_{13} K_{7n})] = 0 \qquad (4.3.7)$$

$$\sum_{m=1}^{\infty} (-1)^m \alpha_m^3 [C_{10n} (F_{12} I_{k5} + F_{13} I_{k6}) + C_{11n} (F_{12} I_{k6} - F_{13} I_{k5})$$
$$+ C_{14n} (E_{12} I_{k7} + E_{13} I_{k8}) + C_{15n} (E_{12} I_{k8} - E_{13} I_{k7})]$$
$$+ \beta_n^3 [C_{2n} (-EI\ \beta_n A_{7n} + F_{10} A_{5n} + F_{11} K_{6n})$$
$$+ C_{3n} (-EI\ \beta_n A_{8n} + F_{10} A_{6n} - F_{11} K_{5n})$$
$$+ C_{6n} (-EI\ \beta_n B_{7n} + E_{10} B_{5n} + E_{11} B_{6n})$$
$$+ C_{7n} (-EI\ \beta_n B_{8n} + E_{10} B_{6n} - E_{11} B_{5n})] = 0 \qquad n \geq 1 \qquad (4.3.8)$$

$$\beta_n^3 [C_{2n} (EI\ \beta_n A_{6n} - F_{10}A_{8n} + F_{11}A_{7n})$$
$$+ C_{3n} (-EI\ \beta_n A_{5n} + F_{10}A_{7n} + F_{11}A_{8n})$$
$$+ C_{6n} (-EI\ \beta_n B_{6n} + E_{10}B_{8n} - E_{11}B_{7n})$$
$$+ C_{7n} (EI\ \beta_n B_{5n} - E_{10}B_{8n} - E_{11}B_{8n})] +$$
$$\sum_{m=1}^{\infty} (-1)^m \alpha_m^4 [C_{10n} (F_5 I_{j5} + F_6 I_{j6}) + C_{11n} (-F_6 I_{j5} + F_5 I_{j6})$$
$$+ C_{14n} (E_5 I_{j7} + E_6 I_{j8}) + C_{15n} (-E_6 I_{j7} + E_5 I_{j8})] = 0$$
$$n \geq 1 \quad (4.3.9)$$

Similarly, for the boundary condition of Equation 3.3.5, the following set of (2n+1) equations are obtained:

$$6\ X_7 C_{22}/a^2 + 6\ X_{10} C_{23}/b^3$$
$$+ \sum_{n=1} (-1)^n \alpha_n^3 [C_{10n} (F_{19}K_{5n} + F_{20}K_{6n}) + C_{11n} (-F_{20}K_{5n} + F_{19}K_{6n})$$
$$+ C_{14n} (E_{19}K_{7n} + E_{20}K_{8n}) + C_{15n} (-E_{20}K_{7n} + E_{19}K_{8n})] = 0$$
$$(4.3.10)$$

$$\beta_n^2 \{ C_{2n} [-\beta_n (-F_{16}A_{6n} + GJK_1 A_{5n}) + F_{14}A_{7n} + F_{15}A_{8n}]$$
$$+ C_{3n} [-\beta_n (+F_{16}A_{5n} + GJK_1 A_{6n}) + F_{14}A_{8n} - F_{15}A_{7n}]$$
$$+ C_{6n} [-\beta_n (-E_{16}B_{6n} + GJK_1 B_{5n}) + E_{14}B_{7n} + E_{15}B_{8n}]$$
$$+ C_{7n} [-\beta_n (E_{16}B_{5n} + GJK_1 B_{6n}) + E_{14}B_{8n} - E_{15}B_{7n}] \}$$
$$+ \sum_{m=1} (-1)^m \alpha_m^3 [C_{10n} (F_{19}I_{k5} + F_{20}I_{k6}) + C_{11n} (F_{19}I_{k6} - F_{20}I_{k5})$$
$$+ C_{14n} (E_{19}I_{k7} + E_{20}I_{k8}) + C_{15n} (E_{19}I_{k8} - E_{20}I_{k7})] = 0$$
$$n \geq 1 \quad (4.3.11)$$

$$6\, X_9 J_{5n} C_{23}/b^3 +$$

$$\beta_n^2 \Big\{ C_{2n} [\beta_n (F_{16}A_{7n} + GJK_1A_{8n}) - F_{14}A_{6n} + F_{15}A_{5n}]$$

$$+ C_{3n} [\beta_n (F_{16}A_{8n} - GJK_1A_{7n}) + F_{14}A_{5n} + F_{15}A_{6n}]$$

$$+ C_{6n} [-\beta_n (E_{16}B_{7n} + GJK_1B_{8n}) + E_{14}B_{6n} - E_{15}B_{5n}]$$

$$+ C_{7n} [-\beta_n (E_{16}B_{8n} - GJK_1B_{7n}) - E_{14}B_{5n} - E_{15}B_{6n}] \Big\}$$

$$+ \sum_{m=1} (-1)^m \alpha_m^2 [C_{10n} (F_{17}I_{j5} + F_{18}I_{j6}) + C_{11n} (F_{17}I_{j6} - F_{18}I_{j5})$$

$$+ C_{14n} (E_{17}I_{j7} + E_{18}I_{j8}) + C_{15n} (E_{17}I_{j8} - E_{18}I_{j7})] = 0$$

$$n \geq 1 \qquad (4.3.12)$$

Thus, the determinant of the symmetric mode shape, which will yield the transcendental frequency equation, consists of 4 (2n+1) equations given by Equations 4.2.5, 4.2.6, 4.2.7, 4.2.8, 4.2.9, 4.2.10, 4.2.11, 4.2.12, 4.2.13, 4.2.14, 4.2.15 and 4.2.16 (see Figure 4.1). Similarly, for the anti-symmetric mode shapes, the determinant equation consists of Equations: 4.3.1, 4.3.2, 4.3.3, 4.3.4, 4.3.5, 4.3.6, 4.3.7, 4.3.8, 4.3.9, 4.3.10, 4.3.11 and 4.3.12 (see Figure 4.2).

4.4 COMPUTER PROGRAM FOR THE NUMERICAL SOLUTION

Rigorous solution of the governing differential equation for the free vibration of a skew orthotropic plate using the classical approach is extremely difficult. Review of the relevant literature has not revealed any published work in this area. In the classical solution presented herein the entire analysis is programmed to obtain the solution of the governing differential equation for the vibration of a 45° skewed

orthotropic plate. The program is written in Fortran IV for an IBM 360 computer for the generation of the even and odd terms, representing symmetric and anti-symmetric mode shapes. The solution of the transcendental frequency equations for the evaluation of the natural frequencies is obtained using the iterative approach. The program is written so that the solution can be obtained for any number of harmonics and for both elastically-supported or free edges. The computer program is applicable only to a skew orthotropic plate having a 45° skew angle and an aspect ratio of unity.

4.4.1 Flow Diagram

The computer program algorithm flow diagram for the solution of the governing differential equation to find the natural frequencies of a skew orthotropic plate is shown in Figure 4.3. The program starts by reading the input data which consists of the number of harmonics to be considered, the elastic properties such as D_x, D_y, D_1, D_2, D_{xy}, D_{yx}, the dimensions of the length and width of the analyzed plate, the parameters defining the types of the mode shapes to be analyzed, and the list of parameters to be printed. The first check is to classify the category to which the analyzed plate belongs; this is done by comparing its flexural rigidities, D_x and D_y, with the effective torsional rigidity, H. If the computer finds that the skew plate is other than flexurally stiff and torsionally weak, it will print the input data and stop. Otherwise, it will proceed to the next check. The next check is to test if the flexural rigidity is greater or smaller than the frequency term. A third test is made to check that the value under the sign of the square root, given in Equation 3.3.14, is

greater than the effective torsional rigidity. If the first, second and third tests are found to be negative, positive and positive, respectively, the computer will print the input data and will proceed to calculate the roots of the mode shape function, which are K_1, K_2 and K_3; otherwise it will stop and print the input data only. Then the subroutine CONSTANT will be called to calculate the constants which are functions of the mass, the rigidities, number of harmonics, and the geometry of the slab. If the symmetric mode shapes are required, the proper harmonic number will be considered, and the subroutine COEFF will generate the transcendental frequency equation, as shown in Figure 4.1. After the computer has determined the symmetric modes, a subroutine ANTIS is called and the transcendental frequency equation for the anti-symmetric modes will be evaluated, as shown in Figure 4.2. The subroutine MINVRS, available in the University of Windsor computer library, is then called to find the roots for the symmetric and anti-symmetric transcendental frequency equations. A listing of the program is included in Appendix E.

$$
\begin{bmatrix}
S_n(1,1) & S_n(1,2) & S_n(1,3) & S_n(1,4) & 0 & 0 & 0 & S_n(1,8) & S_n(1,9) & S_n(1,10) & 0 & S_n(1,12) \\
S_n(2,1) & S_n(2,2) & S_n(2,3) & S_n(2,4) & S_n(2,5) & S_n(2,6) & S_n(2,7) & S_n(2,8) & 0 & S_n(2,10) & 0 & S_n(2,12) \\
0 & 0 & 0 & 0 & S_n(3,5) & S_n(3,6) & S_n(3,7) & S_n(3,8) & 0 & 0 & 0 & 0 \\
S_n(4,1) & S_n(4,2) & S_n(4,3) & S_n(4,4) & 0 & 0 & 0 & 0 & 0 & 0 & S_n(4,11) & S_n(4,12) \\
S_n(5,1) & S_n(5,2) & S_n(5,3) & S_n(5,4) & S_n(5,5) & S_n(5,6) & S_n(5,7) & S_n(5,8) & 0 & 0 & 0 & 0 \\
0 & 0 & 0 & 0 & S_n(6,5) & S_n(6,6) & S_n(6,7) & S_n(6,8) & 0 & 0 & 0 & 0 \\
0 & 0 & 0 & 0 & S_n(7,5) & S_n(7,6) & S_n(7,7) & S_n(7,8) & 0 & 0 & 0 & S_n(7,12) \\
S_n(8,1) & S_n(8,2) & S_n(8,3) & S_n(8,4) & S_n(8,5) & S_n(8,6) & S_n(8,7) & S_n(8,8) & 0 & 0 & 0 & 0 \\
S_n(9,1) & S_n(9,2) & S_n(9,3) & S_n(9,4) & S_n(9,5) & S_n(9,6) & S_n(9,7) & S_n(9,8) & 0 & 0 & 0 & S_n(9,12) \\
0 & 0 & 0 & 0 & S_n(10,5) & S_n(10,6) & S_n(10,7) & S_n(10,8) & 0 & S_n(10,10) & S_n(10,11) & S_n(10,12) \\
S_n(11,1) & S_n(11,2) & S_n(11,3) & S_n(11,4) & S_n(11,5) & S_n(11,6) & S_n(11,7) & S_n(11,8) & 0 & 0 & 0 & S_n(11,12) \\
S_n(12,1) & S_n(12,2) & S_n(12,3) & S_n(12,4) & S_n(12,5) & S_n(12,6) & S_n(12,7) & S_n(12,8) & 0 & 0 & 0 & S_n(12,12)
\end{bmatrix}
\begin{bmatrix} C_{1n} \\ C_{4n} \\ C_{5n} \\ C_{8n} \\ C_{9n} \\ C_{12n} \\ C_{13n} \\ C_{16n} \\ C_{17} \\ C_{20} \\ C_{21} \\ C_{24} \end{bmatrix}
=
\begin{bmatrix} 0 \\ 0 \\ 0 \\ 0 \\ 0 \\ 0 \\ 0 \\ 0 \\ 0 \\ 0 \\ 0 \\ 0 \end{bmatrix}
$$

FIGURE 4.1 MATRIX EQUATION OF (8N+4) EQUATIONS FOR SYMMETRIC MODE SHAPES OF A 45° SKEW ORTHOTROPIC PLATE

$$
\begin{bmatrix}
0 & 0 & 0 & 0 & 0 & 0 & 0 & 0 & 0 & A_n(1,10) & 0 & A_n(1,12) \\
0 & 0 & 0 & 0 & A_n(2,5) & A_n(2,6) & A_n(2,7) & A_n(2,8) & 0 & 0 & 0 & 0 \\
A_n(3,1) & A_n(3,2) & A_n(3,3) & A_n(3,4) & A_n(3,5) & A_n(3,6) & A_n(3,7) & A_n(3,8) & A_n(3,9) & 0 & A_n(3,11) & 0 \\
0 & 0 & 0 & 0 & 0 & 0 & 0 & 0 & 0 & 0 & 0 & A_n(4,12) \\
0 & 0 & 0 & 0 & A_n(5,5) & A_n(5,6) & A_n(5,7) & A_n(5,8) & 0 & 0 & 0 & 0 \\
A_n(6,1) & A_n(6,2) & A_n(6,3) & A_n(6,4) & A_n(6,5) & A_n(6,6) & A_n(6,7) & A_n(6,8) & 0 & 0 & 0 & 0 \\
0 & 0 & 0 & 0 & A_n(7,5) & A_n(7,6) & A_n(7,7) & A_n(7,8) & 0 & 0 & A_n(7,11) & A_n(7,12) \\
A_n(8,1) & A_n(8,2) & A_n(8,3) & A_n(8,4) & A_n(8,5) & A_n(8,6) & A_n(8,7) & A_n(8,8) & 0 & 0 & 0 & 0 \\
A_n(9,1) & A_n(9,2) & A_n(9,3) & A_n(9,4) & A_n(9,5) & A_n(9,6) & A_n(9,7) & A_n(9,8) & 0 & 0 & 0 & 0 \\
0 & 0 & 0 & 0 & A_n(10,5) & A_n(10,6) & A_n(10,7) & A_n(10,8) & 0 & 0 & A_n(10,11) & A_n(10,12) \\
A_n(11,1) & A_n(11,2) & A_n(11,3) & A_n(11,4) & A_n(11,5) & A_n(11,6) & A_n(11,7) & A_n(11,8) & 0 & 0 & 0 & 0 \\
A_n(12,1) & A_n(12,2) & A_n(12,3) & A_n(12,4) & A_n(12,5) & A_n(12,6) & A_n(12,7) & A_n(12,8) & 0 & 0 & 0 & A_n(12,12)
\end{bmatrix}
\begin{bmatrix} C_{2n} \\ C_{3n} \\ C_{6n} \\ C_{7n} \\ C_{10n} \\ C_{11n} \\ C_{14n} \\ C_{15n} \\ C_{18} \\ C_{19} \\ C_{22} \\ C_{23} \end{bmatrix}
=
\begin{bmatrix} 0 \\ 0 \\ 0 \\ 0 \\ 0 \\ 0 \\ 0 \\ 0 \\ 0 \\ 0 \\ 0 \\ 0 \end{bmatrix}
$$

FIGURE 4.2 .MATRIX EQUATION OF (8N+4) EQUATIONS FOR SYMMETRIC MODE SHAPES OF A 45° SKEW ORTHOTROPIC PLATE

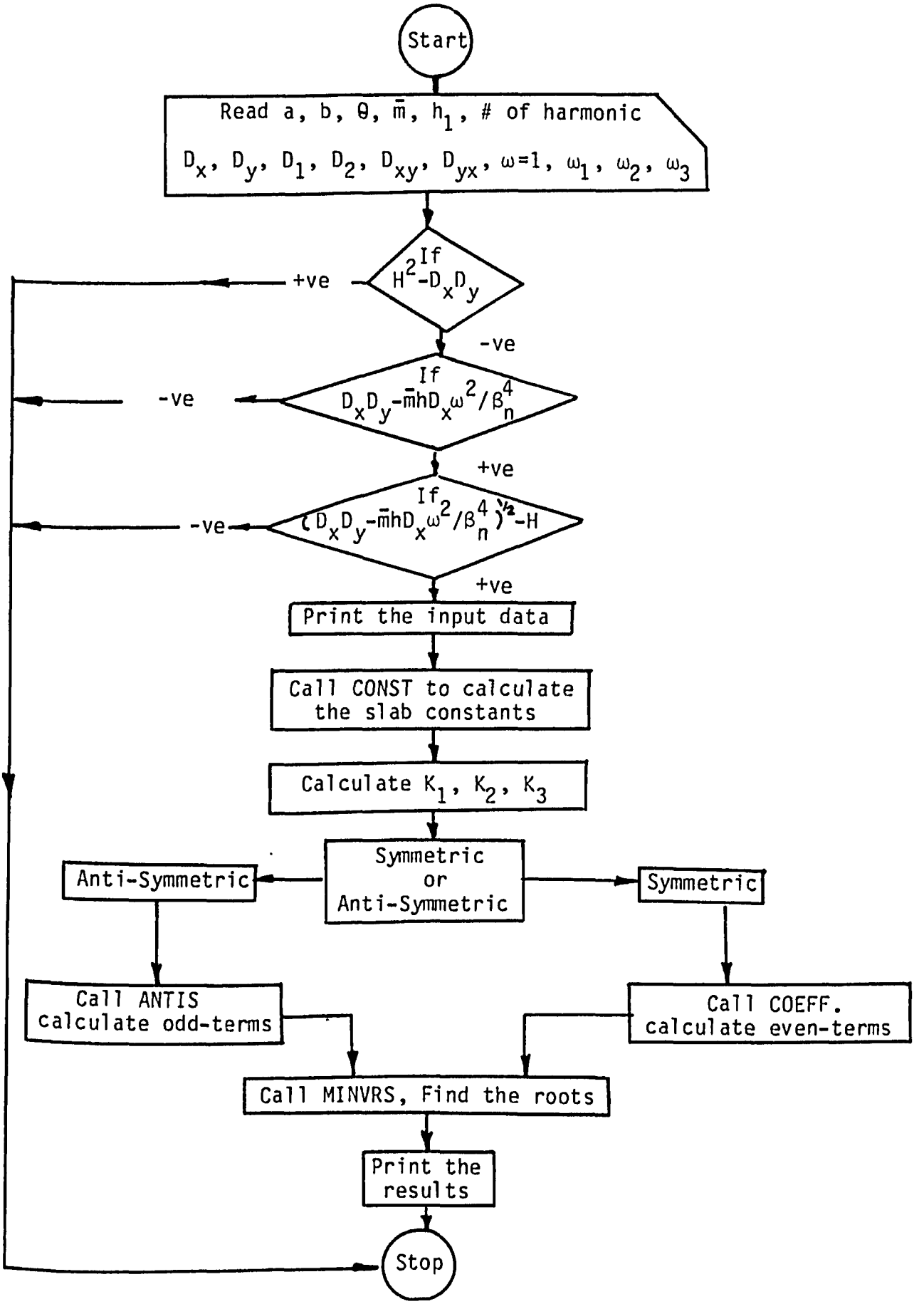

FIGURE 4.3 FLOW DIAGRAM TO CALCULATE THE NATURAL FREQUENCIES OF A 45° SKEW ORTHOTROPIC PLATE FOR THE SYMMETRIC AND ANTI-SYMMETRIC MODES

CHAPTER V

EXPERIMENTAL INVESTIGATION

5.1 INTRODUCTION

This chapter is concerned with the experimental investigation, models set-up, materials and procedures for the static, dynamic, fatigue and ultimate load tests of two bridge models. Visits were made to five different universities in Ontario to determine the most accurate and reliable instrumentation, needed for this experimental study, such as accelerometers, linear variable differential transformers, D.C. differential transformers, dynamic-fatigue strain gages, and data acquisition system. These visits were also necessary to determine and to build the best excitation system to be used as a source for the dynamic loading and fatigue loading through which a resonance fatigue can be induced to the models. The "moving mass" and the modified Gilmore hydraulic actuator combination performed quite satisfactorily for the dynamic and the fatigue loadings. The performance of this modified system, which was modified by the help of Mr. Kiss, the technician in the Department of Civil Engineering, left no doubt as to the ability of this loading system to induce the required stress levels during the resonance-fatigue tests.

The range of the models' accelerations, strains, and displacements were estimated first so that the sensors range and sensitivity would be of the same order. The capability of the data acquisition system, recently purchased by the Civil Engineering Department, was quite satisfactory in all tests. Interfacing this data acquisition system with the IBM Personal

Computer enabled the transmission of the measured data to the main computer system. Hence, data reduction was performed and the most meaningful data was obtained.

5.2 SCOPE OF EXPERIMENTAL PROGRAM

The fundamental objective of this experimental work was to evaluate the theoretical derivation of the free vibration analysis of continuous composite bridges, and to substantiate the theoretical results. Another aspect of this experimental program was to use the dynamic characteristics of bridges as a periodic inspection tool, in addition to visual inspection, to examine and detect fatigue failure of any of the bridge elements during its life.

In order to achieve these goals and obtain the most meaningful experimental data, two 1/4 scale models of a two-span continuous composite bridge were built. This scale was the most suitable for prestressing requirements and the available space in the laboratory.

Each model was free along the sides, parallel to the traffic. The two ends were simply supported and the middle was continuous over an intermediate hinged support. The two continuous composite bridge models I and II were exactly identical, except bridge model II had a prestressed post-tensioned concrete deck around the intermediate support, i.e. in the vicinity of the negative moment area. Each model was made of three longitudinal steel beams connected rigidly with five transverse steel diaphragms located at each support and at the middle of each span. The concrete deck was connected to the main beams by means of Nelson stud shear connectors. In order to avoid any fatigue failure in the tensioned flanges

at the intermediate support, no shear connectors were located within six inches of the intermediate support. The elastic properties of the concrete, steel beams and diaphragms, prestressed and reinforcement bars were determined according to the American Society for Testing and Materials Specifications.

A series of experimental tests were carried out on the two models, I and II. These tests comprised of static, dynamic, fatigue and ultimate load tests. Bridge Model I was subjected to a concentrated static load applied at the span center of the middle girder to confirm the findings from earlier tests (37). The dynamic tests on Models I and II comprised of: (i) the sweep or sine-wave test; (ii) the log decay test, and (iii) the natural mode shapes test, to determine their dynamic characteristics, such as natural frequencies, damping ratio, and the associated mode shapes. Dynamic tests were conducted before commencement of the fatigue test as well as after fatigue failure. One and two actuators were used to conduct the dynamic and fatigue tests on Model I and II, respectively. Ultimate load test was conducted on bridge Model I after the fatigued model was repaired, while in Model II the ultimate load test was conducted on the fatigued and unfatigued spans to determine the load carrying capacity after fatigue cracks had occurred.

To measure the most significant and meaningful data due to dynamic and fatigue tests on the two models at high frequency range (18-35 Hz), the models were instrumented by several accelerometers, linear variable differential transformers, D.C. differential transformer, and dynamic-fatigue strain gages. All of these sensors were connected to the Megadac 2000 data acquisition system which interfaced with the University of

Windsor main-frame computer. The fast Fourier transform concept was used for data reduction and to obtain the time history of the model's signature and the spectrum responses from which the natural frequencies were obtained. The interfacing programs were developed with the help of Mr. Jerry Monforton from the Electrical Engineering Department.

The evaluation of the theoretical analysis of the free vibration of the skew orthotropic plate, explained in Chapter IV, was made possible by comparing the obtained theoretical results with the experimental work carried out by El-Sebakhy, et al. which is described elsewhere (19).

5.3 MATERIALS

5.3.1 Concrete

The concrete mixes used for bridge Model I and II were composed of high early strength cement, coarse and fine aggregates and natural water. The high early strength Portland cement (CSA) manufactured by Canada Cement company provides high strength within a week. The water cement ratios were 60% and 40% for bridge Model I and II, respectively. The size range of the coarse aggregates (crushed stones) was restricted to 1/8 inch (3.17mm) to 1/4 inch (6.35mm). This maximum size of coarse aggregates was determined based on the concrete cover on the top of the shear connectors. The combination of the coarse and fine aggregates was prepared by mixing 60% coarse aggregate to 40% fine aggregate, which gave a well graded combined aggregate according to the ACI code. An Eerich Concrete Mixer Model EA2 (2W), having a charging capacity of five cubic feet ($0.14m^3$), was used for mixing the two concrete mixes for models I and II. The cylinder tests were made by obtaining a concrete sample from each batch. The compressive

strength of the concrete mix for bridge model I was about 4.0 ksi (27.58 MPa), while for bridge model II it was about 6.0 ksi (41.37 MPa).

5.3.2 Grout

Cement grout having a compressive strength of 4.45 ksi (30.68 MPa) was used to bond the prestressed bars in the postensioned concrete region at the intermediate support of bridge model II. High early strength cement mixed with sand and natural water was used. To ensure good workability and high strength of the cement grout, six trial mixes were made. Also, an Intraplast-N expanding grouting aid provided by Sika Canada Incorporated was added to the mixes. It was experienced that this grouting aid increased fluidity and produced a slow, controlled, expansion prior to hardening. Furthermore, Intraplast-N content does not contain any chemicals potentially dangerous as to stress corrosion in prestressed bars. Table 5.1 shows the property of the five mixes and their strength after seven days. The injection was applied at one end of the prestressed concrete portion until it was forced out of the other end. Because of the Intraplast-N product a few psi pressure was found to be sufficient for this short bar. It should be noted that this grout mix was designed in such a way that neither bleeding nor segregation would occur. This grouting mix and the required pressure was first experimented on a small prestressed slab 4'x2' (1.22m x 0.61m), before using it on bridge model II as shown in Figure 5.1.

5.3.3 Sikadur Hi-Mod Epoxy Adhesive

Sikadur Hi-Mod epoxy adhesive provided by Sika Canada Incorporated was

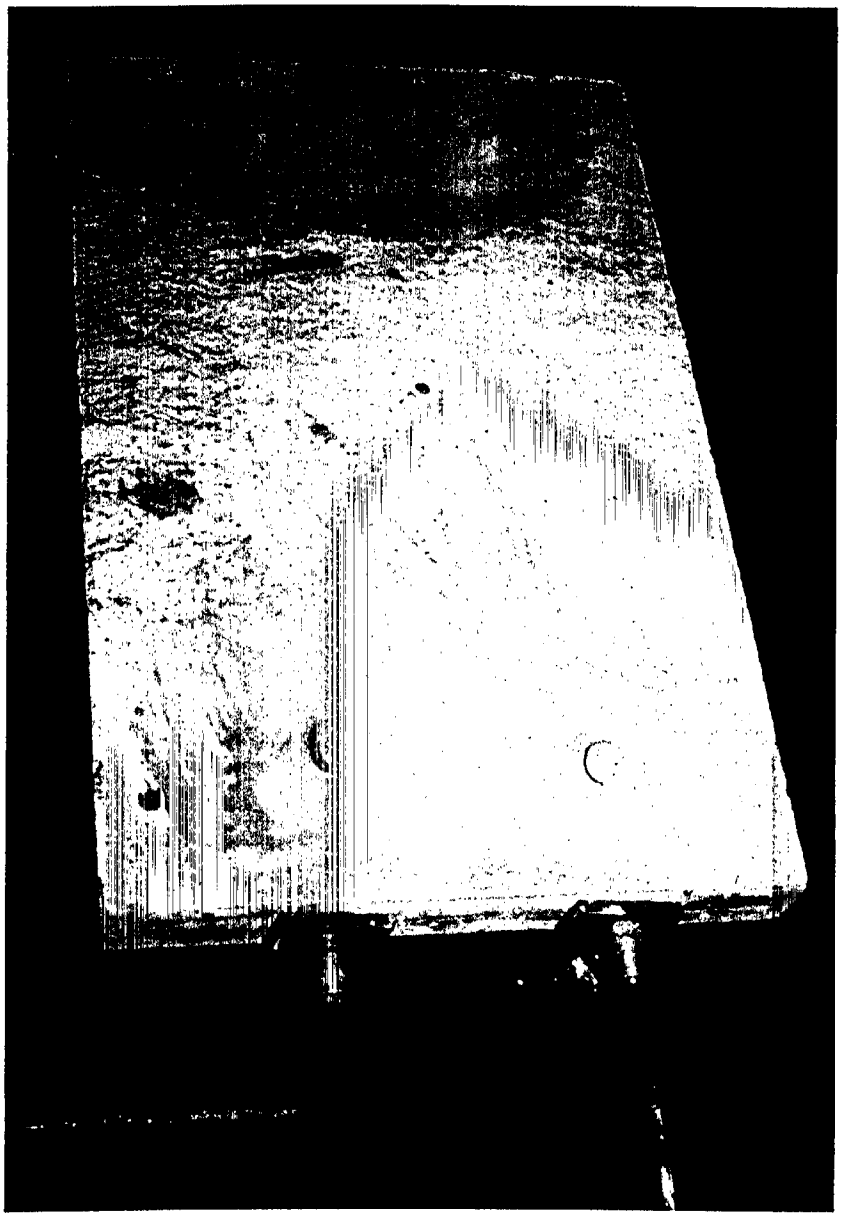

FIGURE 5.1 SMALL PRESTRESSED MODEL FOR TESTING GROUT PROCEDURES

used to bond the fresh reinforced concrete portions to the hardened prestressed concrete portion of bridge model II. The fresh reinforced concrete was placed against the prestressed concrete deck while Hi-Mod was still tacky, in between. Using this product resulted in no joints between the prestressed concrete and reinforced concrete portions, thus uniform rigidity was assured along the two-spans. The two equal-part components A and B of this product were mixed for three minutes using a low speed drill until the blend had a uniform color, and then applied by brush on the two ends of the prestressed concrete deck. Typical physical characteristics of this product was provided by the company as shown in Table 5.2

5.3.4 Steel Beams

The longitudinal steel beams were S 5 x 14.75 of G40.21-M300W grade; the transverse diaphragms had a section of S 3 x 7.5 of the same grade of steel. Mechanical properties such as yield stress, tensile strength and percentage of elongation of the longitudinal girders and transverse diaphragms were obtained from tensile coupons cut from supplied steel. These properties are shown in Table 5.3. In addition, the properties of the steel beams are given in Table 5.4. The 120-kip (533.76 KN) Tinus Olsen Universal machine was used to test the coupons at 0.025 inch per minute (0.635 mm per minute) speed until fracture occurred.

5.3.5 Stud Shear Connectors

Stud shear connectors of 0.5 inch (12.7 mm) diameter and 1.5 inches (38.1 mm) long provided by Nelson Stud Welding Division of TRW Canada Ltd. were used in bridge models I and II. The connectors were welded to the top

TABLE 5.1

PROPERTIES AND STRENGTH OF THE GROUT MIXES

MIX NO.	CEMENT RATIO WT.	WATER (RATIO) WT.	SAND (RATIO) WT.	STRENGTH (PSI)	WORKABILITY
1	1.0	1.0	0.0	3.04	Extremely fluid
2	1.50	1.0	0.25	3.20	Fluid
3	1.75	1.0	0.25	3.45	Medium to thick fluid
4	2.0	1.0	0.25	4.45	Dense grout
5	2.25	1.0	0.0	5.69	Very dense grout
6	2.50	1.0	0.0	6.53	Extremely dense grout

TABLE 5.2

TYPICAL PHYSICAL CHARACTERISTICS
FOR SIKADUR HI-MOD EPOXY ADHESIVE

COMPRESSIVE STRENGTH PSI (7 DAYS)	E PSI (28 DAYS)	BOND STRENGTH PSI (14 DAYS)	SHEAR STRENGTH PSI (14 DAYS)	TENSILE STRENGTH PSI (14 DAYS)
9,000	540,000	1,900	5,900	4,800

(1 PSI = 6.895×10^3 Pa)

TABLE 5.3 AVERAGE MECHANICAL PROPERTIES OF STEEL BEAMS

YIELD STRESS (KSI)	TENSILE STRENGTH (KSI)	PERCENT ELONGATION IN 2"
42.0	72.0	24

TABLE 5.4 ROLLED STEEL BEAM PROPERTIES

NOMINAL SIZE AND WEIGHT PER FOOT	TOTAL AREA	I_x	S_x	I_y	S_y	DEPTH d	WIDTH b	MEAN THICKNESS w	WEB THICKNESS
(LB)	IN^2	IN^4	IN^3	IN^4	IN^3	IN.	IN.	IN.	IN.
S 5x14.75	4.29	15.0	6.0	1.7	1.0	5.0	3.28	0.326	0.494
S 3x7.5	2.17	2.9	1.9	0.59	0.47	3.0	2.51	0.260	0.349

flange of the longitudinal steel beams by using Nelson stud equipment, which provided equal shear in all directions, eliminated any distortion that might result from hand welding, and permitted more satisfactory compaction of concrete around the connectors.

Nelson Company provided a complete line of stud welding system and power source to meet this research requirement. The simplest and most common procedure for locating stud positions was followed by laying them out and then center punch through holes in a templet. This method usually resulted in a good tolerance. Electric-arc stud welding is the most common process and was utilized for welding the shear connectors. The Nelson NS-20A HD, which is a heavy duty stud welding unit designed specifically to weld small diameter stud was used along with the welding gun which is a semi-automatic, lightweight, pistol shaped tool.

The stud was held in the welding gun with the end of the stud placed against the top flange. The cycle was started by depressing the trigger button start switch. The fastener is then automatically retracted from the top flange to establish an arc. The arc continued for a predetermined period of time until a portion of the stud and the top flange have been melted. The molten metal was held in place by a ceramic ferrule which also served to shield the arc. The weld metal was deoxidized by a flux in the weld end of the stud. This procedure resulted in a strong weld which developed the full strength of the stud and the top flange as was experienced in the static and fatigue push-out tests. The welding currents ranged from 250 to 3000 amps. Figure 5.2 shows the welding machine, welding gun, stud and ceramic ferrule. The mechanical properties of the headed studs are given in Table 5.5.

TABLE 5.5
MECHANICAL PROPERTIES OF HEADED STUD SHEAR CONNECTORS

DIAMETER	NOMINAL AREA	TENSILE STRENGTH	YIELD STRENGTH
(IN.)	(IN^2)	(KIPS)	(KIPS)
0.5	0.196	11.78	9.82

(IN = 25.4 mm, KIP = 4.448 KN)

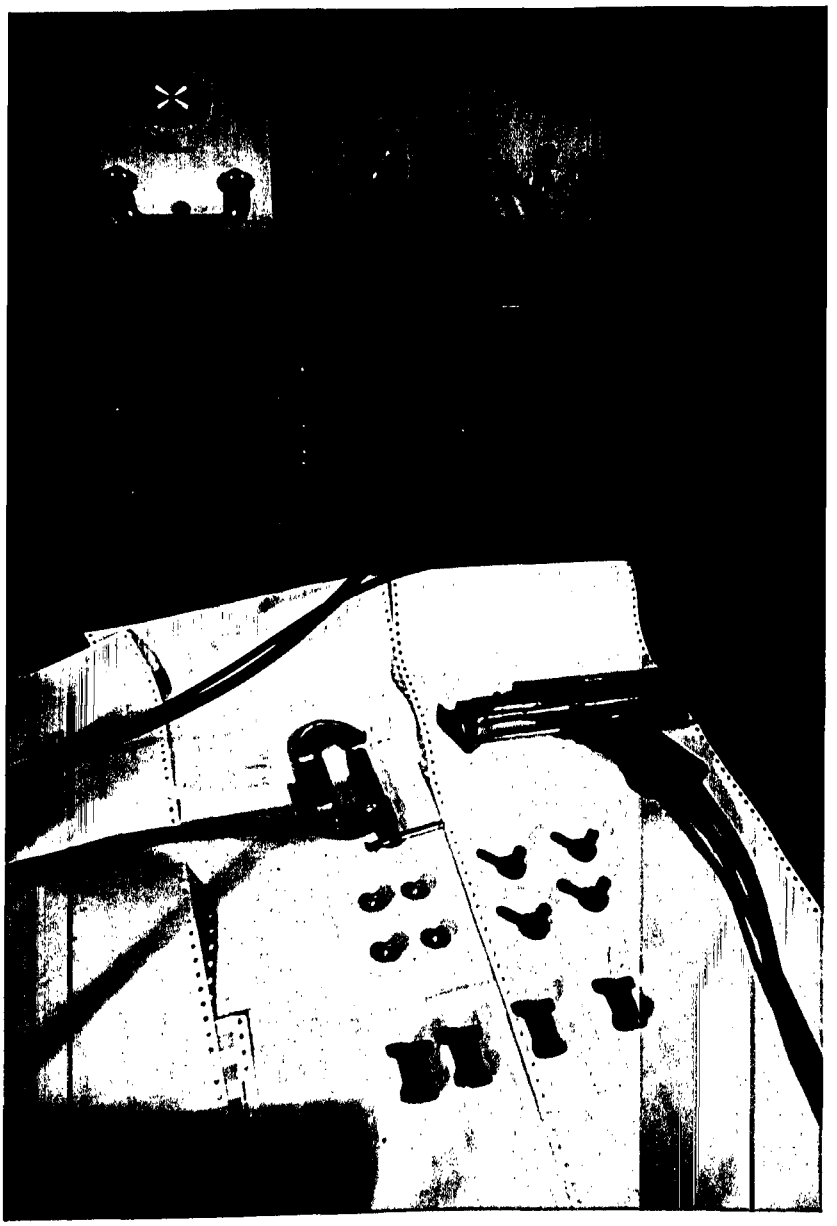

FIGURE 5.2 NELSON STUD WELDING SYSTEM

5.3.6 Reinforcing Steel

5.3.6.1 Steel for Reinforced Concrete Deck Slab

Two layers of plain mild steel bars of 3/16 inch diameter (4.76 mm) were used as reinforcing steel in the top and in the bottom of the reinforced concrete slab of bridge model I and in the reinforced concrete slab portions of bridge model II. The bars were cleaned from oil and hooks were provided at both ends for the longitudinal and transverse reinforcement. The stress-strain relationship for the reinforcing bars is shown in Figure 5.3. The modulus of elasticity was found to be 28.5×10^3 ksi (196.8×10^3 MPa) a yield stress of 78 ksi (537.8 MPa) and an average ultimate strength of 89 ksi (613.66 MPa).

5.3.6.2 High Tensile Steel for the Post-Tensioned Concrete

High tensile steel wires of 0.276 in. (7.01 mm) in diameter were used for prestressing the concrete deck in bridge model II. The typical stress-strain relationship for the prestressing steel is shown in Figure 5.4. It indicated a minimum yield stress of 190 ksi (1310 MPa) and minimum tensile strength of 236 ksi (1627 MPa). The wire exhibited a smooth surface and good resistance against slippage from the grips, in providing good control on the amount of the required prestressing force.

5.3.8 Formwork

The forms consisted of 3/4 inch (19.1 mm) thick plywood, and were supported on brackets of 2x6 inches (50.8 x 152.4 mm) and 2x2 inches (50.8 x 50.8 mm) plywood posts as shown in Figure 5.5. The brackets were spaced about three feet apart and rested on the floor. This arrangement was used

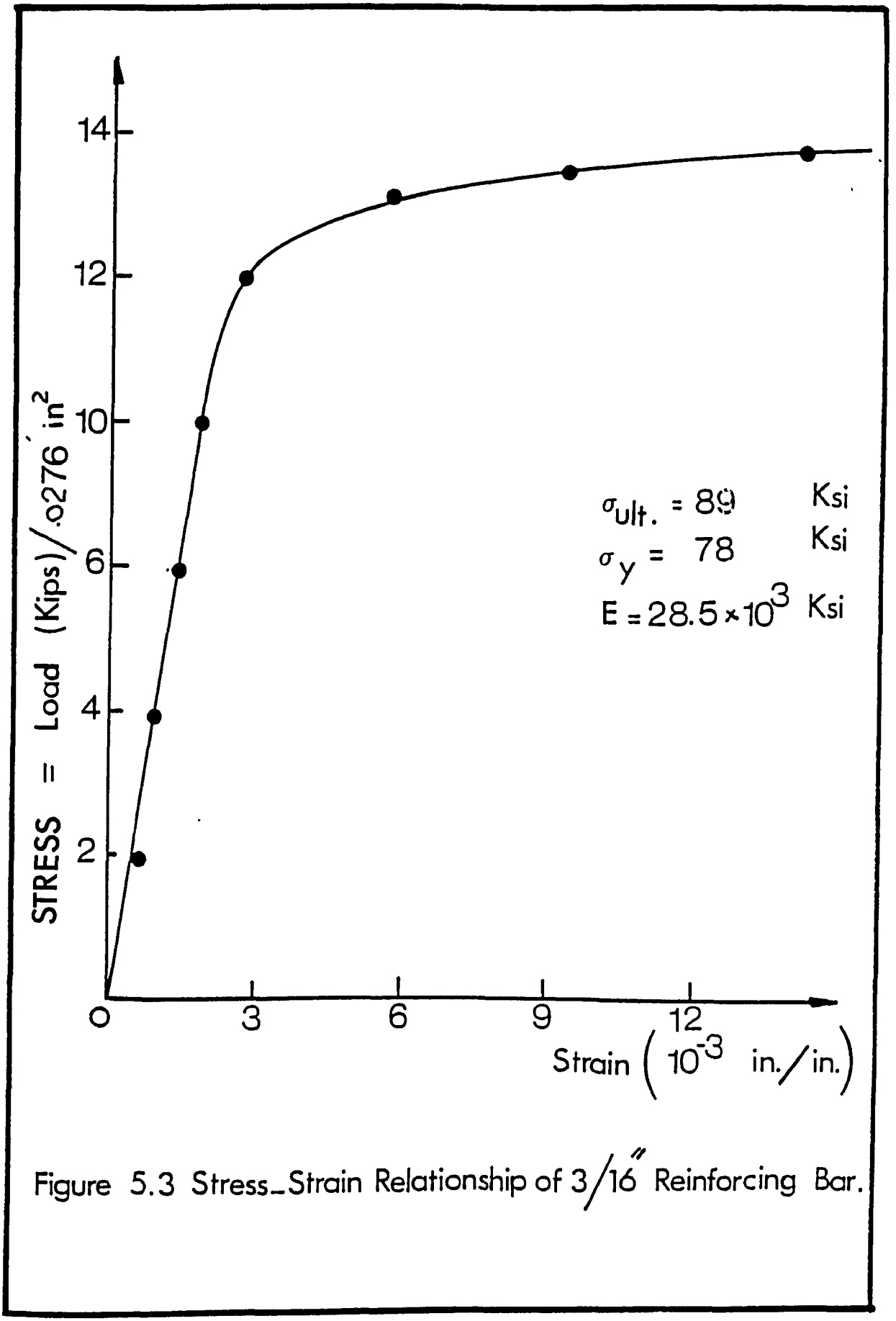

Figure 5.3 Stress-Strain Relationship of 3/16" Reinforcing Bar.

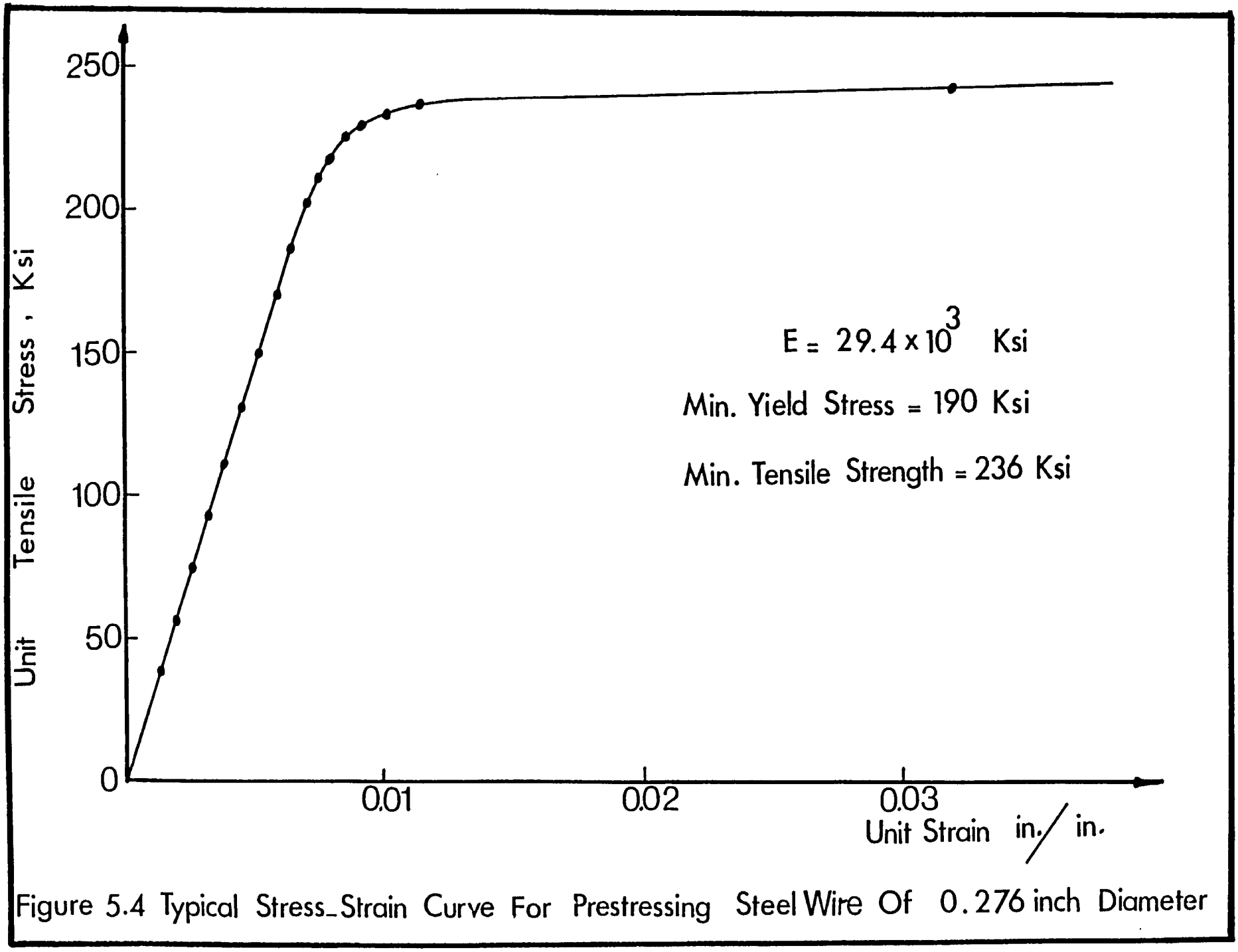

Figure 5.4 Typical Stress_Strain Curve For Prestressing Steel Wire Of 0.276 inch Diameter

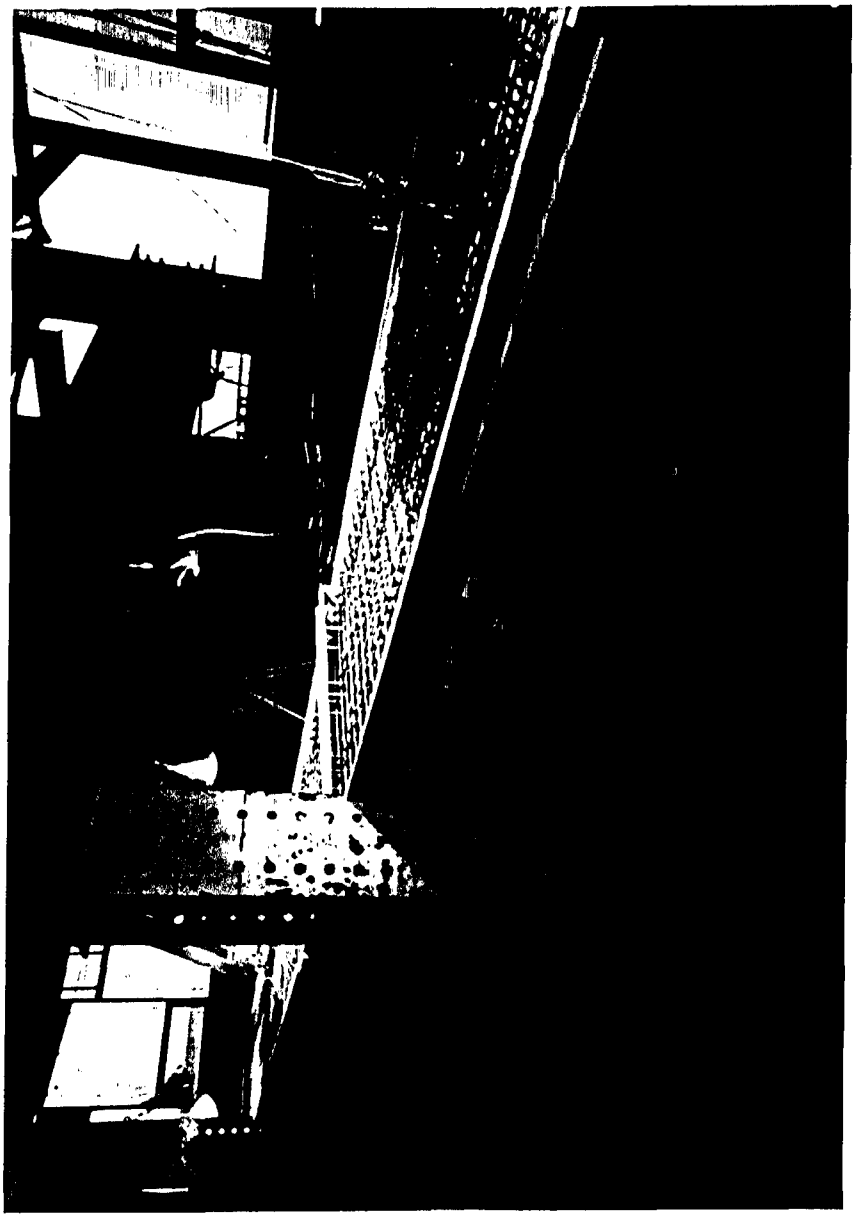

FIGURE 5.5 ARRANGEMENT OF THE FORM BRACKET SYSTEM

in both models I and II, and provided a rigid form. Figures 5.6 and 5.7 show the prestressed and non-prestressed slab formwork with the longitudinal and transverse reinforcement of bridge model II, respectively.

5.4 EXPERIMENTAL MODELS

5.4.1 Design Procedures and Construction of Bridge Model I

The model that was adopted in this investigation had two spans, each span being 12.0 feet (3.66 m) long and 3.0 feet (0.91 m) wide. Figure 5.8 shows the dimension of the cross-sections and the layout of bridge model I. The three S5 x 14.75 beams for each bridge model, together with five (S3x7.5) steel diaphragms were assembled into a single frame by fillet welding to ensure interaction between the longitudinal steel beams and the transverse diaphragms; the diaphragms were located at each support and at the middle of each span; the beams were spaced 1.0 foot (0.305 m) apart. Each beam was cut from nominal length 30-foot (9.12 m) rolled sections. The excess pieces were used to provide material for tension tests of the steel and for push-out tests. The shear connectors were welded to the top flange of each of the longitudinal beams; the shear connectors were over-designed compared to the OHBDC recommendations (53). This was necessary to test the model under resonance-fatigue.

All studs were placed in pairs and were distributed uniformly along the three distinct lengths, namely, from the support to the mid-span, from the mid-span to the point of contraflexure and from this point to the intermediate support. However, no shear connectors were located within 6 inches from the intermediate support to avoid any possible fatigue failure in the top steel flanges. Before welding the studs to the steel beams, the

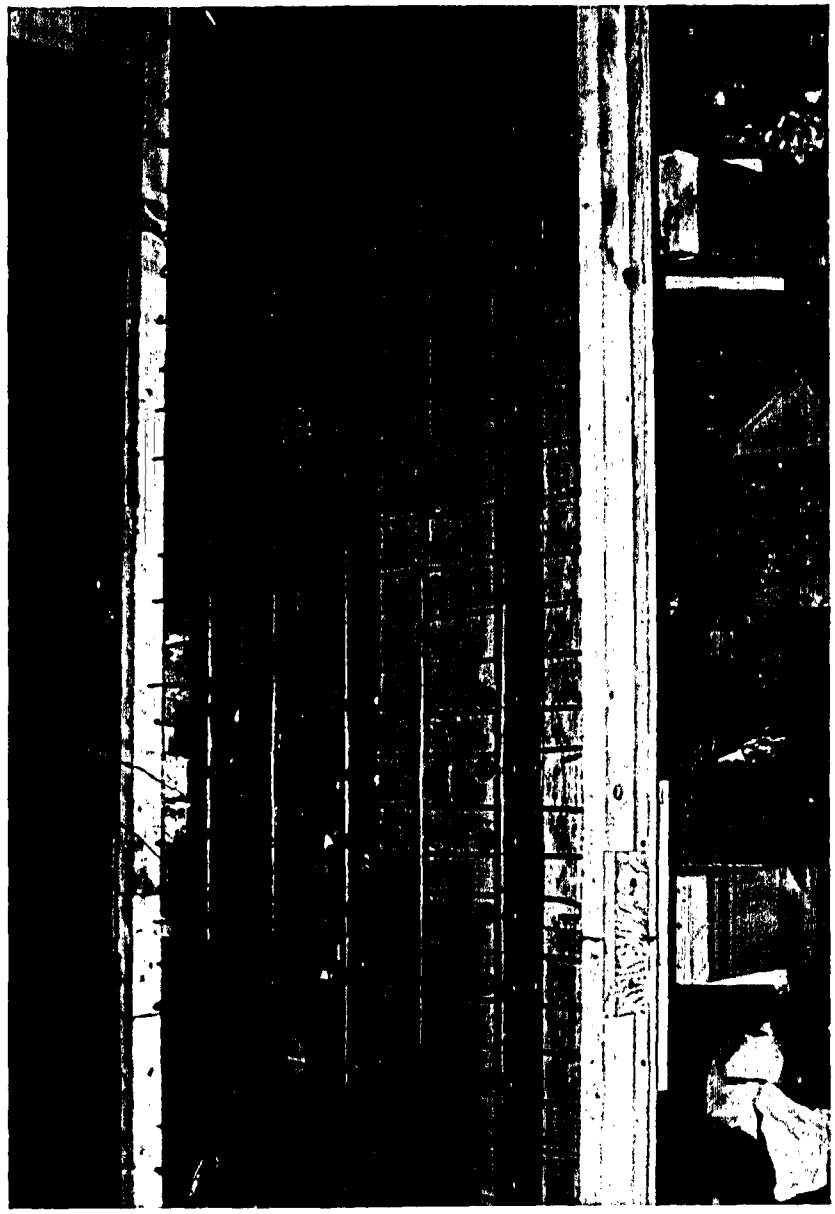

FIGURE 5.6 FORMWORK FOR PRESTRESSED CONCRETE PORTION OF BRIDGE MODEL II

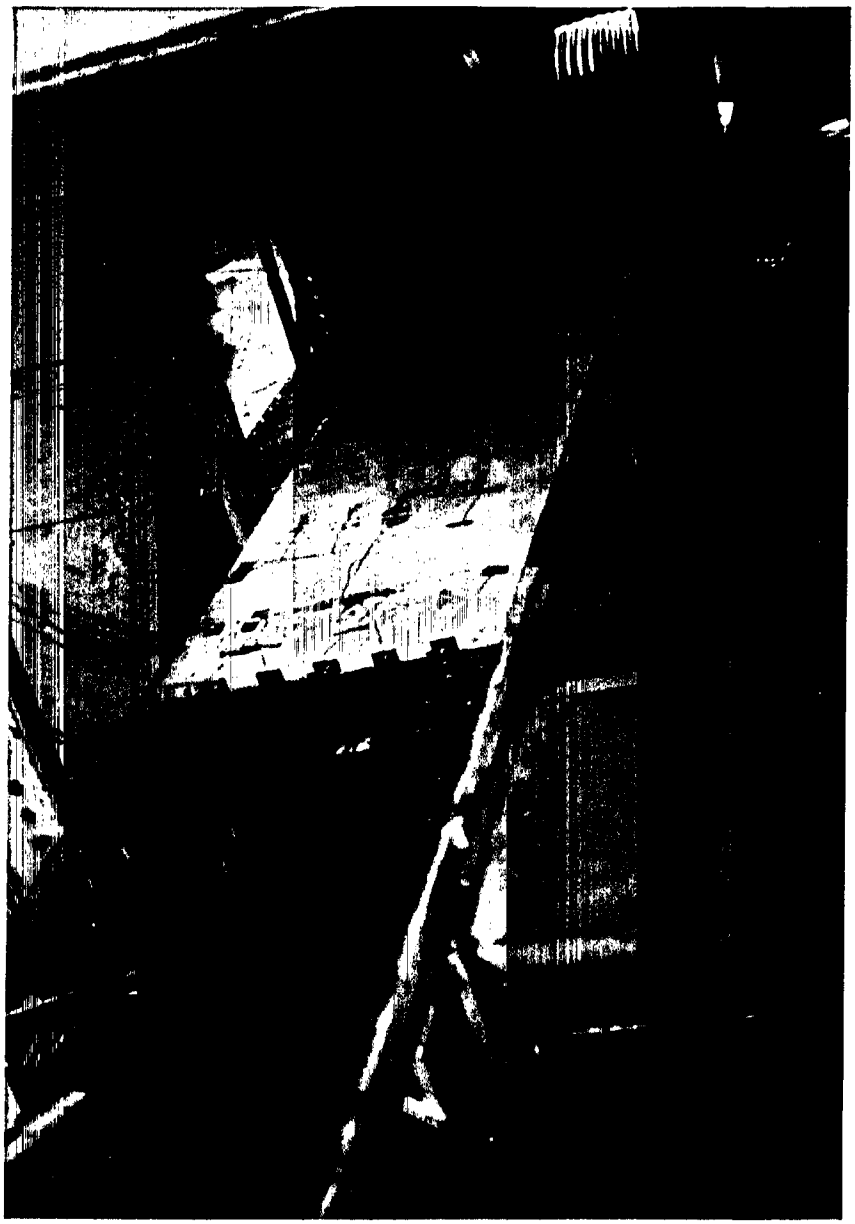

FIGURE 5.7 CLOSE-UP OF FORMWORK FOR BRIDGE MODEL II

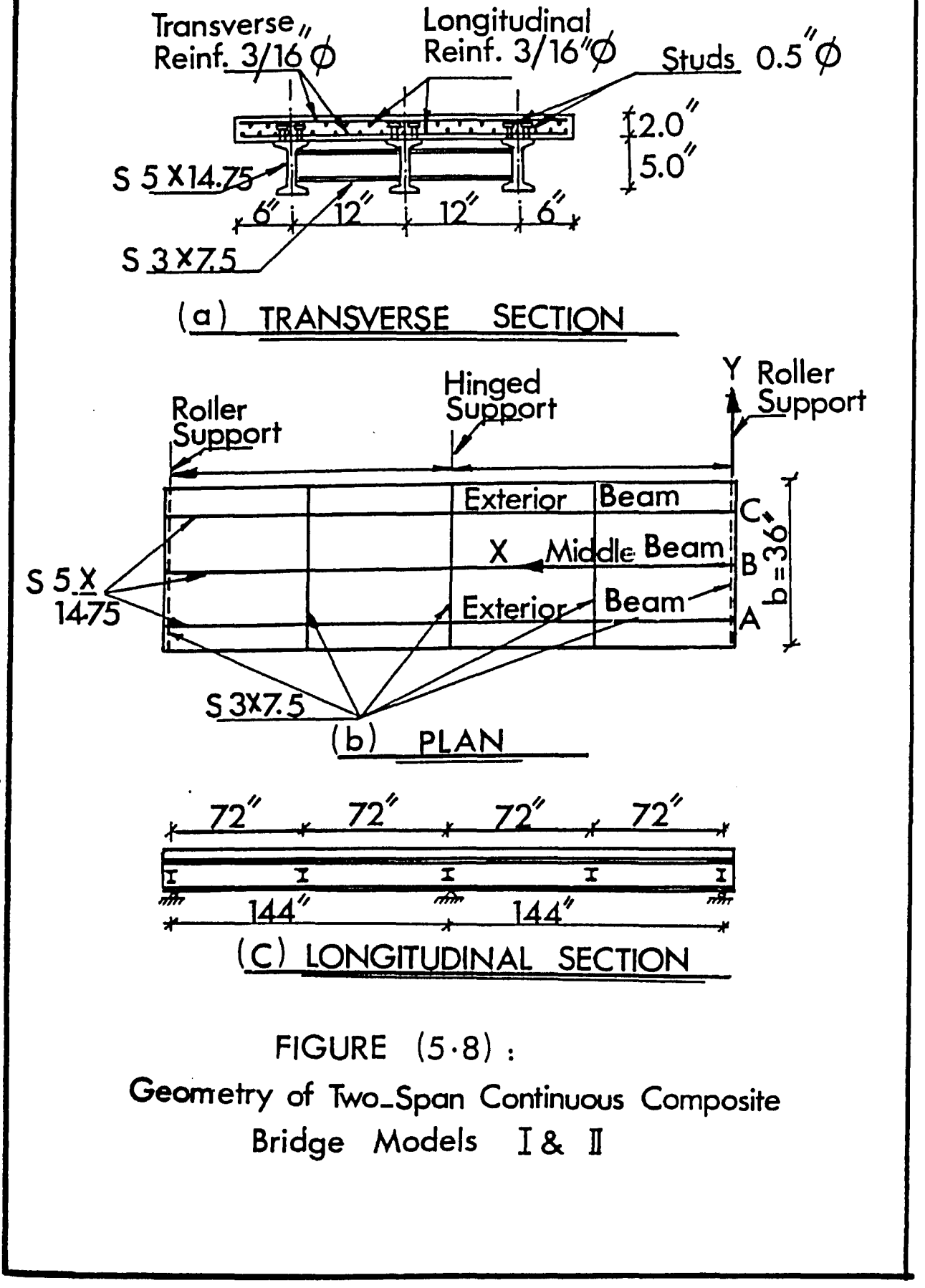

FIGURE (5·8) :

Geometry of Two-Span Continuous Composite Bridge Models I & II

welding equipment was tested and examined by welding several studs to the excess lengths of beams that were cut off. The quality of the welds was verified by Nelson Stud Welding Ltd.'s representative using standard inspection procedures. The number of the stud shear connectors was enough to ensure 100% interaction between the slab and the longitudinal steel beams.

In order to mount the rectangular base of the actuator at the middle of the span, four holes 1/2 inch (12.7 mm) in diameter were drilled in the top flange of the longitudinal steel beams. Care was taken to locate the holes properly with the actuator base bolts. Since these holes were to be through the depth of the concrete deck, extreme care was taken to ensure that the holes were square (perpendicular) to the concrete surface so that no distortion would occur with the actuator mounted.

The required forms were prepared and then painted with three layers of grease material, Vitrea oil 150, for easy form release after the concrete had hardened. Since it was realized that the dynamic and resonance fatigue loading would impose high tensile stresses in the slab, the area of the longitudinal steel reinforcement was made approximately three percent of the transverse cross-sectional area of the concrete deck, in order to maintain the integrity of the slab; two layers of steel were provided. Furthermore, since the model would be subjected to torsional mode of vibration, it was decided to provide an area of transverse reinforcement equal to four percent of the longitudinal cross-section. The transverse reinforcement was also placed in double layers (55). The longitudinal and transverse reinforcements were supported on steel wire chairs which provided a clear cover of 0.25 inch (6.35 mm) from the bottom face of the

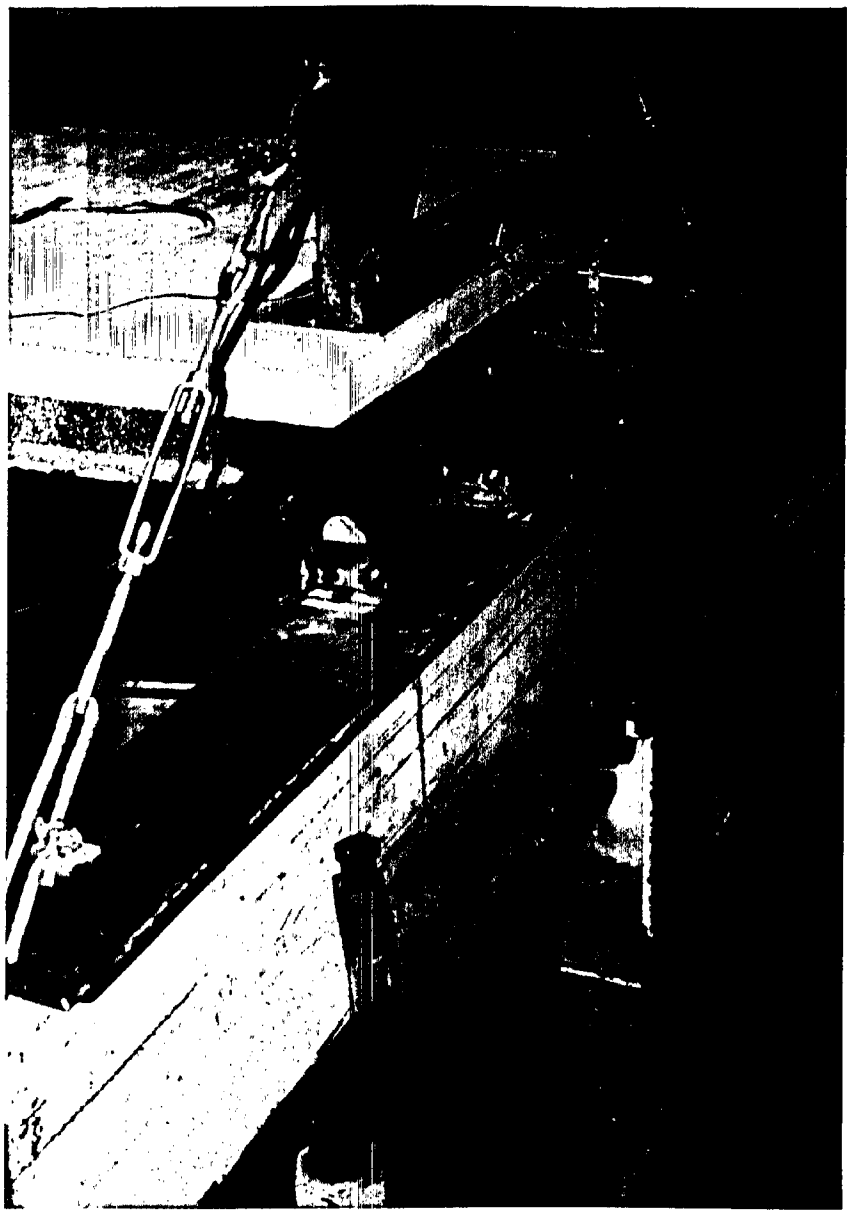

FIGURE 5.9 TIE-DOWN SYSTEM FOR BRIDGE MODELS I AND II

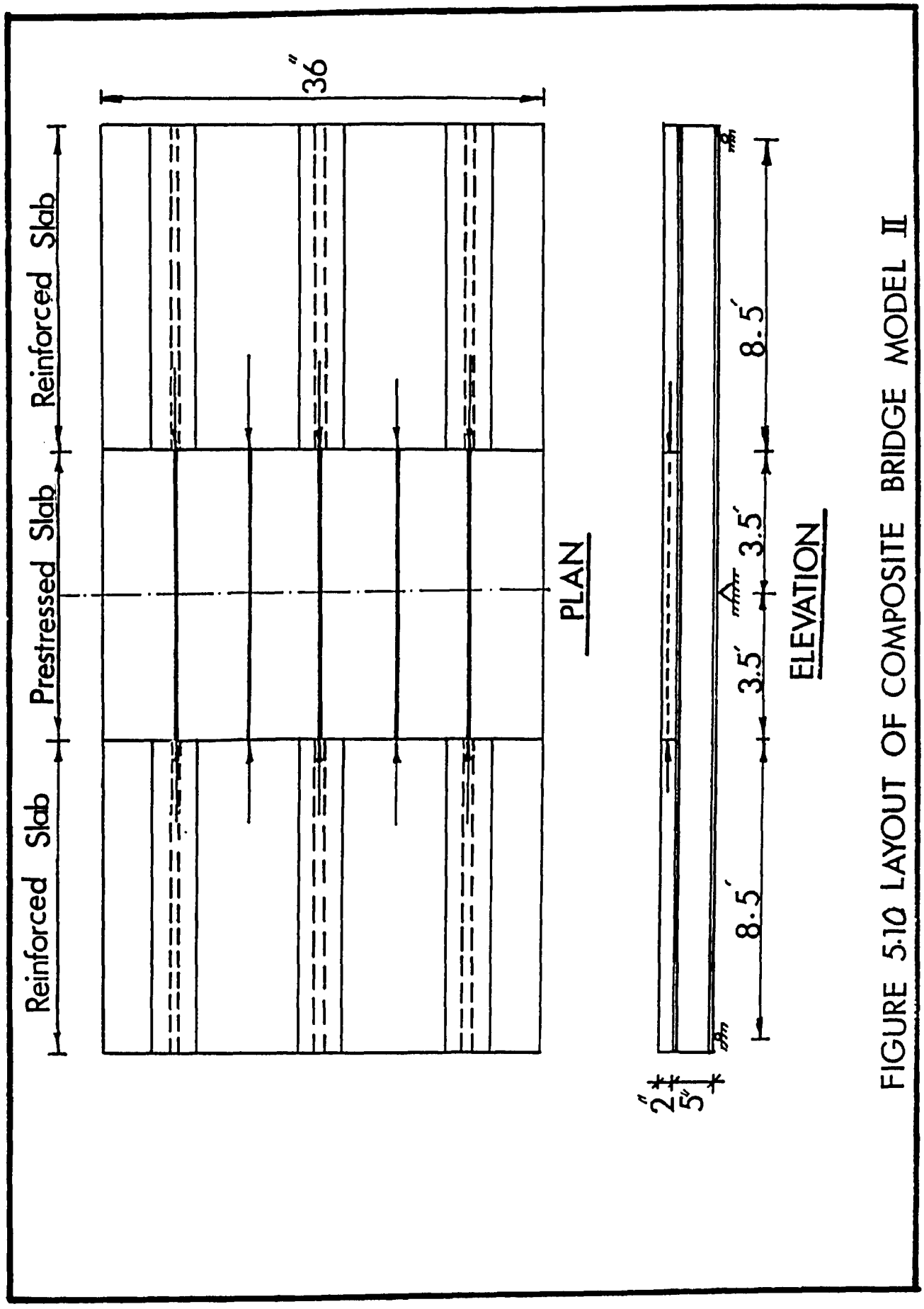

FIGURE 5.10 LAYOUT OF COMPOSITE BRIDGE MODEL II

slab deck. Air-entrained concrete mix of 4,000 psi (27.58 MPa) compressive strength was used; concrete placement began at one exterior support and progressed to the other exterior support. Compaction was accomplished by using a high frequency needle vibrator. In addition, tamping rods were used to tamp the sides; to avoid honeycombing, the sides of the forms were lightly hammered. The final finish and smooth surface were obtained by hand troweling. Twenty-four hours later the forms were removed. To determine the compressive strength of the concrete, seven 3x6 inch (76.2 x 15.24 mm) cylinders were cast at the time of placing the concrete slab. Both the slab and the seven test cylinders were moist-cured for seven days with the exposed surface covered with wet burlap and a polyurethylene sheet. Then the model deck and the test cylinders were allowed to cure under dry conditions for at least seven days. In order to avoid any uplift at the supports, the model was tied down to the transverse supporting beams through steel cables, the transverse supported beams were clamped to the supporting steel bases which were bolted to the ground floor. This is shown in Figure 5.9. It should be noted that the end supports provided translation and rotation freedom while the intermediate support provided translational constraint.

5.4.2 Design Procedure and Construction of Bridge Model II

The dimensions of bridge model II and layout of the prestressed and nonprestressed concrete portions are shown in Figure 5.10. It should be noted that bridge models I and II are exactly identical except bridge model II had a prestressed concrete deck around the intermediate support. Furthermore, the number of connectors in bridge model II was 50% less than

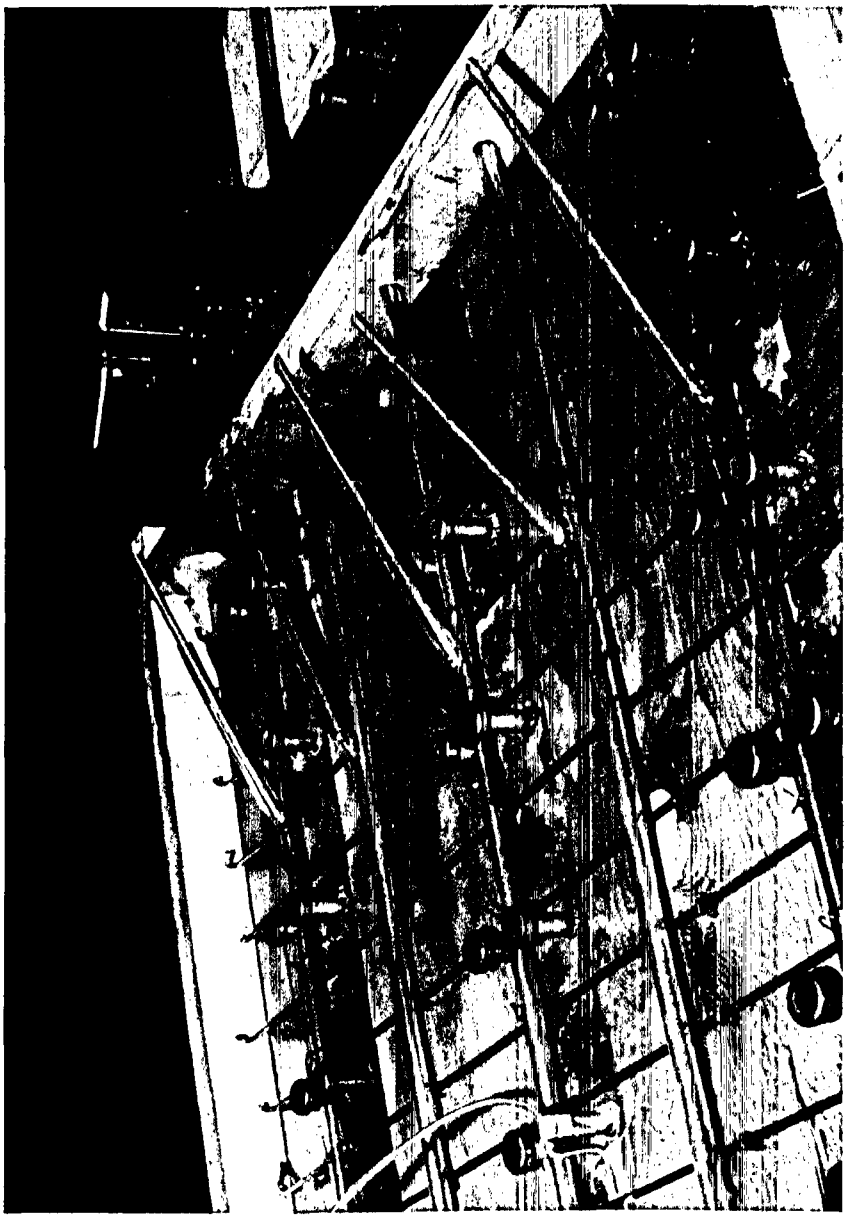

FIGURE 5.11 RUBBER HOSES USED AS CONDUIT FOR PRESTRESSING WIRES AND GROUT PURPOSE

FIGURE 5.12 PRESTRESSED CONCRETE PORTION OF BRIDGE MODEL II AFTER GROUTING

FIGURE 5.13 INSTRUMENTED STUD SHEAR CONNECTORS IN THE VICINITY OF THE PRESTRESSED CONCRETE PORTION OF BRIDGE MODEL II

that provided in bridge model I, following the OHBDC recommendations (53). The same procedures were followed as in bridge model I to connect the main beams with the diaphragms, and the connectors to the top flange of the main beams.

Rubber hoses having an inner diameter of 0.25 inch (6.4 mm) and 0.375 inch (9.5 mm) outside diameter were used as conduits for the prestressing wires and grout, as shown in Figure 5.11. Five prestressing wires were used for prestressing the slab in the negative moment region. The five rubber hoses were placed at the mid-depth of the slab, transverse top and bottom reinforcement in the slab were also used. Eight hours after placing of the air-entrained concrete of 6,000 psi compressive strength, five cores were created by withdrawing the rubber hoses without much effort because of the lateral shrinkage of the rubber under the pull force. In order to maintain the rubber hoses straight during concreting, they were stiffened internally by inserting steel bars in the hoses. Steel chairs were used at 12.0 inch (304.8 mm) intervals to maintain the rubber hoses in position during concreting. After seven days of water curing, the slab was allowed to dry for 7 days. The prestress force, applied to the slab after it gained the desired strength (Figure 5.12), was applied in two stages to minimize the prestressing losses due to jacking and elastic shortening. The length of the prestress wires was about 20 feet (6.1 m), which provided sufficient embedment length in the non-prestressed portions of the slab.

In order to place the prestress jack in the right position for prestressing the slab, eight studs on each steel beam on one side of the slab were sawed off to 1/4 of their height. Then six longitudinal steel

rods, each 2 feet (609 mm) long, were welded to the top of the remaining portions of the studs after the slab was successfuly prestressed to complensate for the removed portions.

Cement grout was injected through a prepared hole on the top of each conduit; the injection was applied at one end of the slab until it was forced out of the other end. To ensure good bond, grouting under pressure was made using a strong spring-loaded oil gun. After the grout was discharged from the far end, that end was plugged and the pressure was applied once again at the injecting end. This procedure ensures that the grout was compacted.

A formwork was prepared to cast the right and left parts of the non-prestressed concrete slab; the reinforcement arrangement was similar to that in bridge model I. In order to bond fresh concrete to hardened concrete, the prestressed concrete side surfaces were first cleaned by using sand blasting, and then by using a brush three layers of Sikadur Hi-Mod were applied to each side surface of the prestressed concrete. The procedures for casting and curing the reinforced concrete slab portion were the same as described earlier.

5.5 VIBRATION EXCITATION SYSTEM

An important decision that needed to be made in planning the dynamic and fatigue testing program was the type of excitation that was to be used, to produce measurable motions within a reasonable frequency range. To perform such dynamic and fatigue tests on the two bridge models, it was decided to use the excitation supplied by the Gilmore closed-loop electro-hydraulic system with modifications. The excitors were constructed by

turning the actuators upside-down and attaching weights (steel blocks) to the top of the pistons. This modified (Gilmore) rebuilt structural system in conjunction with the electronic console unit provided complete control of the stroke and the frequency range required and imposed by the nature of the dynamic and fatigue tests. The same arrangement was used successfully elsewhere using an MTS product (55).

5.5.1 Attached Moving Weight

A total of 600 lbs. (2.66 KN), weight made of six 12x12x2 inch (305 x 305 x 5.1 mm) steel plates of 100 lbs. (444.8 N) each was used as a moving mass for all the fatigue and dynamic tests. The dynamic or fatigue forces were adjusted by adding or removing part of the moving mass, since the dynamically imposed force is a function of the mass and the acceleration of the actuator rod.

5.5.2 Modified Actuators

Gilmore 20-kip (88.9 KN) hydraulic actuators were used in testing both bridge models. The actuator was bolted down to the top flange of the middle steel beam at the mid-span of the model. The attachment was made by means of four 1/2 inch (12.7 mm) diameter high-strength bolts and one steel plate on the top of the concrete deck. Hydra-stone was used to level the steel plate. The bracing system was made of four adjustable length channels of 2x1.5x0.25 inches, and were welded to a square steel plate mounted on the top of the concrete deck and bolted to the top flange of the two exterior beams by means of four 1/2 inch (12.7 mm) high-strength bolts through the depth of the slab. Figure 5.14 shows the support arrangement

and the attachment system for the 20-kip (88.9 KN) servo-controlled hydraulic actuators. The location of the excitor was chosen with extreme care to ensure that it would not be located on a mode line and therefore will not be able to excite the associated mode. One actuator carrying 600 lb. (2.6 KN) moving mass was used in testing bridge model I while two actuators, each carrying a 600 lb. (2.6 KN) moving mass, were used for testing bridge model II.

5.5.3 Gilmore Hydraulic and Electronic Control System

Unfortunately, Gilmore Industries, Inc. was out of business and the author had to search all over Canada and the United States for the necessary parts that were required to repair and use the system efficiently. Several parts were replaced in the hydraulic section, such as tuning up the two actuators, flush and clean the oil pump, and reclamp properly all of the hydraulic lines. Furthermore, the amplifier had to be replaced.

The Gilmore structural loading system consisted of three main sections, namely: 1) Two actuators, model 433-20, each one included a position transducer, a velocity feedback transducer and a load cell; 2) The hydraulic pump of 20 GPM, and 3) Control console unit, which included the servo-amplifiers, signal conditioners, rate programmer and the control push buttons.

The electronic console unit, after being repaired, was functioning as a closed-loop (feedback) system. The servo-amplifier controlled the servo-valve of the actuator, the rate of flow of oil into the actuator, the static set point, gain and damping.

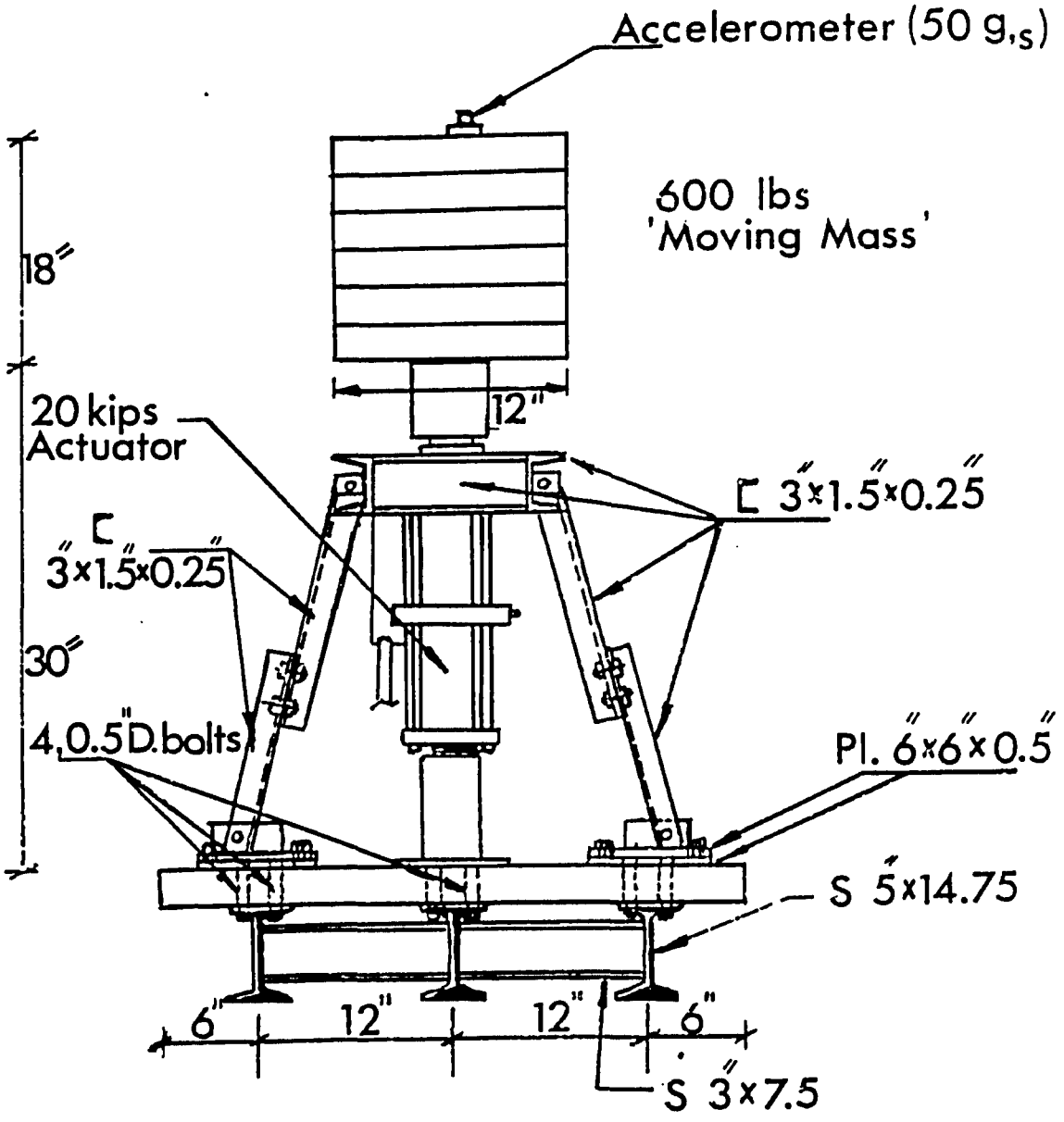

FIGURE 5.14 Support Arrangement For 20-Kip Actuator

Model 416 position signal conditioner controlled the mode of the actuator through the gain and phase adjustments and the LVDT output signal was fed to the servo-amplifier. Model 429 function generator was used to generate the required wave function. The available dynamic frequency range was between 1 and 34 cycles per second.

Three controlled parameters were used to control the exciting force such as the moving mass, the stroke of the hydraulic actuator and the excited frequency, including the option to use either 10%, 20%, 50% or 100% of the full capacity of the actuator. Figure 5.15 shows the connected actuator and the moving mass.

5.6 PRESTRESSING EQUIPMENT

Ten end bearing steel plates 2 x 1-3/4 inches (50.8 x 44.5 mm) of 1/2 inch (12.7 mm) thick with holes of 0.3 inch (7.62 mm) diameter were used at both ends of the prestressed wires in bridge model II to distribute the prestressing force from the wires to the concrete slab, as shown in Figure 5.16. A hydraulic jack of 20-kip (89 KN) capacity and mechanical gripping devices of the open grip type were used for post-tensioning. The prestressing equipment was manufactured by Cable Covers, Ltd., England.

5.7 INSTRUMENTATION

5.7.1 Introduction

During the planning of the dynamic and fatigue tests, consideration was given to the purpose of the tests, the instrumentation, the analytical method to be used for data reduction and its compatibility with the instrumentation and the final use of the information generated. It was

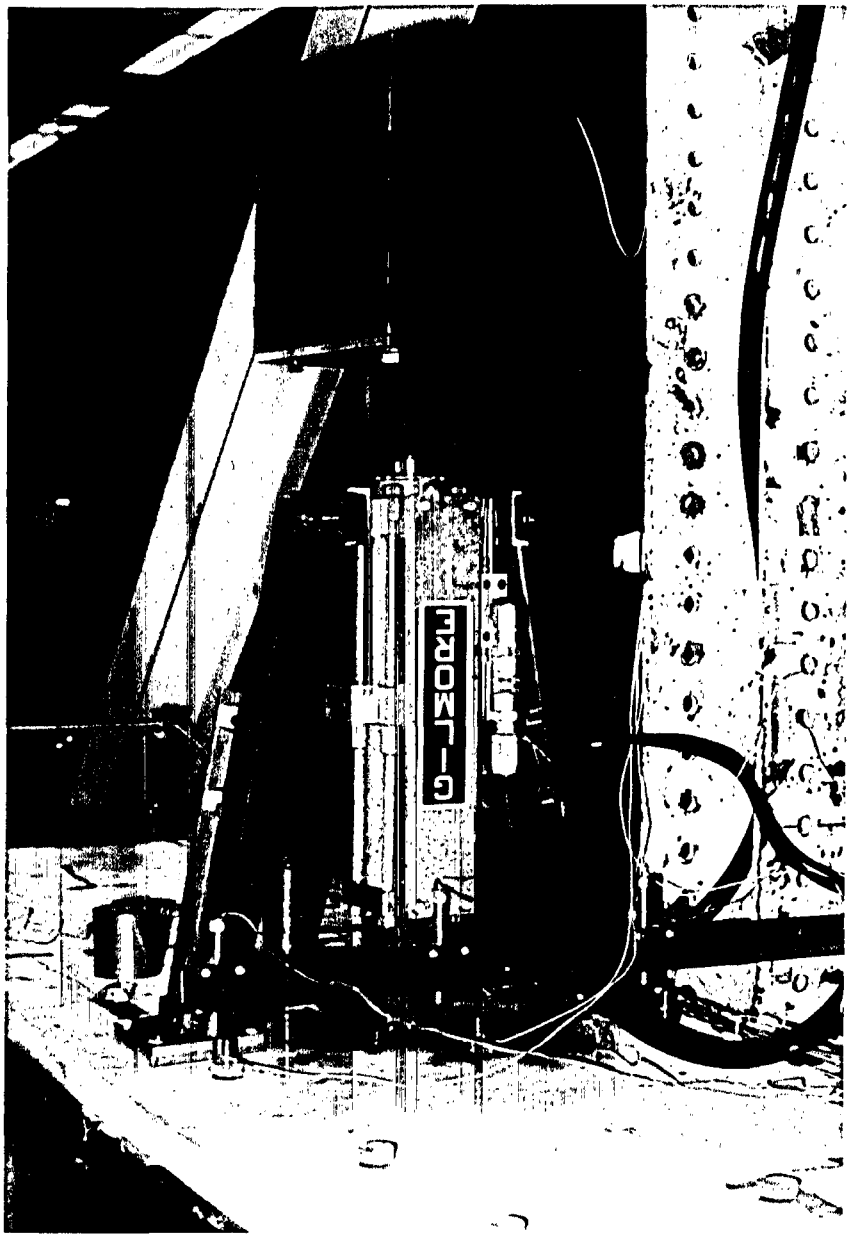

FIGURE 5.15 20-KIP HYDRAULIC ACTUATOR CARRYING 600 LB. "MOVING MASS".

FIGURE 5.16 END BEARING SYSTEM, BRIDGE MODEL II

possible to obtain useful and meaningful data with the simplest set of instrumentation when appropriately deployed. The scope of the measurement program was clearly outlined from the beginning and the temptation to measure and record everything was eliminated. A programmable monitoring program such as the initiation of the recording process based on a predetermined trigger level of a signal was used during the fatigue tests on bridge models I and II. Only few dynamic measuring points were needed to be monitored continuously, since these points could be related to the model properties. A digital recording technique was used to permit simultaneous sampling of a large number of channels (64 channels were used). Extreme care was taken to shield the used cables and ground the components so as to avoid pickup of electrical noise.

Four different types of electronic transducers were utilized during the dynamic and fatigue tests of two models. These sensors consisted of piezoelectric accelerometers, D.C. differential transformers, linear variable differential transformers and dynamic-fatigue steel and concrete strain gages. Besides the electronic transducers, two Megadac 2000 data acquisition systems of 64 and 16 channels each were used in recording and transmitting the data to an IBM Personal Computer, and then to the main computer of the University of Windsor. Interfacing between the data acquisition system and the personal computer was made by means of an RS-232C electronic card. Necessary software for controlling and programming the data acquisition as well as transmitting the data was developed.

The following sections describe each type of the four transducers, the circuits connection that was used and the locations of the transducers

throughout the dynamic and fatigue tests. Figure 5.17 shows the data acquisition system connected to all the sensors used on the two bridge models.

5.7.2 Megadac 2000 Data Acquisition System

The Megadac data acquisition system embodies numerous options. Some of these options were useful during the dynamic tests and some were most useful during the fatigue tests and prestressing the slab. The system has a maximum sampling rate of 20,000 samples per second. However, only 160 to 600 samples per second were required throughout the tests; it has a capacity of 128 channels, but only 64 channels were used. Signal conditioning and bridge completion modules including constant current and constant voltage energization were used to energize the strain gages, the LVDT's and the DC DT. A high and low alarm level was set on individual channels for real time monitoring during fatigue tests. Data was captured and stored on a 300-foot (91.5 m) long magnetic tape cartridge. The capacity of the 300-foot (91.5 m) magnetic tape was about 32 mega bits (14 x 10^6 samples). This allowed a continuous recording for about 30 minutes. However, a 600-foot (183.0 m) magnetic tape of 67 mega bits (32 x 10^6 samples) was used for longer time recording periods.

Furthermore, the front panel keyboard and display were most useful to allow the megadac to function as stand-alone device without the computer host. Four high speed analog to digital input modules of 16 channels each (AD-1614D) with differential inputs and 15 input scaling ranges with a maximum system gain of 400:1 were used. Eight signal conditioning modules

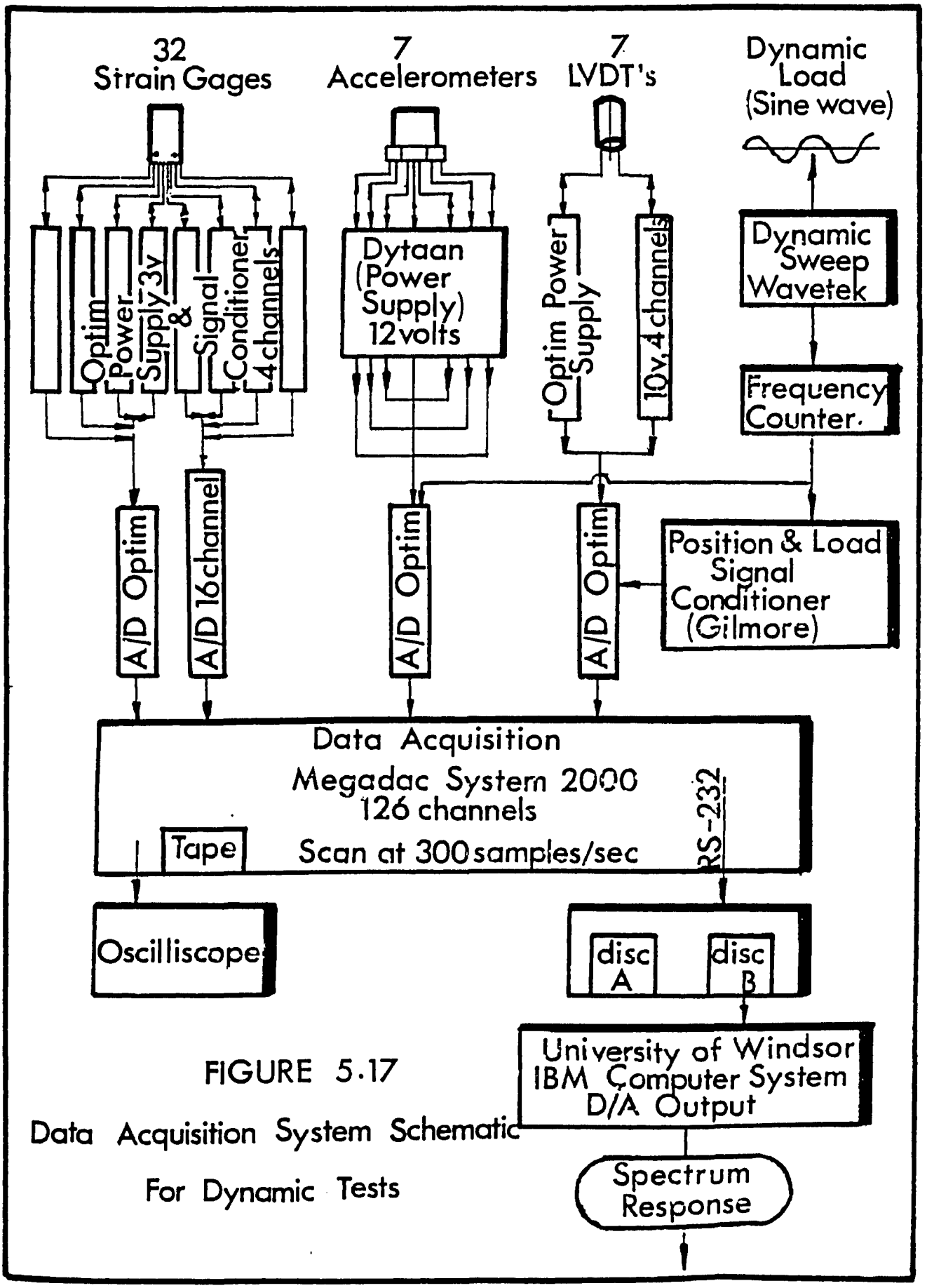

FIGURE 5.17

Data Acquisition System Schematic

For Dynamic Tests

of 4 channels each (SCI-884/350) with a twin constant current source of 3.50 mA per arm were used for connecting 32 strain gages. They have internal quarter bridge completion for 350 ohms gages, allowing connection of quarter, half and full bridges. Another four signal conditioning module (SCV-884) of four channels each were used in connecting the linear variable differential transformer and the D.C. differential transformer. These modules have a constant voltage output per channel, with excited voltage of 4, 6, 8 or 12 volts. They were designed only for a full bridge type transducer.

The 64K buffer memory in the Megadac mainframe allowed continual sampling with the parking of data in the memory awaiting transfer. However, during the fatigue tests, it allowed storing and overwriting continuously until an alarm was sounded.

The Megadac was controlled by the host IBM Personal Computer via an RS-232-C interface by sending different commands to the system. However, in the absence of the host computer, it was controlled through the keys on the front panel.

In order to operate the Megadac, three tables were initialized through its software. These tables were Mode Table, Scan Table and Scan Entries Table. The Mode Table was used to establish the communication profile with the host computer, while the Scan Table was used to specify and designate scanning and sampling parameters.

The scan entries contained the most important information pertaining to the mapping from hardware ports to positions in the recorded data files. Through the scan entries the high strain and acceleration limits were imposed and these were used for starting and stopping the recording

process. A 19.2K Baud Rate was used while the R-232-C port was operating. High resolution of 12 bits was used during the recording. More details regarding recording and transmitting data from the data acquisition system to a floppy disk through the host computer and from the floppy disk to a hard disk on the University of Windsor computer main frame can be found in Appendix D.

Figure 5.18 shows a schematic circuit diagram for connecting full bridge current energization which was used for the prestressed load cell, while Figure 5.19 shows the circuit of voltage energization that was used for all of the LVDTs and DCDTs. Furthermore, Figure 5.20 shows the quarter bridge 3-wire connection utilized for all of the concrete and steel dynamic-fatigue strain gages.

Four terminal boxes were designed and built so that the circuit connections for accelerometers, LVDTs and strain gages would be easy, simple and straight-forward. The author had the opportunity to design these terminal boxes, with the guidance of Dr. G. R. Monforton, to be compatible with the Megadac data acquisition and any type of sensors. These boxes comprised of: (1) an A/D box of 144-gold plated terminal representing four A/D modules of 16 channels each; (2) an SCV box of 72-gold plated terminals which represent four SCV modules of 4 channels each, and (3) two boxes of SCI-I and SCI-II with 64 gold plated terminals each, representing the 8 SCI modules of 4 channels each. All of the wires of each box were gathered in one large diameter cable connected at its end by a 37-pin connector "male type", which was compatible with the female type connection at the back of the data acquisition system. Furthermore, these boxes were connected together externally by means of 48-pin ribbon

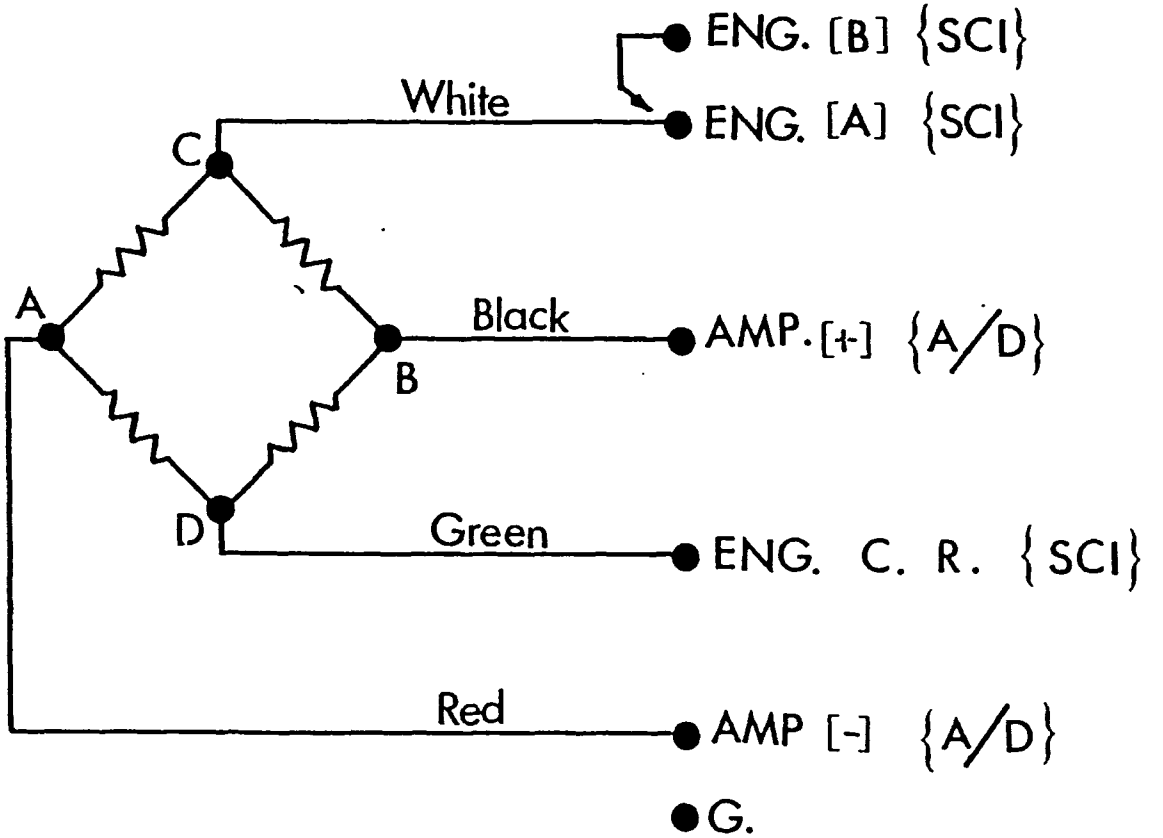

Figure 5.18 Schematic Circuit Diagram For Full Bridge Current Energization

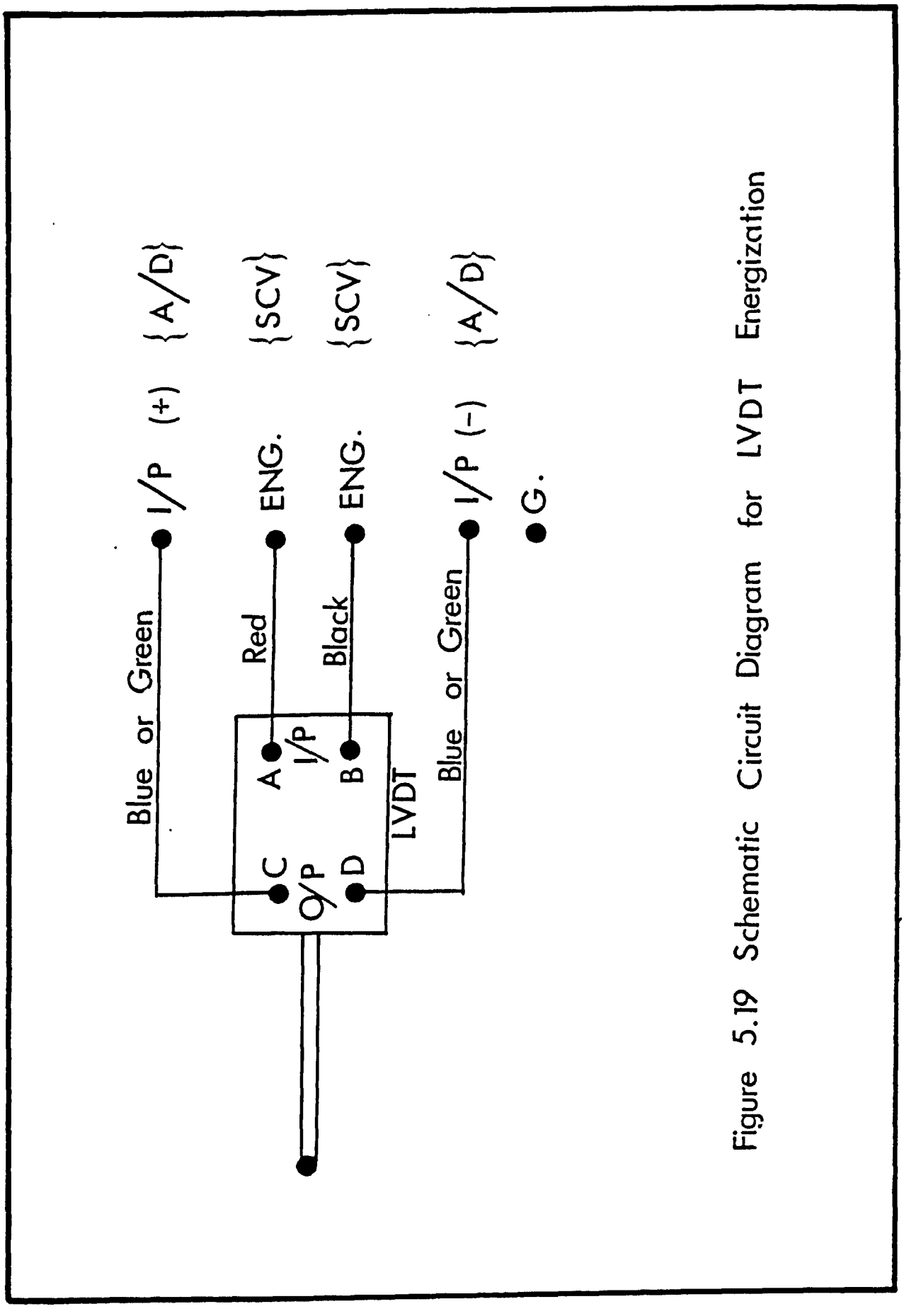

Figure 5.19 Schematic Circuit Diagram for LVDT Energization

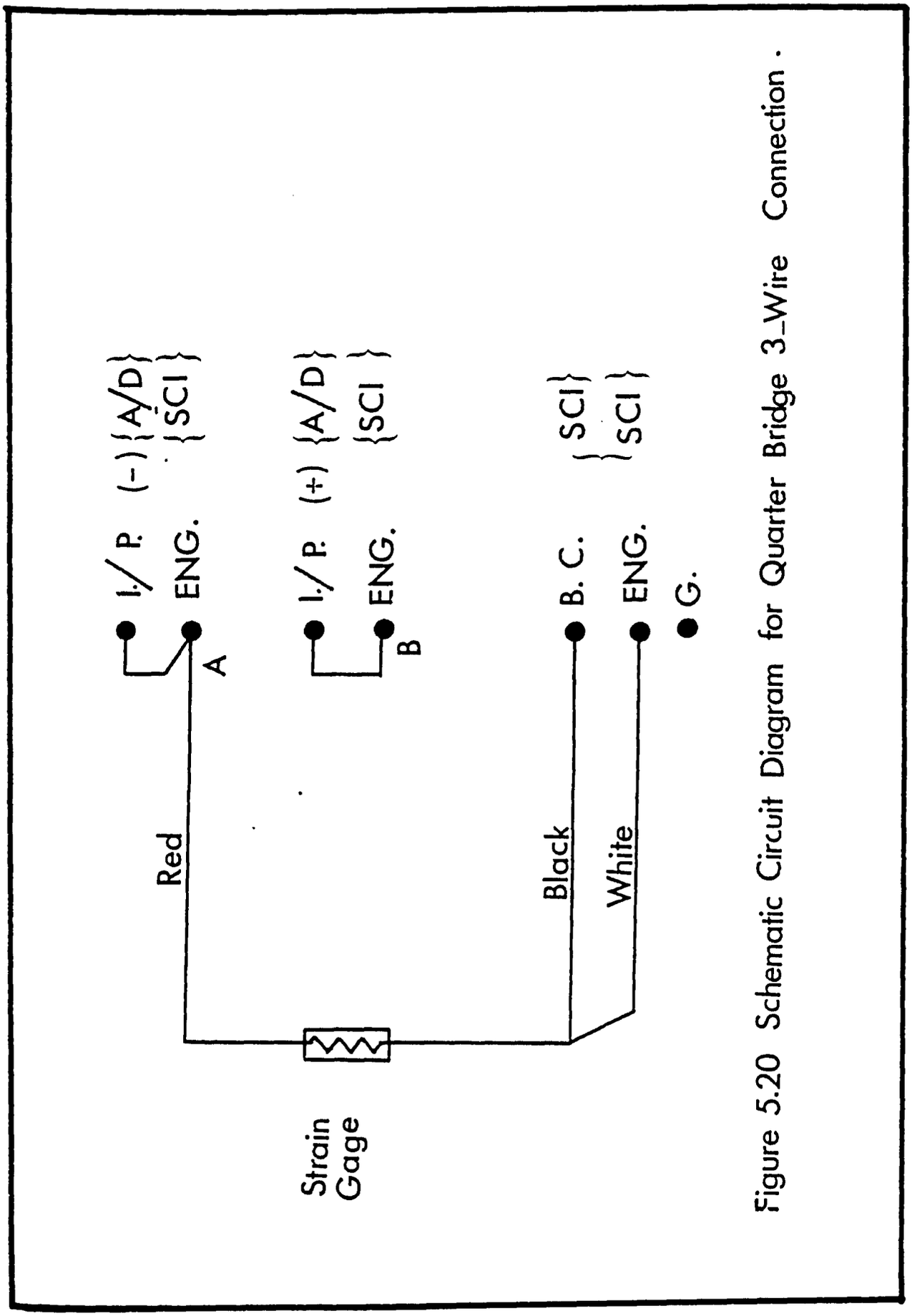

Figure 5.20 Schematic Circuit Diagram for Quarter Bridge 3_Wire Connection.

connector to achieve any circuit connection for any type of application. All connections and construction of the boxes were done with the help of the Electronic Design Centre at the University of Windsor.

5.7.3 Piezoelectric Accelerometers

Six piezoelectric "Dytran" Model 3100A 25g accelerometers were used throughout the dynamic and fatigue tests, as shown in Figure 5.22; one 50g accelerometer was used on the top of moving mass to sense the absolute acceleration of the actuator rod, as shown in Figure 5.21. The accelerometers were self-generating quartz crystals and a seismic mass to convert acceleration to an analogous, low impedance, electronic signal. The acceleration acting upon the base of the accelerometer was transferred to the seismic mass through the crystals creating a force equal to the acceleration times the mass in accordance with Newton's Second Law of Motion; this released some of the preload force on the crystal generating a voltage proportional to the acceleration. Each accelerometer had an IC built-in amplifier. The voltage output range was between ± 5 volts, while the sensitivity was about 100 mv/g over a frequency range of 1 to 3500 Hz at 0.5 dB. To install these accelerometers properly on the surface of the concrete deck of the bridge models, 1.0 inch (25.4 mm) diameter plexi-glass mounting locks with a smooth clean surface were used so that the base of the accelerometers were in intimate contact with the plexi-glass mounting block surface. The mounting blocks were attached to the top of the concrete deck by means of 5 minute epoxy glue. Care was taken to develop sufficient flatness on the concrete surface at each accelerometer location by spotfacing and grinding. This was necessary to avoid straining the

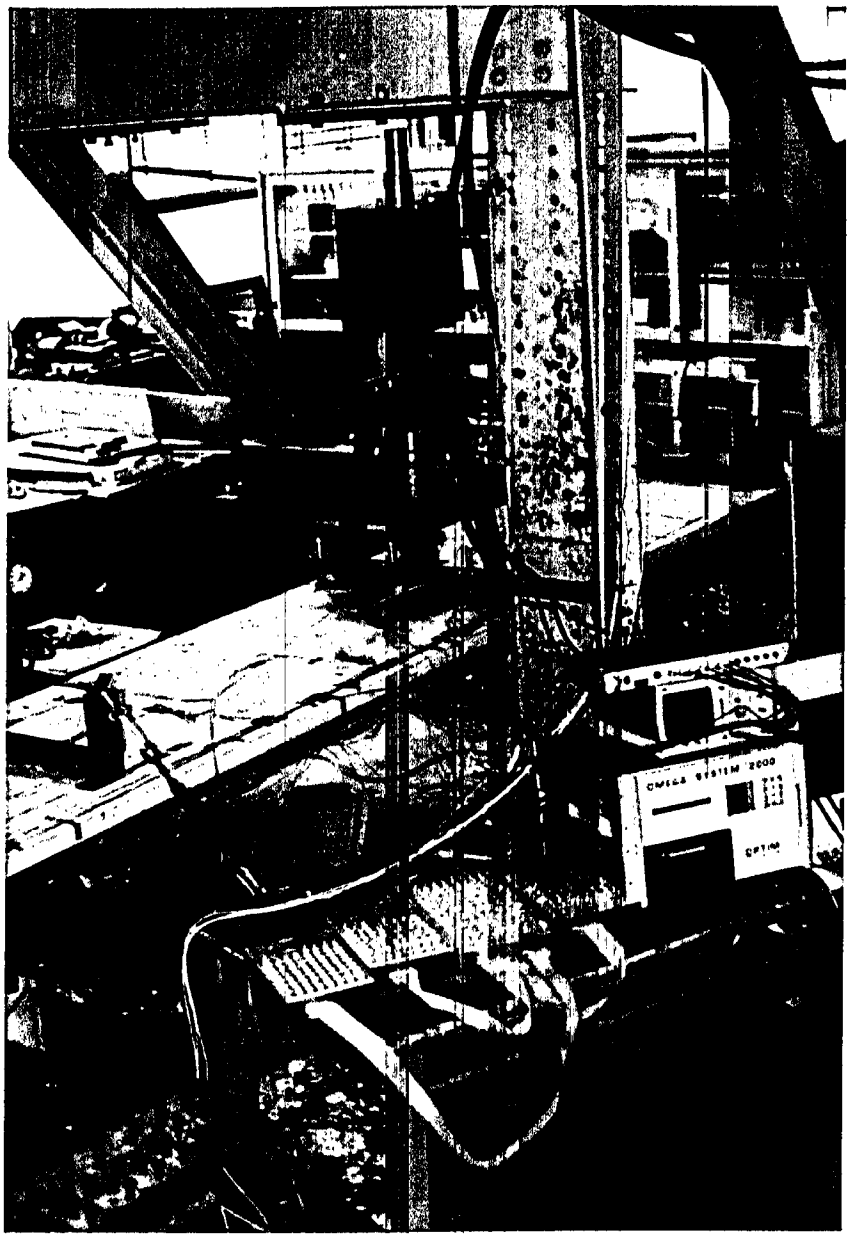

FIGURE 5.21 A/D, SCV, SCI-I AND SCI-II TERMINAL BOXES

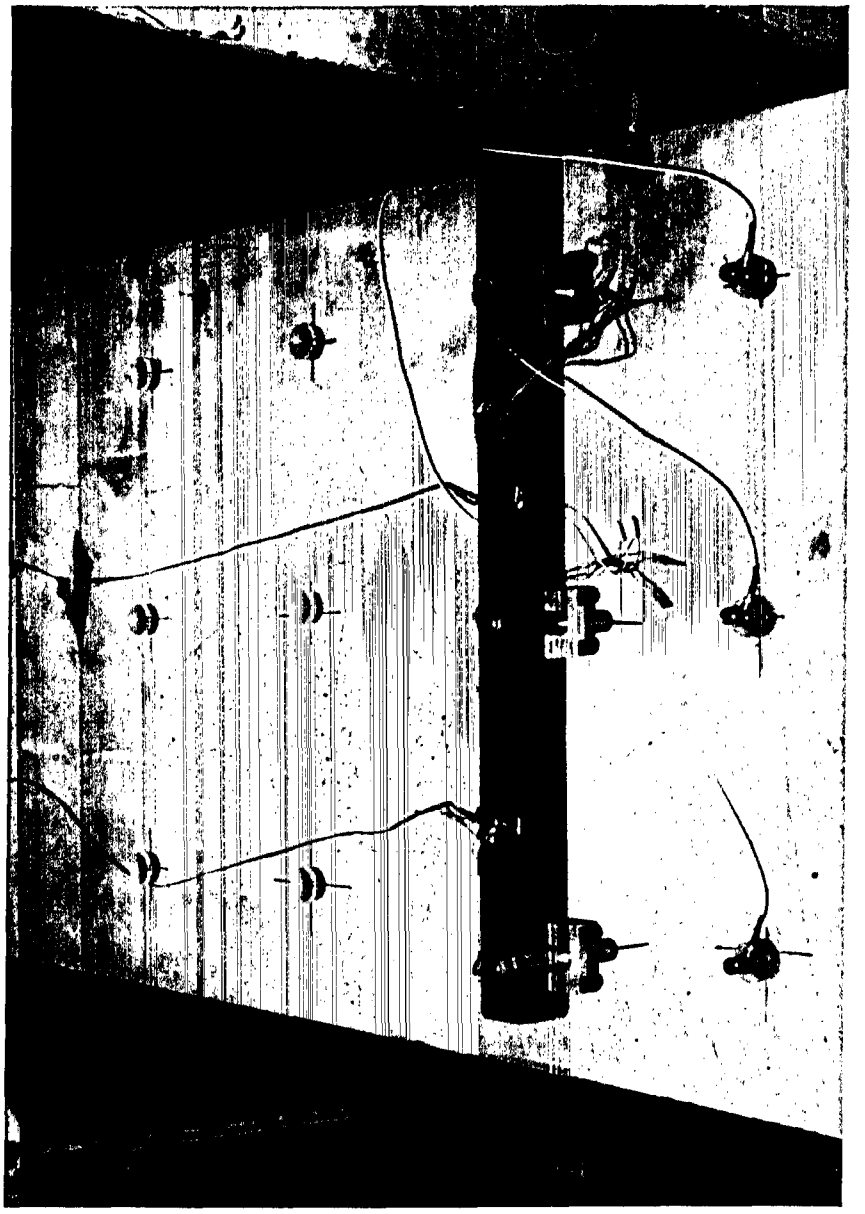

FIGURE 5.22 25g ACCELEROMETERS MOUNTED ON BRIDGE MODELS I AND II

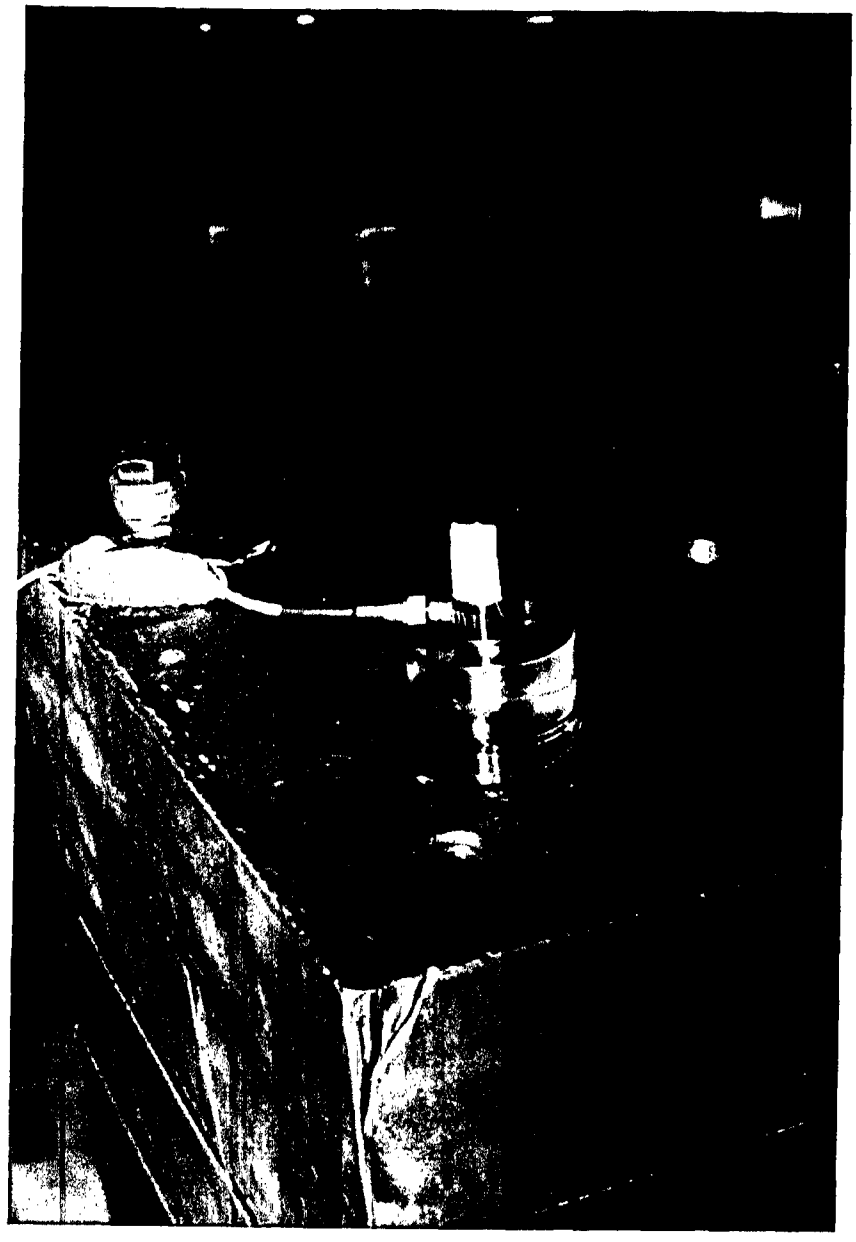

FIGURE 5.23 50g ACCELEROMETER ON THE TOP OF THE MOVING MASS

accelerometer's base. A drill #21 of 0.159-inch (4.0 mm) diameter and a tap of 10-32 UNF-2B were used to drill a 0.250-inch (6.35 mm) deep threaded hole for threading the mounting stud Model 6200 into the plexi-glass blocks. The stud was screwed into the accelerometer by hand until the stud was seated on the flange located at the center of the stud; this flange prevented the stud from bottoming inside the accelerometer where it could have stressed the base during mounting. Finally, all of the accelerometers were torqued to secure them to the block surfaces with approximately 20 to 25 in lb. (225.5 to 281.9 cm. N.) of torque. Co-axial cables Model 6010 with a microdot and PNC connectors at each end were used between the accelerometers and the power supply.

5.7.4 Accelerometers Power Supply

Dytran Model 4121 rack mountable power unit of constant current source (2 to 20 mA "adjustable"), for voltage mode 2-wire accelerometer, was used. The unit contained a regulated DC power supply and 12 channels of adjustable constant current circuit. The front panel has 12 BNC output jacks which were used to transfer the accelerometer output analog signals to the A/D modules of the data acquisition system, while the rear panel contained 12 sets of "input" BNC connectors for energizing the accelerometers. The unit can provide an exitation voltage up to +24 V DC. An available rotary selector switch on the front panel allowed continuous monitoring of the bias voltage of each accelerometer.

5.7.5 DC Differential Transformer

One DC differential transformer located at the end of each model was

used to measure the differential movement between the concrete deck and the longitudinal steel beams. The DCDT was mounted on the web of the steel beam while the core measured the movement of the concrete deck. The DCDT has a linear range of ±1.0 inch (25.4 mm) and sensitivity of 0.33 mv/0.001 inch (0.33 mv/0.025 mm) The DCDT was a spring-loaded type of D-500 series made by Schaevitz em Limited.

5.7.6 Linear Variable Differential Transformer

Six LVDTs were used to measure the static and dynamic displacements of the bridge models. Three LVDTs were located across the middle of one span and the other three were on the middle of the other span. Each LVDT was mounted exactly on the top of each longitudinal steel beam. The LVDT had a capacity of ± 1.0 inch (25.4 mm) displacement of D-500 series made by Schaevitz em Limited. It should be noted that the LVDTs were attached to non-movable brackets (reference location) and only the core was in contact with the top of the concrete deck.

5.7.7 Dynamic-Fatigue Strain Gages

5.7.7.1 Strain Gages on the Prestressing and Reinforcing Wires

The longitudinal prestressing wires used in bridge model II were instrumented with strain gages, type WK-06-125BB 350. Two strain gages were mounted on the top and bottom of each prestressing wire. Using fine silicon carbide paper and chlorothene, the surface of the prestressing wire was cleaned and prepared for mounting the strain gages. The gages were mounted using M-Bond AE10 adhesive with 200 catalyst as bonding agent according to the manufacturer's recommendation for proper attachment for

dynamic-fatigue environmental conditions. These WK-Series gages were a family of fully encapsulated K-alloy strain gages, having integral high-endurance lead ribbons with a backing and encapsulated matrix consisting of a high-temperature phenolic resin system reinforced with glass fiber. The WK-Series have a maximum strain limit of ±15% and fatigue life of 10^8 cycles at ±2000μin./in. Furthermore, the lead wire system comprised of two flat high-endurance leads to each tab permitting a 3-wire system to be carried directly to the gage. The gage factor was 2.04, while the gage length was 0.125 inch (3.2 mm). After soldering the lead wire, mechanical protection was provided for each strain gage against the grout by using an M-coat F; this consisted of "M-coat FT" self adhering teflon film," M-coat FB "Butyl rubber sealant," M-coat FN" Neoprene rubber sheet, "M-coat FA" aluminum foil tape and an "M-coat BT" air drying Nitrile rubber coating. The same type of strain gages were mounted on the reinforcing bars of bridge model I to predict any failure due to fatigue, as shown in Figure 5.24.

5.7.7.2 Strain Gages on the Longitudinal Steel Beams

Strain gages of type WK-06-250BG-350 were used to measure the strain on the top and the bottom flanges of the longitudinal beams and the transverse diaphragms. The locations of the strain gages are shown in Figures 5.24 and 5.25. The procedures, explained in 5.7.7.1 were followed for mounting these strain gages.

5.7.7.3 Strain Gages on the Stud Shear Connectors

An attempt was made to measure, qualitatively, the load on individual studs and detect any failure during fatigue tests, Figure 5.13. This was done by attaching strain gages on the underside of the top flange of the

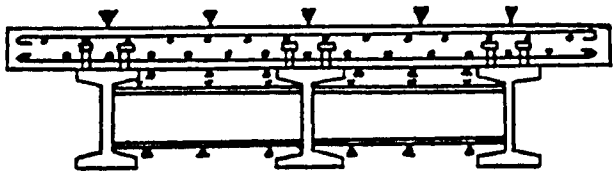

LOCATION OF TRANSVERSE STRAIN GAGES AT MID_SPAN

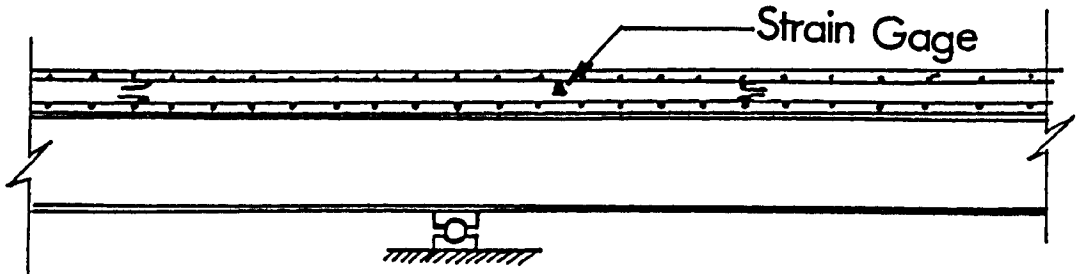

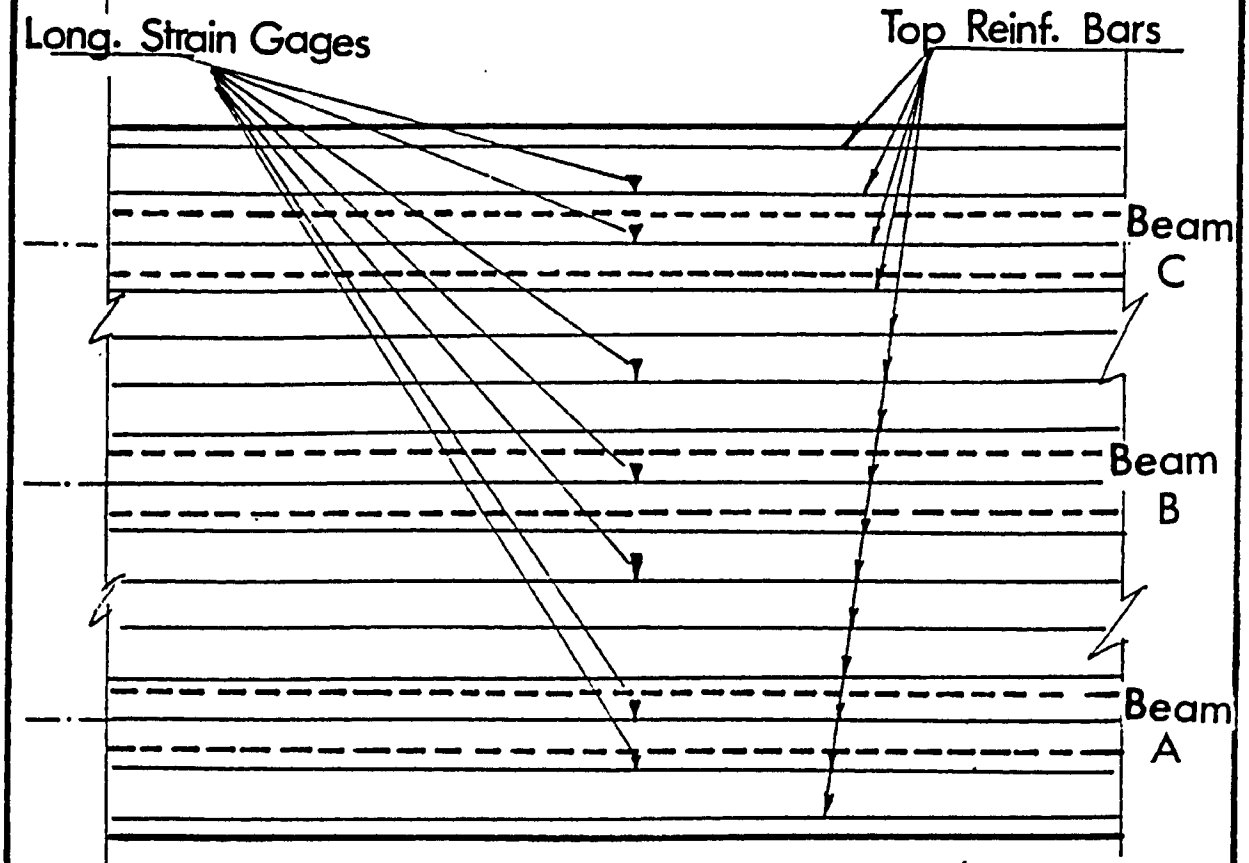

FIGURE 5·24

LOCATION OF STRAIN GAGES AT INTERMEDIATE SUPPORT, BRIDGE MODEL I

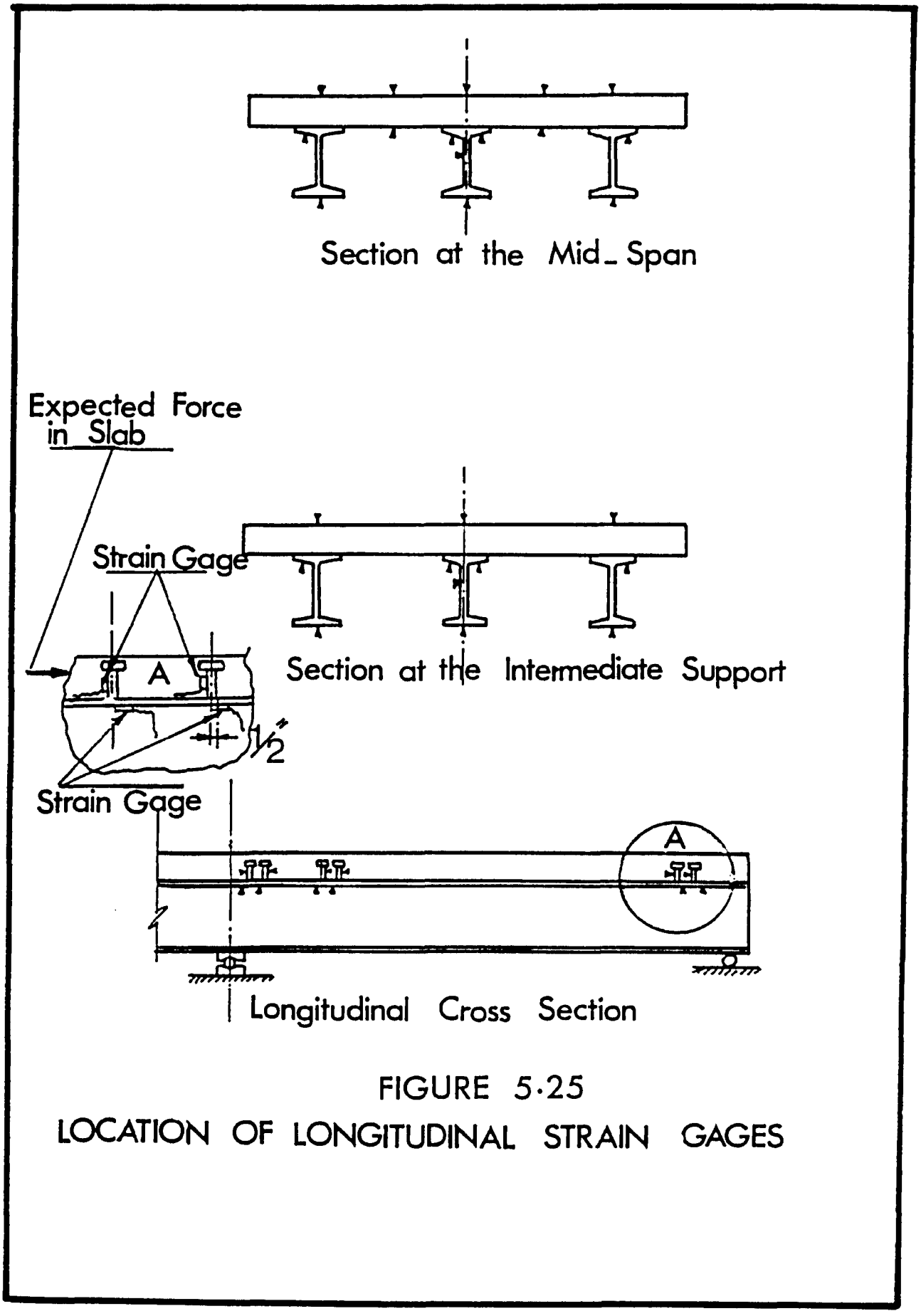

FIGURE 5·25

LOCATION OF LONGITUDINAL STRAIN GAGES

steel beams in the immediate vicinity of the stud in two zones, namely: (1) close to one of the end supports; and (2) at the intermediate support. Also, a strain gage was attached to the same stud in the vertical direction. This was done based on the work reported by Torpac (65). The expected force on individual studs created localized deformation in the top flange which reflected on the strain gage reading. Continuous monitoring of such strains was carried out to detect any failure in the studs, and thus establish their fatigue life. The same type of strain gages, described in 5.7.7.2 were used as shown in Figure 5.25.

5.7.7.4 Strain Gages on the Concrete

To measure the strain in the longitudinal and transverse directions on the top and the bottom surface of the concrete slab, the 2.0 inches (50.8 mm) long of WK-06-20CBW-350 strain gages were used. Surface cavities were filled by applying an epoxy of high strength (RTC), which was mixed by one volume activator B, and the same volume of resin A. Same procedures were followed for mounting the strain ages. Figure 5.26 shows the locations of the concrete strain gages.

5.8 EXPERIMENTAL SET-UP AND TEST PROCEDURE

Figures 5.27 and 5.28 show the experiment set-ups for both bridge models I and II, respectively. It should be noted that the reason for using two actuators in bridge model II was to impose a high negative moment on the prestressed concrete portion during the fatigue test. This was not necessary in bridge model I and one actuator was sufficient to create the cracking negative moment at the intermediate support. The test procedure comprised of static, dynamic, fatigue and ultimate load tests on bridge

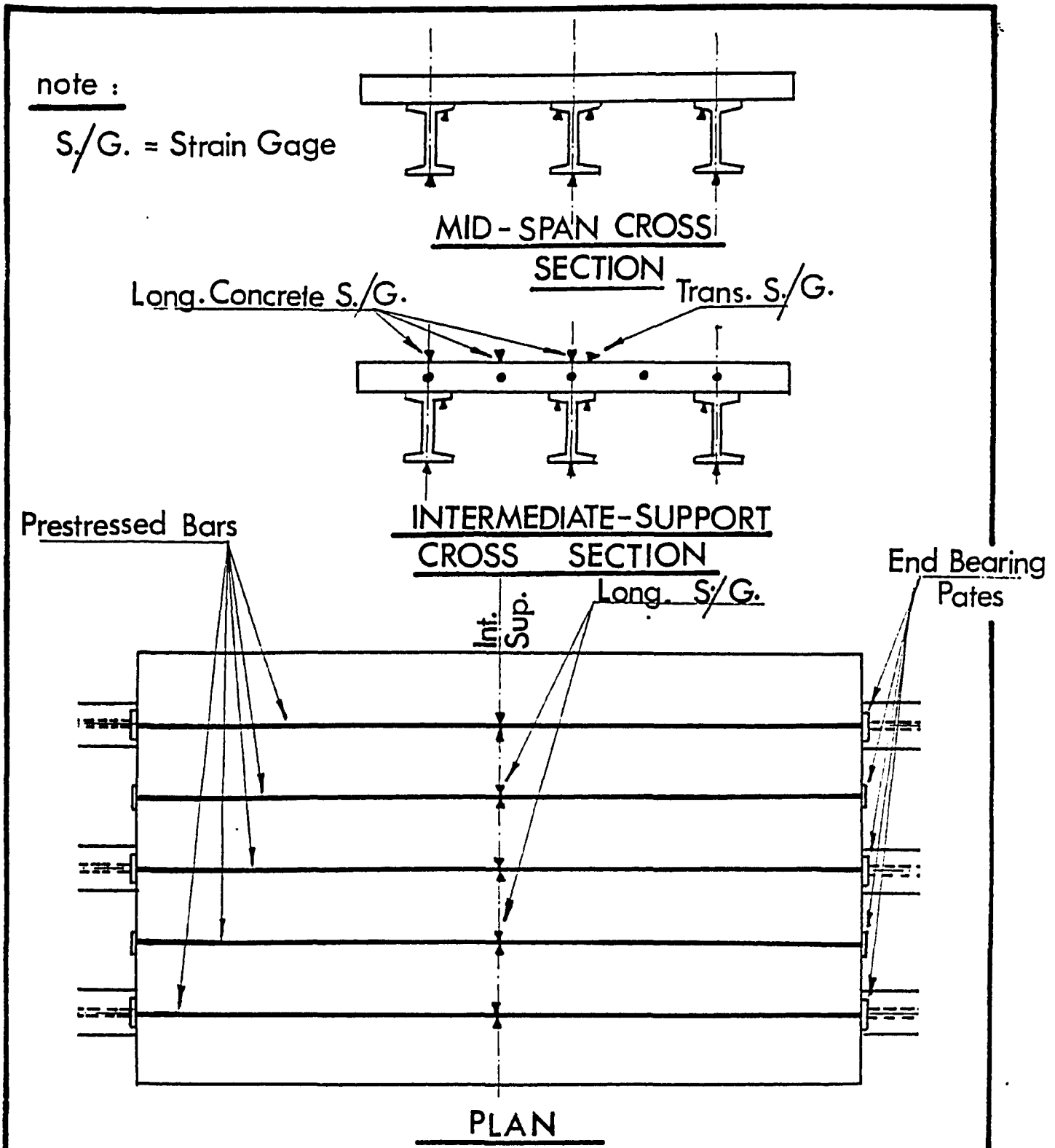

FIGURE 5·26 LOCATION OF LONGITUDINAL AND TRANSVERSE STRAIN GAUGES ON BRIDGE MODEL II

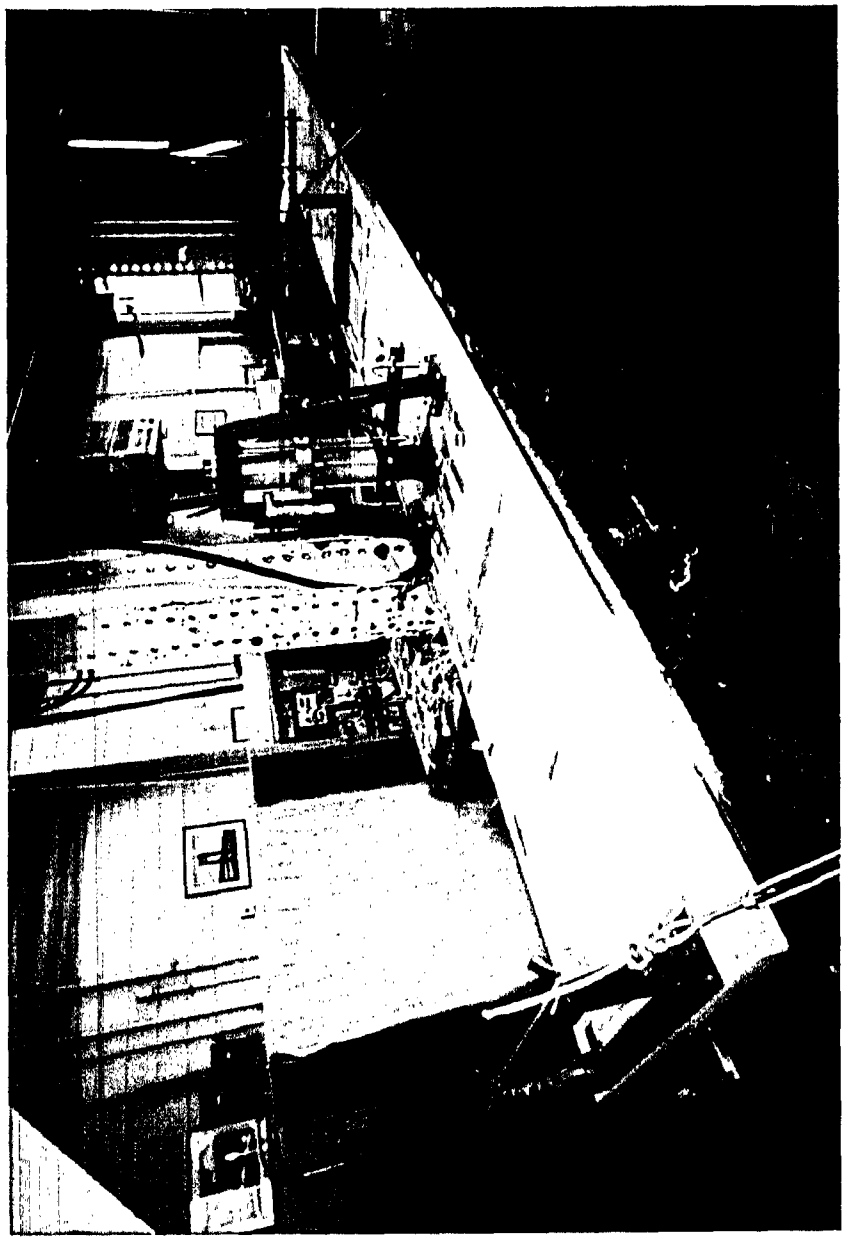

FIGURE 5.27 DYNAMIC AND FATIGUE TEST SET-UP FOR BRIDGE MODEL I

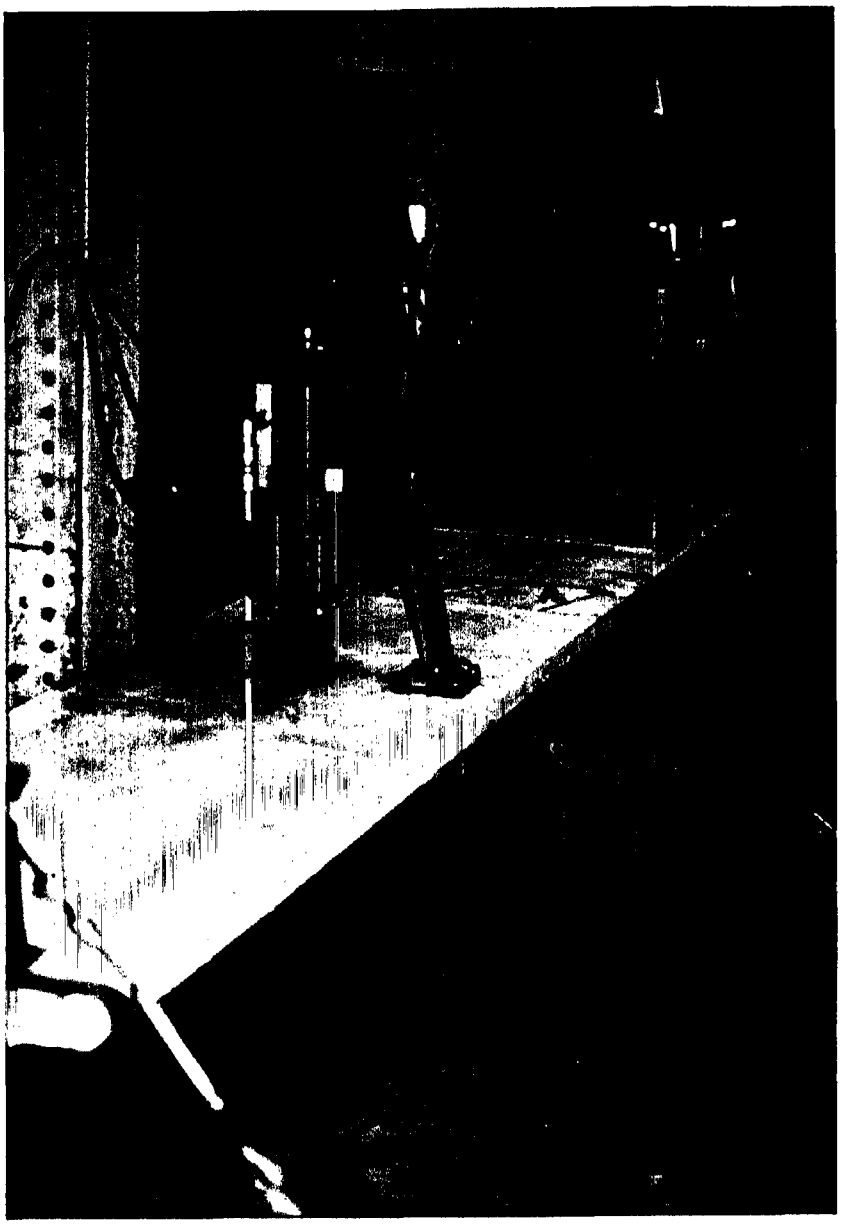

FIGURE 5.28 DYNAMIC AND FATIGUE TEST SET-UP FOR BRIDGE MODEL II

model I, while bridge model II was subjected to the same tests excluding the static test.

5.8.1 Static Test

The actuator mounted on bridge model I was used to apply a static load on the center longitudinal beam at the middle of one span. This single concentrated load test was important to confirm the finding from earlier research (21, 36, 37). This was done by loading the model in the elastic range and measuring the deflection and strain in the longitudinal and transverse directions of the steel beams, diaphragms and concrete deck.

5.8.2 Dynamic Test

Three modes of vibration and its associated natural frequencies were of interest. These modes of vibration of were: the first bending mode, the first torsional mode, and the second bending mode. In order to excite these modes and to obtain the dynamic characteristics as well as the models' vibration signature, the following set of dynamic tests were performed twice on each model, once at the beginning and then at the end of the fatigue test:

1. Sweep-sine wave test.
2. Normal modes test.
3. Log-decrement test (transient test)

The sweep-sine wave test was performed by continuously and slowly varying the actuator excited frequency over a frequency range of 8 to 40 cycles/second. The moving mass and the actuator stroke were kept as constant as possible. The data acquisition system was continuously

recording and transmitting the recorded data to the IBM PC computer via an RS-232-C. The computer was continuously chart recording the output signal from the data acquisition system. This gave a complete picture of the model behavior and understanding of the models' vibration signature over this frequency range. It was expected that the first three natural frequencies were in this frequency range.

After having the sweep tests results on a hard disk in the computer center, a Fast Fourier transform program was used to obtain the spectrum response charts from the acceleration time history charts for each accelerometer. This spectrum chart identified the natural frequencies of each bridge model.

Knowing the first three natural frequencies of each model led to the next dynamic test which was the normal modes test. This test was performed by exciting each bridge model at each of the three natural frequencies creating three resonance modes of vibration. The steady state responses of the two models during the first three modes of vibration were measured at 18 stations to establish the configuration shape of each mode for the two bridge models. This was done directly by feeding the measured data into an available subroutine ZETAPLOT.

Finally, the third test of log-decrement test was performed by exciting each bridge model at their first natural frequency, then the hydraulic power was turned off to set the model to undergo a decaying free vibration. The transient response of the decaying free vibration time history was plotted by using the computer. As a result, the associated geometric and material damping was ascertained by using the logarithmic decrement method.

5.8.3 Fatigue Test

A resonance fatigue test was carried out at the first bending natural frequency of the two bridge models to observe any fatigue failures. The dynamic strains on the steel beams, shear connectors, longitudinal prestressing wires, reinforcing bars and concrete deck were monitored and recorded periodically throughout the loading. The bridge model dynamic characteristics were used as inspection tools beside visual inspection to detect any fatigue failure.

5.8.4 Ultimate Load Test

Prior to the initiation of the ultimate load test, bridge model I was repaired after the fatigue failure of its longitudinal beams. Figure 6.56, Chapter 6, shows bridge model I after being repaired from fatigue failure. However, bridge model II was not repaired from the fatigue damage and was tested under ultimate load directly after the conclusion of the fatigue test. This facilitated a comparison between the repaired and unrepaired models under ultimate loads. Two hydraulic jacks, one in each span, were used in testing bridge model II under ultimate load while only one hydraulic jack located in the middle of one span was used in bridge model I. Two universal static flat load cells, having a capacity of 50 kips (222.4 KN) and 150 kips (667.0 KN) were used. The load was slowly and continuously increased until plastic hinges were developed at the mid-span and at the intermediate support. Figure 5.30 shows the ultimate load test set-up for bridge model II.

5.9 PUSH-OUT TESTS OF STUD SHEAR CONNECTORS

The purpose behind the tests of push-out specimens was to study the type of failure in the stud shear connector under static or fatigue loading. Furthermore, to estimate the static load capacity of each connector. Six push-out specimens, four under static load and two under fatigue loading were tested; all specimens were identical. The same stud shear connectors, concrete mix and the longitudinal steel beams used in constructing the two models were also used in the push-out specimens. Nelson stud welding equipment was used to attach the stud connectors. This was important to simulate the same conditions as found in the bridge models.

A push-out specimen consisted of a short steel beam 30 inches (762 mm) long of S 5 x 14.75 and two concrete slabs 2 inches (50.8 mm) thick, one attached to each flange of the beam by means of two studs. The slab was reinforced by using the same reinforcing bars used in the bridge models. Figure 5.29 shows the forms and the reinforcement arrangement for the push-out specimens. As shown in this figure, two studs were welded to each flange of the beam and embedded in a 24x12x2.0 inch (610 x 305 x 50.8 mm) concrete slab. Strain gages were attached along each connector and on the bottom face of the flanges underneath the stud itself. Mechanical protection was provided to all the strain gages as explained before in 5.7.7.1. All the slabs were cast simultaneously in the vertical direction; then the specimens were placed in a moist condition for seven days for curing. Figure 5.30 shows the push-out test set-up for static loading while Figure 5.31 shows the set-up for fatigue test using a Gilmore 100-kip hydraulic actuator. During the static test, the slip between the beam and

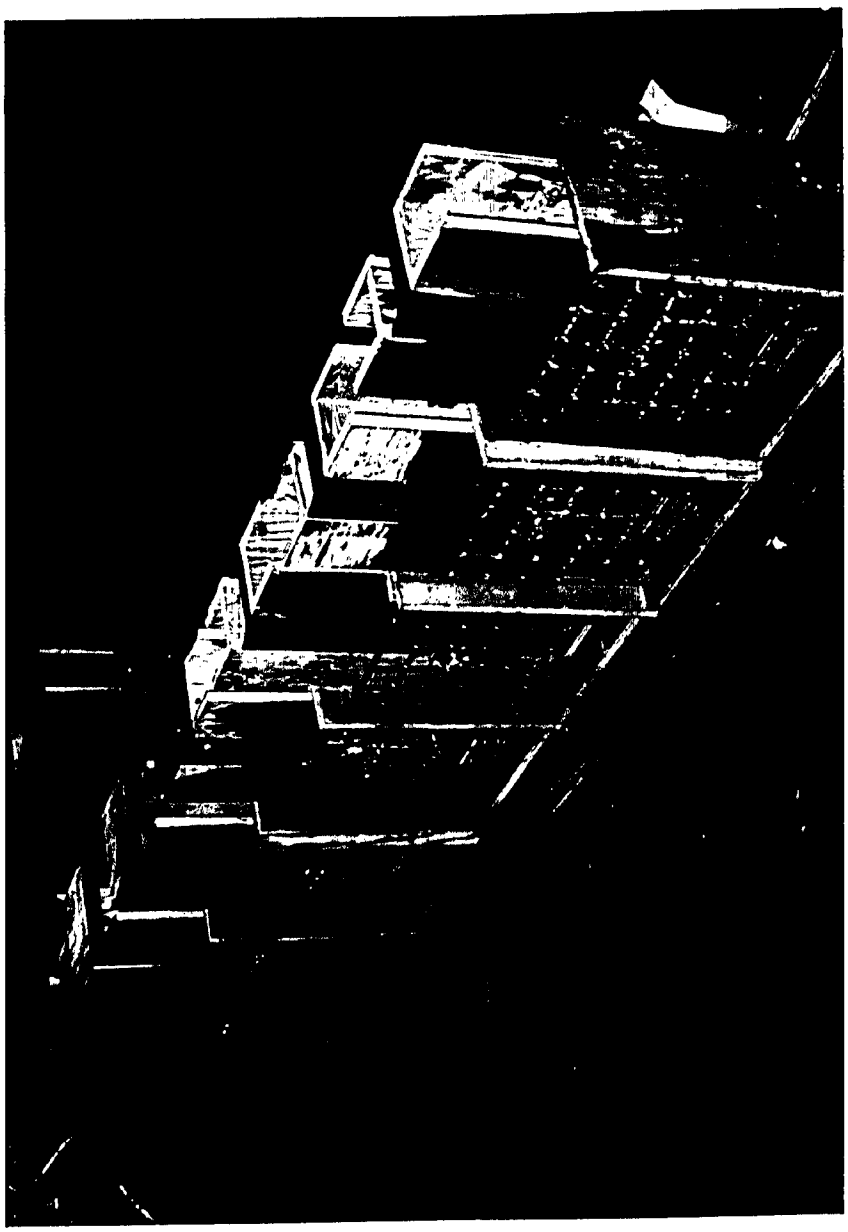

FIGURE 5.29 FORMS FOR THE PUSH-OUT SPECIMENS

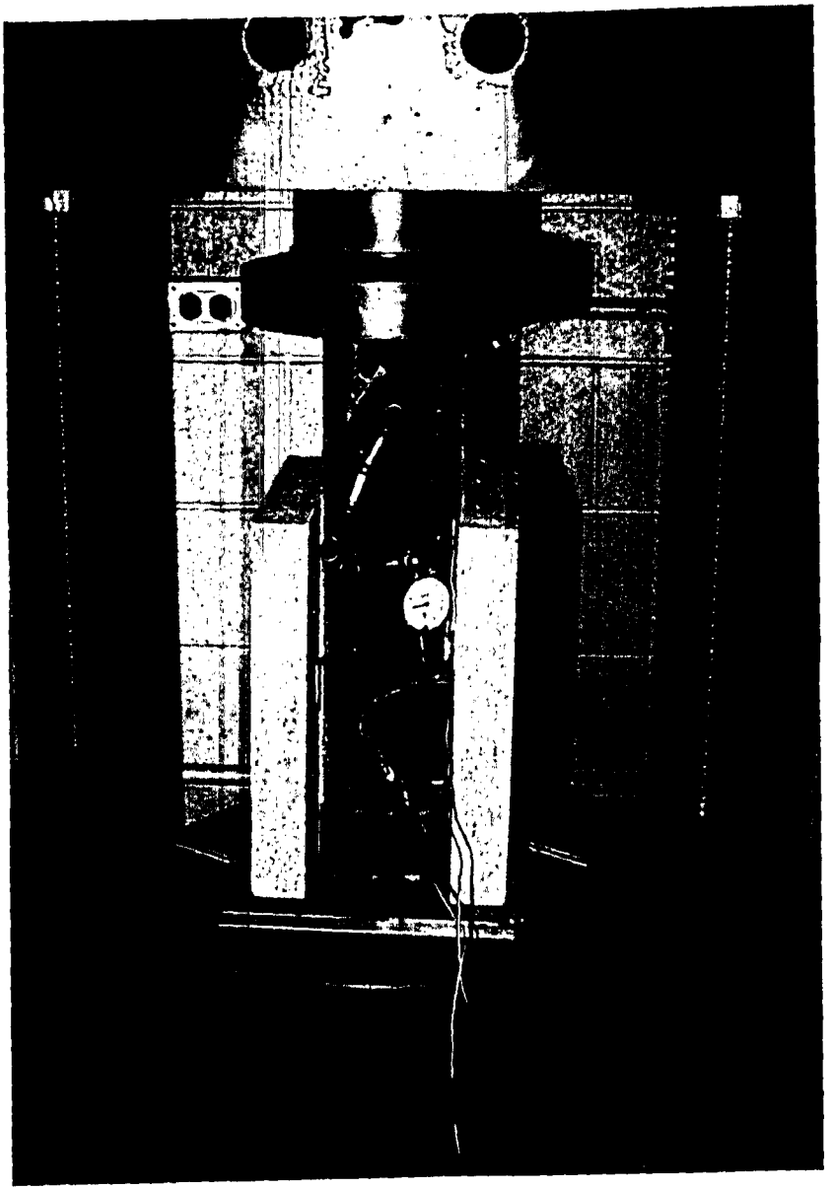

FIGURE 5.30 SET-UP FOR STATIC PUSH-OUT TESTS

the slabs was measured at four locations by means of four 0.001-inch (0.025 mm) dial gages. The dial gages were mounted rigidly to the beam's web with the stem bearing against brackets glued to the inner faces of the slabs. During the static tests the load was applied in increments of 2.0 kips (8.88 KN) each until failure. The slip and strain on the connector and on the flange were recorded continuously. The duration of each test varied from 1 to 2 hours. However, during the fatigue test the load range was kept constant at 2 kips (8.88 KN) and the rate of loading was 4 cycles per second. The load was applied to the top of the beam and transferred from the beam to the slabs through the four shear connectors on each beam. It should be noted that the load, at the beginning of the test, was transmitted to the slabs not only by the shear connectors, but also in part by kinetic friction and bond. Care was taken to apply only a concentric load, with respect to the beam so that each connector would carry an equal part of the load. Unfortunately, all the fatigue push-out tests were conducted before acquiring the data acquisition system. However, a static electronic strain indicator of 80 channels capacity and a one-sample per second scan rate was used for recording the strain during the static and fatigue tests. Results will be discussed in Chapter VI.

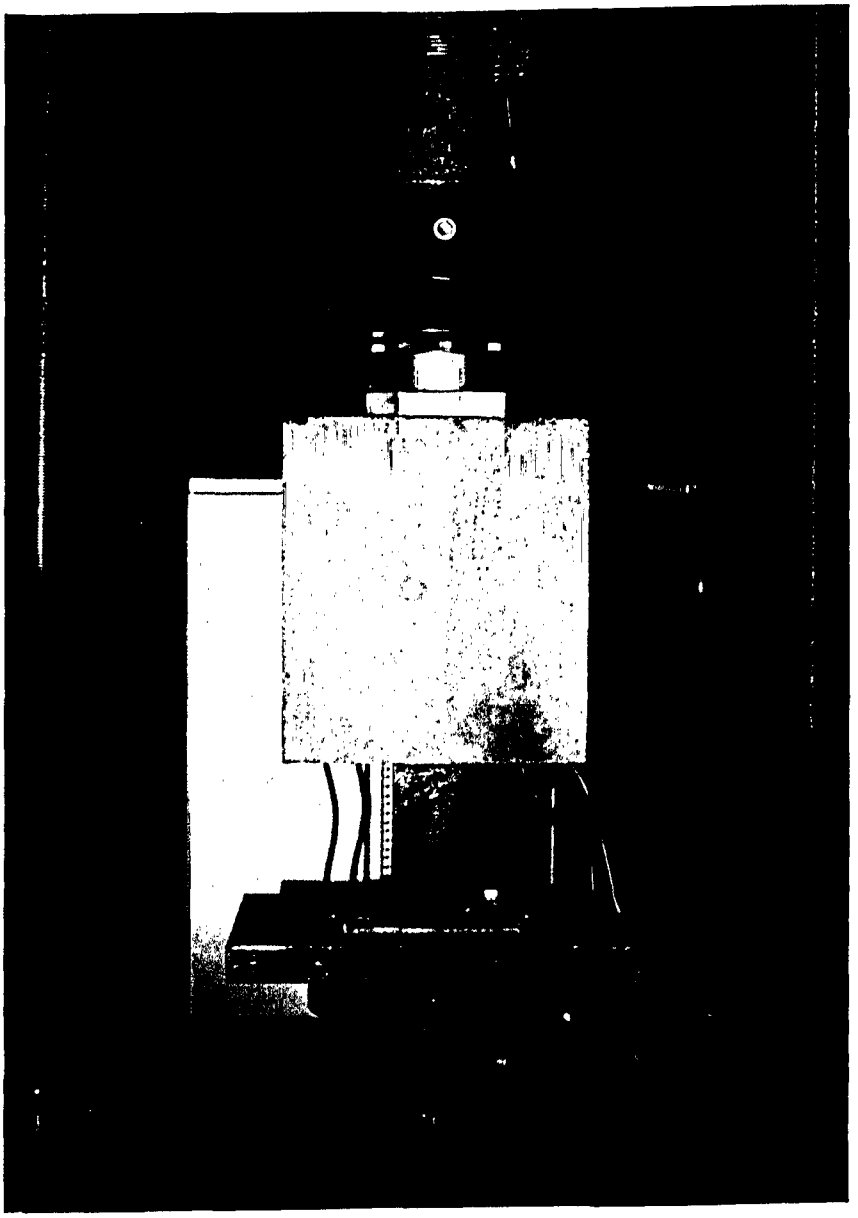

FIGURE 5.31 SET-UP FOR FATIGUE PUSH-OUT TESTS

CHAPTER VI

DISCUSSION OF RESULTS

6.1 INTRODUCTION

The results of the dynamic tests obtained from the two bridge models are discussed in this chapter to evaluate and demonstrate the accuracy of the analytical method developed earlier in Chapter III. The mathematical treatment of the free vibration problem of the skew orthotropic plate is substantiated by the experimental results obtained by El-Sebakhy, et al. (19) on a skew prestressed waffle slab. In addition to the experimental results, the most recent version of STRUDL-DYNAL computer program (59), developed by McDonnell Douglas Automation Company, as well as SAP IV finite element computer program (5), were used as other sources for comparison. Furthermore, a parametric study on the effect of different skew angles, aspect ratios and rigidities on the dynamic behavior of skew orthotropic plates is undertaken and discussed. A comparison study is presented between the skew waffle slab and the skew solid slab having the same volume of concrete (i.e., the same mass) and the same planeform geometry.

The analogy in the dynamic characteristics between a two-span continuous composite bridge and a single-span orthotropic plate, with different boundary conditions, is presented. Also, the dynamic response of an orthotropic plate having fixed-simply supported and free-free boundary conditions is presented; the influences of aspect ratio and rigidity ratio (Dx/Dy) on the natural frequencies are examined and compared to those obtained from beam theory.

Confirmation of earlier research on the structural response of composite bridges under static loads (21,37) is discussed using the results obtained from the static tests on bridge model I.

The structural responses of some components of the two bridge models such as shear connectors, longitudinal steel reinforcing and prestressing wires at the intermediate support, longitudinal beams and transverse diaphragms under resonance-fatigue tests are examined. Effect of the fatigued-elements of the bridge models on the dynamic characteristics as well as on the ultimate load carrying capacity is discussed.

6.2 FINITE ELEMENT METHOD

The finite element method is a generally acceptable method for deducing the natural frequencies and the associated mode shapes of structure, using numerical solution. Consequently, the available finite element computer programs, such as SAP IV and STRUDL, are used to verify the mathematical solutions of the free vibration of continuous composite bridges and skew orthotropic plates. The basis of the finite element method is the replacement of the continuum of the bridge by a substitute model consisting of a number of discrete elements, such as a quadrilateral plate and three-dimension beam elements, representing the top slab and the steel beams of the composite bridge or the concrete ribs of a skew waffle slab. These elements are connected together at discrete nodal points where continuity is expressed and can be generated automatically.

6.2.1 Structural Analysis Computer Program; SAP IV

One of the finite element computer programs adopted in this chapter is

the Structural Analysis Program, Version IV SAP(IV), (5) developed at the University of California, Berkeley. In order to model bridge models I and II, two approaches were used. In the first approach, the model was made of isotropic plate elements representing the cement deck slab, resting on three-dimensional beam elements in the longitudinal and transverse directions, modeling the longitudinal steel beams and the transverse diaphragms, as shown in Figure 6.1. In this model, the number of quadrilateral plate elements was 288, while the number of beam elements was 164.

This number of elements was necessary to achieve accurate results. The aspect ratio of the quadrilateral plate element was equal to one as recommended by the user's manual. Figures 6.2 and 6.3 show the associated number of the degrees of freedom and the local axes orientation with respect to the global axes of the quadrilateral plate element and the three dimensional beam element. This approach of modeling the composite bridge will be denoted as composite action in the comparison of results.

In the second approach, the model was made of an equivalent quadrilateral orthotropic plate element reflecting the properties of the equivalent orthotropic plate of the continuous composite bridge. Using the following relations:

$$D_x = \frac{E_x h_1^3}{12} \tag{6.1}$$

$$D_y = \frac{E_y h_1^3}{12} \tag{6.2}$$

$$D_1 = \frac{\bar{\bar{E}}\ h_1^3}{12} \tag{6.3}$$

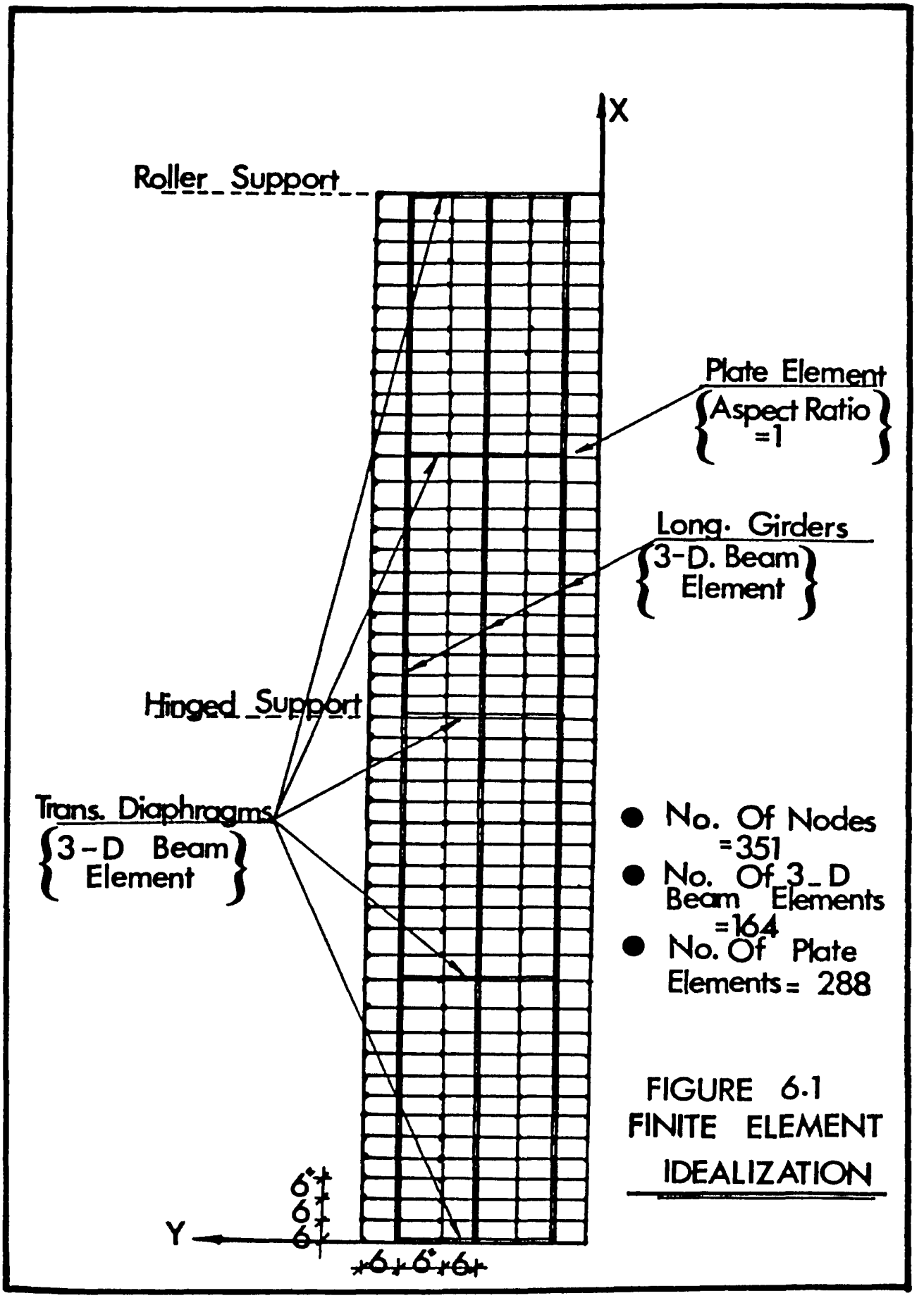

FIGURE 6.1
FINITE ELEMENT IDEALIZATION

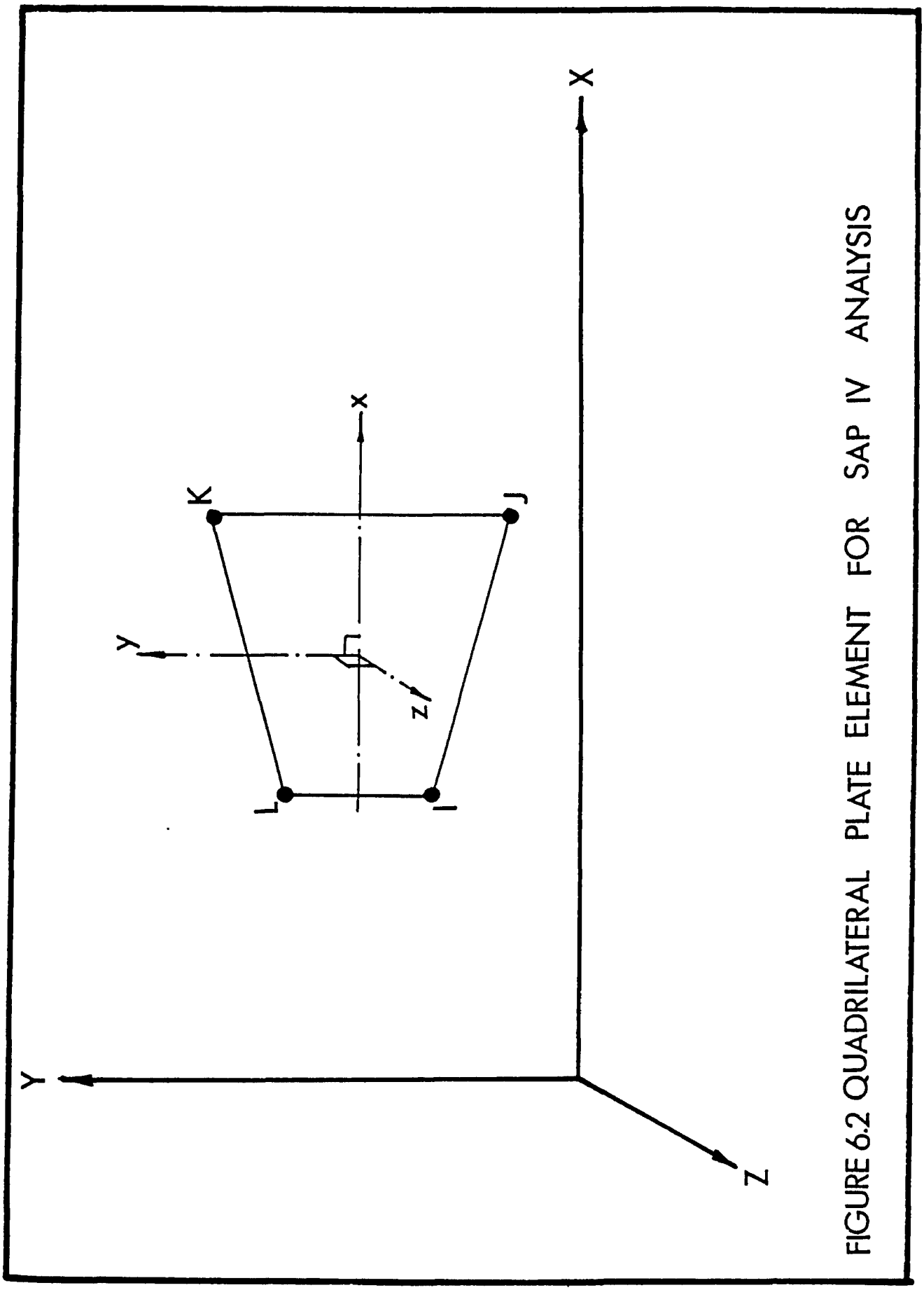

FIGURE 6.2 QUADRILATERAL PLATE ELEMENT FOR SAP IV ANALYSIS

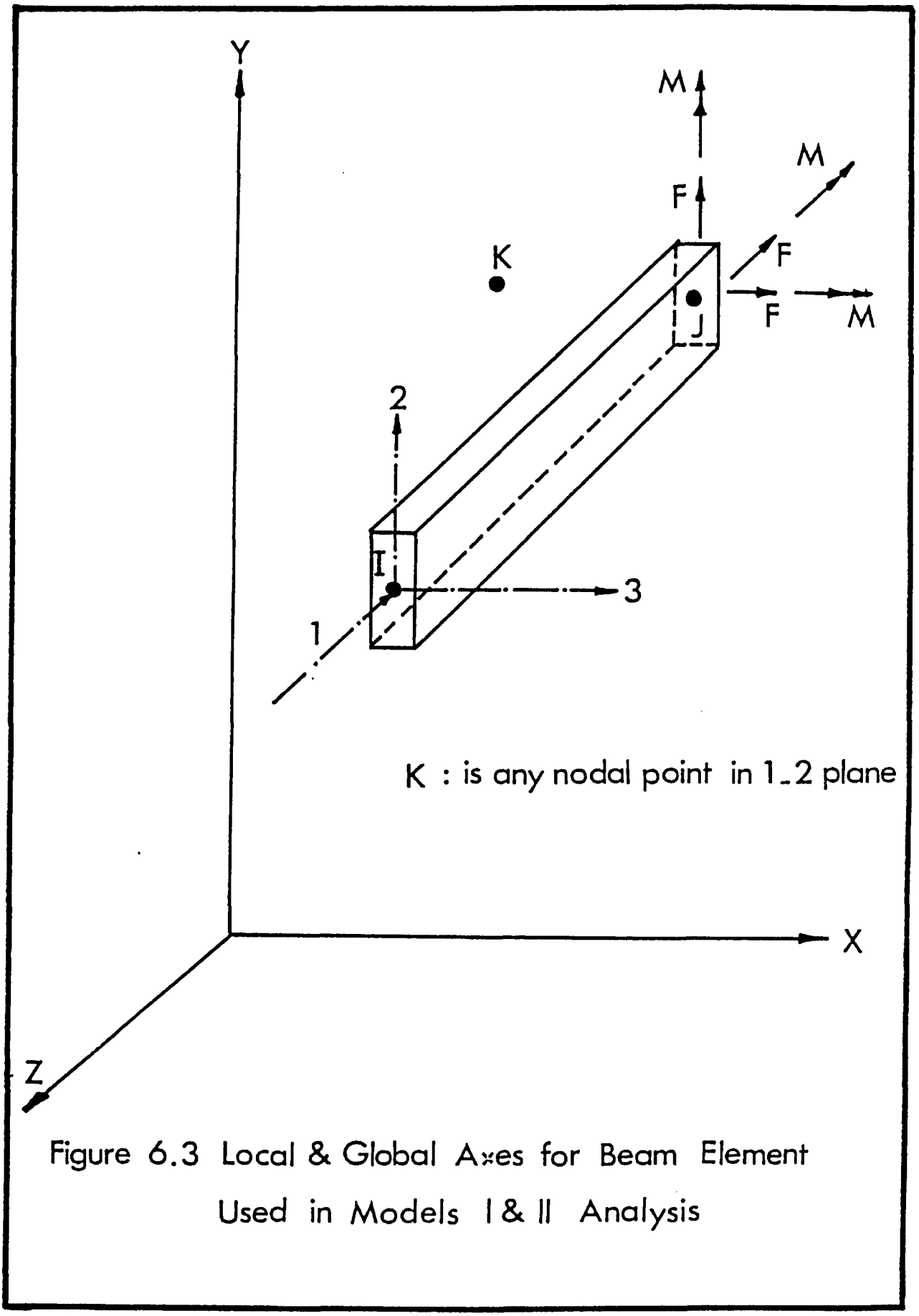

Figure 6.3 Local & Global Axes for Beam Element Used in Models I & II Analysis

$$D_2 = \frac{\bar{\bar{E}} \quad h_1^3}{12} \tag{6.4}$$

$$D_{xy} = \frac{Gh_1^3}{12} \tag{6.5}$$

and knowing the values of D_x, D_y, D_1, D_2 and D_{xy} the values $\bar{E}_x$, $\bar{E}_y$, average of $\bar{E}$ and $\bar{\bar{E}}$, and G can be calculated and used for formulating the material matrix, (5). This approach of modeling the composite bridge will be denoted as an orthotropic plate.

To use SAP IV in modelling the skew waffle slab, additional boundary elements, besides the quadrilateral plate elements, were required at the two simply supported ends (7). This was important to correctly model the boundary conditions since it was not possible to align the principal flexural rigidities D_x and D_y, and the supported edges with the same global axes system. A typical section of the waffle skew slab is given in Figure 6.4. The input data requirements for modeling the continuous composite bridge and the skew waffle slab are given in the user's manual (5) and are discussed here.

6.2.2 Structural Design Language Computer Program; STRUDL-DYNAL

The original version of the STRUDL was conceived, developed, and initially released by the Massachusetts Institute of Technology (MIT). McDonnell Douglas Automation Company (MCAUTO) provides a much enhanced system of STRUDL compared with the basic system from MIT. In particular, a major enhancement has been the implementation of a reliable dynamics analysis capability. This capability resulted from the merger of the

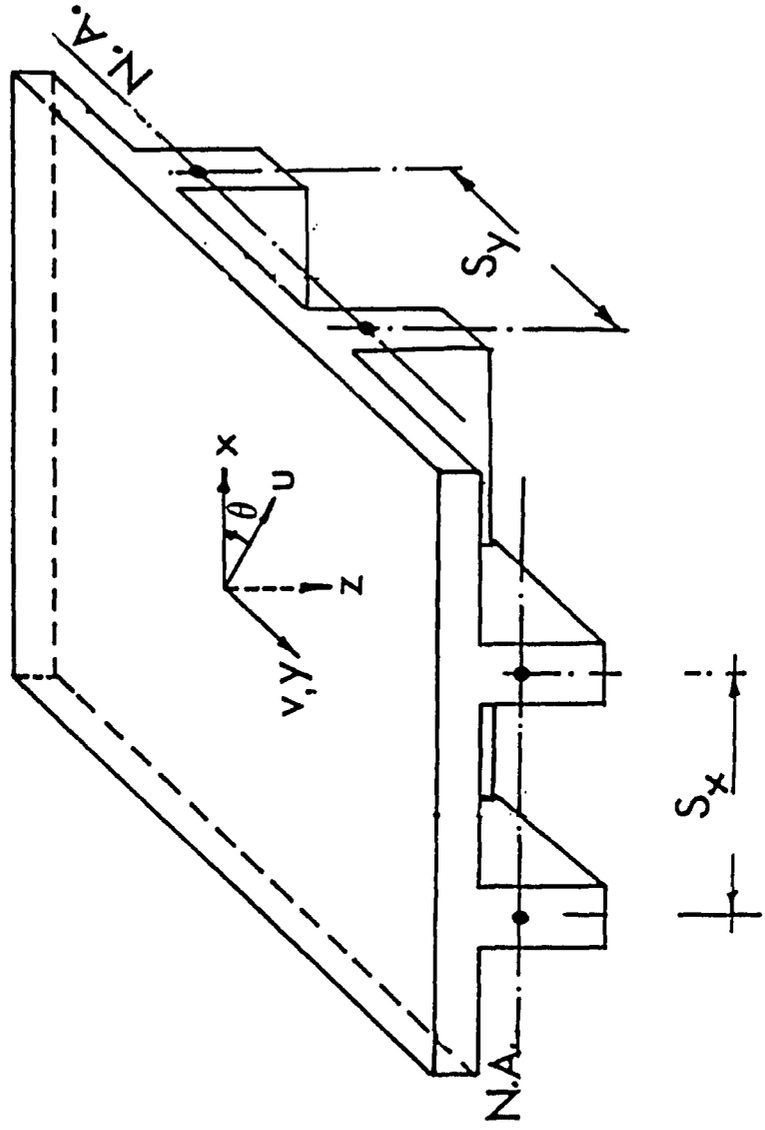

FIGURE 6.4 TYPICAL CROSS-SECTION OF WAFFLE SLAB

proprietary STRUDL and MCAUTO Dynamic Analysis System, DYNAL. The dynamics portion of STRUDL is called STRUDL-DYNAL, which is used in this chapter to model the skew waffle slab. This program is a series of subprograms for solving different dynamic problems in structural engineering. The commands are interpreted by the Integrated Civil Engineering System (ICES), which automatically provides everything necessary to solve the dynamic problem. These commands are made up of engineering words. However, details of the content of STRUDL-DYNAL computer program and its use will not be discussed here, but can be found elsewhere (59).

This program was used to analyze skew and rectangular waffle slabs and to calculate the natural frequencies and the associated mode shapes. Furthermore, the program was utilized to conduct a parametric study on the waffle slab by varying the skew angle and aspect ratio. Typical bottom plan layout of the rectangular and skew waffle slabs that were used in this analysis are shown in Figures 6.5 and 6.6, respectively. An equivalent orthotropic plate bending (PBR) element of an aspect ratio equal to one was used to model both the rectangular and skew waffle slabs; the program automatically generates all the required nodes as well as the required elements, as shown in Figures 6.7 and 6.8. For the rectangular slab, the model is made from 288 elements and 325 nodes, while the skew model is made from 155 elements and 195 nodes for small skew angle. However, a larger numbers of elements were used to deal with large skew angles to ensure high accuracy.

6.3 CONFIRMATION OF EARLIER RESEARCH

Bridge model I was tested first under static load to confirm earlier

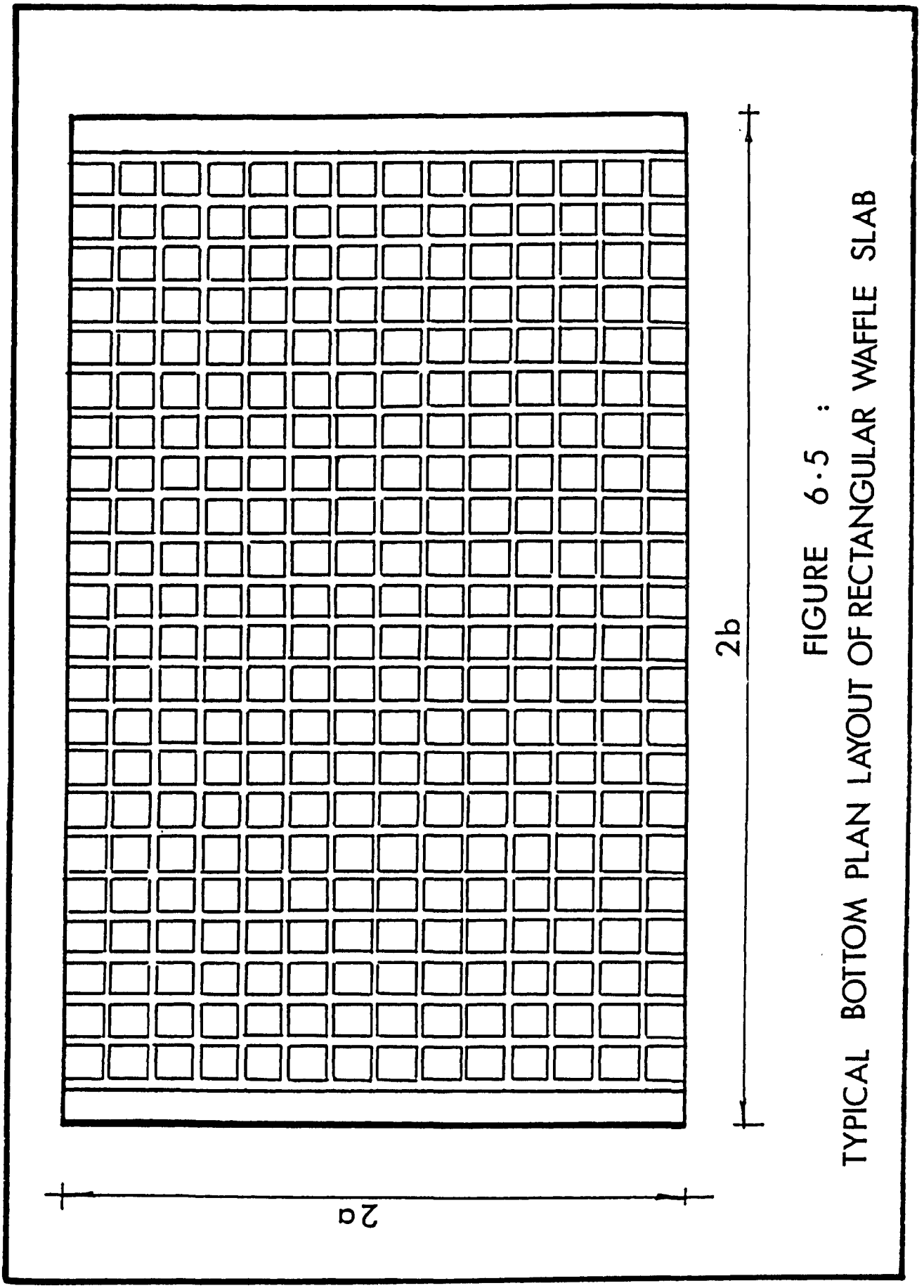

FIGURE 6·5 : TYPICAL BOTTOM PLAN LAYOUT OF RECTANGULAR WAFFLE SLAB

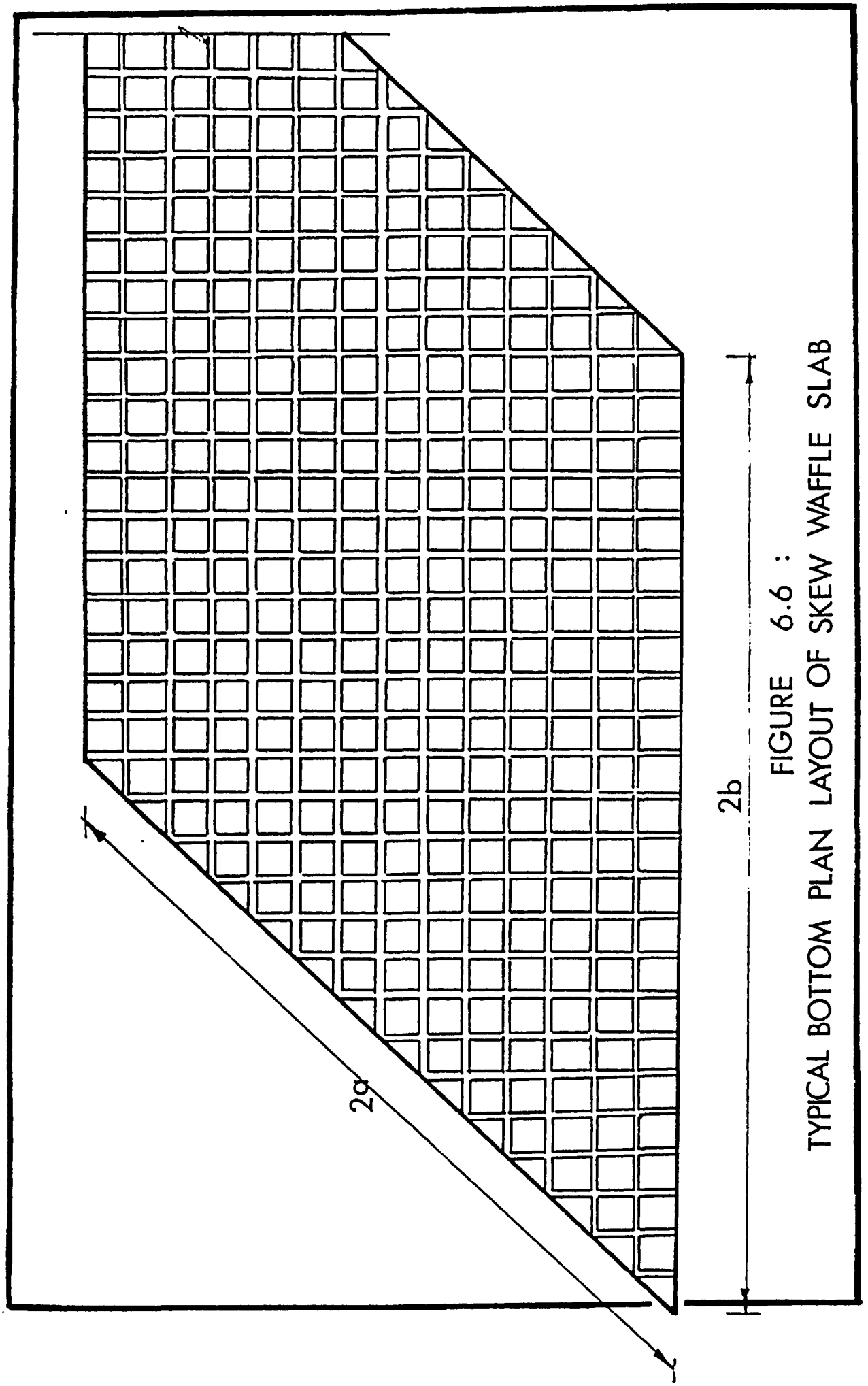

FIGURE 6.6 : TYPICAL BOTTOM PLAN LAYOUT OF SKEW WAFFLE SLAB

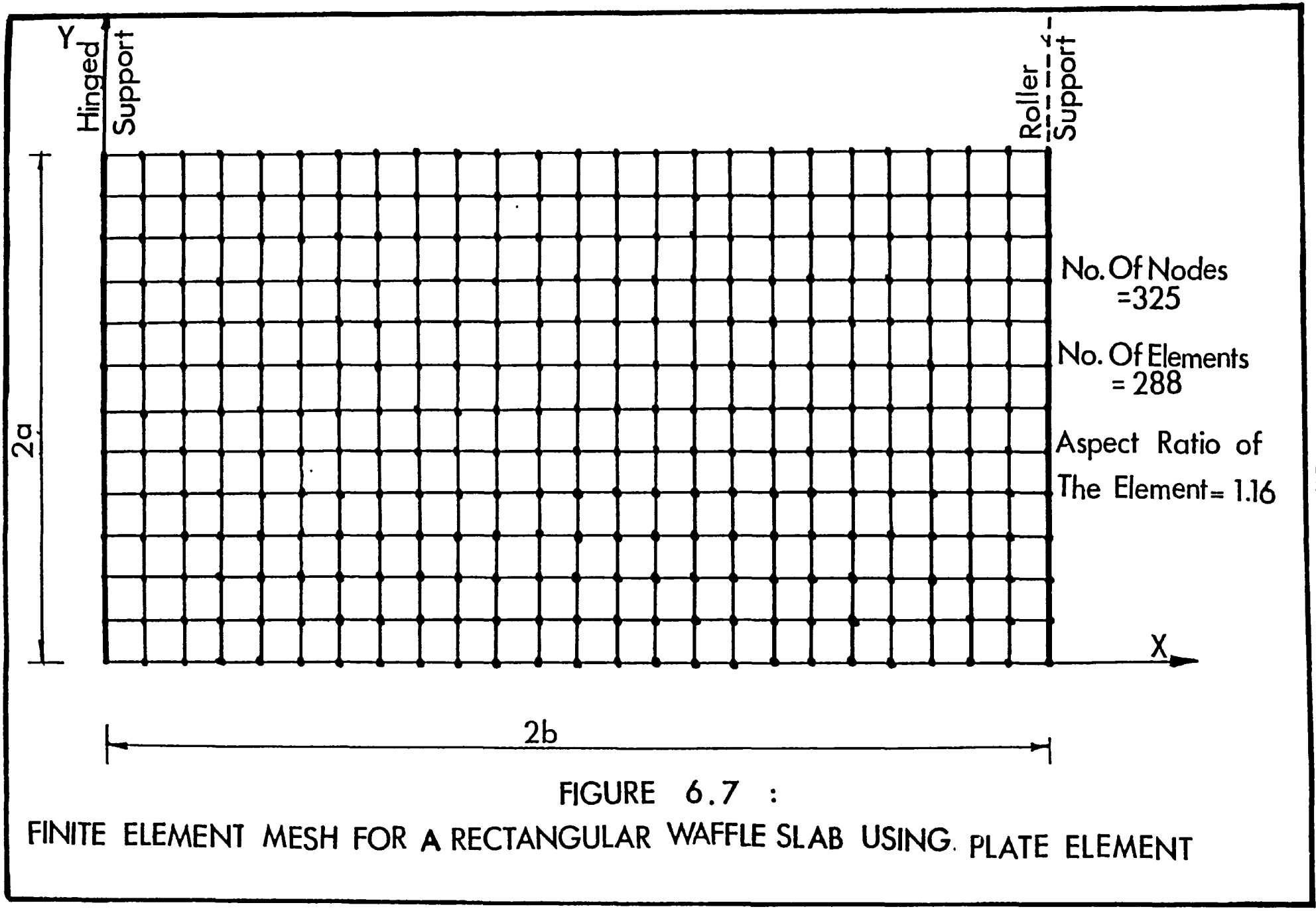

FIGURE 6.7 :

FINITE ELEMENT MESH FOR A RECTANGULAR WAFFLE SLAB USING PLATE ELEMENT

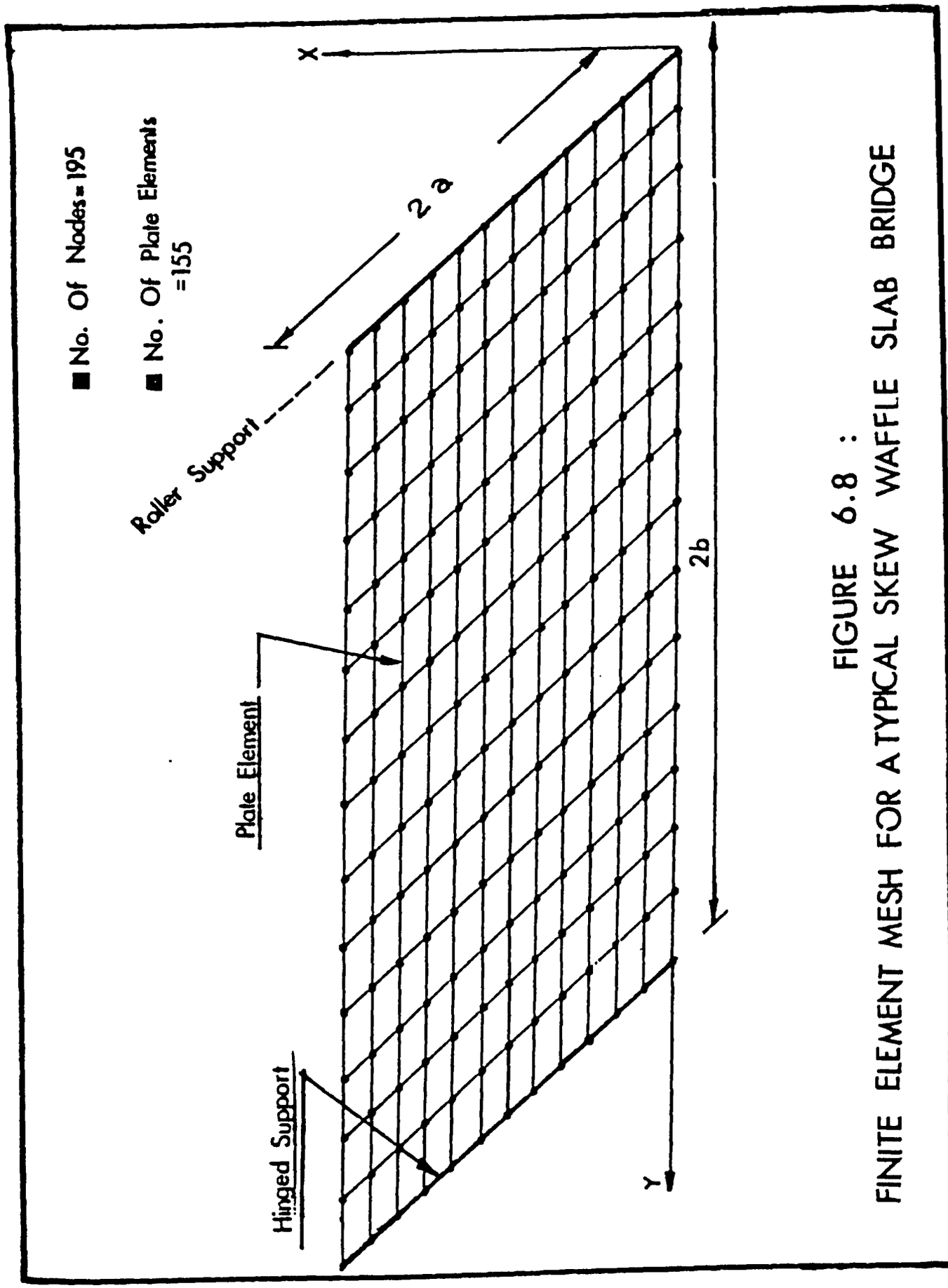

FIGURE 6.8 : FINITE ELEMENT MESH FOR A TYPICAL SKEW WAFFLE SLAB BRIDGE

results obtained by Grace and Kennedy (22, 37). This earlier research concluded that the presence of the steel beam diaphragms, when rigidly connected to the longitudinal girders, enhanced significantly the transverse load distribution as well as the effectiveness of the orthotropic theory in predicting the elastic response of a continuous composite bridge.

The lateral distribution of the deflection of the three longitudinal steel beams of bridge model I due to a concentrated load on the middle beam at mid-span is given in Table 6.1. The lateral distribution of the deflection is presented by expressing the deflection of the individual beams as a percentage of the total deflection of all three beams at the cross-section under consideration. This was to facilitate a direct comparison of the experimental deflection behavior of bridge model I with that predicted by the other theoretical methods. Furthermore, the distribution of the longitudinal and the transverse bending moments experienced by bridge model I are also compared with the predicted theoretical values at the mid-span section in Tables 6.2 and 6.3, respectively. It should be noted that the distribution of the longitudinal bending moment was taken to be the same as the distribution of the strains measured at the center of the bottom face of the steel beams at the mid-span section, while the distribution of the transverse bending moment was taken to be the same as the distribution of strains measured in the transverse direction at the bottom face of the concrete slab at each beam at the same section. The distribution of the longitudinal bending moment at the intermediate support is shown in Table 6.4. The strain distribution

TABLE 6.1

DEFLECTION DISTRIBUTION AT MID-SPAN USING DIFFERENT METHODS

	PERCENTAGE OF TOTAL DEFLECTION			
	EXPERIMENT	FOURIER SERIES	F.E. (ORTHOTROPIC PLATE ELEMENT)	F.E. COMPOSITE ACTION (PLATE & BEAM ELEMENTS)
Girder A(*)	33.1	33.0	33.1	33.2
Girder B	33.9	33.9	33.7	33.6
Girder C	33.1	33.0	33.1	33.2

TABLE 6.2

LONGITUDINAL BENDING MOMENT DISTRIBUTION AT MID-SPAN

USING DIFFERENT METHODS

	PERCENTAGE OF TOTAL LONGITUDINAL MOMENT (My)			
	EXPERIMENT	FOURIER SERIES	F.E. (ORTHOTROPIC PLATE ELEMENT)	F.E. COMPOSITE ACTION (PLATE & BEAM ELEMENTS)
Girder A(*)	32.9	30.3	31.1	31.5
Girder B	36.1	38.9	37.7	36.9
Girder C	31.0	30.3	31.1	31.5

(*) A and C are exterior beams and B is an interior beam.

TABLE 6.3

TRANSVERSE BENDING MOMENT DISTRIBUTION AT THE MID-SPAN SECTION USING DIFFERENT METHODS

	PERCENTAGE OF TOTAL TRANSVERSE BENDING MOMENT (Mx)			
	EXPERIMENT	FOURIER SERIES	F.E. (ORTHOTROPIC PLATE ELEMENT)	F.E. COMPOSITE ACTION (PLATE & BEAM ELEMENTS)
Girder A(*)	7.0	9.1	9.5	6.9
Girder B	86.0	81.9	81.0	86.1
Girder C	7.0	9.1	9.5	6.9

TABLE 6.4

LONGITUDINAL BENDING MOMENT DISTRIBUTION AT THE INTERMEDIATE SUPPORT USING DIFFERENT METHODS

	PERCENTAGE OF TOTAL LONGITUDINAL BENDING MOMENT (My)			
	EXPERIMENT	FOURIER SERIES	F.E. (ORTHOTROPIC PLATE ELEMENT)	F.E. COMPOSITE ACTION (PLATE & BEAM ELEMENTS)
Girder A(*)	34.1	33.3	33.1	33.7
Girder B	35.7	33.4	33.8	34.6
Girder C	30.2	33.3	33.1	32.7

(*) A and C are exterior beams and B is an interior beam.

in the composite section at the mid-span and at the intermediate support in the longitudinal direction is shown in Figure 6.9.

The theoretical values for the distribution of the lateral deflection, longitudinal moments at the mid-span and at the intermediate support sections, and the transverse bending moment at the mid-span were calculated using two methods: the orthotropic plate theory, in which a Fourier series deflection function was utilized as discussed elsewhere (21, 26, 37), and the finite element computer program SAP IV.

The pertinent rigidities of the equivalent orthotropic plate, calculated according to reference (21), were used in predicting the theoretical values given in Tables 6.1 to 6.4. Close agreement is observed not only between the experimental results and the orthotropic plate theory results, but also with the results from the finite element method in which two different models were used to model the composite bridge. It should be noted that modeling bridge model I by either the orthotropic plate element or the composite action, resulted in good correspondence with the experimental results; this shows that the suggested formulae for calculating the orthotropic plate rigidities are reliable. These formulae considered the effectiveness of the diaphragms in the transverse direction, while the OHBDC (53) usually neglected the effect of diaphragms in the design of bridges.

In order to calculate the contribution of the diaphragms to the slab in carrying the transverse bending moment, the transverse strain on the top and on the bottom flanges of the diaphragm and on the slab at the middle of the diaphragms were plotted, as shown in Figure 6.10. Strain on the bottom flange of the diaphragm is about four times the strain on the top flange,

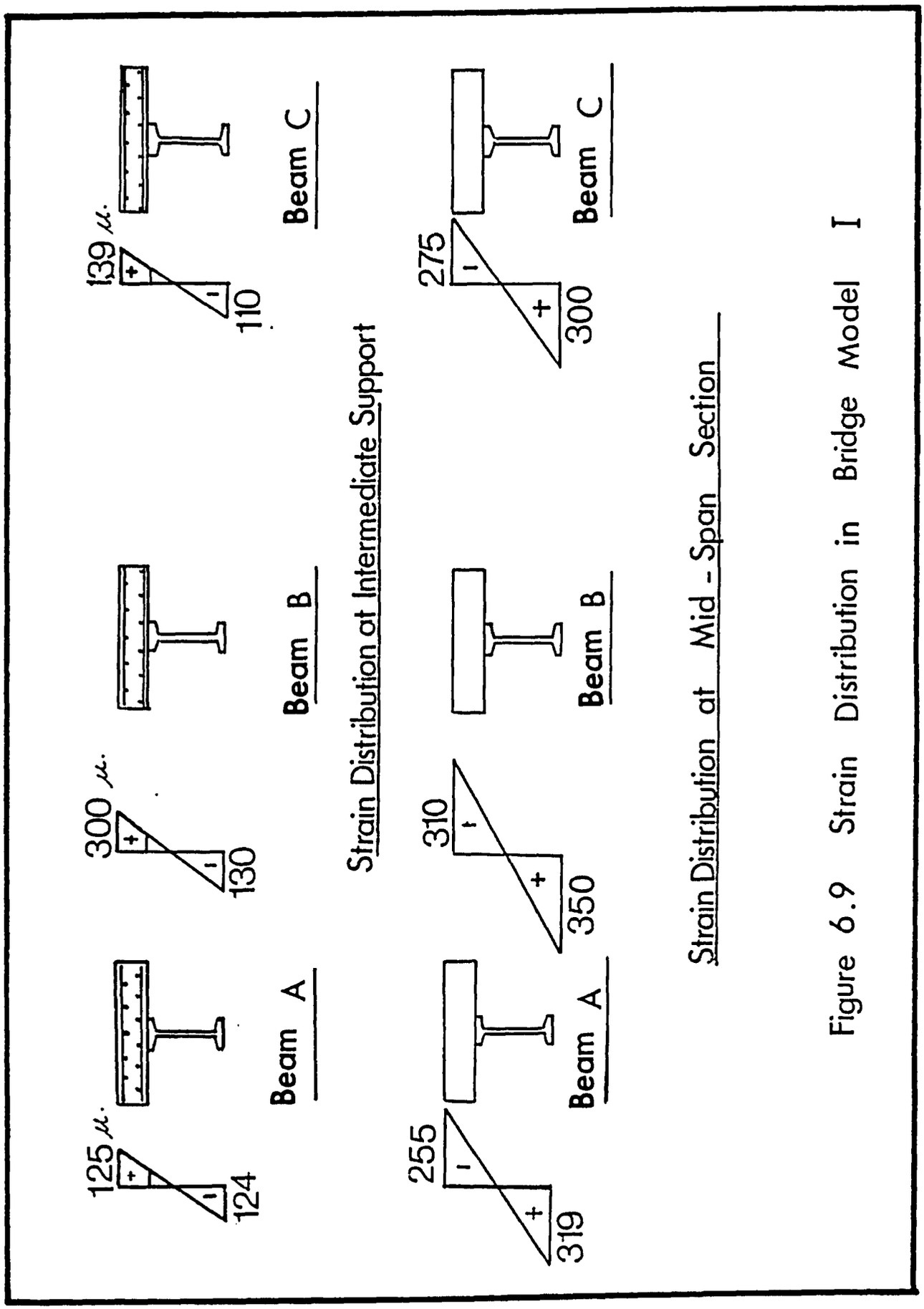

Figure 6.9 Strain Distribution in Bridge Model I

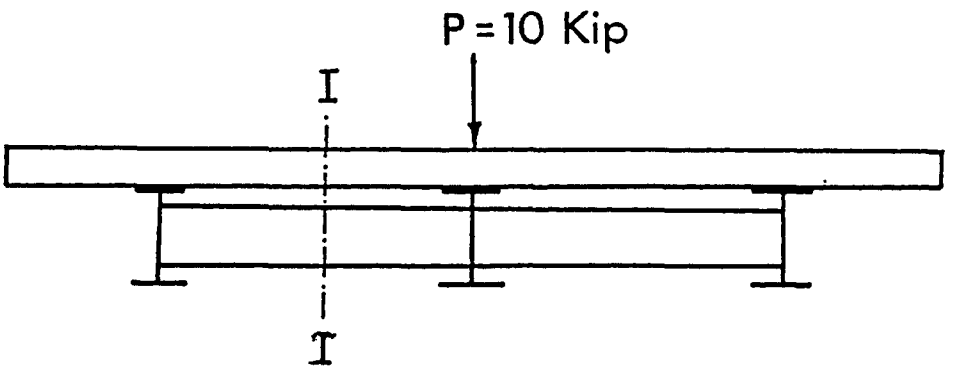

Cross – Section

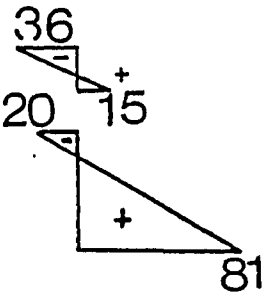

Section I-I

Figure 6.10 Strain Distribution on the Diaphragm & Slab in Transverse Direction

which explains that the neutral axis was forced to move towards the slab and is not at the middle of the diaphragm cross-section. Moreover, the strain on the top of the concrete slab is about twice the strain on the bottom of the slab, which again means that the neutral axis of the slab has been pushed towards the diaphragm. This observation proves that the slab and diaphragms are acting together to some significant degree, which is estimated to be approximately 70% in the present case. It is therefore expected as mentioned elsewhere (37) that a more economical design will result using the load distribution method, suggested by the OHBDC, when the pertinent rigidities are calculated as recommended in Reference (21).

6.4 ANALYSIS OF DYNAMIC TEST RESULTS

6.4.1 Sweep-Sine Wave Tests

The objective of conducting the sweep-sine wave tests on the two bridge models was to obtain the vibration signature of the acceleration time histories at different locations on each model. The forcing function that was used for the sweep test was sinusoidal as shown in Figure 6.11. Before analyzing the results, the adequacy and quality of data were verified by visual examination on a strip chart obtained from a computer-plotted trace; this was necessary to avoid any introduced distortions into the computed results caused by signal clipping, "blips" or record gaps. A typical acceleration time history at the mid-span of bridge model I close to the resonance frequency is shown in Figure 6.12. The extraction of useful information invariably requires the computation of Fourier Transform. Therefore, in order to express the acceleration response in a frequency domain instead of time domain, Fourier Transform technique was

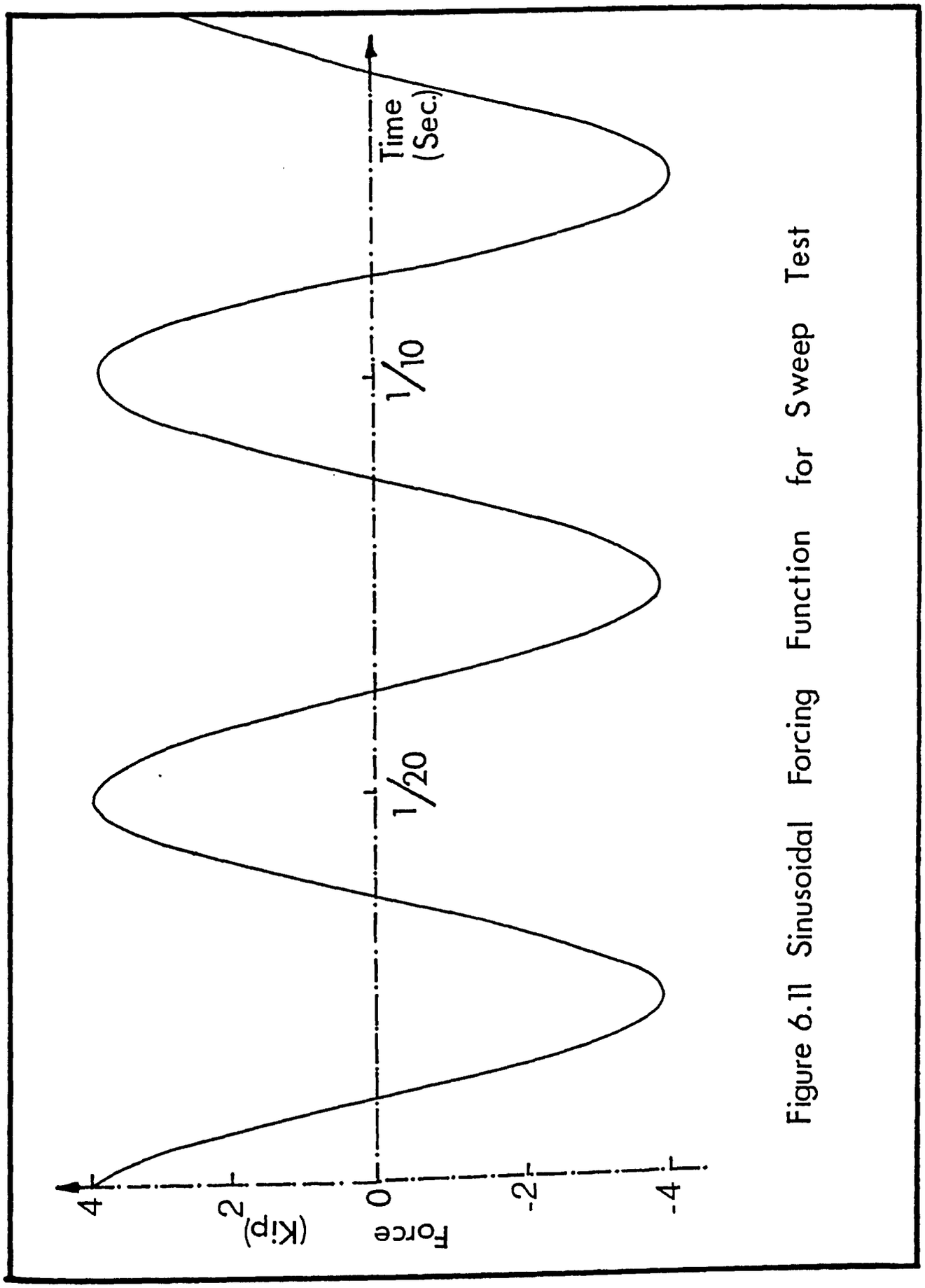

Figure 6.11 Sinusoidal Forcing Function for Sweep Test

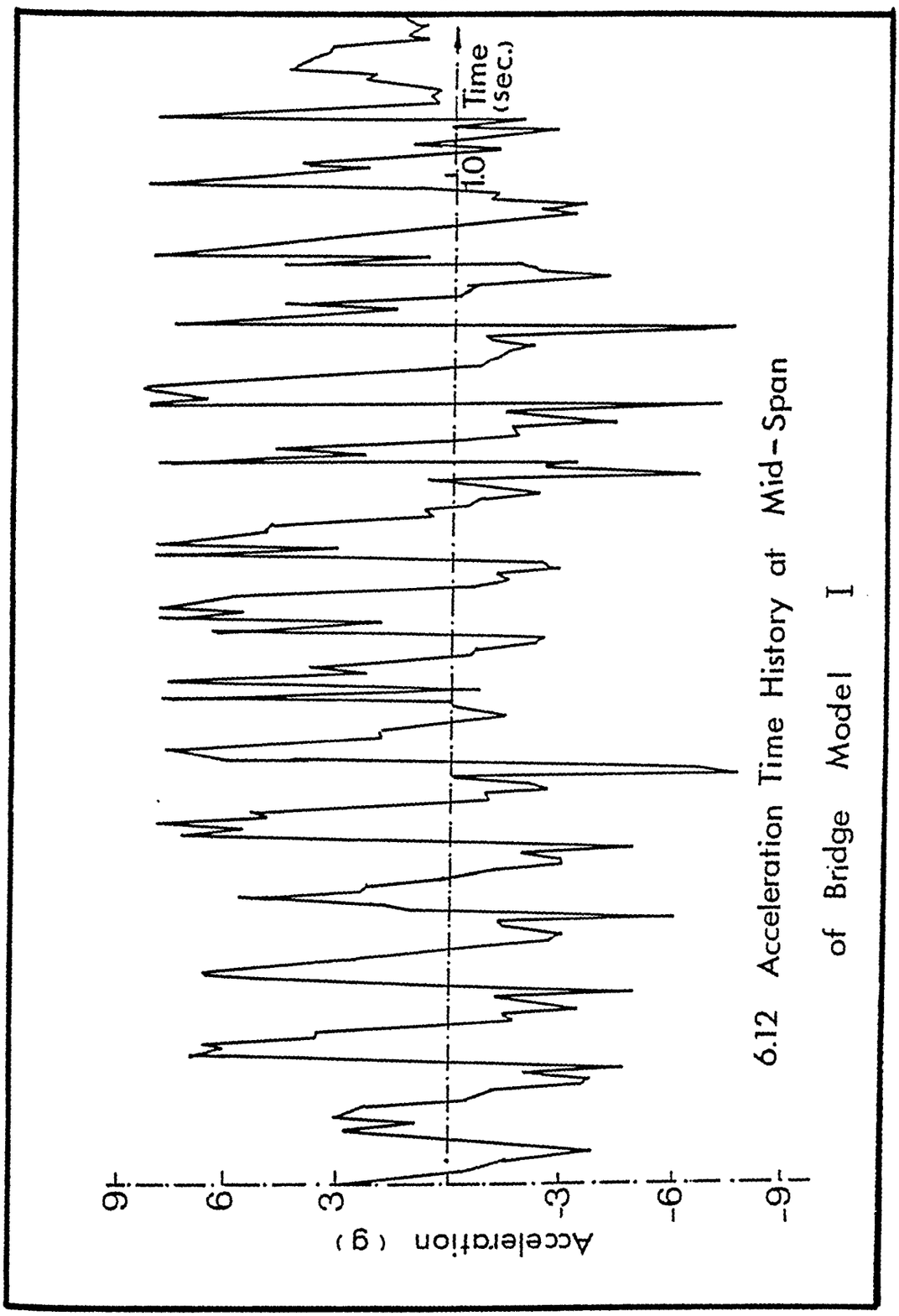

6.12 Acceleration Time History at Mid-Span of Bridge Model I

used. The continuous time signal, shown in Figure 6.12, was transformed into frequency domain by using the following relation:

$$\ddot{X}(\omega) = \sum_{-\infty}^{\infty} \ddot{X}(t)\, e^{\pm i\omega t}\, \Delta t \qquad (6.6)$$

where

$\ddot{X}(\omega)$ = Fourier transform function

$X(t)$ = Time domain function

ω = Circular frequency

t = Time

$i = \sqrt{-1}$, for an imaginary quantity

The Fourier transform can be expressed as a complex function in the form

$$X(\omega) = a(\omega) + ib(\omega) \qquad (6.7)$$

where

$a(\omega)$ = real part of Fourier transform

$b(\omega)$ = imaginary part of Fourier transform

A computer program was developed, with the help of the Electrical Engineering Department, to apply Equation 6.6 and produce the fast Fourier transform program (FFT). The output of the FFT was plotted by using Zetta plot subroutines available at the University of Windsor computer library. A list of the FFT and Zetta plot subroutine are given in Appendix C. A sweep test result as acceleration output of bridge model I of the middle beam is shown in Figure 6.12; using this acceleration output as an input to the FFT computer program gave the spectrum response of bridge model I in the frequency domain, as shown in Figure 6.13.

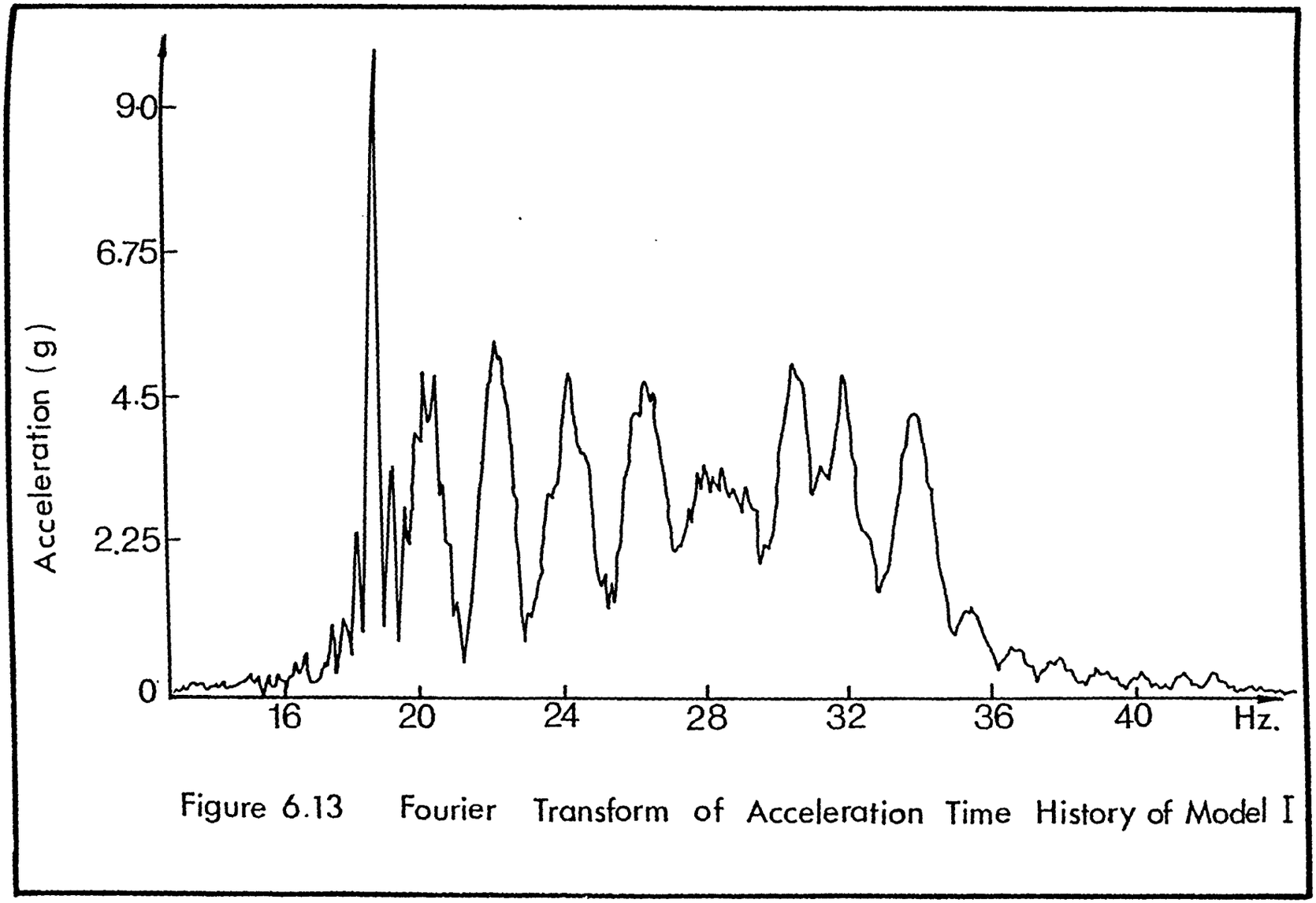

Figure 6.13 Fourier Transform of Acceleration Time History of Model I

This Fourier transform of the acceleration in the frequency domain provided the first four natural frequencies of bridge model I. The first natural frequency was clearly identified while the other three natural frequencies were not very well separated. The complex character of the acceleration response curve near resonance was, perhaps, a result of the transverse and the longitudinal cracks in the concrete deck, caused by the static test. However, by using the time history response in the time domain, and noticing the phase angle, whether it is in phase or out of phase, between different locations in the longitudinal and transverse direction, the second, third and fourth natural frequencies were identified. This Fourier transform technique was suitable for identifying and extracting the natural frequencies, from the time history response, as evidenced by the sweep test.

Bridge model II was tested using the same sweep forcing function applied slowly and continuously for the same range of frequencies. Acceleration time history of the middle beam and the corresponding Fourier transform are shown in Figures 6.14 and 6.15. The first three natural frequencies were well separated, similar to that for a single degree of freedom structure, perhaps because there were no cracks at that time. Also, the presence of the prestressed portion helped in maintaining constant rigidity along the entire deck. The acceleration response on the middle and exterior beams are shown in Figures 6.16 and 6.18 respectively. The corresponding Fourier transform are given in Figures 6.17 and 6.19, which were almost identical and yielded the same natural frequencies as the one given by Figure 6.15. It is observed from Figures 6.17 and 6.19 that

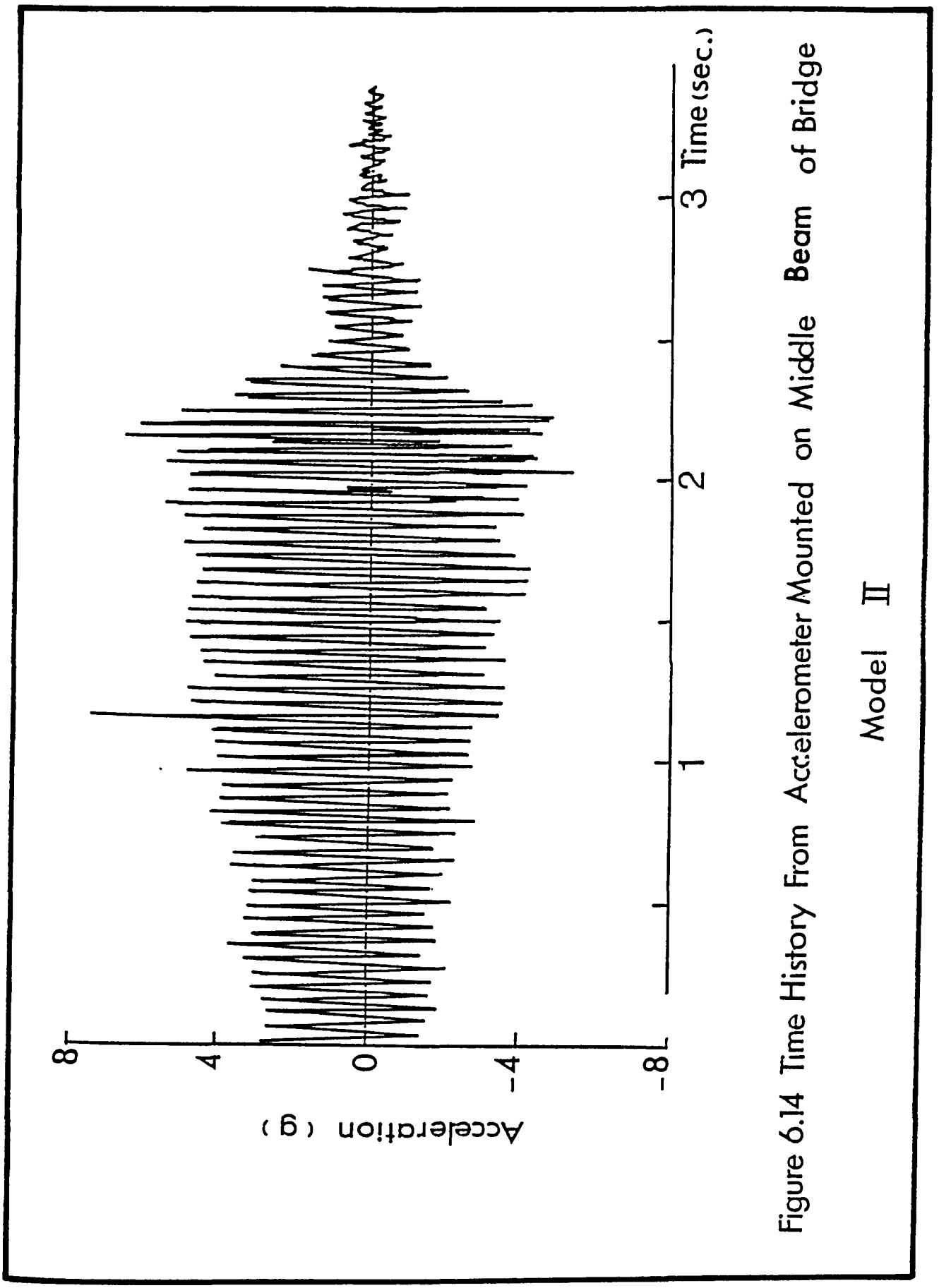

Figure 6.14 Time History From Accelerometer Mounted on Middle Beam of Bridge Model II

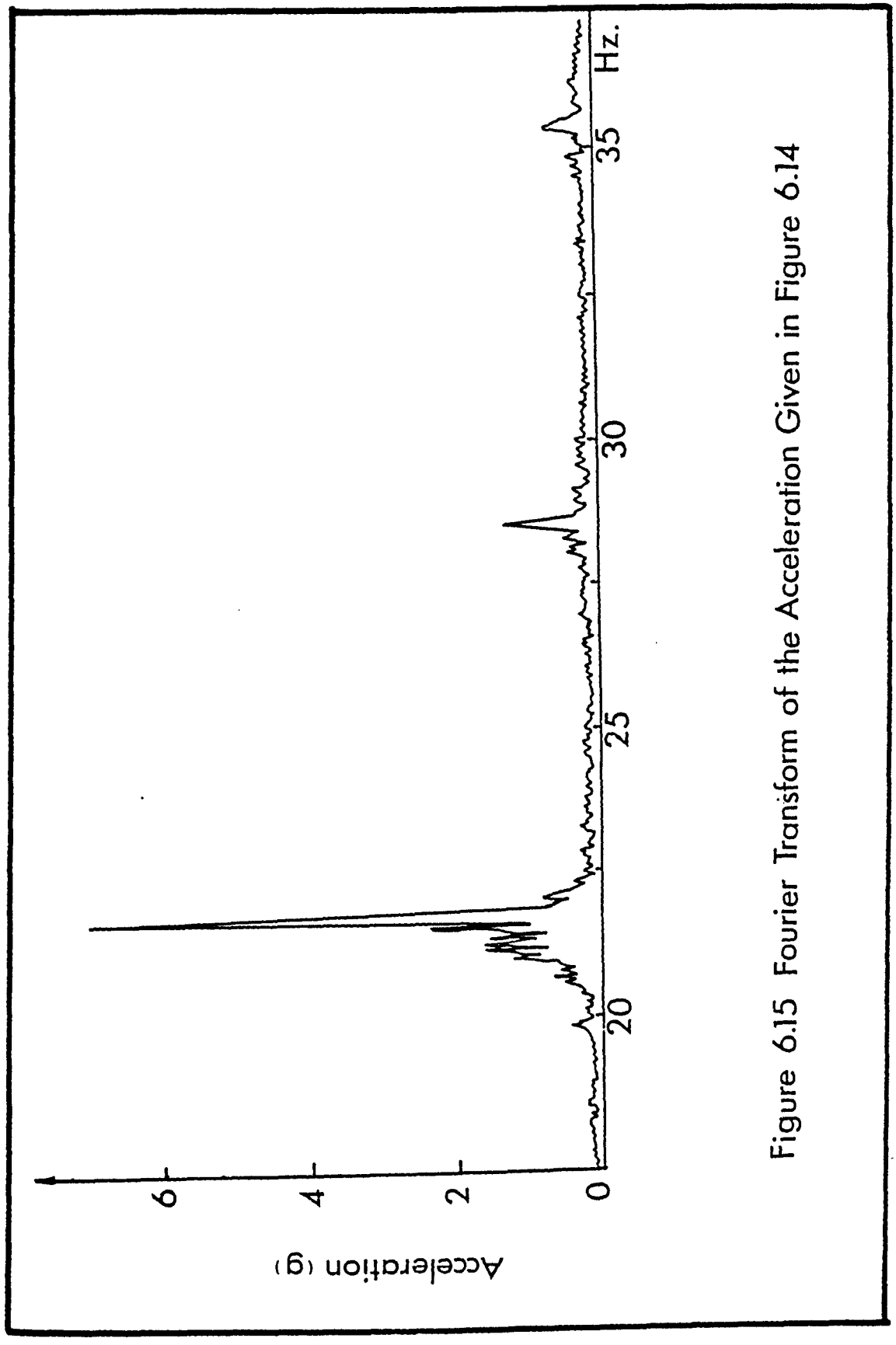

Figure 6.15 Fourier Transform of the Acceleration Given in Figure 6.14

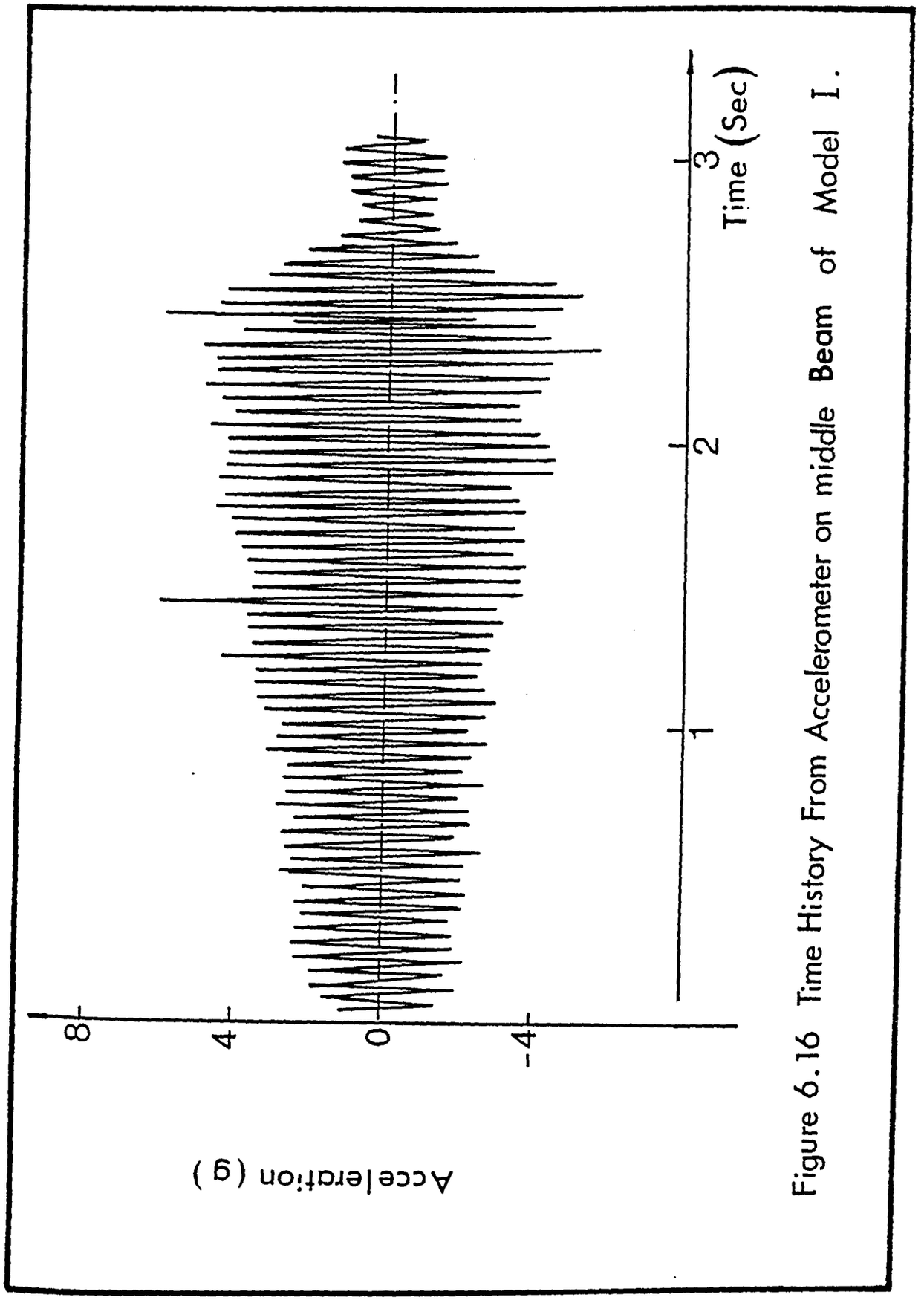

Figure 6.16 Time History From Accelerometer on middle Beam of Model I.

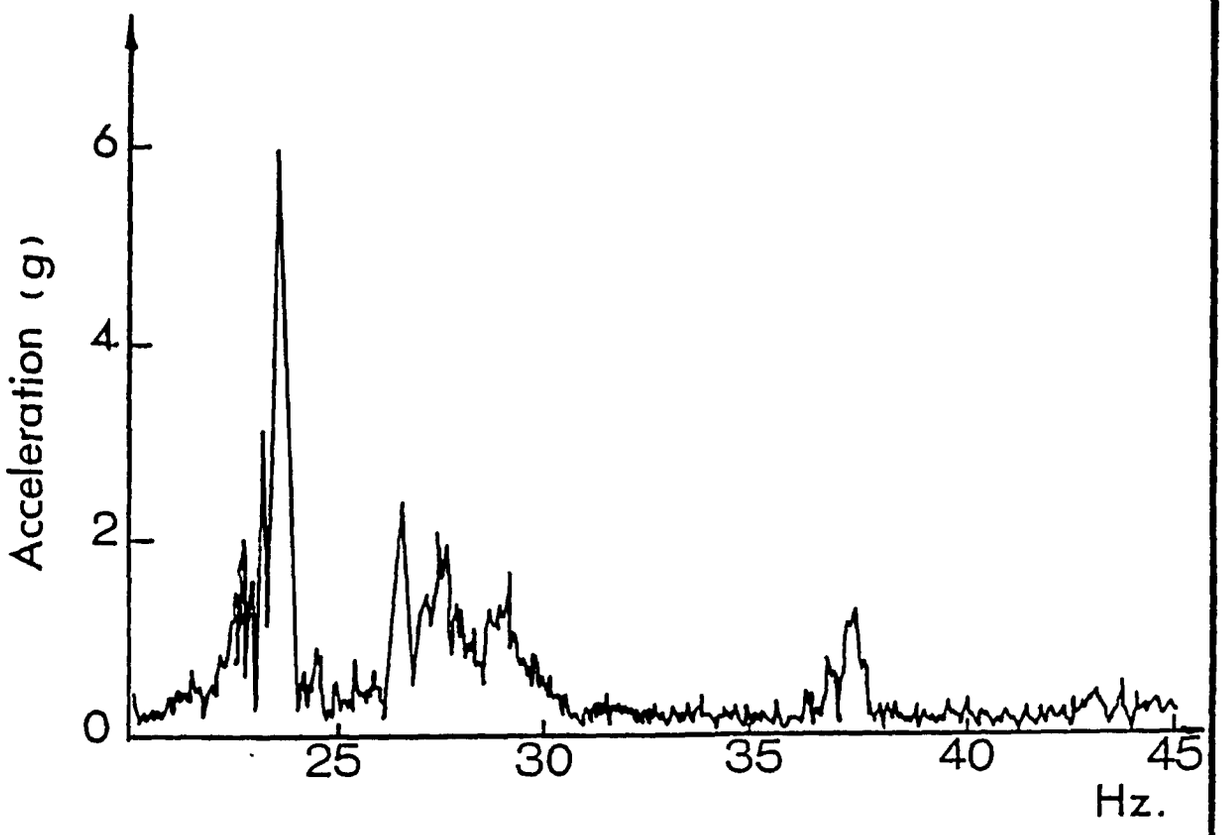

Figure 6.17 Fourier Transform of Acceleration Time History Given in Figure 6.16

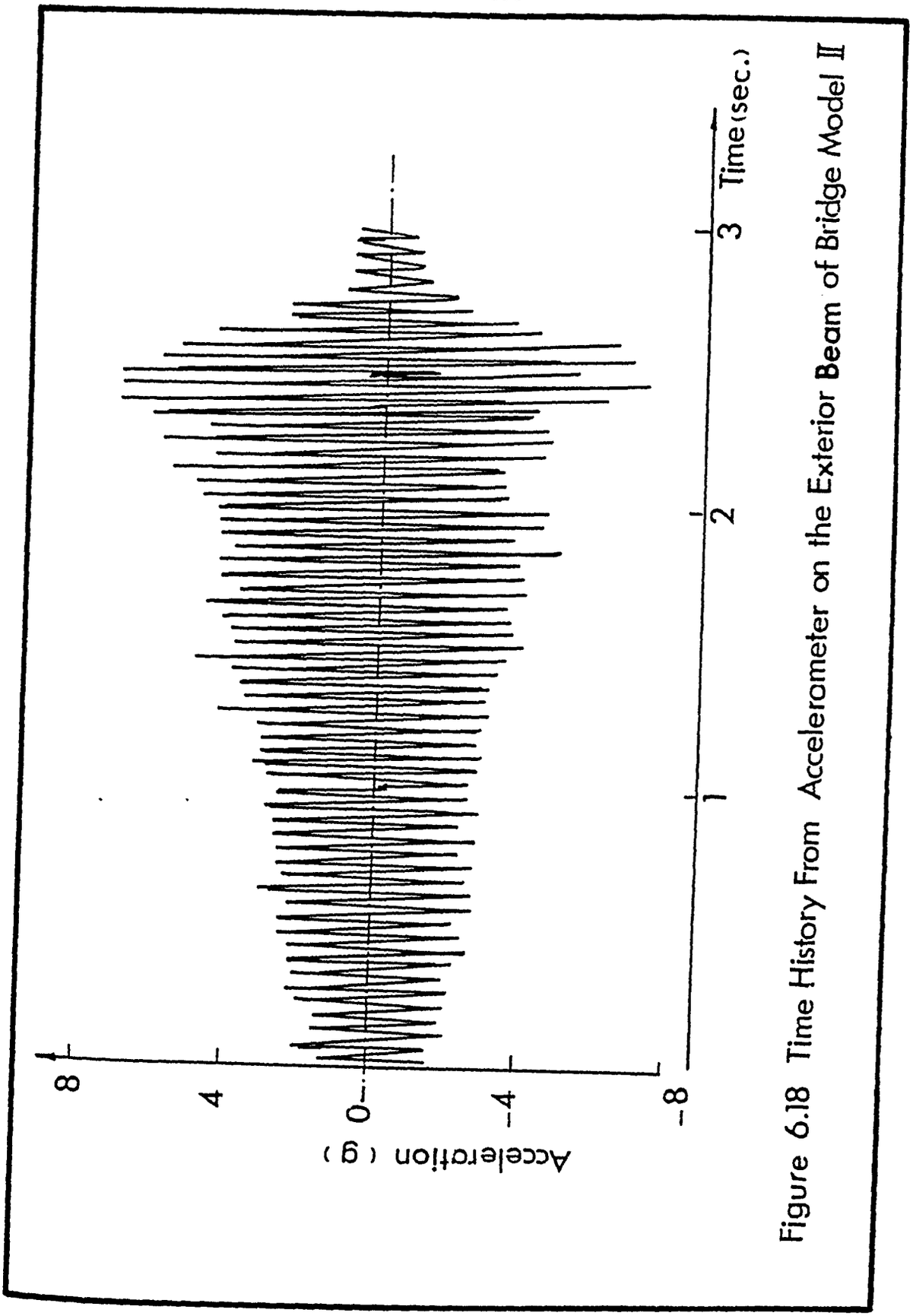

Figure 6.18 Time History From Accelerometer on the Exterior Beam of Bridge Model II

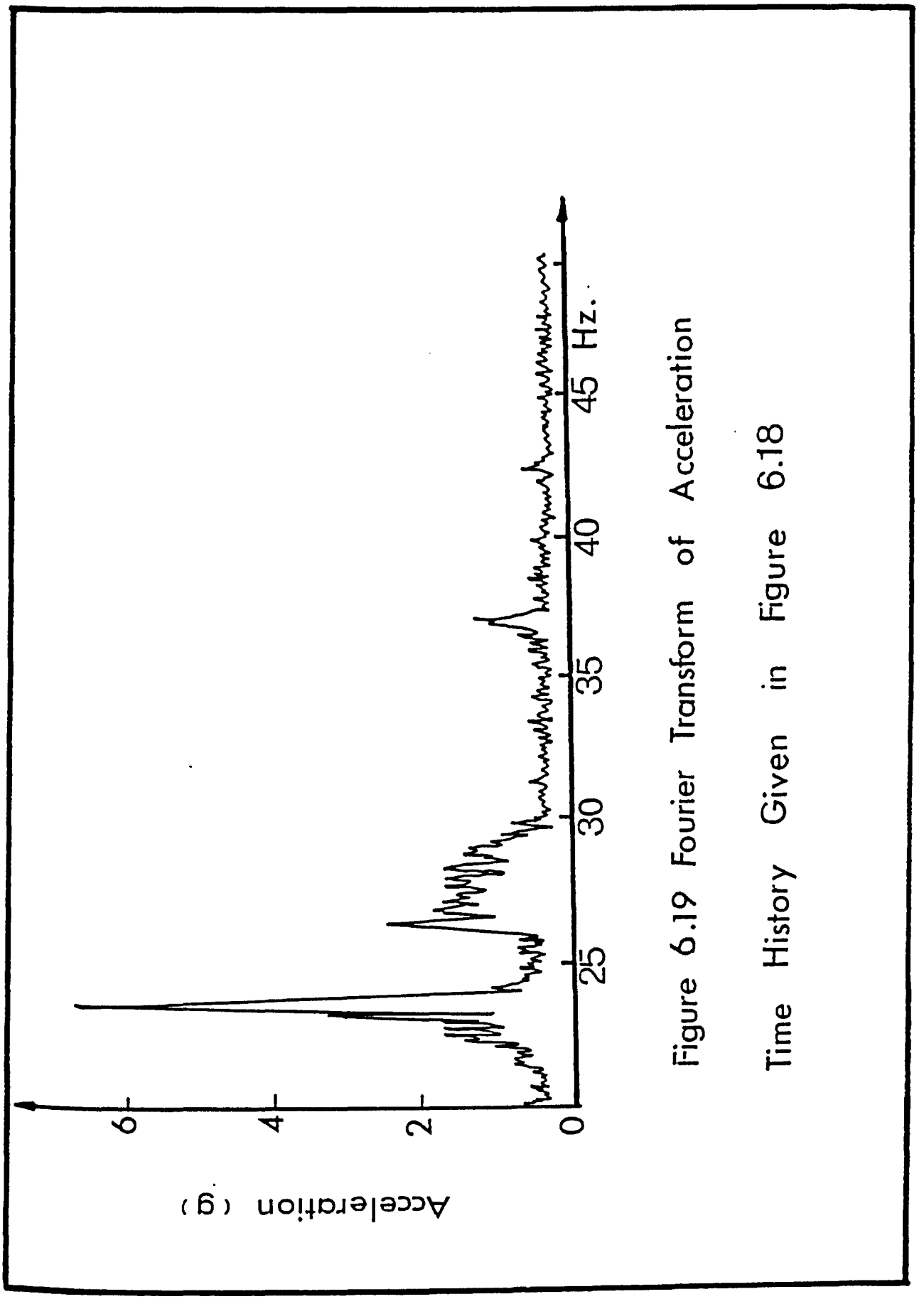

Figure 6.19 Fourier Transform of Acceleration Time History Given in Figure 6.18

the second natural frequency was not clearly identifiable as was the case in Figure 6.15.

6.4.2 Normal Modes Tests

The objective of this test was to obtain the mode shapes of bridge models I and II after determining their natural frequencies. The steady state vibration at the first three mode shapes were measured at 18 locations along the entire deck of each model and plotted using the Zita subroutine. Fast Fourier transform was used to find the vibration levels in the frequency domain at the first three mode shapes of bridge models I and II. The identification of the associated mode shapes required the determination of phase between the signals from the 18 measuring locations. This was achieved by simple addition and subtraction of signals and observing how the amplitude of the Fourier transform peaks changed. Frequency components that were in phase resulted in increasing resonance peaks of added signal; out-of-phase signals resulted in decreasing resonance peaks. It should be noted that this method is applicable if the real part of the frequency components are either in-phase or out-of-phase since they constitute normal modes with only real components. It was noticed that the vibration levels, in terms of g's, of bridge model II were slightly less than the vibration levels experienced by bridge model I. This could be attributed to the effect of prestressing a portion of the concrete deck around the intermediate support in bridge model II, which helped in eliminating the transverse cracks in the vicinity of the intermediate support. The first three mode shapes of bridge models I and II were plotted as shown in Figures 6.20, 6.21 and 6.22.

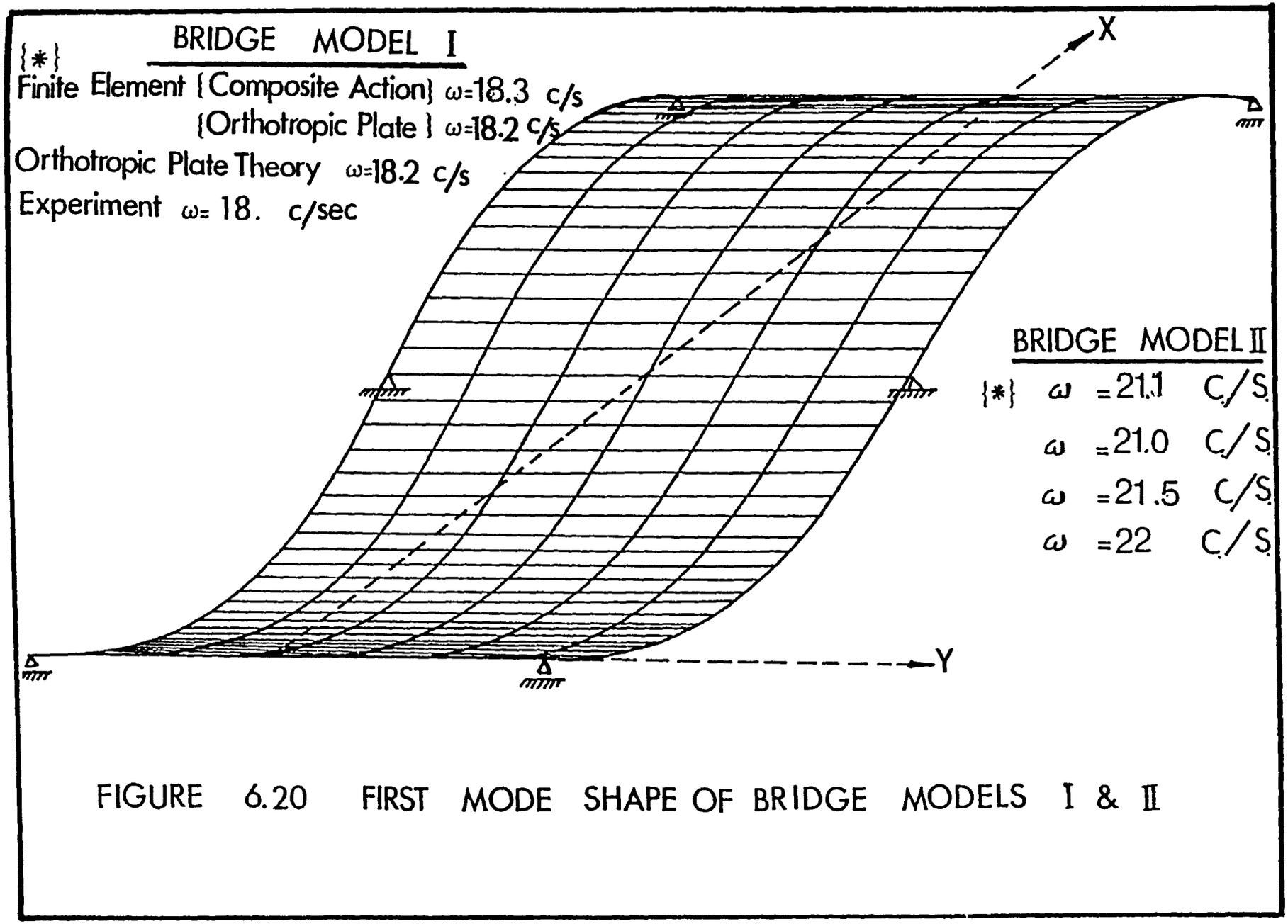

FIGURE 6.20 FIRST MODE SHAPE OF BRIDGE MODELS I & II

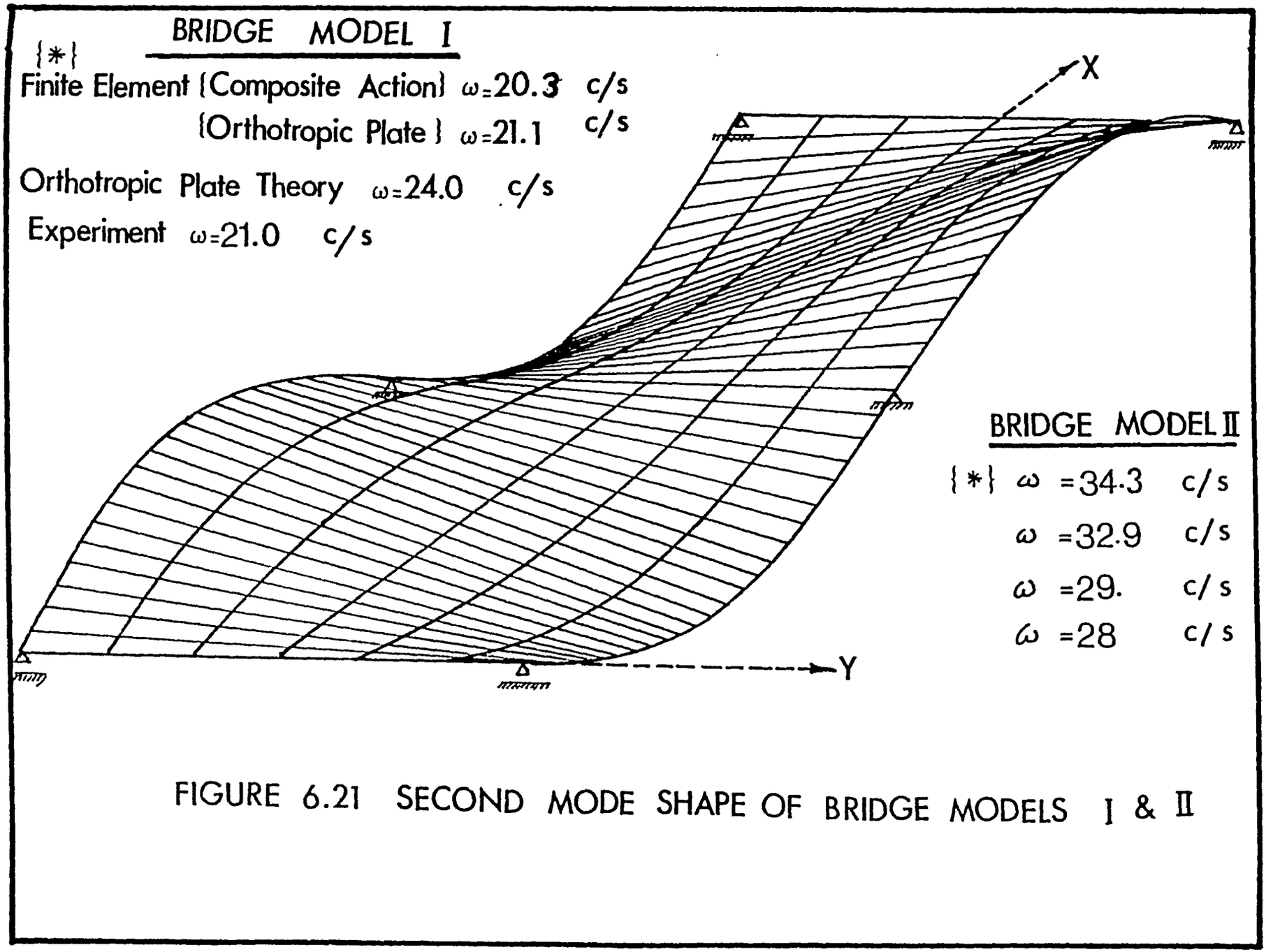

FIGURE 6.21 SECOND MODE SHAPE OF BRIDGE MODELS I & II

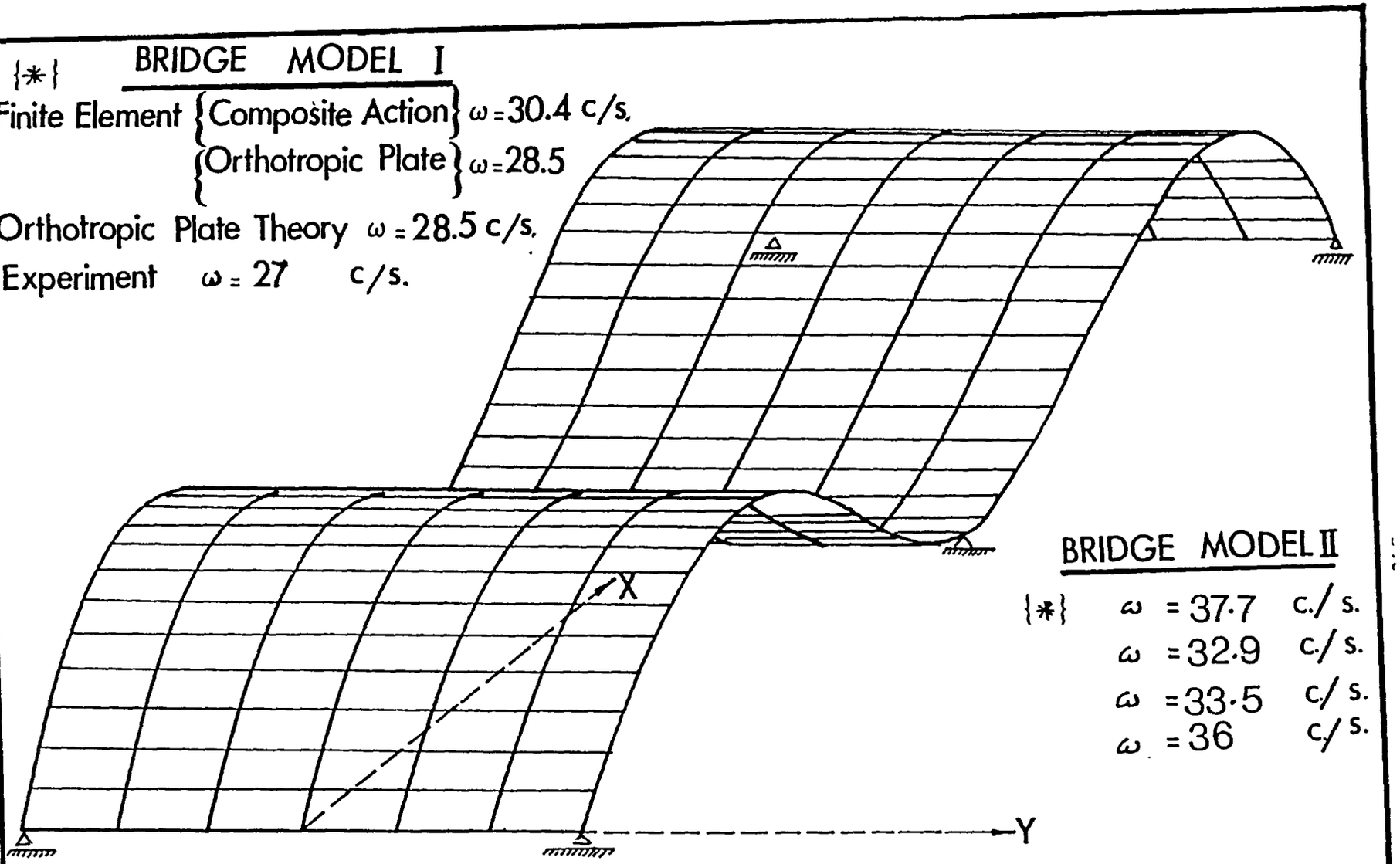

FIGURE 6.22 THIRD MODE SHAPE; BRIDGE MODELS I & II

The first mode shape was anti-symmetric in the longitudinal direction about the intermediate support, and symmetrical about the longitudinal x-axis in the transverse direction. This mode shape is simply a flexural mode, while the second mode shape is a torsional mode, which was anti-symmetrical about the intermediate support and the longitudinal x-axis. The third mode shape was symmetrical about the intermediate support and the longitudinal axis, which means that it is a flexural vibration mode. The fourth mode shape up to the eight mode of vibration were plotted as shown in Figures 6.23 to 6.27, using the results obtained from the orthotropic plate theory and were verified by results from the finite element computer program, SAP IV. The fourth, sixth and eight mode shapes are torsional modes, while the fifth and the seventh modes are flexural modes. Usually, the first three fundamental modes of vibration in any structure are of the most concern in any analysis. However, the reason for calculating the first eight mode shapes of vibration of the continuous composite bridge will be explained later on in Section (6.7.3).

6.4.3 Logarithmic Decay Response of Bridge Models I and II

Damping can be determined by a number of methods. However, the logarithmic decay test is one of several types of dynamic tests, which can be conducted as a means of determining the equivalent viscous damping ratio. The logarithmic decrement method is valid for a multi-degree-of-freedom system provided that the continuous composite bridge model system vibrates in a single mode. The logarithmic decrement method is fairly easy to apply by utilizing the solution of the equation of motion for a single-

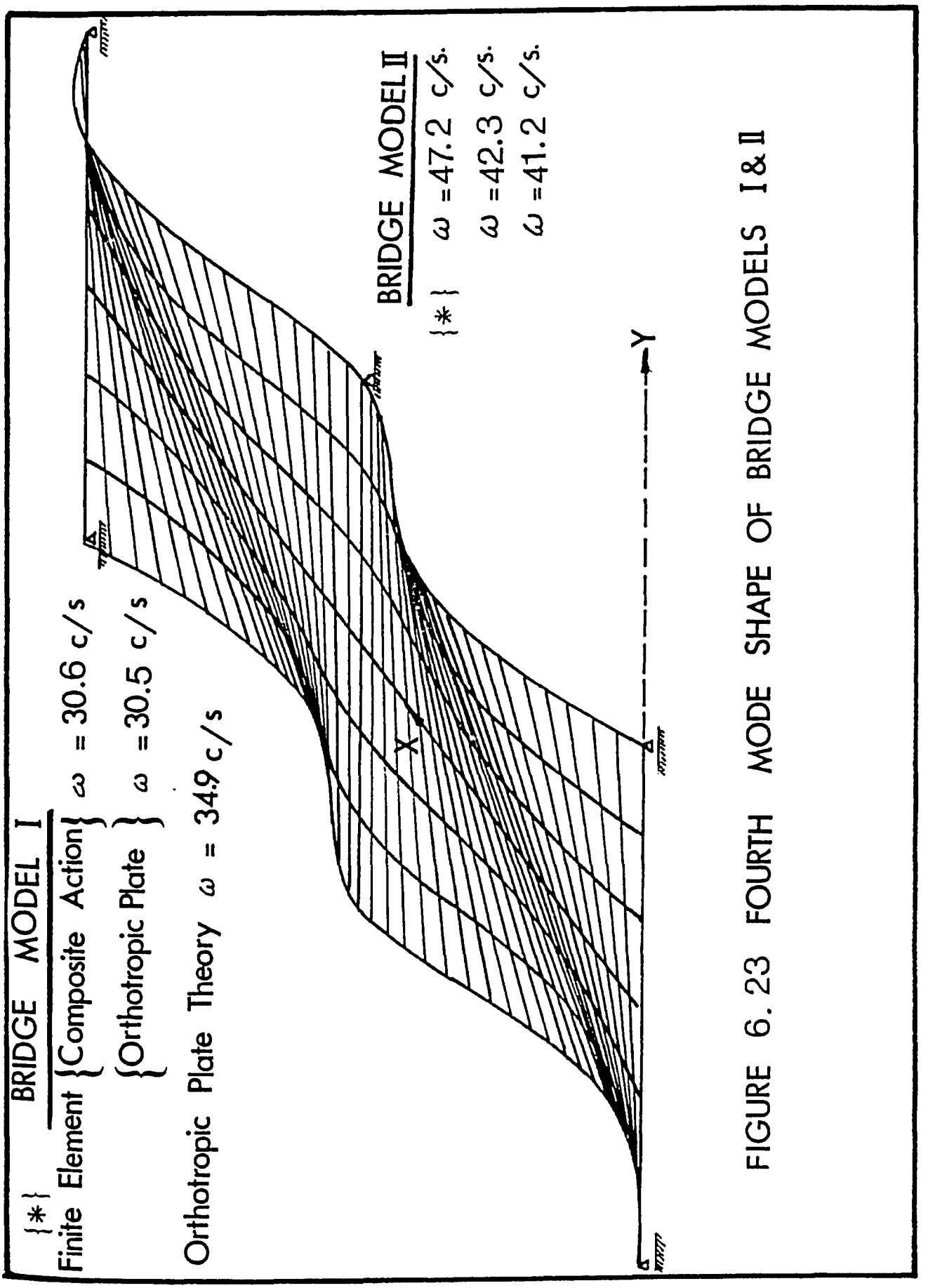

FIGURE 6.23 FOURTH MODE SHAPE OF BRIDGE MODELS I & II

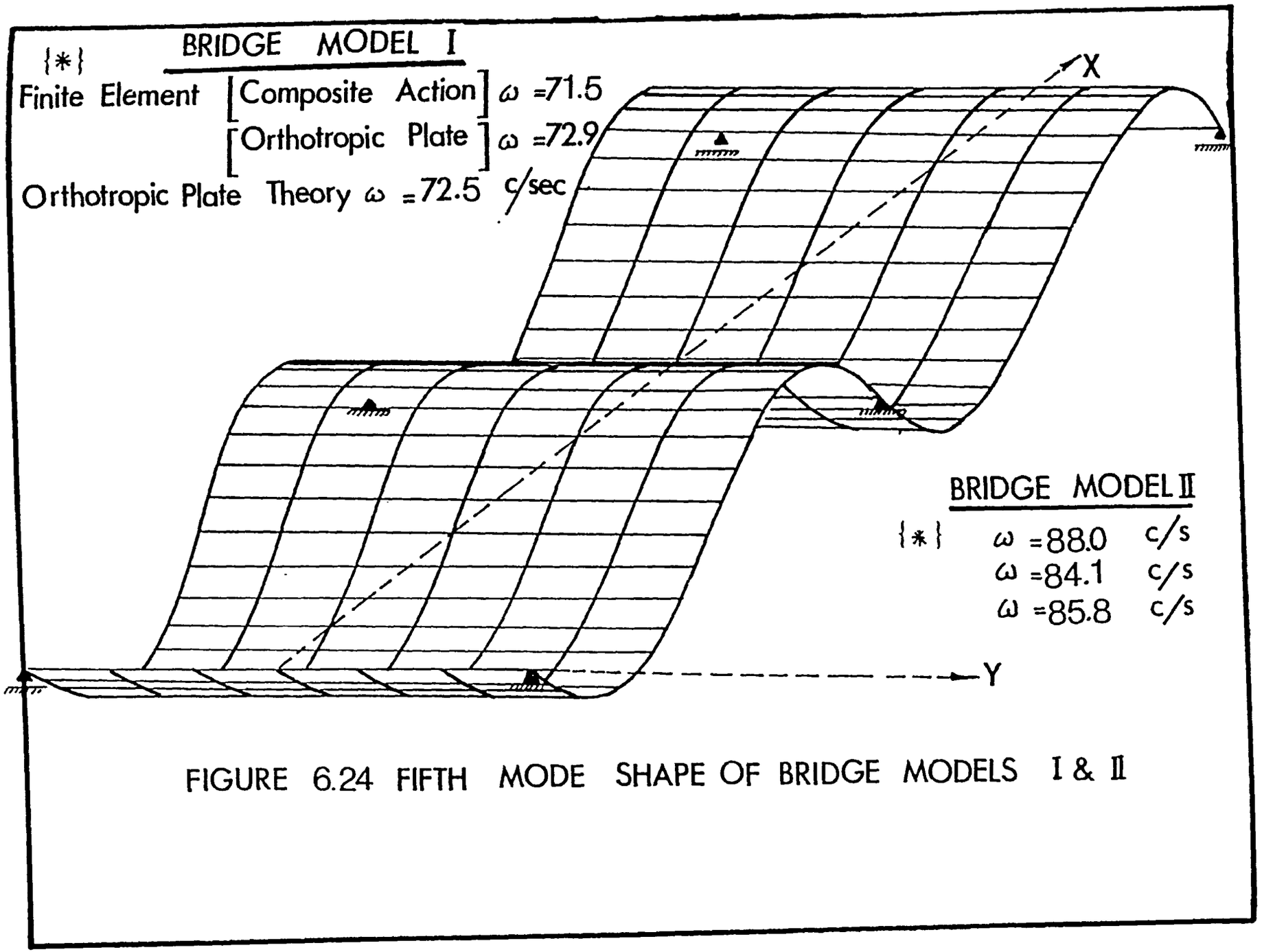

FIGURE 6.24 FIFTH MODE SHAPE OF BRIDGE MODELS I & II

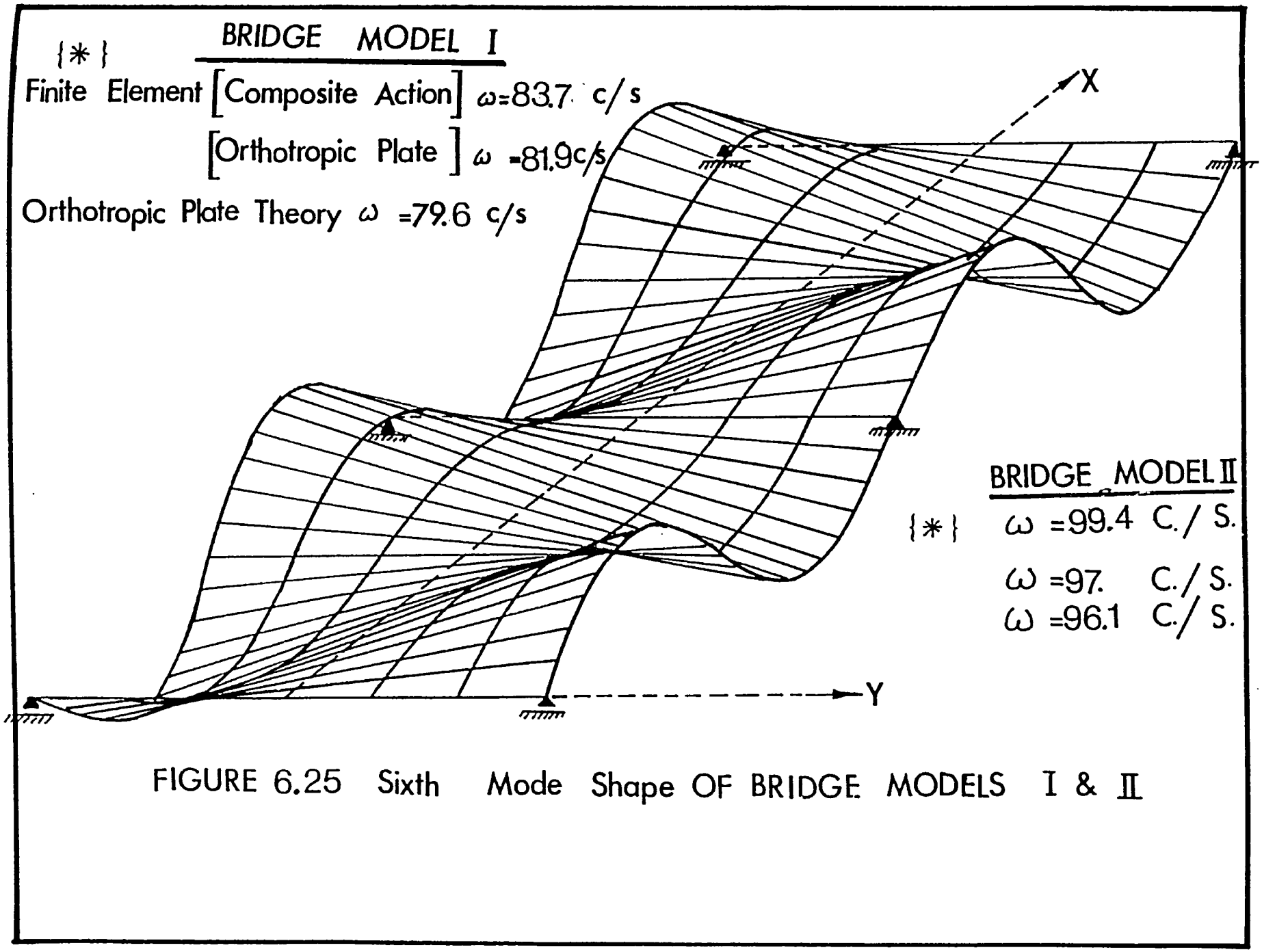

FIGURE 6.25 Sixth Mode Shape OF BRIDGE MODELS I & II

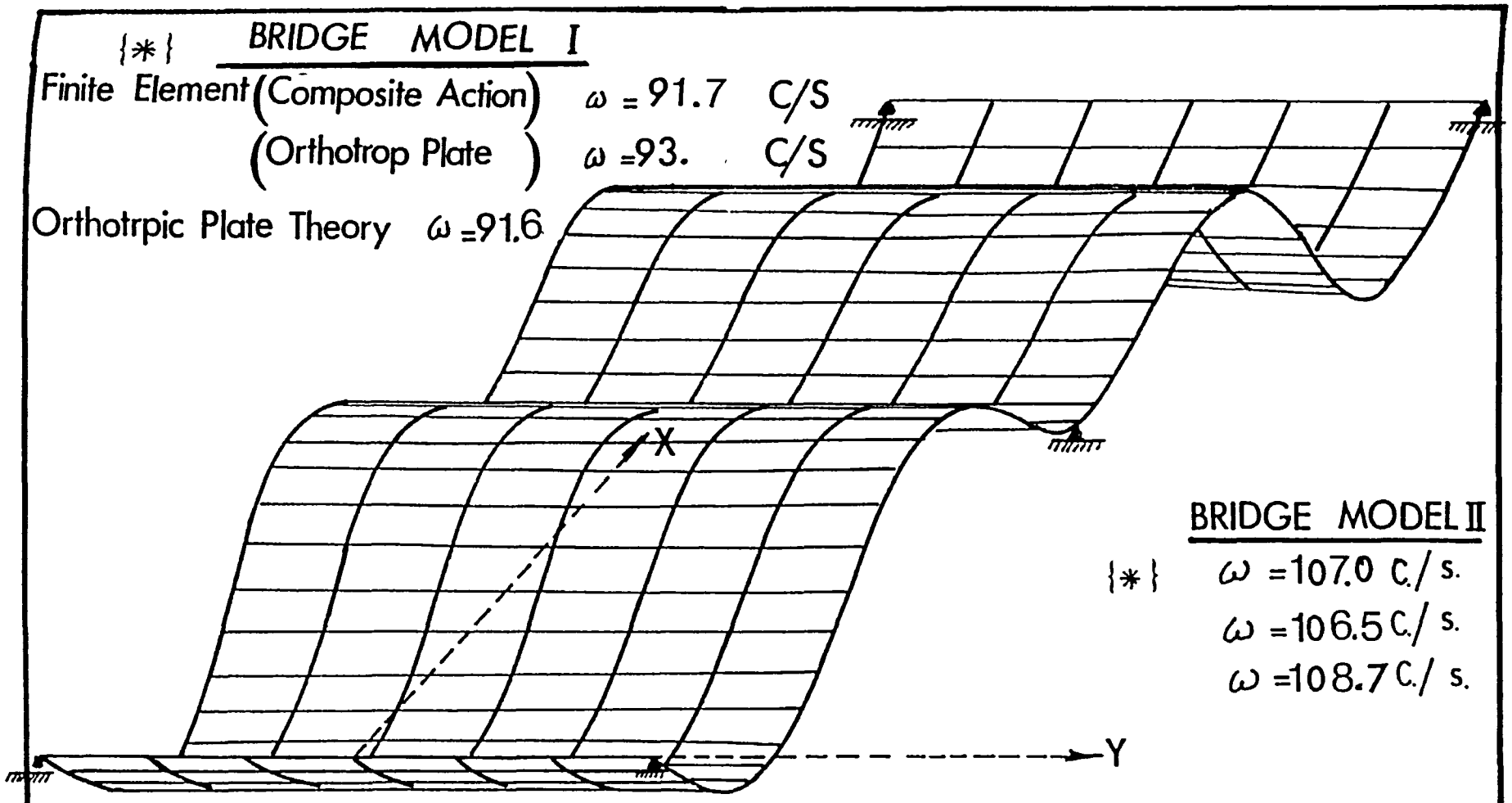

FIGURE 6.26 SEVENTH MODE SHAPE OF MODELS I & II

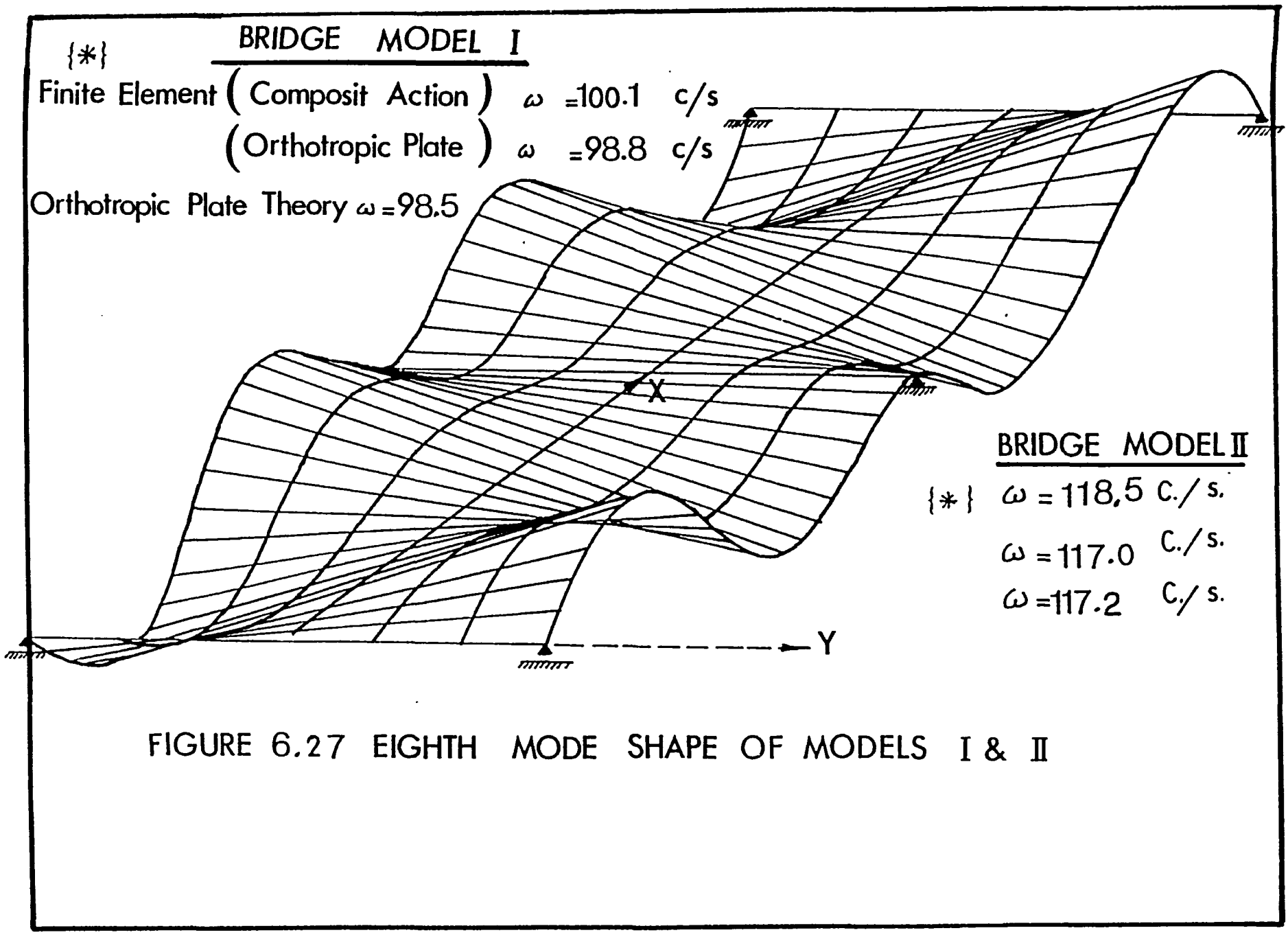

FIGURE 6.27 EIGHTH MODE SHAPE OF MODELS I & II

degree of freedom system; the natural logarithm of the ratio of an initially selected single peak to the nth successive single peak is given by

$$\xi = \frac{1}{2n\pi} \ln \left(\frac{\ddot{X}_1}{\ddot{X}_{n+1}}\right) \qquad n = 1,2,3,4,... \qquad (6.7)$$

where

ξ = Linear viscous damping ratio

$\ddot{X}$ = Acceleration, initial single peak

$\ddot{X}_{n+1}$ = Acceleration, single peak after n cycles

n = number of cycles

The acceleration response for transient vibration at the first natural frequency of bridge model I is shown in Figure 6.28. This signal contains only one mode response from which the equivalent viscous damping ratio was calculated using the logarithmic decrement method. The damping ratio was found to be 3.2%. This damping ratio also represents the material friction and coulomb friction present between the concrete deck, shear connectors, and steel girders, and at the supports. It should be noted that the calculated damping ratio is based on the decay rate in the free vibration system only.

For bridge model II, the damping ratio at the same location was found to be about 2.4%, as shown in Figure 6.29. This means that the damping ratio of bridge model II is about 35% less than the damping ratio of bridge model I. Two other locations on bridge model II were tested and the damping ratios were found to be 2.2% and 2.4%, as shown in Figures 6.30 and 6.31. The variation in damping between bridge models I and II was expected

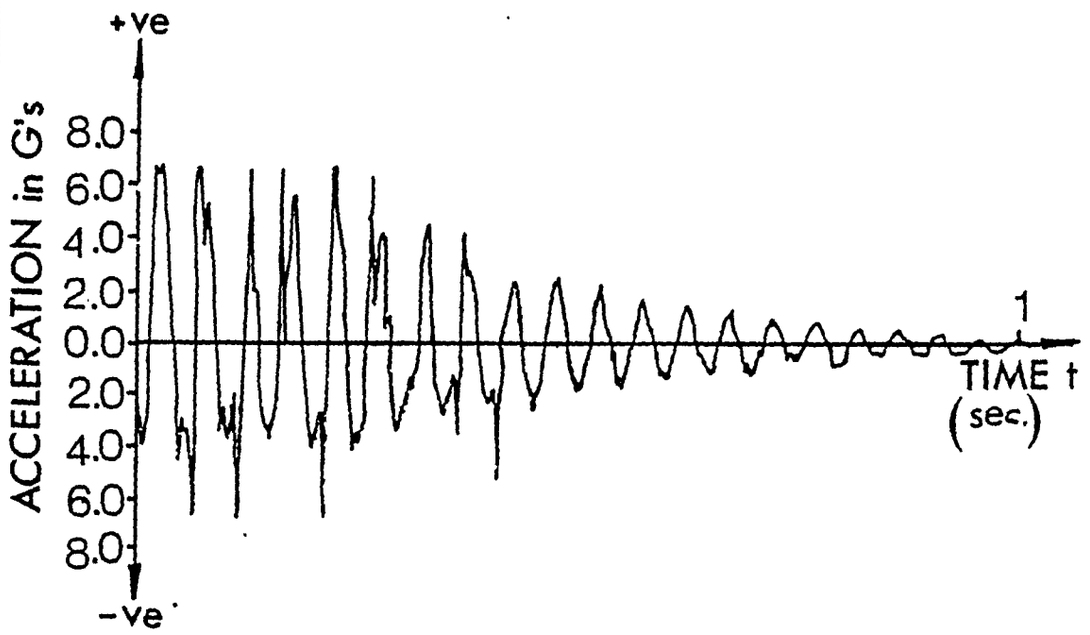

Figure 6.28
Acceleration Response For Transient Vibrations of Model I

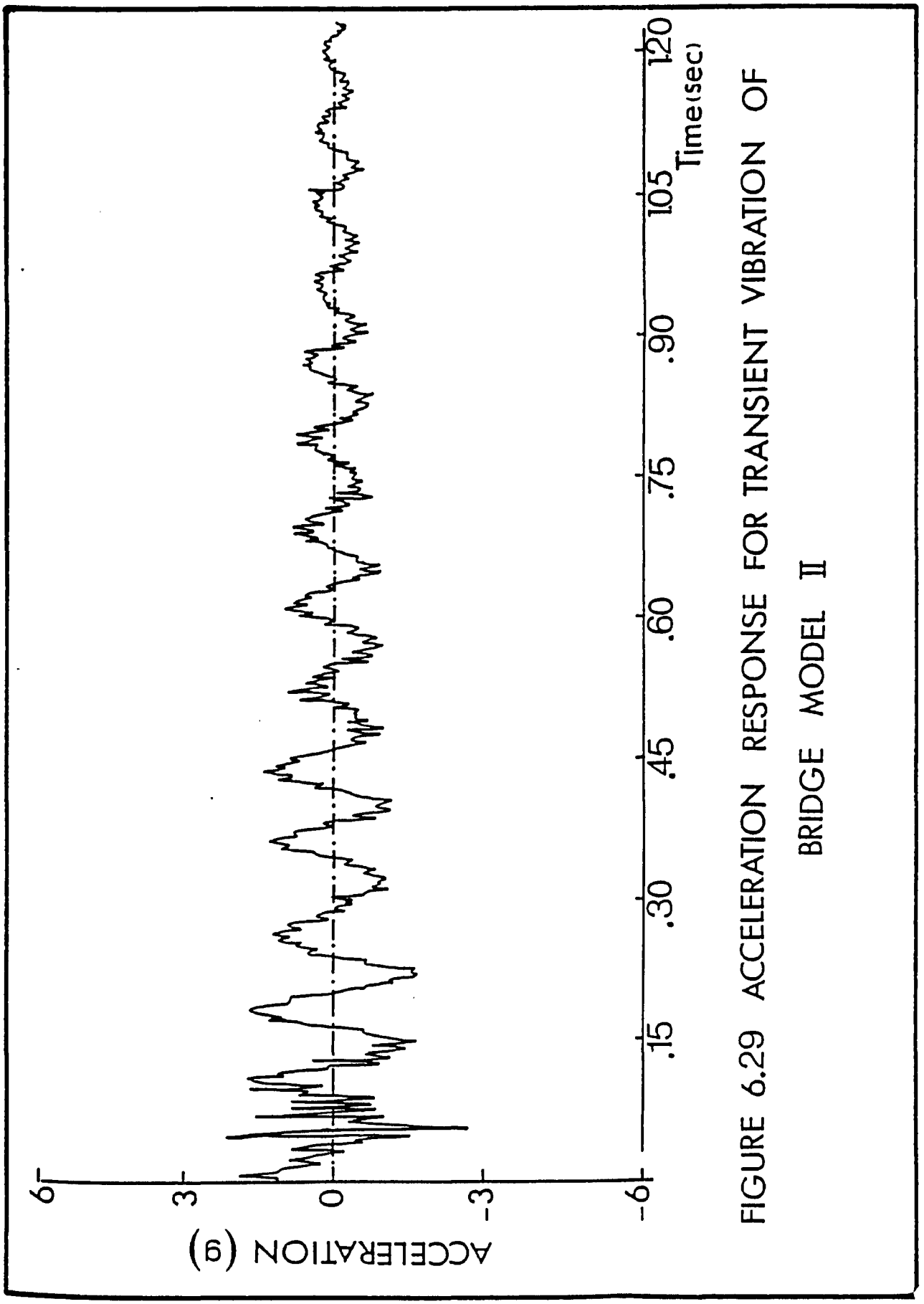

FIGURE 6.29 ACCELERATION RESPONSE FOR TRANSIENT VIBRATION OF BRIDGE MODEL II

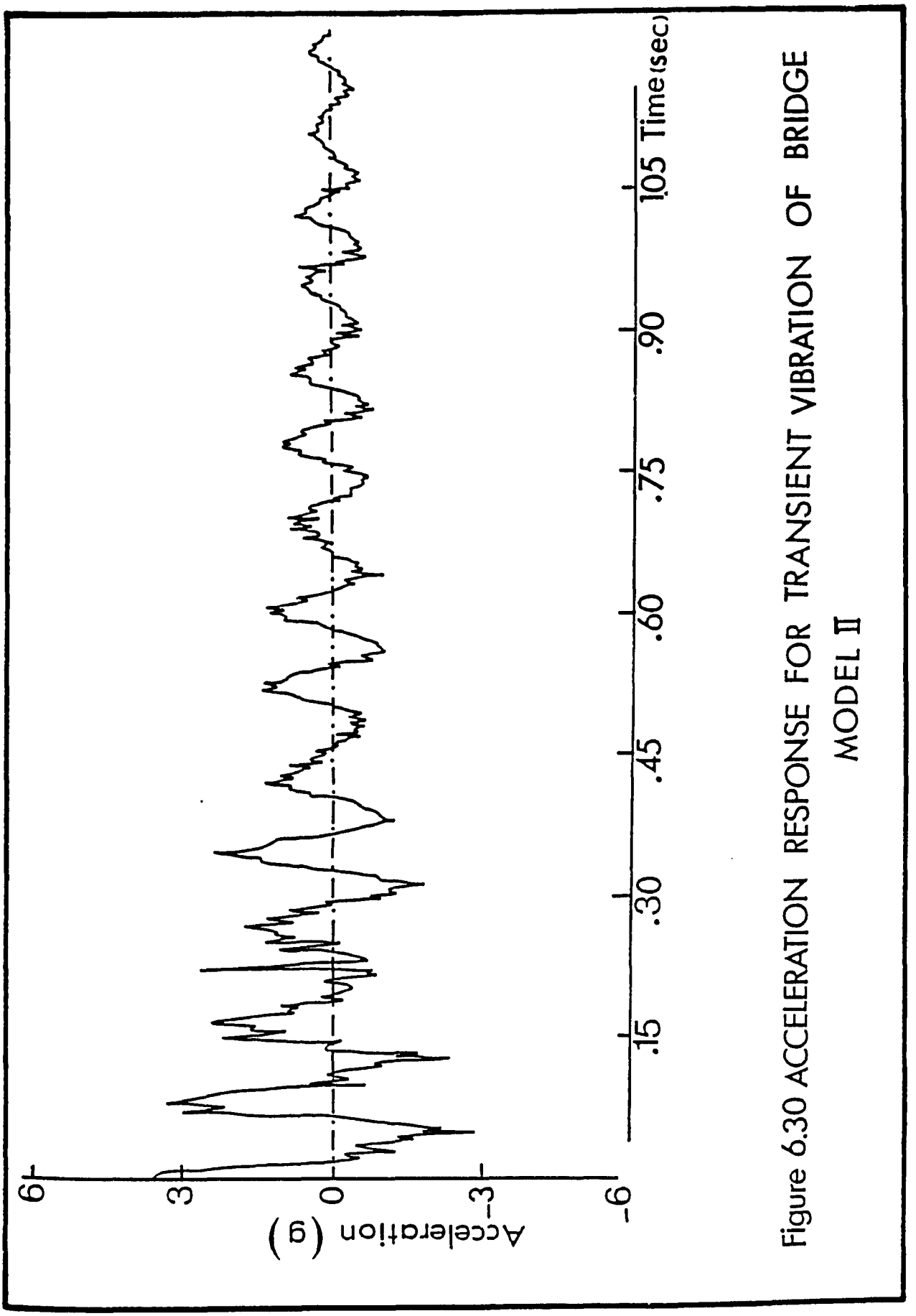

Figure 6.30 ACCELERATION RESPONSE FOR TRANSIENT VIBRATION OF BRIDGE MODEL II

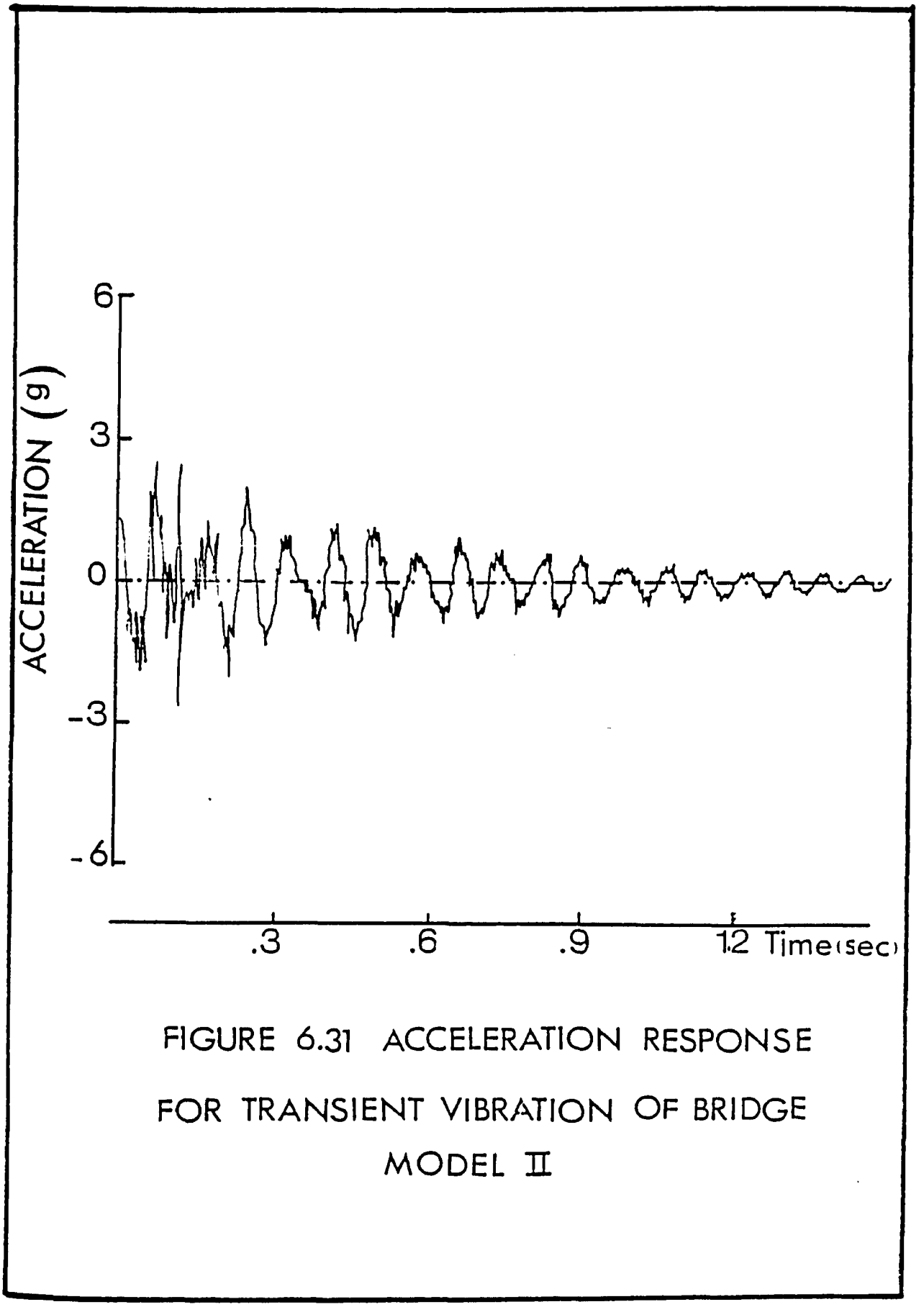

FIGURE 6.31 ACCELERATION RESPONSE FOR TRANSIENT VIBRATION OF BRIDGE MODEL II

because bridge model I had some transverse cracks at the intermediate support in contrast to the situation in bridge model II. Therefore, one can conclude that cracking of the concrete deck is an important parameter which influences damping in a composite bridge, i.e., more cracks means higher damping.

Damping ratio in a continuous composite bridge may be less than three percent if the prestress forces are sufficient to prevent tension cracks from developing at the intermediate support. However, if transverse tension cracks are allowed to develop on a microscopic scale, damping ratio can be expected to be in the order of 3 percent. If larger transverse cracks are permitted to develop, one should expect much higher value of damping.

6.5 COMPARISON BETWEEN THE NATURAL FREQUENCIES OF BRIDGE MODELS I AND II

It should be noted that during the dynamic tests, bridge model II had two actuators mounted at the middle of each span, while bridge model I had just one actuator mounted at the middle of one span. Comparison between the effect of the weight of the two actuators mounted on bridge model II, and the effect of the weight of one actuator is given in Table 6.5, using the orthotropic plate theory and the finite element computer program SAP IV. This comparison shows that the presence of the two actuators had reduced bridge model II natural frequencies by about 20%, compared to the case of a single actuator.

Comparison between the theoretical natural frequencies of bridge models I and II obtained by using the orthotropic plate theory, shows that if one actuator would have been used on bridge model II, the enhancement

TABLE 6.5

EFFECT OF OWN WEIGHT OF THE ACTUATORS AND THE MOVING MASS ON THE NATURAL FREQUENCIES OF BRIDGE MODEL II

MODE NUMBER	NATURAL FREQUENCIES C/SEC						
	ORTHOTROPIC PLATE THEORY		FINITE ELEMENT, SAP (IV)				
			ORTHOTROPIC PLATE THEORY		PLATE AND BEAM ELEMENT		
	(A)	(B)	(A)	(B)	(A)	(B)	EXPERIMENT
1	26.6	21.5	26.1	21.0	26.1	21.9	22
2	35.3	29.0	40.8	32.9	40.9	34.3	28
3	41.6	33.5	40.8	32.9	42.3	37.8	36
4	50.9	41.2	52.5	42.3	53.8	47.7	--

(A) Considering the weight of one actuator
(B) Considering the weight of two actuators

of the natural frequencies, due to the presence of the prestressed concrete portion around the intermediate support, and the higher concrete strength used in Model II, would have been in the order of 46%, as shown in Table 6.6. However, the actual enhancement in the natural frequencies of bridge model II compared to the natural frequencies of bridge model I, considering the presence of the two actuators mounted on bridge model II, is in the order of 18%, as shown in Table 6.6.

The obtained experimental natural frequencies from the dynamic tests of bridge models I and II, compared to the theoretical values obtained from the finite element computer solution programs, are shown in Table 6.7. Furthermore, the theoretical results obtained from the orthotropic plate theory compared to those based on the beam theory are also shown. Generally, the comparison between the results of the orthotropic plate theory and the finite element showed a discrepancy of approximately 2% in the first natural frequency of bridge models I and II. The discrepancy is slightly higher for higher modes of vibration. The beam theory yields quite comparable results for flexural modes, but it fails to predict reliably the natural frequencies corresponding to the torsional modes of the orthotropic plate. It should be noted that the longitudinal and transverse cracks in the concrete deck, near the top of the intermediate support of bridge model I affected all flexural and torsional frequencies.

From an engineering point of view, the experimental results are in good agreement with the theoretical ones. Furthermore, modeling bridge models I and II as composite action model or an an equivalent orthotropic plate model yields fairly good results which gives confidence in the use of the formulae for the orthotropic rigidities for bridges (21).

TABLE 6.6

ENHANCEMENT OF THE NATURAL FREQUENCIES DUE TO PRESTRESSED CONCRETE IN THE NEGATIVE MOMENT REGION USING ORTHOTROPIC PLATE THEORY

MODE NUMBER	NATURAL FREQUENCIES C/SEC. BRIDGE MODEL I (*)	BRIDGE MODEL II (*)	BRIDGE MODEL II (**)	IMPROVEMENT A % (**)	IMPROVEMENT B % (*)
1	18.2	26.6	21.5	18	46
2	24.0	35.3	29.0	21	47
3	28.5	41.6	33.5	18	46
4	34.9	50.9	41.2	18	46

(*) Due to one actuator on model
(**) Due to two actuators on model II

TABLE 6.7

NATURAL FREQUENCIES OF BRIDGE MODELS I AND II USING DIFFERENT APPROACHES

	NATURAL FREQUENCIES CYCLES/SEC.								
	ORTHOTROPIC PLATE THEORY		FINITE ELEMENT, SAP IV				EXPERIMENTAL		
			ORTHOTROPIC PLATE ELEMENT		PLATE AND BEAM ELEMENT				
MODE NUMBER	BRIDGE MODEL I	BRIDGE MODEL II	BRIDGE MODEL I	BRIDGE MODEL II	BRIDGE MODEL I	BRIDGE MODEL II	BRIDGE MODEL I	BRIDGE MODEL II	FLEXURAL BEAM THEORY
1	18.2	21.5	18.2	21.0	18.3	21.1	18	22	21.0
2	24.0	29.0	21.1	32.9	20.3	34.3	21	28	--
3	28.5	33.5	28.5	32.9	30.4	37.7	27	36	32.9
4	34.9	41.2	30.5	42.3	30.6	47.2	30	--	--

6.6 NATURAL FREQUENCIES AND MODE SHAPES OF RECTANGULAR AND SKEW WAFFLE SLABS

6.6.1 Natural Frequencies of Rectangular Waffle Slabs

Natural frequencies of a rectangular waffle slab were calculated using the theoretical classical approach that was outlined in Chapter III. The flexural and torsional rigidities for the equivalent orthotropic plate were calculated according to the formulae recommended by Kennedy and El-Sebakhy (39,17) for an uncracked and the cracked waffle slab. The first four natural frequencies were calculated along with the associated mode shapes; the results are summarized in Table 6.8. The calculated frequencies reveal that the first and the third natural frequencies of the uncracked waffle slab are nearly double those of the cracked slab. This means that if the waffle slab is fully and effectively prestressed in such a way that no cracks are permitted to form, its natural frequencies will be nearly twice as high as those of a cracked reinforced concrete waffle slab. This results shows that by increasing the stiffness of a waffle slab by means of prestressing and keeping the mass constant the slab's natural frequencies are enhanced, which helps in avoiding resonance under low frequency excited source of vibration.

In order to verify this conclusion and confirm the derivation of the classical approach of the rectangular waffle slab, the calculated natural frequencies were compared with the experimental natural frequencies of the same rectangular waffle slab reported by El-Sebakhy, et. al. (19), as shown in Table 6.8. Since the tested rectangular waffle slab had some cracks in the transverse direction along the mid-span, the first three experimental natural frequencies compared well with the classical approach frequencies

calculated on the basis of cracked rigidities of the equivalent orthotropic plate. The good agreement shown between the experimental and the theoretical natural frequencies gave verification of the assumptions made in the derivation of the theoretical analysis, and also confirmed the adequacy of the loading system capability in conducting the dynamic tests.

The finite element computer program SAP IV was used as a second source to check the accuracy of the obtained frequencies using the equivalent quadrilateral orthotropic plate elements to model the rectangular waffle slab, shown in Figure 6.7. The finite element natural frequencies for cracked and uncracked sections are tabulated also in Table 6.8; they are in good agreement with both the experimental and theoretical results. It is of interest to mention that the CPU computer time used to execute the finite element program was as much as ten times the CPU time for the developed orthotropic plate theory computer program. Furthermore, Table 6.8 gives the natural frequencies using the beam theory for cracked and uncracked cross-section. The first and third natural frequencies associated with the flexural modes match well with the experimental, classical theoretical and finite element results. However, the beam theory failed to predict the torsional mode natural frequencies of a wide rectangular slab.

The first four mode shapes associated with the cracked natural frequencies, reported in Table 6.8, are shown in Figures 6.32, to 6.35 using the orthotropic plate theory. The first and third flexural modes of vibration are symmetrical in the transverse direction about the longitudinal x-axis, while the second and fourth torsional modes of vibration are anti-symmetrical in the transverse direction about the x-

TABLE 6.8

NATURAL FREQUENCIES FOR RECTANGULAR WAFFLE SLAB

MODE SHAPE NUMBER	MODE SHAPE	BEAM THEORY		CLASSICAL APPROACH (ORTHOTROPIC PLATE THEORY)		SAP IV (QUADRILATERAL PLATE ELEMENTS)		EXPERIMENTAL RESULTS (19)
		UNCRACKED C/SEC.	CRACKED C/SEC.	UNCRACKED C/SEC.	CRACKED C/SEC.	UNCRACKED C/SEC.	CRACKED C/SEC.	C/SEC.
1	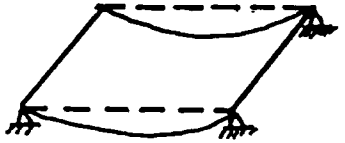	14.3	7.5	14.4	7.5	14.1	7.3	8.0
2	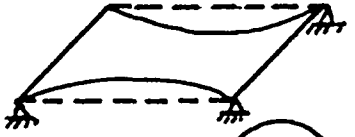	--	--	22.3	14.5	24.9	19.3	16.0
3	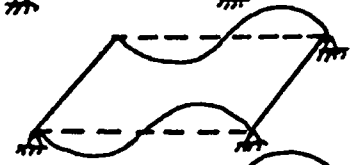	57.3	30.0	57.3	29.3	56.4	29.3	29.5
4	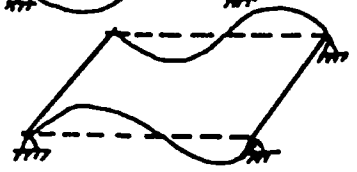	--	--	69.9	40.1	69.6	46.1	--

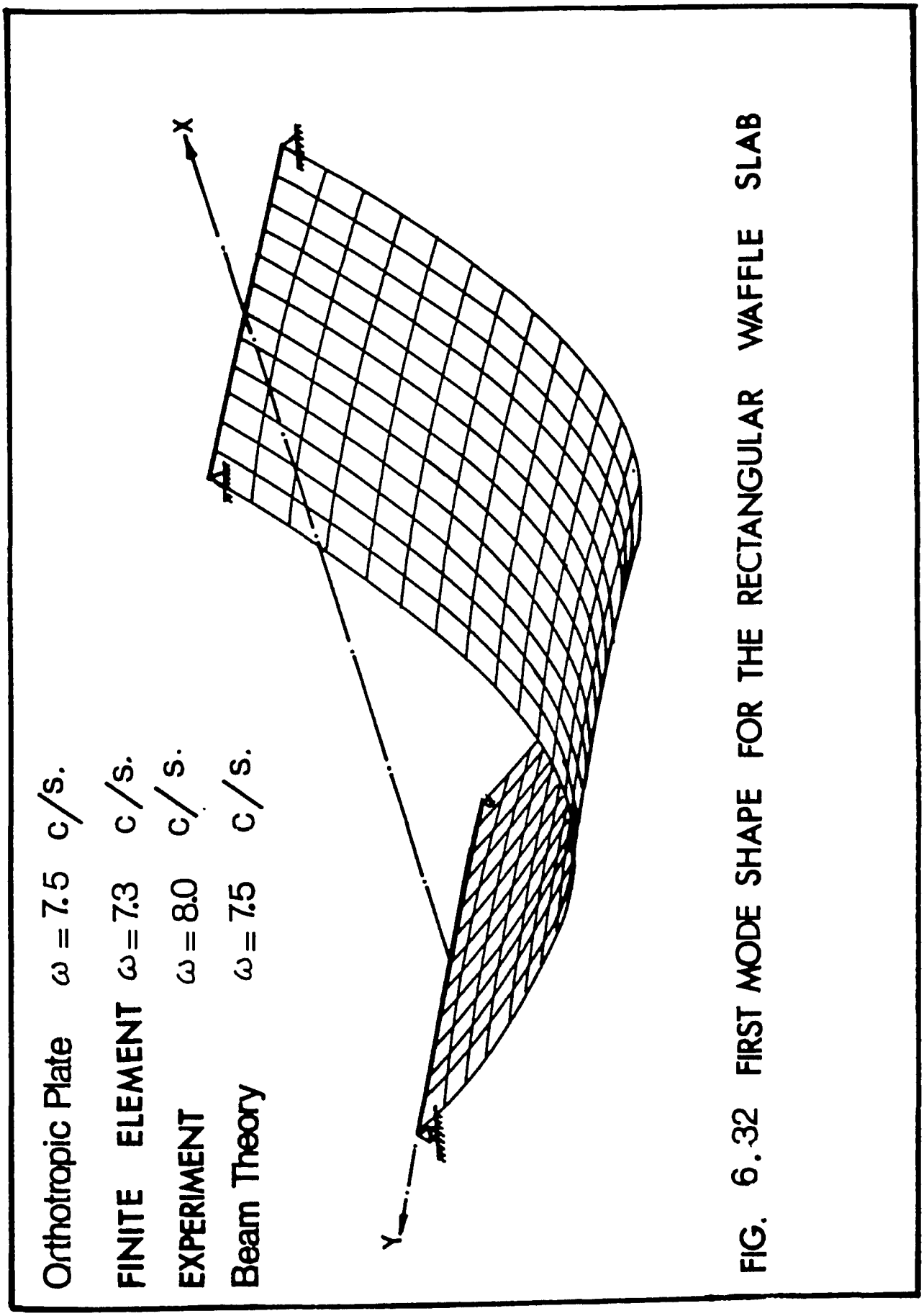

FIG. 6.32 FIRST MODE SHAPE FOR THE RECTANGULAR WAFFLE SLAB

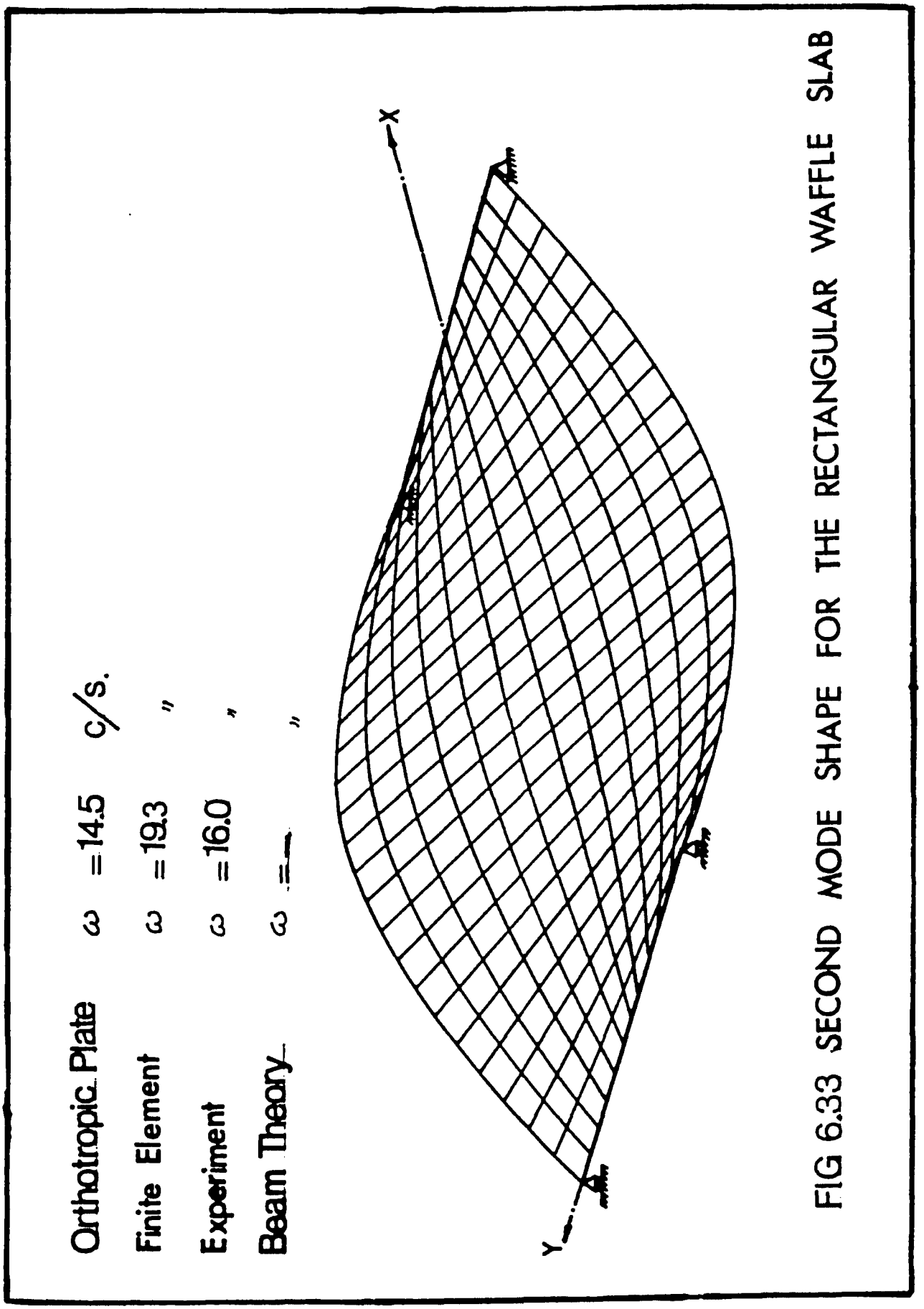

FIG 6.33 SECOND MODE SHAPE FOR THE RECTANGULAR WAFFLE SLAB

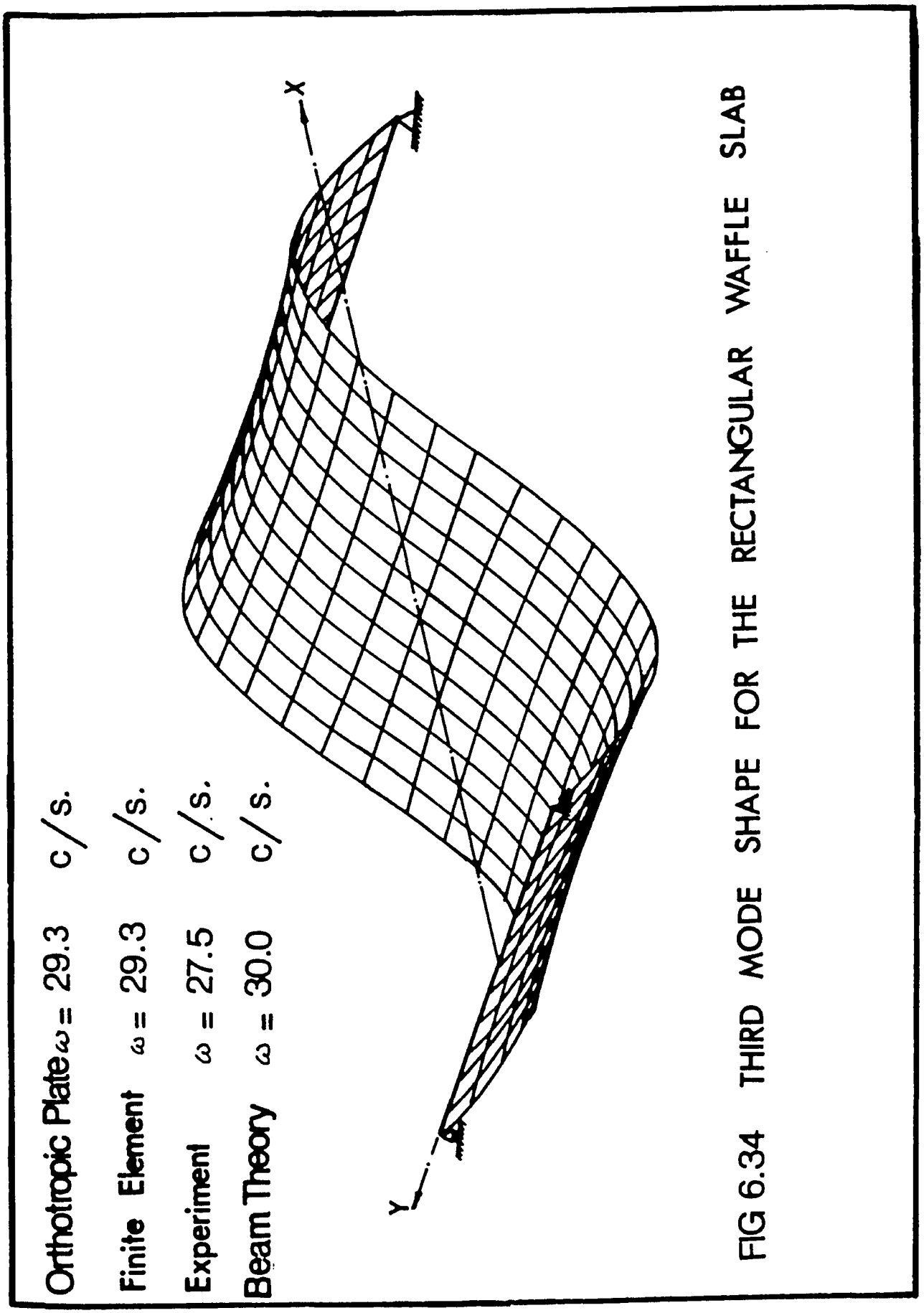

FIG 6.34 THIRD MODE SHAPE FOR THE RECTANGULAR WAFFLE SLAB

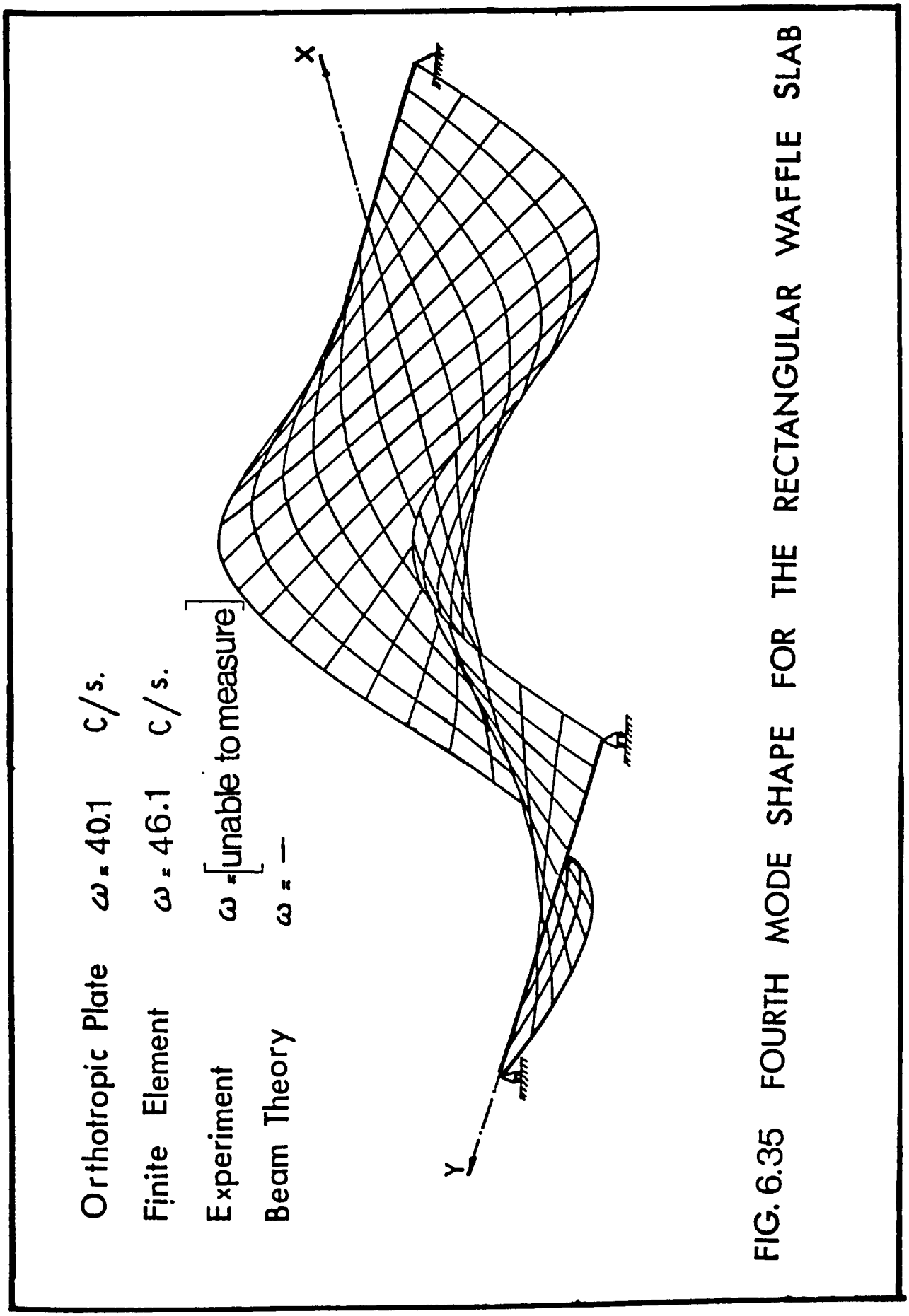

FIG. 6.35 FOURTH MODE SHAPE FOR THE RECTANGULAR WAFFLE SLAB

axis; the first and the second modes are half sine-waves while the third and fourth modes are two-half sine-waves.

6.6.2 Natural Frequencies of 45° Skew Waffle Slab

The first three natural frequencies of a 45° skew waffle slab were obtained by using the equivalent orthotropic plate theory concept explained in Chapter III. Using the transcendental frequency equation for the symmetric modes of vibration, given in Chapter IV, yielded the first and the third (flexural) modes of vibration while the transcendental frequency equation of the anti-symmetrical mode yielded the second (torsional) mode of vibration. Four harmonics were considered for the symmetric modes, while five harmonics were considered for the anti-symmetric modes. This number of harmonics was necessary to obtain the most accurate natural frequencies. It should be emphasized that the theoretical analysis given in Chapter III can predict up to the third mode natural frequency; from an engineering point of view, the first three natural frequencies are the most important in structural analysis. However, if higher modes of vibration are desired, the mathematical derivation for the skew orthotropic plate theory can be readily adjusted to accommodate higher modes of vibration.

The obtained theoretical natural frequencies are in good comparison with the experimental results, shown in Table 6.9; the experimental results were obtained by testing a 45° skew prestressed waffle slab (19). The details of the experimental model and test set-up procedures will not be discussed here and can be found elsewhere (19); this experimental work was conducted by El-Sebakhy et al. and directed towards the enhancement of the

TABLE 6.9

NATURAL FREQUENCIES FOR 45° SKEW WAFFLE SLAB

MODE SHAPE NUMBER	BEAM THEORY C/SEC.	CLASSICAL APPROACH ORTHOTROPIC PLATE THEORY C/SEC.	FINITE ELEMENT COMPUTER PROGRAM		EXPERIMENTAL (19) C/SEC.
			SAP IV C/SEC.	STRUDL-DYNAL C/SEC.	
1	14.3(*) 28.6(**)	24.4(a)	23.3	24.8	23.5
2	--	25.3(b)	24.9	26.1	25
3	57.3(*) 114.5(**)	53.8(a)	52.7	41.7	--

(*) Based on the exact span length
(**) Based on the span length perpendicular to the end supports
(a) # of harmonics = 4
(b) # of harmonics = 5

vibration levels of skew waffle slabs prestressed longitudinally and transversely.

The finite element computer programs, STRUDL and SAP IV, were used as a second source to substantiate the theoretical natural frequencies derived from the classical orthotropic plate theory. These results, given in Table 6.9, are in fair agreement with both the experimental and the theoretical results. Furthermore, the beam theory was utilized to calculate the flexural mode natural frequencies by considering the span of the beam either equal to the exact free span of the slab or equal to the perpendicular length between the two support ends. The results reveal that beam theory is not only incapable of predicting the torsional mode natural frequency, but also yield unrealistic flexural mode natural frequencies for the skew orthotropic plate as shown in Table 6.9.

The first and the third (flexural) modes of vibration of the 45° skew waffle slab are quadrant symmetric about the center of the polar coordinates, as shown in Figures 6.36 and 6.38, while the second and the fourth (torsional) modes of vibration are quadrant anti-symmetric as shown in Figures 6.37 and 6.39. These mode shapes were plotted using STRUDL-DYNAL computer capabilities. The experimental first and second vibration mode shapes, obtained from (19), confirm the STRUDL's mode shapes.

Comparison between the theoretical natural frequency of the uncracked rectangular waffle slab, Table 6.8, and of the skew waffle slab, Table 6.9, deduced by using the classical orthotropic plate theory, Chapter III, reveals that the first natural frequency of the skew waffle slab is as high as 58% of that of the rectangular waffle slab, even though the boundary conditions are exactly identical; the spans and the widths are slightly

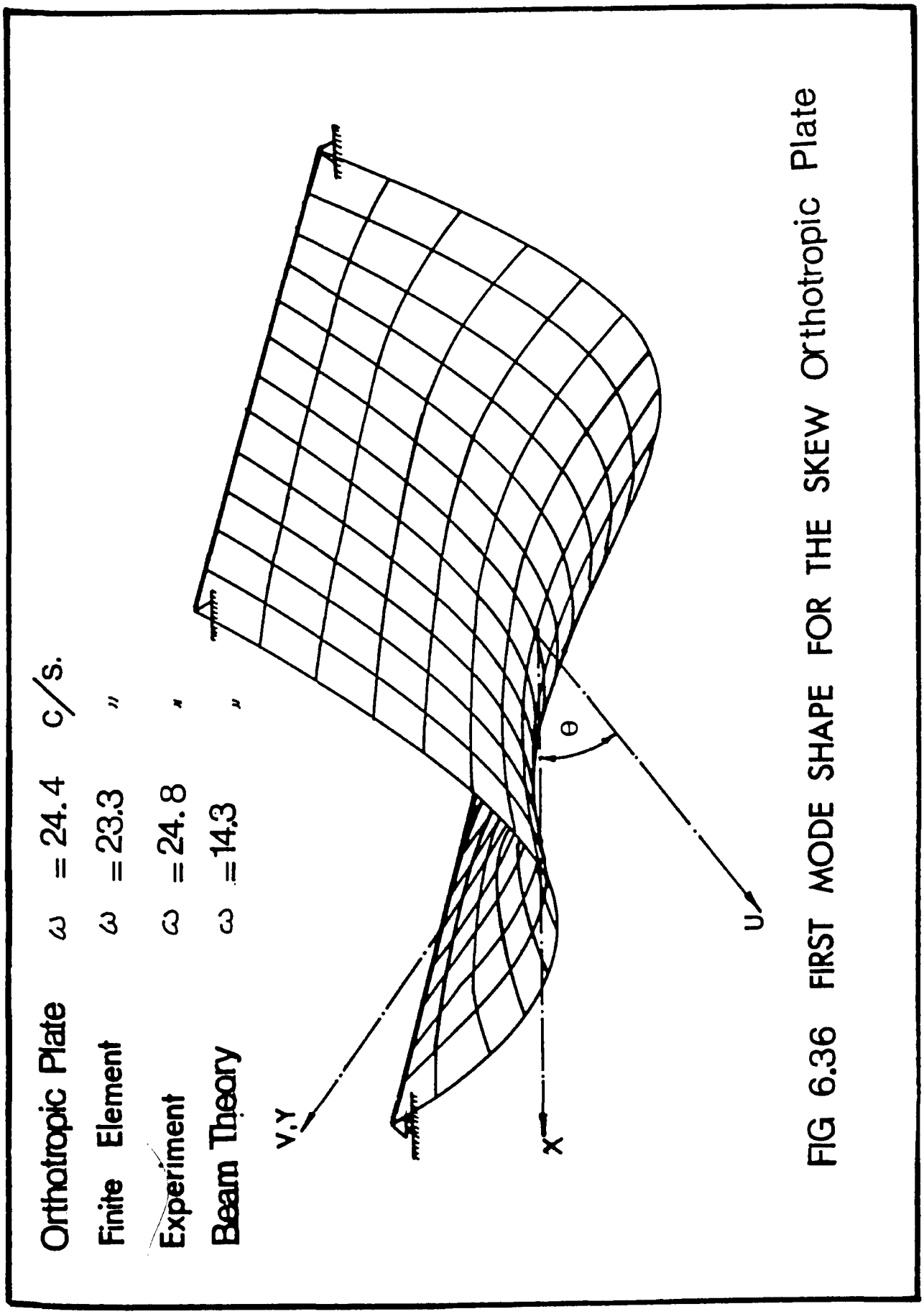

FIG 6.36 FIRST MODE SHAPE FOR THE SKEW Orthotropic Plate

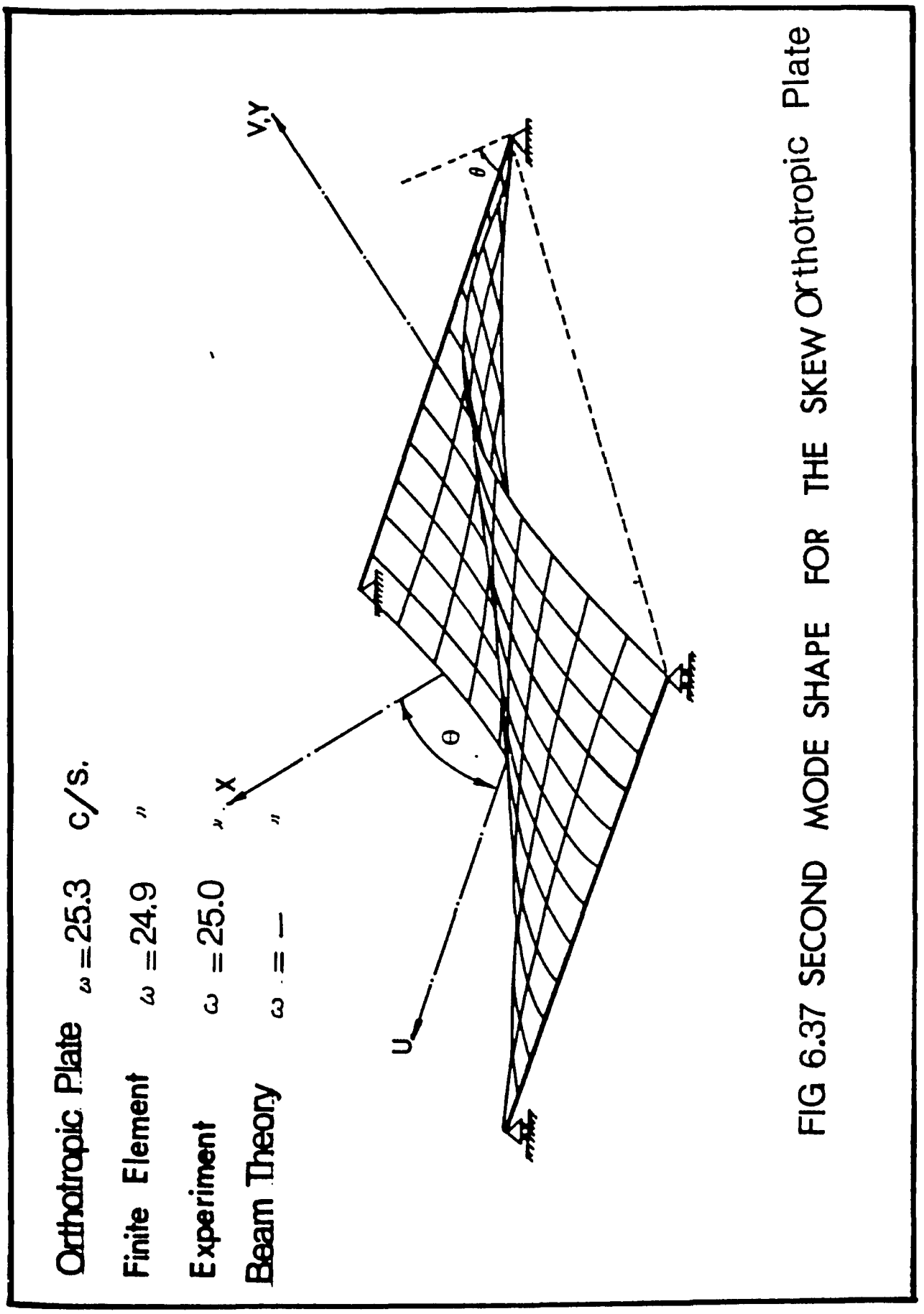

FIG 6.37 SECOND MODE SHAPE FOR THE SKEW Orthotropic Plate

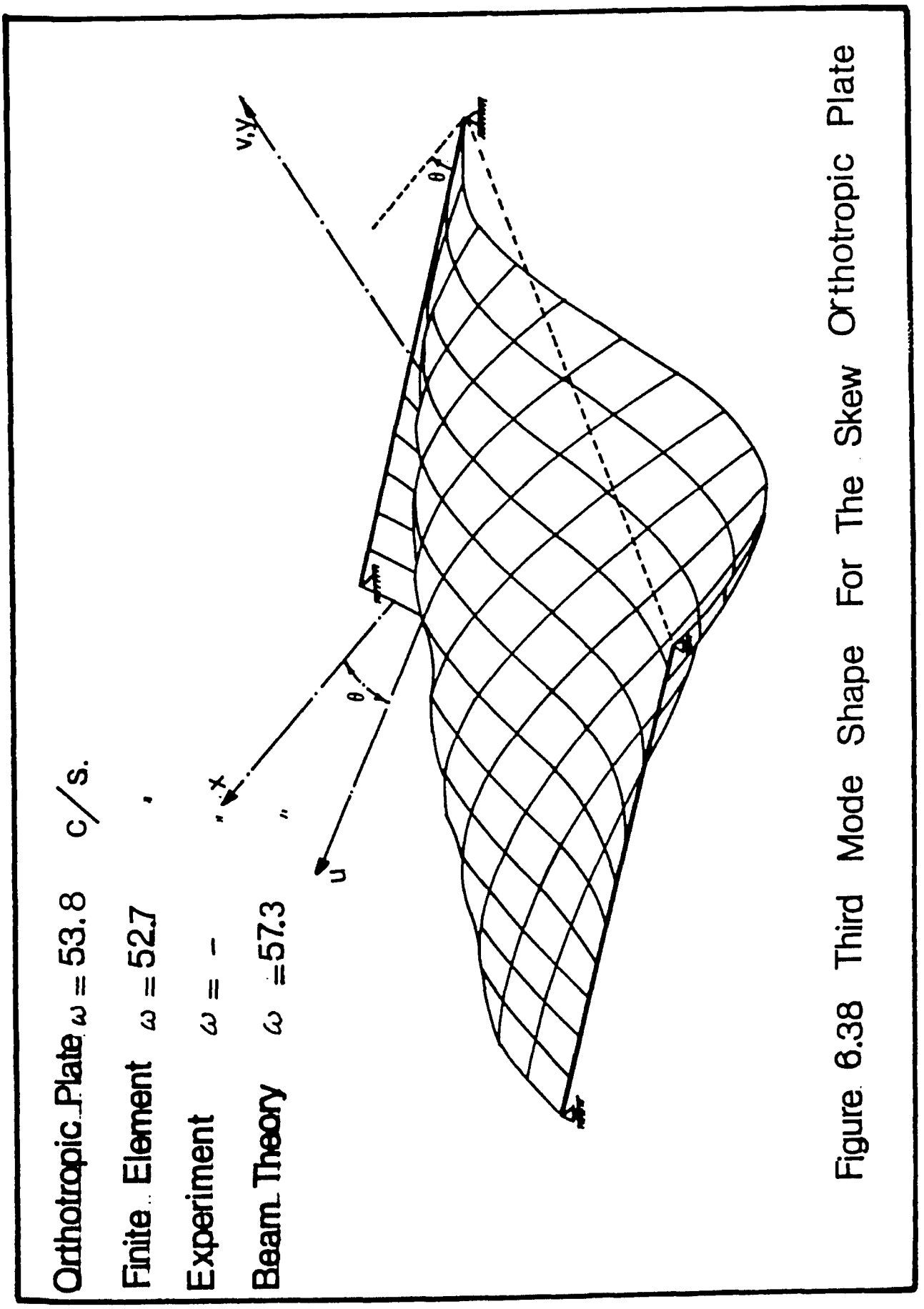

Figure 6.38 Third Mode Shape For The Skew Orthotropic Plate

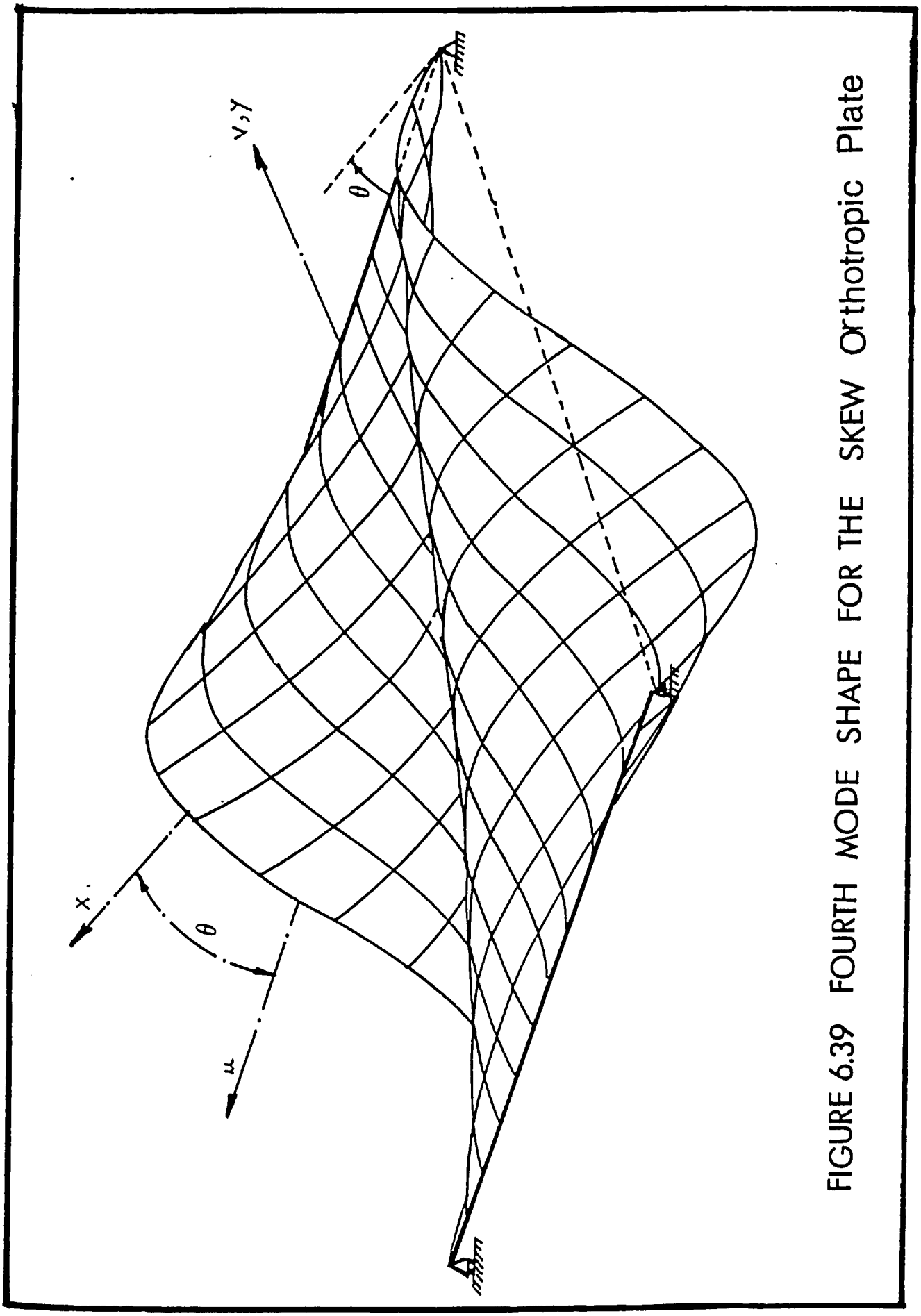

FIGURE 6.39 FOURTH MODE SHAPE FOR THE SKEW Orthotropic Plate

different. This comparison between the rectangular and skew waffle slabs reflects the influence of the 45° skew angle on the first natural frequency. This is not a surprising observation since with increasing skew angle, the stiffness is dramatically increased, which leads to an increase in the natural frequency. Mode shape wise, Figures 6.32 to 6.39 are almost the same, except in the skew slab there is a quadrant symmetry, while in the rectangular slab it is half symmetry about the longitudinal x-axis and about the mid-span line.

6.7 FREE VIBRATION OF A SINGLE SPAN ORTHOTROPIC PLATE WITH DIFFERENT BOUNDARY CONDITIONS

6.7.1 Fixed-Simply Supported Plate

The dynamic response of orthotropic plate structures having fixed simply supported and free-free boundary conditions is investigated using the classical orthotropic plate theory. A plan view of an orthotropic plate structure with end conditions is shown in Figure 6.40. The boundary conditions are:

At the simple support (x=0)

$$w(x,y,t) = 0 \tag{6.8}$$

and the moment

$$M_x = D_x w_{,xx} + D_1 w_{,yy} = 0 \tag{6.9}$$

At the fixed support (x=a)

$$w(x,y,t) = 0 \tag{6.10}$$

and

$$w_{,x} = 0 \tag{6.11}$$

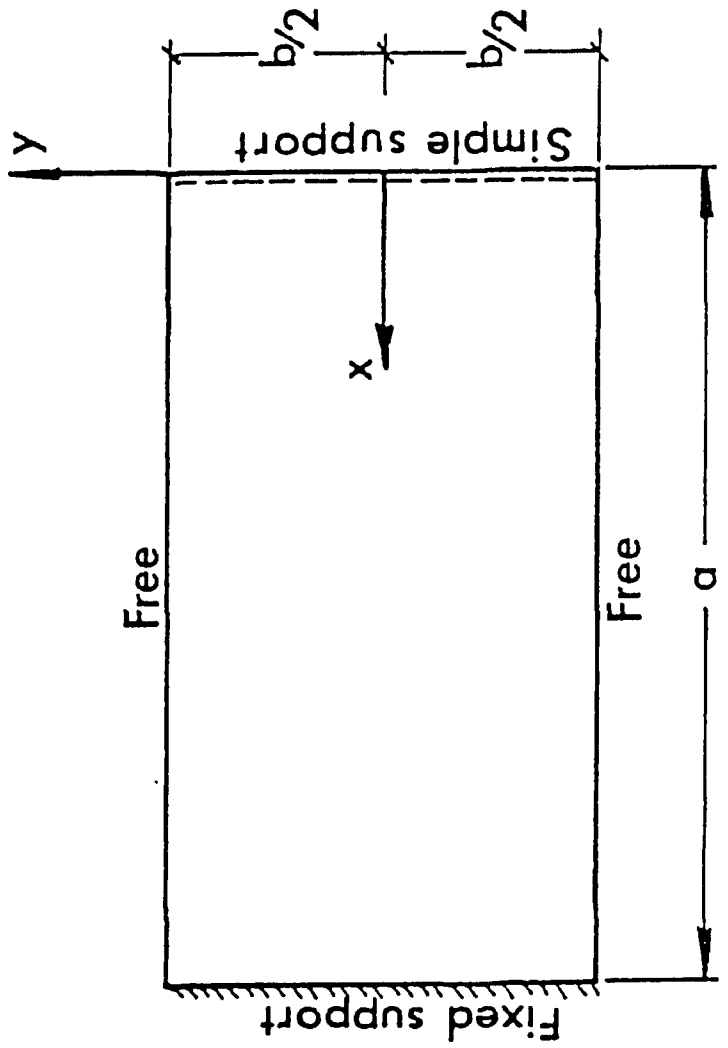

FIGURE 6.40 PLAN VIEW OF ORTHOTROPIC PLATE WITH END CONDITIONS

At the free edges ($y=\pm b/2$): the moment

$$M_y = D_y w_{,yy} + D_2 w_{,xx} = 0 \tag{6.12}$$

and the transverse shear

$$V_y = (D_{xy} + D_{yx} + D_2)\, w_{,xxy} + D_y w_{,yyy} = 0 \tag{6.13}$$

A solution of the governing Equation 3.2.6 is given by Equation 3.2.17. Following the same procedure as explained in Chapter III and satisfying the above boundary conditions and considering the symmetry about the x-axis the first four natural frequencies are obtained and tabulated in Table 6.10. In order to verify the method of solution, results were compared with those derived from a finite element SAP IV computer program as shown in Table 6.10. The aspect ratio of the quadrilateral plate element was unity and the minimum number of elements used along the width of the structure was ten. Also, the flexural natural frequencies utilizing the beam theory derived from the following well-known frequency equation (1)

$$f = \frac{(i+1/4)^2 \pi}{2a^2} \sqrt{\frac{EI}{\bar{m}}} \tag{6.14}$$

where

$\bar{m}$ = mass of beam per unit length

I = moment of inertia of the beam cross-section

f = natural frequency, c.p.s.

are calculated and shown in the same table for comparison purposes. It is observed that the results are in close agreement. The associated four mode shapes are shown in Figure 6.41 as determined by the classical method of analysis presented herein.

TABLE 6.10

COMPARISON OF FREQUENCIES OF FIXED-SIMPLY SUPPORTED SINGLE-SPAN ORTHOTROPIC PLATE

MODE NUMBER	MODE SHAPE	FREQUENCY C/SEC.			
		CLASSICAL APPROACH [ORTHOTROPIC PLATE THEORY]	FINITE ELEMENT (SAP IV)		BEAM THEORY
			BEAM AND PLATE ELEMENTS	ORTHOTROPIC PLATE ELEMENT	
1	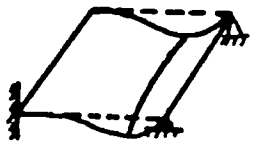	33.1	32.4	32.0	32.5
2		40.4	42.1	41.9	--
3		107.0	105.5	105.0	105.4
4		115.0	116.0	116.3	--

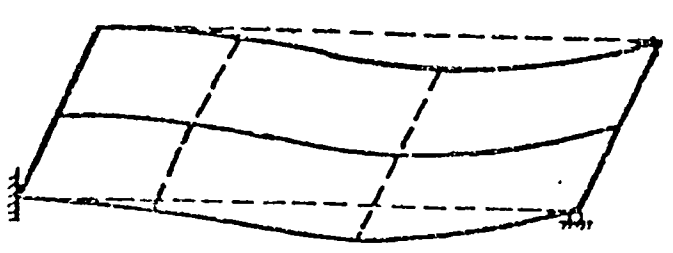

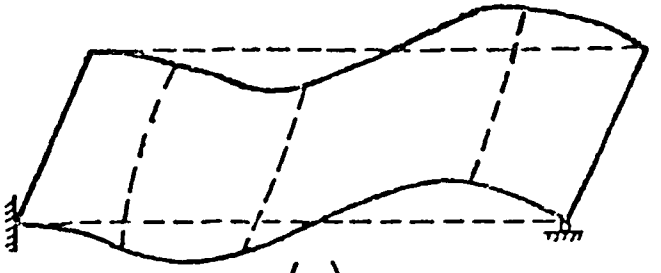

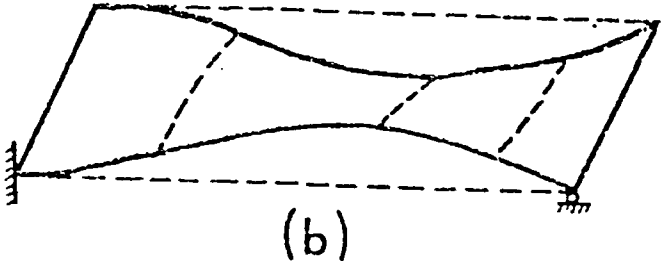

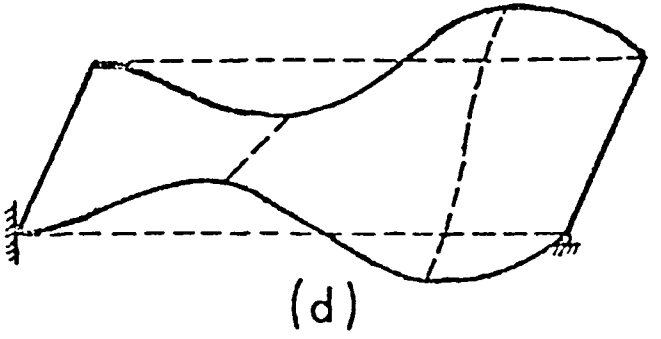

FIGURE 6.41 MODE SHAPES;

(a) FIRST FLEXURAL MODE, i=1 (b) SECOND MODE (TORSIONAL), i=1

(C) THIRD MODE (FLEXURAL), i=2 (d) FOURTH MODE (TORSIONAL), i=2

A parametric study was also undertaken to investigate the influence of aspect ratio (a/b) and the ratio of the rigidities (Dx/Dy) on the frequency response of the structure. Figures 6.42 to 6.45 show the relation between the aspect ratio, the rigidities ratio, and the natural frequencies of the plate. It is observed that for symmetrical modes about the x-axis, Figures 6.42 and 6.44, there is no significant interaction between the aforementioned ratios; that is, for a given Dx/Dy, the frequency appears to be insensitive to the aspect ratio. Furthermore, the results from the beam theory idealization are not too different from those based on the orthotropic plate theory, regardless of the aspect ratio or the ratio Dx/Dy.

However, results for anti-symmetrical modes, shown in Figures 6.43 and 6.45, reveal significant interaction between the ratios (a/b) and (D_x/D_y). Also, considerable discrepancies in the predicted results from the beam theory idealization can be observed. This parametric study is important since many codes of practice (53) base the design on the beam theory idealization and completely disregard the two-way effect.

6.7.2 Simply-Supported Plate

The dynamic response of an orthotropic plate having simply supported ends and free-free boundary conditions, as shown in Figure 6.46, was studied using the orthotropic plate theory. The boundary conditions are identical to the fixed-simply supported plate except at x=a Equation 6.11 was replaced by Equation 6.9 for zero moment. Satisfying the boundary conditions and proceeding as outlined in the case of fixed-simply supported plate the first four natural frequencies are obtained. Table 6.11 shows

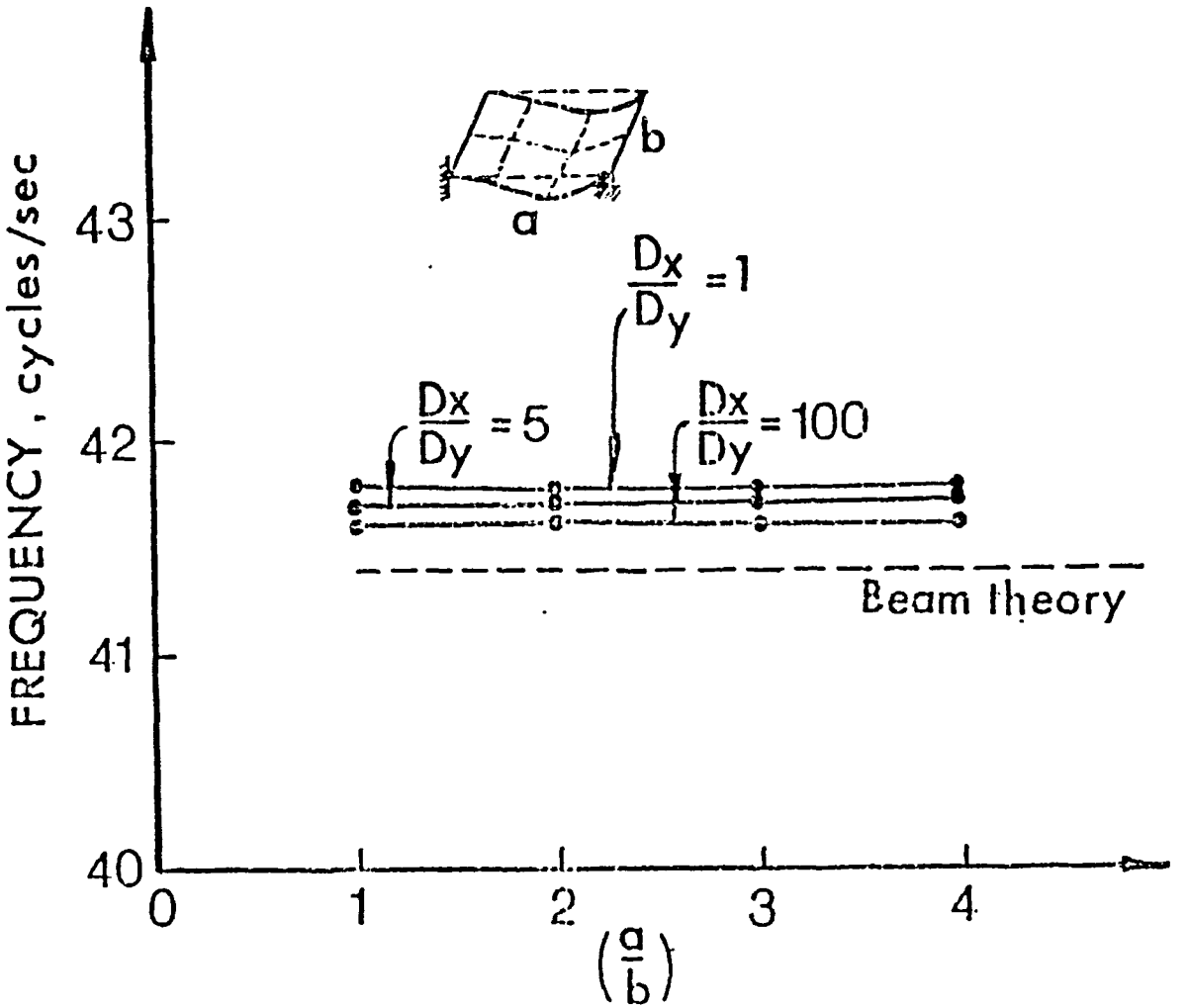

FIGURE 6.42 INFLUENCE OF ASPECT RATIO (a/b) AND RIGIDITY RATIO (D_x/D_y) ON FIRST MODE FREQUENCY

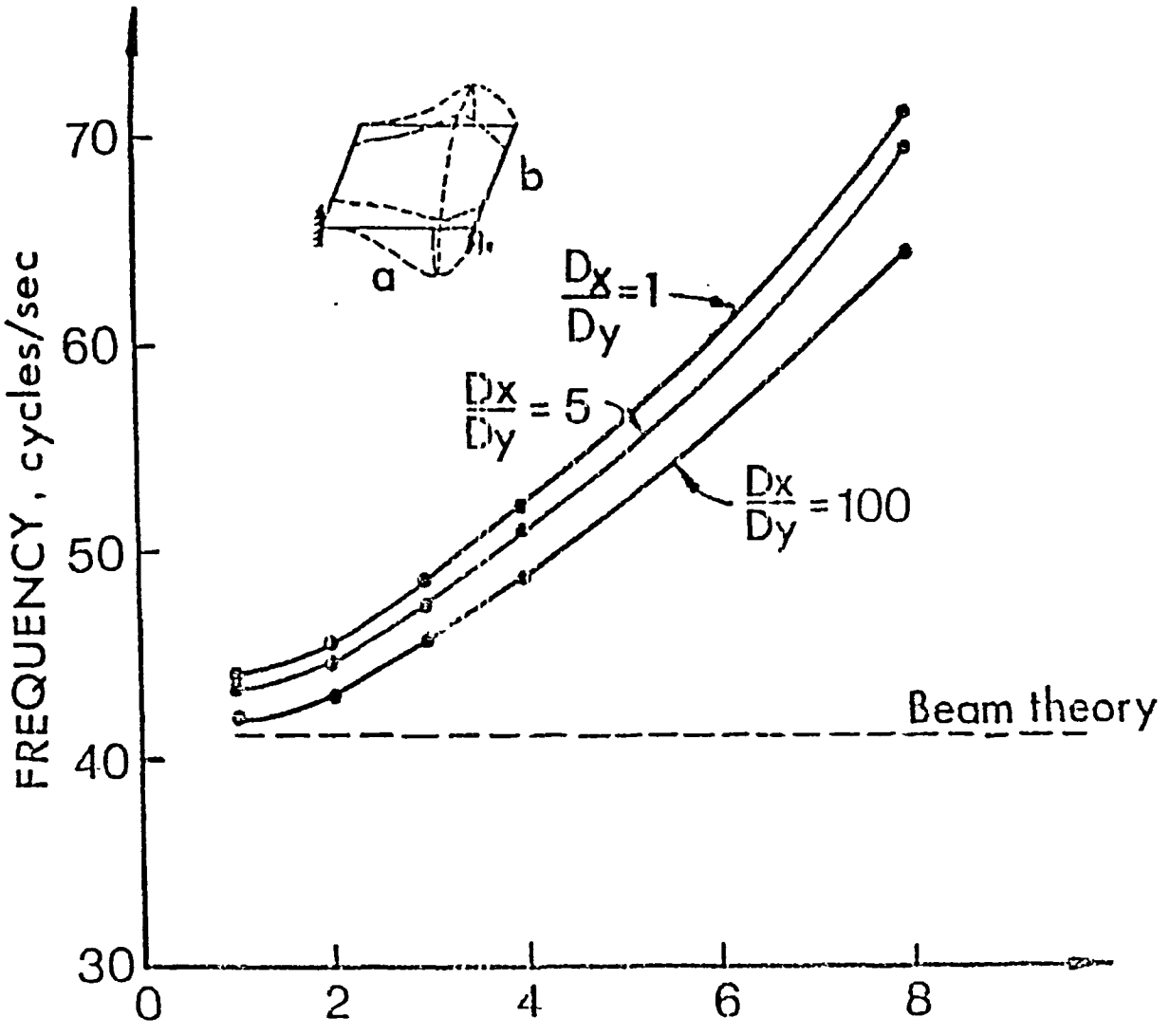

FIGURE 6.43 INFLUENCE OF ASPECT RATIO (a/b) AND RIGIDITY RATIO (D_x/D_y) ON SECOND MODE FREQUENCY

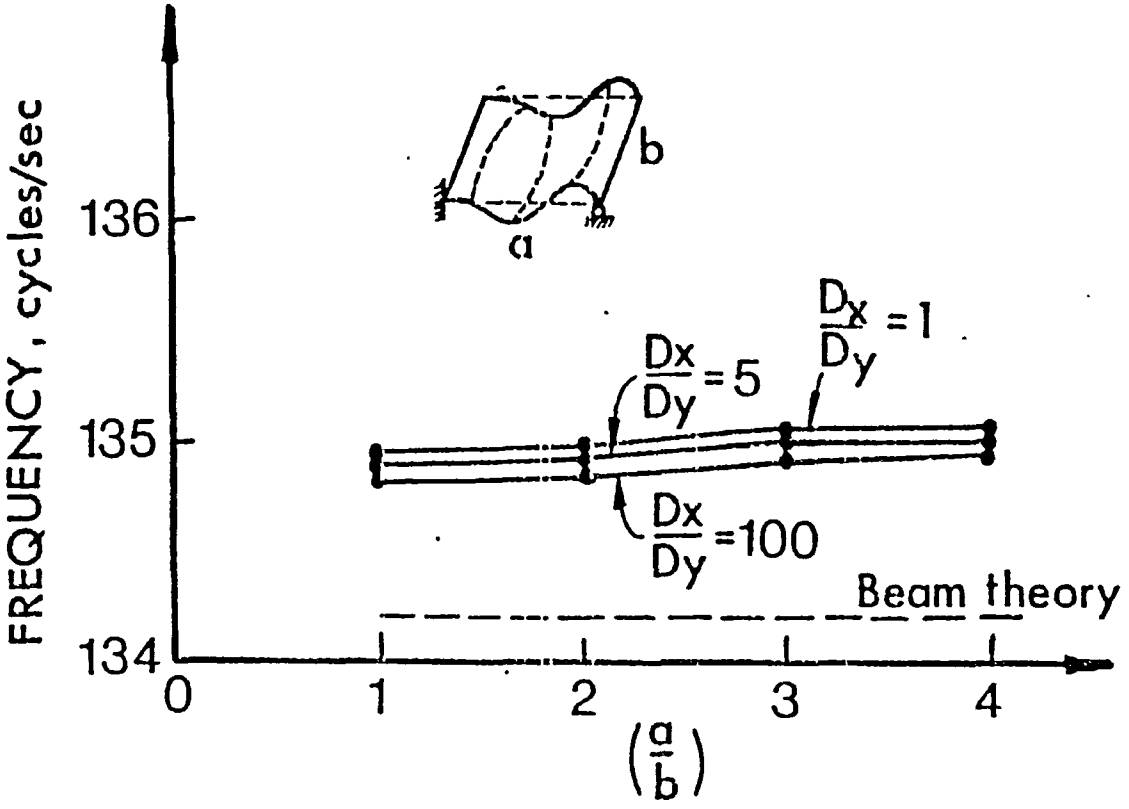

FIGURE 6.44 INFLUENCE OF ASPECT RATIO (a/b) AND RIGIDITY RATIO (D_x/D_y) ON THIRD MODE FREQUENCY

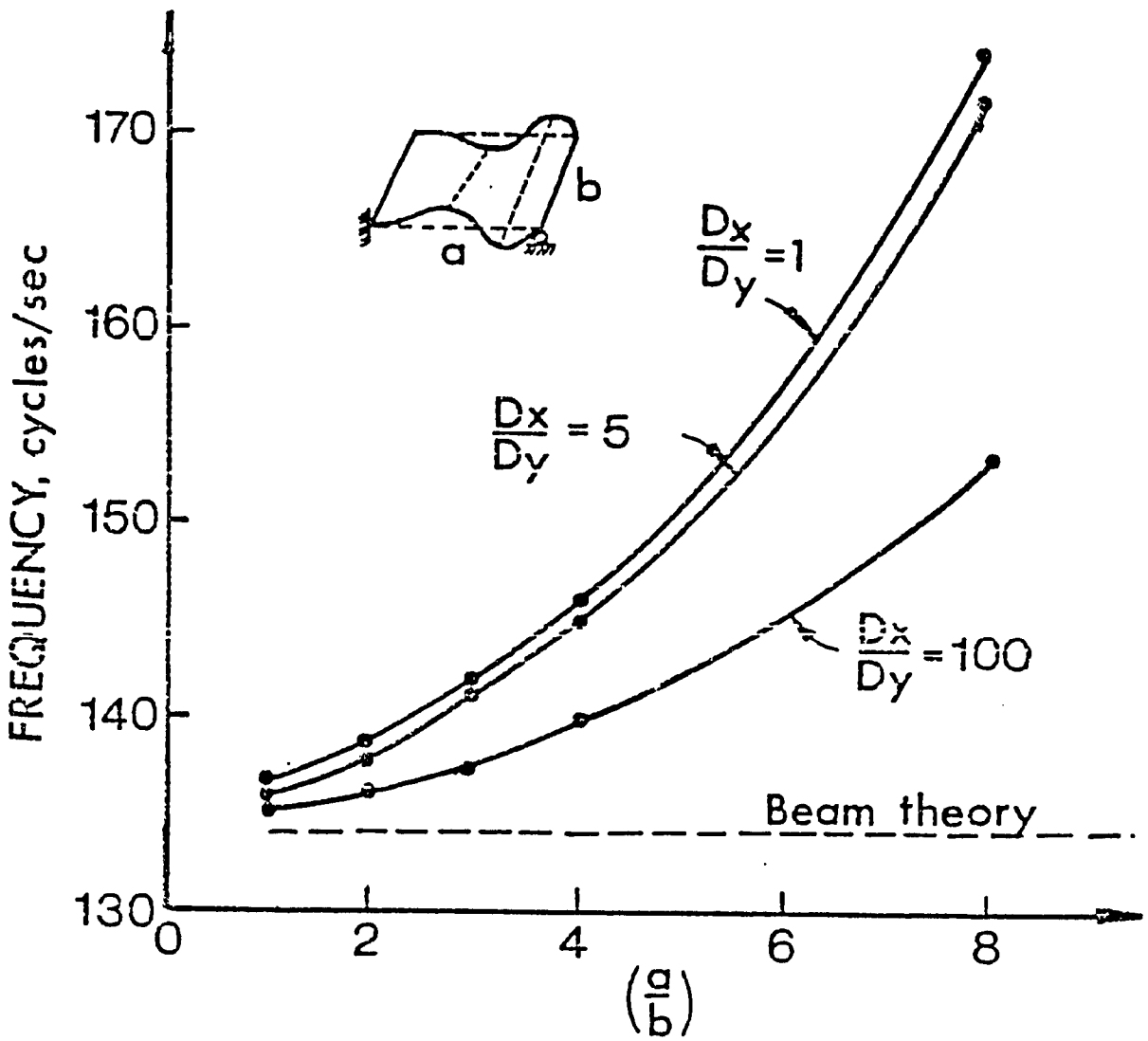

FIGURE 6.45 INFLUENCE OF ASPECT RATIO (a/b) AND RIGIDITY RATIO (D_x/D_y) ON FOURTH MODE FREQUENCY.

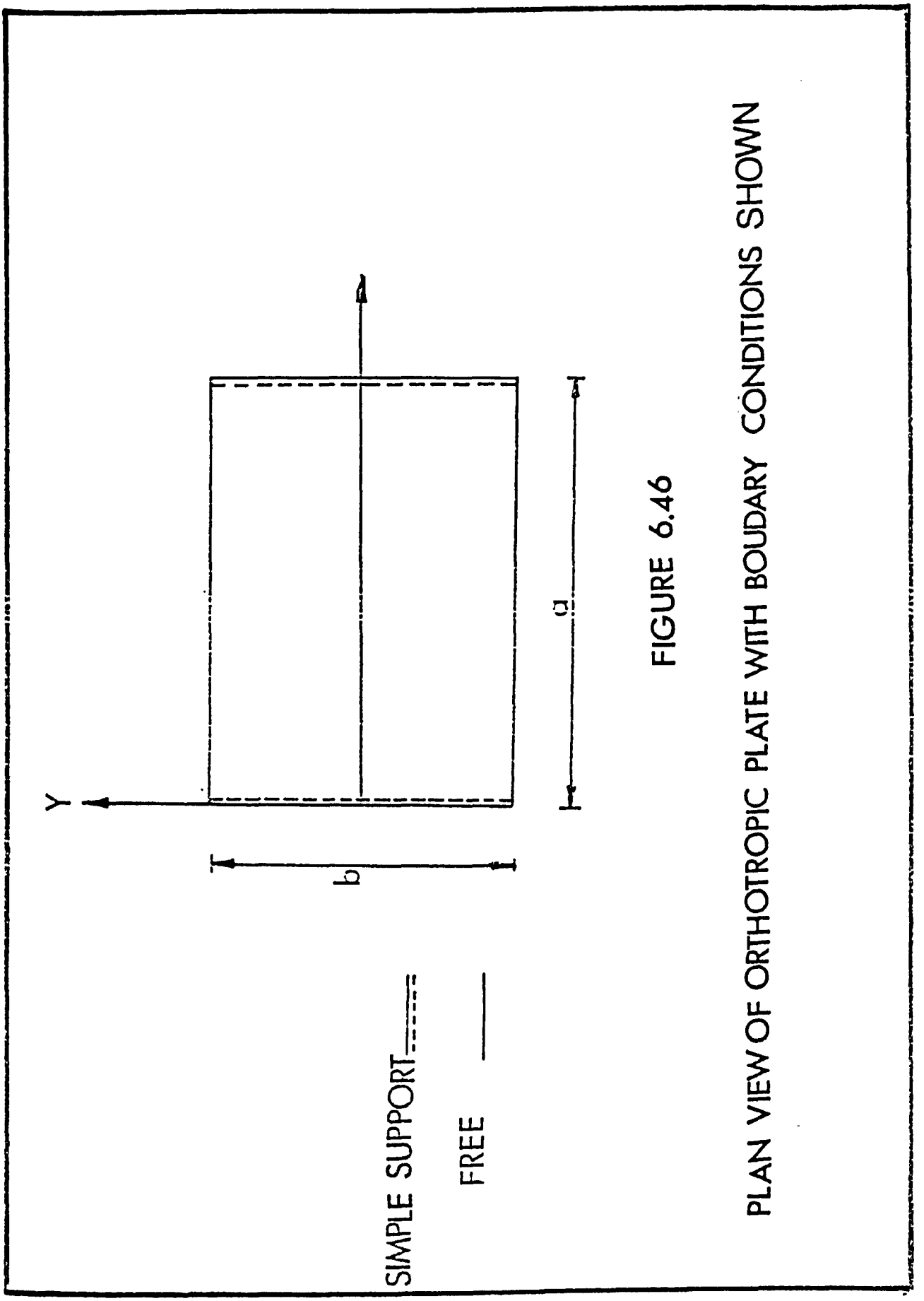

FIGURE 6.46

PLAN VIEW OF ORTHOTROPIC PLATE WITH BOUDARY CONDITIONS SHOWN

TABLE 6.11

COMPARISON OF FREQUENCIES OF SIMPLY-SUPPORTED ENDS ORTHOTROPIC PLATE

MODE NUMBER	MODE SHAPE	FREQUENCY C/SEC. CLASSICAL APPROACH [ORTHOTROPIC PLATE THEORY]	FINITE ELEMENT (SAP IV) BEAM AND PLATE ELEMENTS	FINITE ELEMENT (SAP IV) ORTHOTROPIC PLATE ELEMENT	BEAM THEORY
1		21.1	20.7	20.7	20.8
2	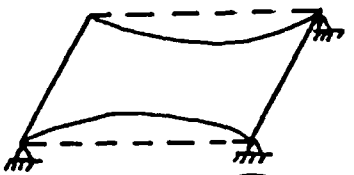	28.4	32.7	31.6	--
3	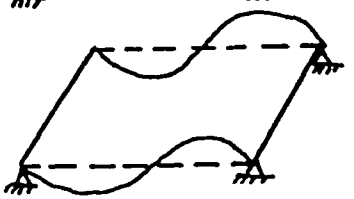	84.5	83.2	82.7	83.2
4	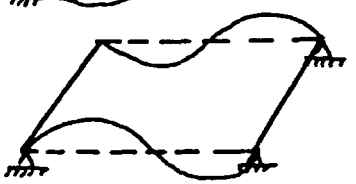	92.7	95.7	95.2	--

comparison of the first four natural frequencies using the finite element approach and the beam theory. The frequencies obtained from the orthotropic plate theory are in good agreement with those obtained from the finite element approach and the beam theory. The associated mode shapes are identical to those previously given in Figures 6.32 to 6.35.

6.7.3 Analogy Between a Continuous Composite Bridge and the Single-Span Orthotropic Plate

All of the aforementioned natural frequencies of the single-span orthotropic plate with the aforementioned boundary conditions are compared with the theoretical natural frequencies of continuous composite bridge models. It my be recalled that model I comprised of a reinforced concrete deck and therefore its rigidities varied due to cracking of the deck slab; while model II with a prestressed deck in the vicinity of the intermediate support had uniform rigidities since the deck slab did not crack. Two methods of analysis were utilized for this comparison, namely, the orthotropic plate theory and the finite element method using SAP IV program. The results obtained using the classical orthotropic plate theory are tabulated in Table 6.12, while those obtained using either the equivalent orthotropic plate elements or plate and beam elements are tabulated in Tables 6.13 and 6.14, respectively. The comparison of results was possible since the first and second mode shapes of the continuous composite bridge coincided with the first and second mode shapes of a single-span orthotropic plate with simply supported ends, while the third and fourth mode shapes of the continuous composite bridge coincided with the first and second mode shapes of a single-span orthotropic plate with

TABLE 6.12

FREQUENCY RATIO OF TWO-SPAN CONTINUOUS BRIDGE TO SINGLE-SPAN ORTHOTROPIC PLATE USING THE ORTHOTROPIC PLATE THEORY

	TWO-SPAN BRIDGE			SINGLE-SPAN BRIDGE		FREQUENCY RATIO	
		NATURAL FREQUENCIES C/SEC.					
MODE NUMBER	MODE SHAPE	MODEL I	MODEL II	MODE SHAPE	NATURAL FREQUENCY C/SEC.	MODEL I/ SINGLE SPAN	MODEL II/ SINGLE SPAN
1	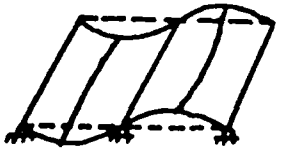	18.2	21.5		21.1	0.86	1.01
2	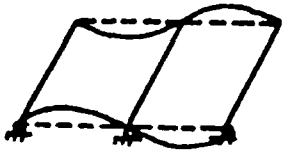	24.0	29.0	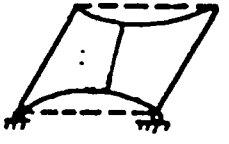	28.4	0.85	1.02
3	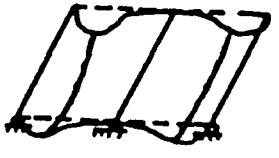	28.5	33.5		33.1	0.86	1.01
4	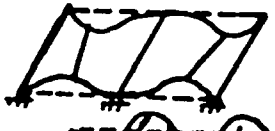	34.9	41.2		40.4	0.86	1.01
5		72.5	85.8		84.5	0.86	1.01
6	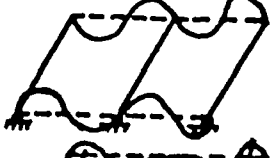	79.6	96.1		92.7	0.86	1.03
7		91.6	108.7		107.0	0.86	1.01
8	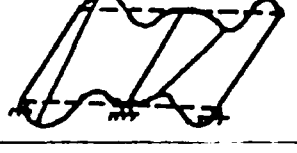	98.5	117.2		115.0	0.86	1.02

TABLE 6.13

FREQUENCY RATIO OF TWO-SPAN CONTINUOUS BRIDGE TO SINGLE-SPAN ORTHOTROPIC PLATE USING SAP IV (QUADRILATERAL PLATE ELEMENTS)

	TWO-SPAN BRIDGE			SINGLE-SPAN BRIDGE		FREQUENCY RATIO	
		NATURAL FREQUENCIES C/SEC.					
MODE NUMBER	MODE SHAPE	MODEL I	MODEL II	MODE SHAPE	NATURAL FREQUENCY C/SEC.	MODEL I/ SINGLE SPAN	MODEL II/ SINGLE SPAN
1	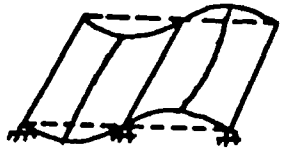	18.2	21.0		20.7	0.88	1.02
2	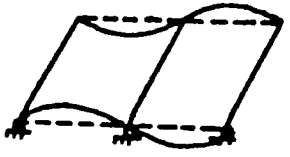	21.1	32.9	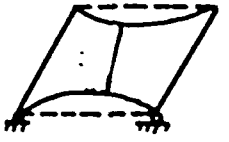	31.6	0.67	1.04
3	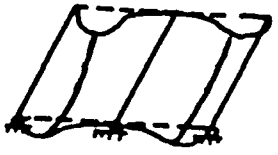	28.5	32.9		33.1	0.86	1.00
4		30.5	42.3		40.4	0.75	1.05
5		72.9	84.1		82.7	0.88	1.02
6		81.9	97.0		95.2	0.86	1.02
7		93.0	106.5		107.0	0.86	1.00
8	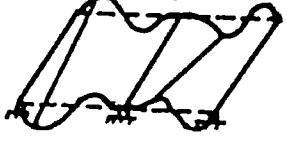	98.8	117.0		115.0	0.86	1.02

TABLE 6.14

FREQUENCY RATIO OF TWO-SPAN CONTINUOUS BRIDGE TO SINGLE-SPAN ORTHOTROPIC PLATE USING SAP IV (ISOTROPIC PLATE AND THREE-DIMENSIONAL BEAM ELEMENTS)

TWO-SPAN BRIDGE				SINGLE-SPAN BRIDGE		FREQUENCY RATIO	
		NATURAL FREQUENCIES C/SEC.					
MODE NUMBER	MODE SHAPE	MODEL I	MODEL II	MODE SHAPE	NATURAL FREQUENCY C/SEC.	MODEL I/ SINGLE SPAN	MODEL II/ SINGLE SPAN
1	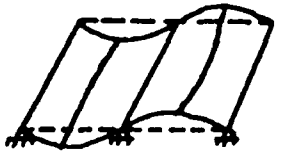	18.3	21.1		20.7	0.88	1.01
2	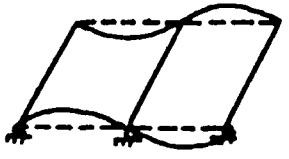	20.4	34.1	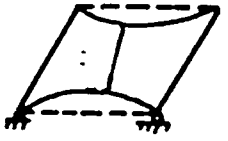	32.7	0.62	1.04
3	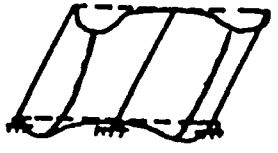	30.4	37.8	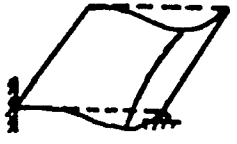	32.4	0.94	1.16
4		30.6	47.2		42.1	0.72	1.12
5		71.5	88.0		83.2	0.86	1.05
6	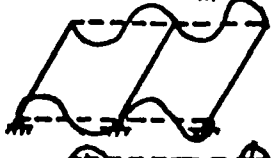	83.7	99.4		95.7	0.87	1.04
7		91.7	107.0		105.5	0.86	1.01
8	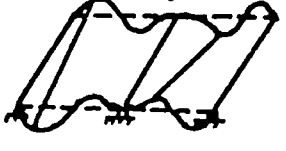	100.1	118.5		116.0	0.86	1.02

simply-fixed ends. The same explanation applies to the fifth up to the eighth modes as shown in the aforementioned tables. The frequency ratio, defined as the ratio between the frequency of the continuous composite bridge to that of the single-span orthotropic plate, is given in the last two columns of each table.

It is interesting to note how closely the appropriate 'single-span plate frequencies' are approached by the 'continuous composite bridge frequencies' even at the lower modes of vibration. This closeness is measured by means of the frequency ratio. This means that the "single-span orthotropic plate frequencies" are the natural frequencies of a continuous two-span composite bridge if the latter has a uniform rigidity along the entire length of the bridge; this state can be readily achieved by prestressing a portion of the concrete deck around the intermediate support.

6.8 FATIGUE TEST RESULTS

The primary purpose of the fatigue test was to monitor the behavior of different elements of bridge models I and II under a resonance fatigue loading, applied very close to the first natural frequency. As mentioned before, the fatigue loading was applied in intervals; this was necessary in order to conduct visual inspection between the loading intervals to locate any fatigue cracks. The piston stroke and the moving mass were coupled in combination with the excitation frequency to produce the fatigue force on the models. Visual inspection is one of the most reliable methods of crack detection; however, cracks must penetrate the surface first to be detected visually. Furthermore, the dynamic signature of the models was used as a

tool for detecting cracks in any of the bridge model elements. Dynamic strain ranges were recorded periodically on different elements in different directions throughout the entire fatigue loading tests. There were five critical elements in bridge models I and II which required monitoring and examination, namely:

1. Top and bottom flanges of the longitudinal steel beams at mid-span and intermediate support sections,
2. Longitudinal reinforcement of bridge model I at the intermediate support,
3. Prestressing wires of bridge model II at the intermediate support,
4. Transverse diaphragms and
5. Shear connectors.

6.8.1 Bridge Model I

Strain variation at the bottom and top flanges of a longitudinal steel beam is shown in Figures 6.47 and 6.48, respectively. It is observed that the stress range at the beginning of the fatigue test was about 41.0 ksi in the bottom flange and about 20.0 ksi in the top flange; at about 400,000 cycles, at the first natural frequency the stress range in the bottom flange increased to 60.0 ksi, while in the top flange it doubled to 42.4 ksi. At about 530,000 cycles the bottom flange of the exterior steel beam experienced the first visible fatigue crack, 1/4 inch wide. This crack propagated from the bottom flange penetrating the web towards the top flange, as shown in Figure 6.49. This dramatic change in the stress range in the top and bottom flanges of the steel beam at mid-span can be attributed to loss in stiffness resulting from the initiation of the

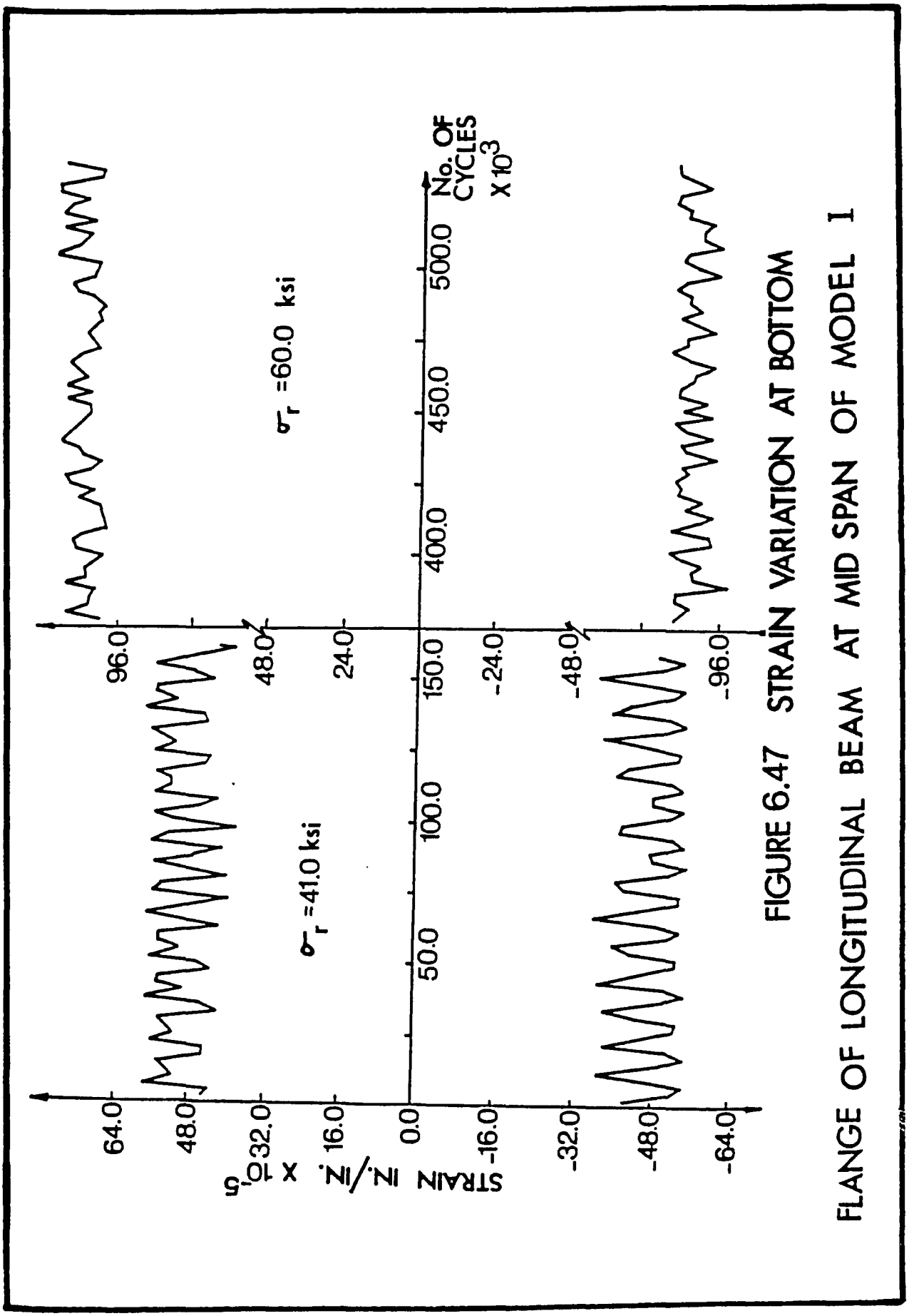

FIGURE 6.47 STRAIN VARIATION AT BOTTOM FLANGE OF LONGITUDINAL BEAM AT MID SPAN OF MODEL 1

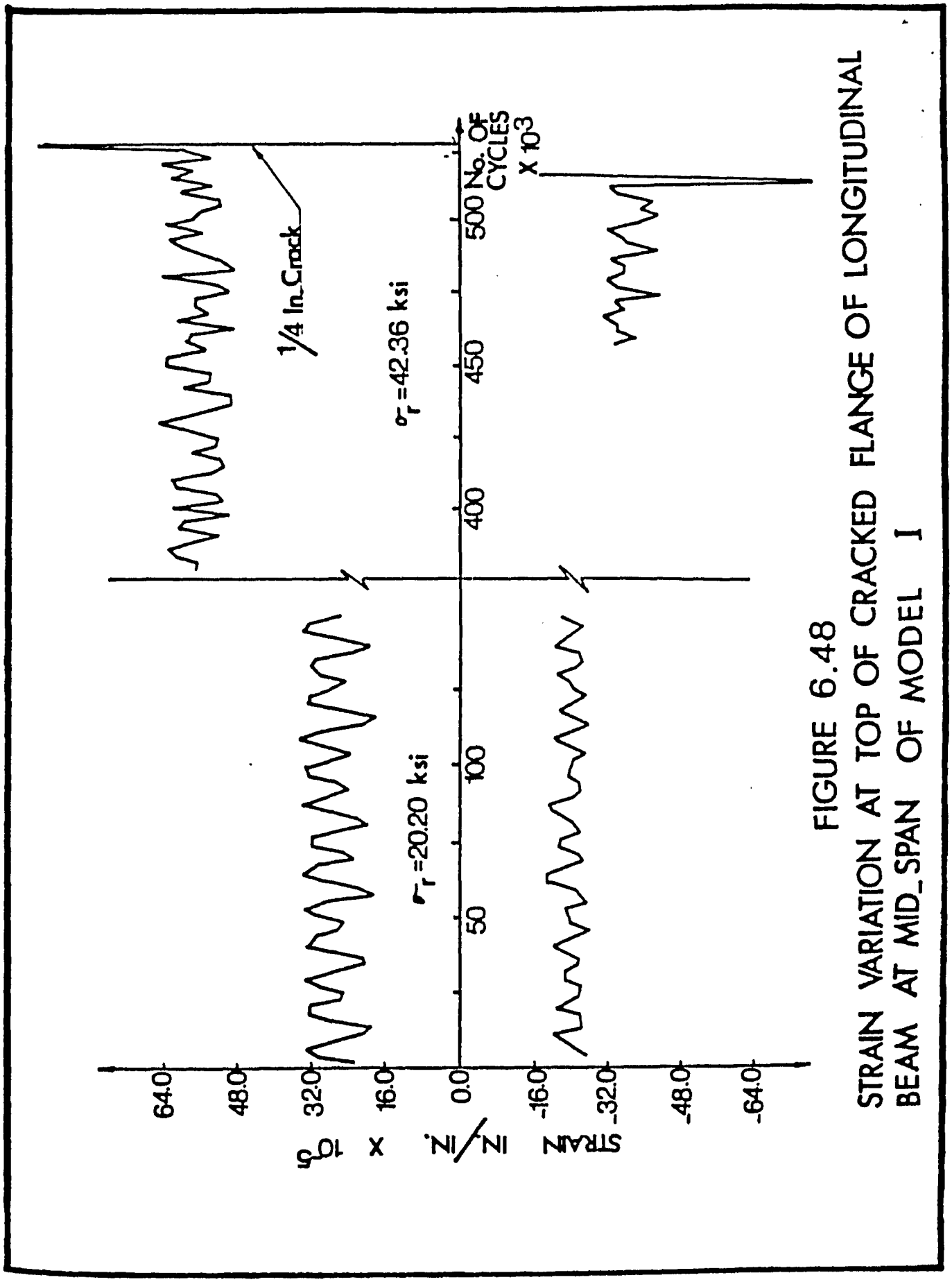

FIGURE 6.48
STRAIN VARIATION AT TOP OF CRACKED FLANGE OF LONGITUDINAL BEAM AT MID_SPAN OF MODEL I

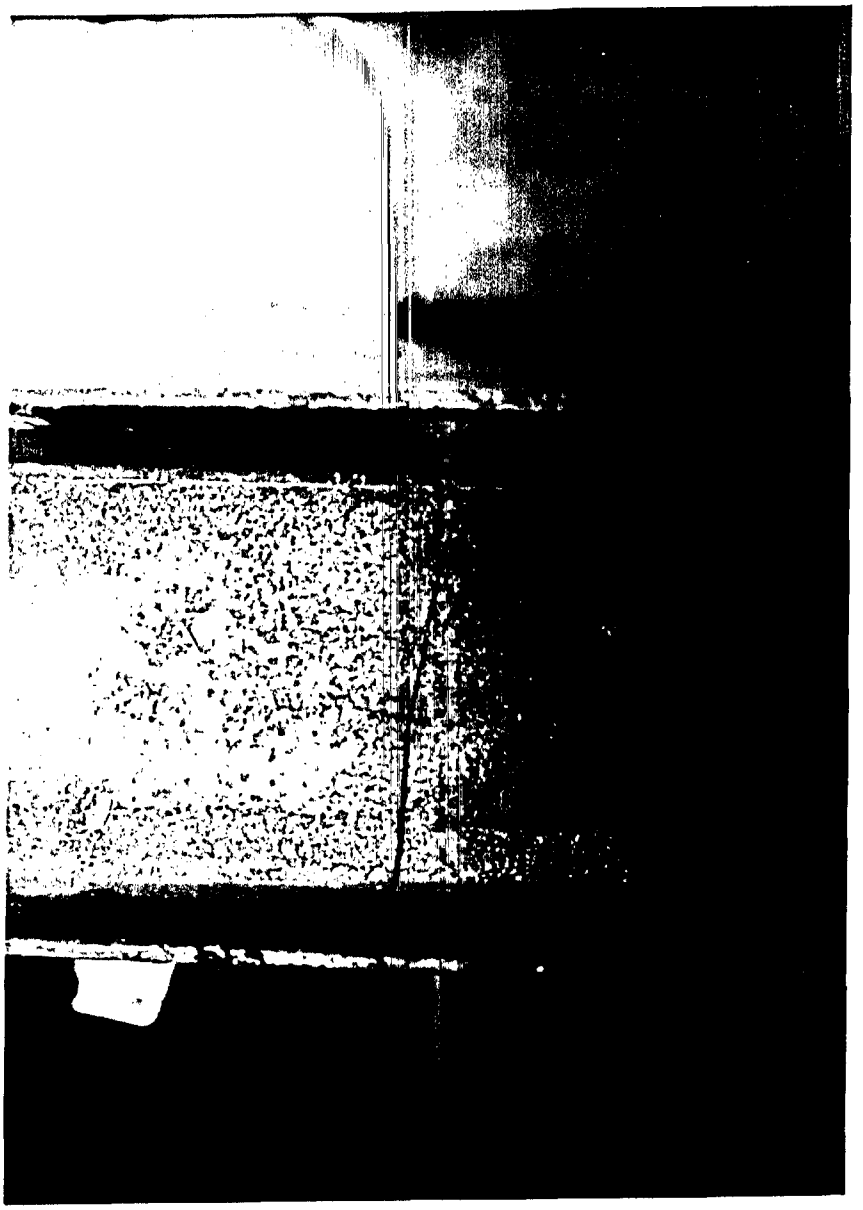

FIGURE 6.49 FATIGUE CRACK PROPAGATION IN BRIDGE MODEL I

transverse cracks along the concrete deck. Extensive transverse cracking of the concrete deck began to develop at the beginning of the fatigue test; this cracking occurred near the intermediate support as well as at mid-span because the dynamic deflection was large enough to create some negative moment even at the mid-span section; these cracks were fairly well stabilized after 10,000 cycles of fatigue loading. This means that the slab was not effective in contributing to composite action of the bridge model, especially not at the intermediate support. The intermediate support section was always subjected to negative moment during the fatigue test. At this section, the effective moment of inertia was at least equal to the cracked slab composite moment of inertia contributed by the steel beam and the longitudinal reinforcement in the concrete slab deck. It should be emphasized that even though there were transverse cracks at mid-span, they were completely closed when the model vibrated at the lowest deflected point; this means uncracked slab composite moment of inertia was completely effective in resisting the downward vibration. However, during the upward vibration, transverse cracks opened and hence, only the cracked slab composite moment of inertia was effective in resisting the upward deflection.

It was not surprising that the cumulative fatigue damage to the bridge model had a considerable influence on the damping ratio associated with the first mode shape as well as on the first natural frequency. Repeating the dynamic tests again on the model revealed that the first natural frequency dropped dramatically, which means the model lost a certain percentage of its stiffness which increased the damping ratio. This increase was a result of the successive transverse cracks in the concrete deck. This

shows that the dynamic characteristics of a bridge can be used as an inspection tool to confirm the existance of fatigue cracks or of impending fatigue failure.

The strain variation of the stress range of the bottom flange of the transverse diaphragms at mid-span is shown in Figure 6.50. Initially, the stress range was about 10 ksi. At about 600,000 it more than doubled due to an invisible crack which was monitored from the strain gage time history. Furthermore, the strain variation in the longitudinal reinforcing bars at the intermediate support was continuously monitored and recorded as shown in Figure 6.51; at about 600,000 cycles, one bar was fatigued; this fatigue crack was a result of the wide transverse cracks which created high stress concenetration at the cracks' locations in the reinforcing bars under the repeated load. Also, an invisible crack was monitored in the top flange of the longitudinal steel beam at the intermediate support by means of changes in the strain time history as shown in Figure 6.52.

Design of the stud shear connectors based on fatigue and flexural requirements are shown in Figure 6.53. However, it was decided to provide, in bridge model I, a larger number of shear connectors beyond the number required by fatigue considerations. This decision was made to eliminate the possibility of separation between the deck and the steel beams, which is likely to occur at resonance fatigue loading. The strain variation in a stud shear connector near the end support is given in Figure 6.54. This figure shows fatigue hair cracks on both sides of the stud; however, after the conclusion of the tests and the slab removed to examine the studs, there were no visible cracks on the studs; which means that the number of

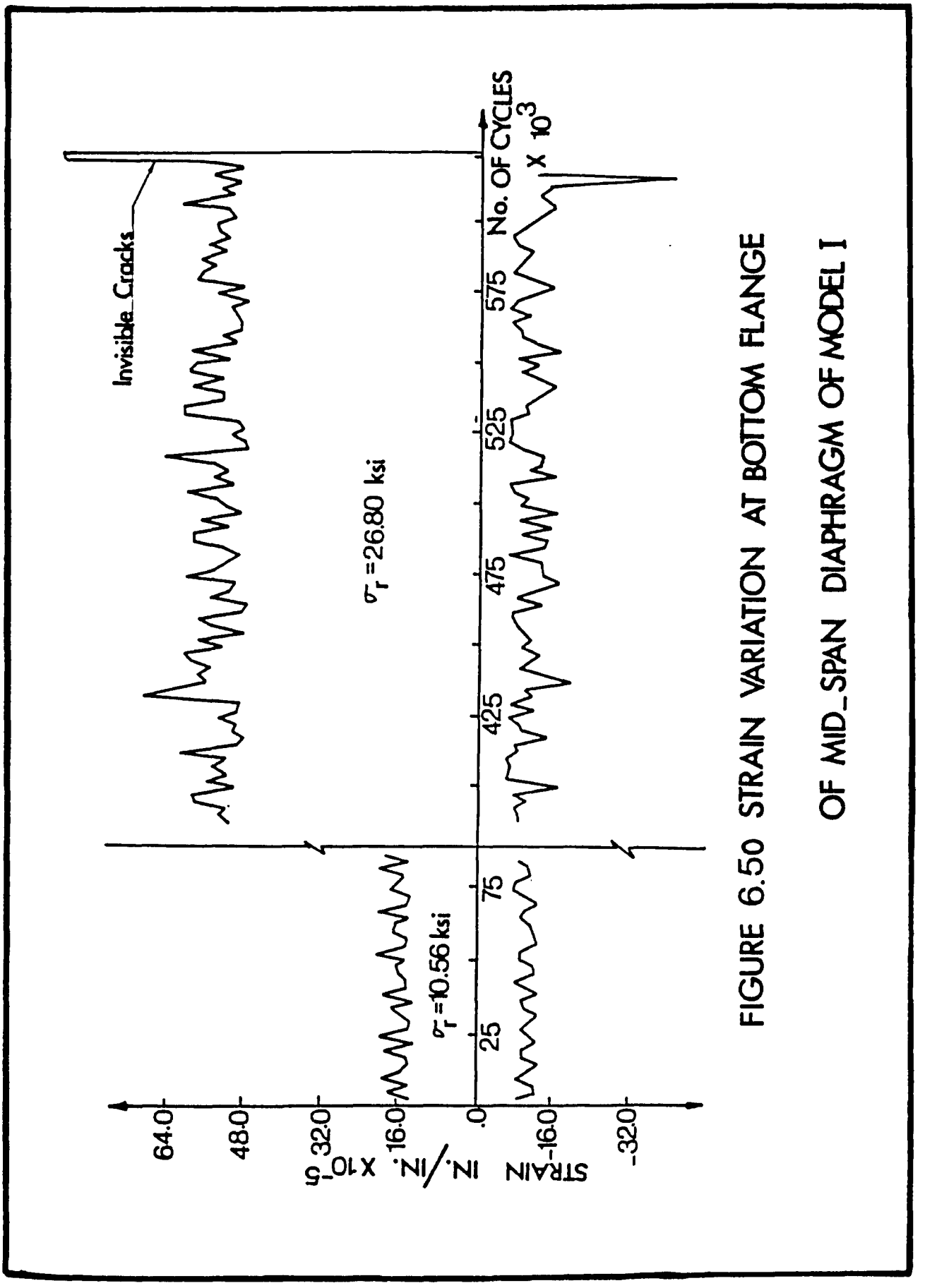

FIGURE 6.50 STRAIN VARIATION AT BOTTOM FLANGE OF MID_SPAN DIAPHRAGM OF MODEL I

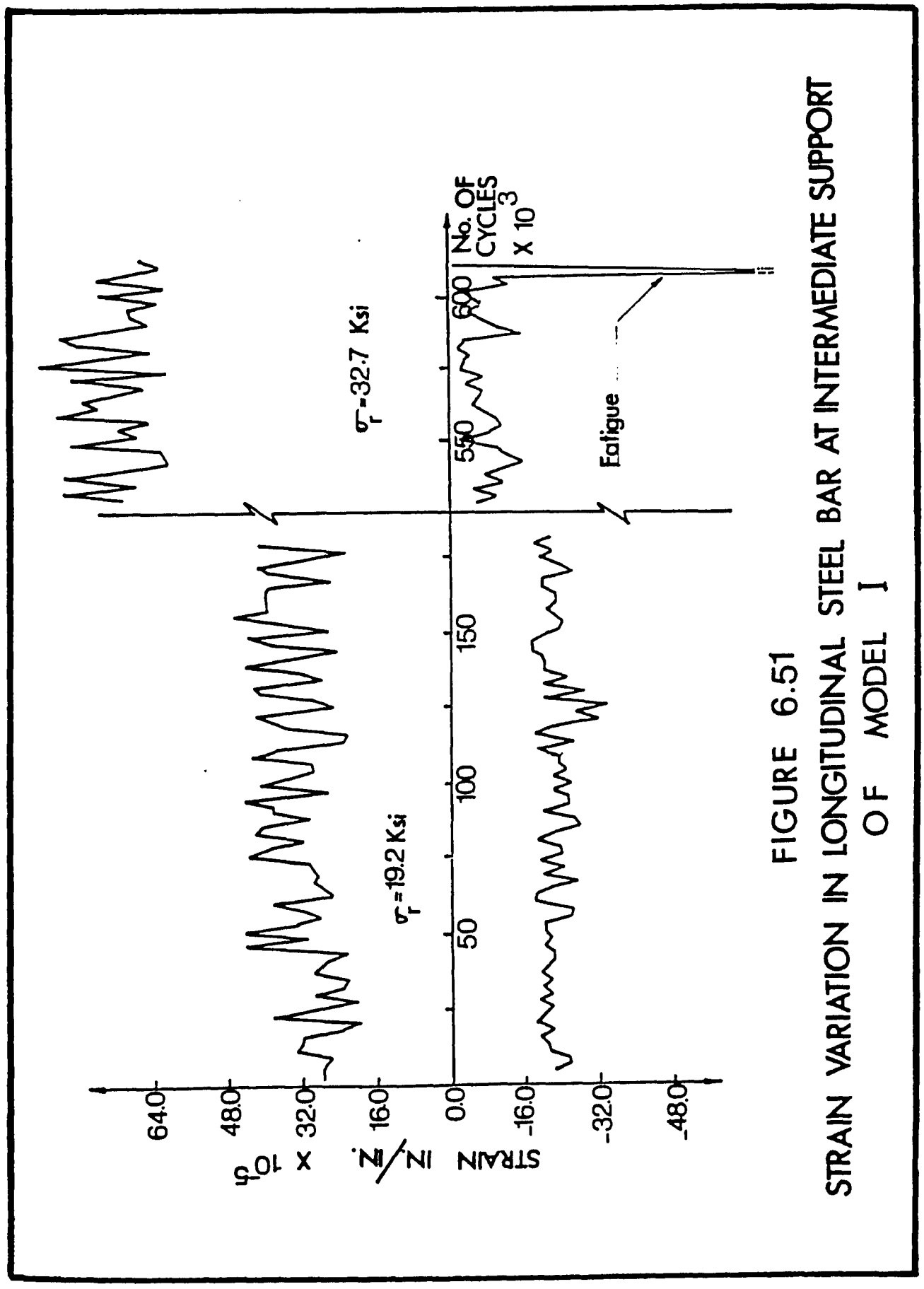

FIGURE 6.51
STRAIN VARIATION IN LONGITUDINAL STEEL BAR AT INTERMEDIATE SUPPORT OF MODEL I

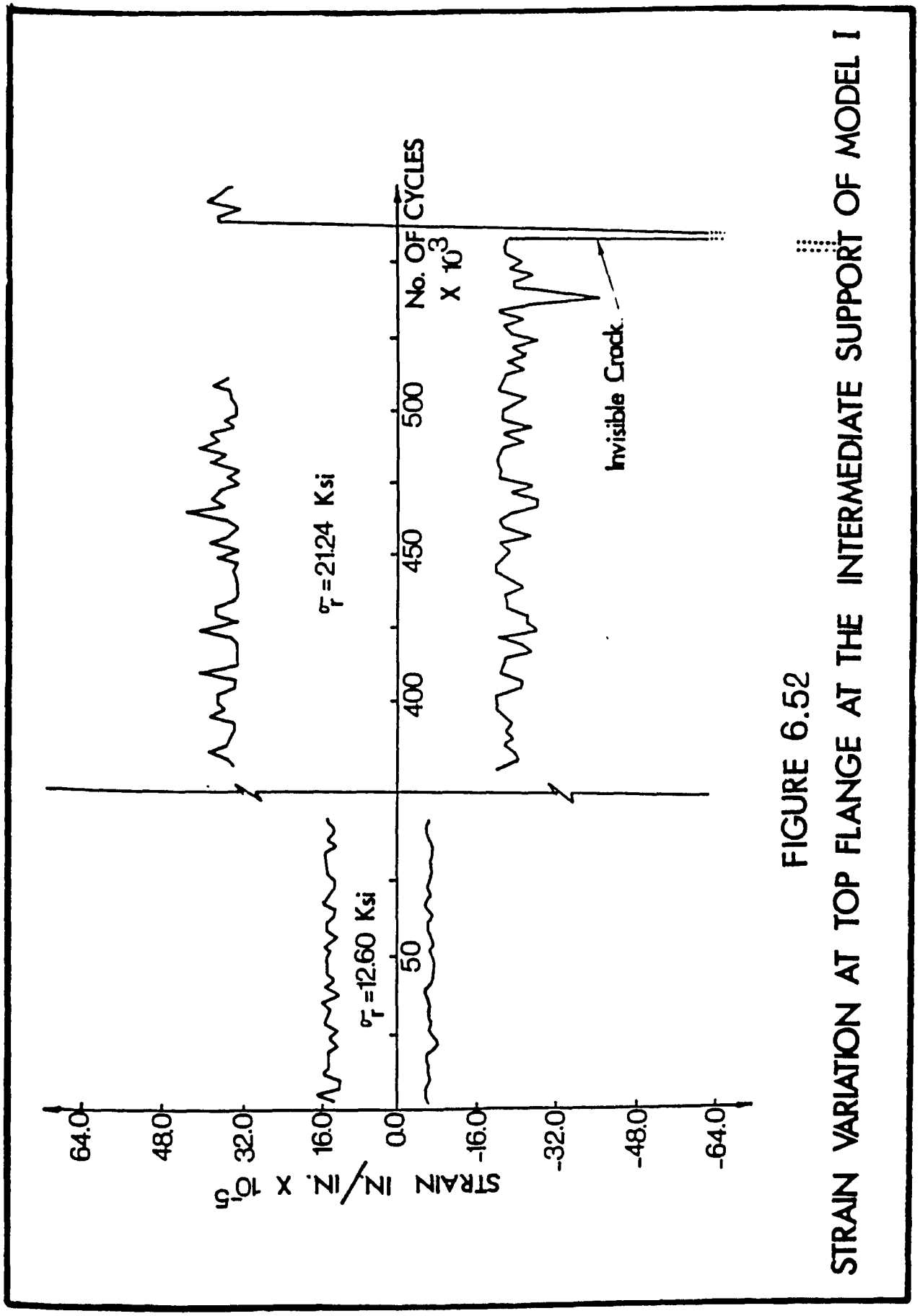

FIGURE 6.52

STRAIN VARIATION AT TOP FLANGE AT THE INTERMEDIATE SUPPORT OF MODEL I

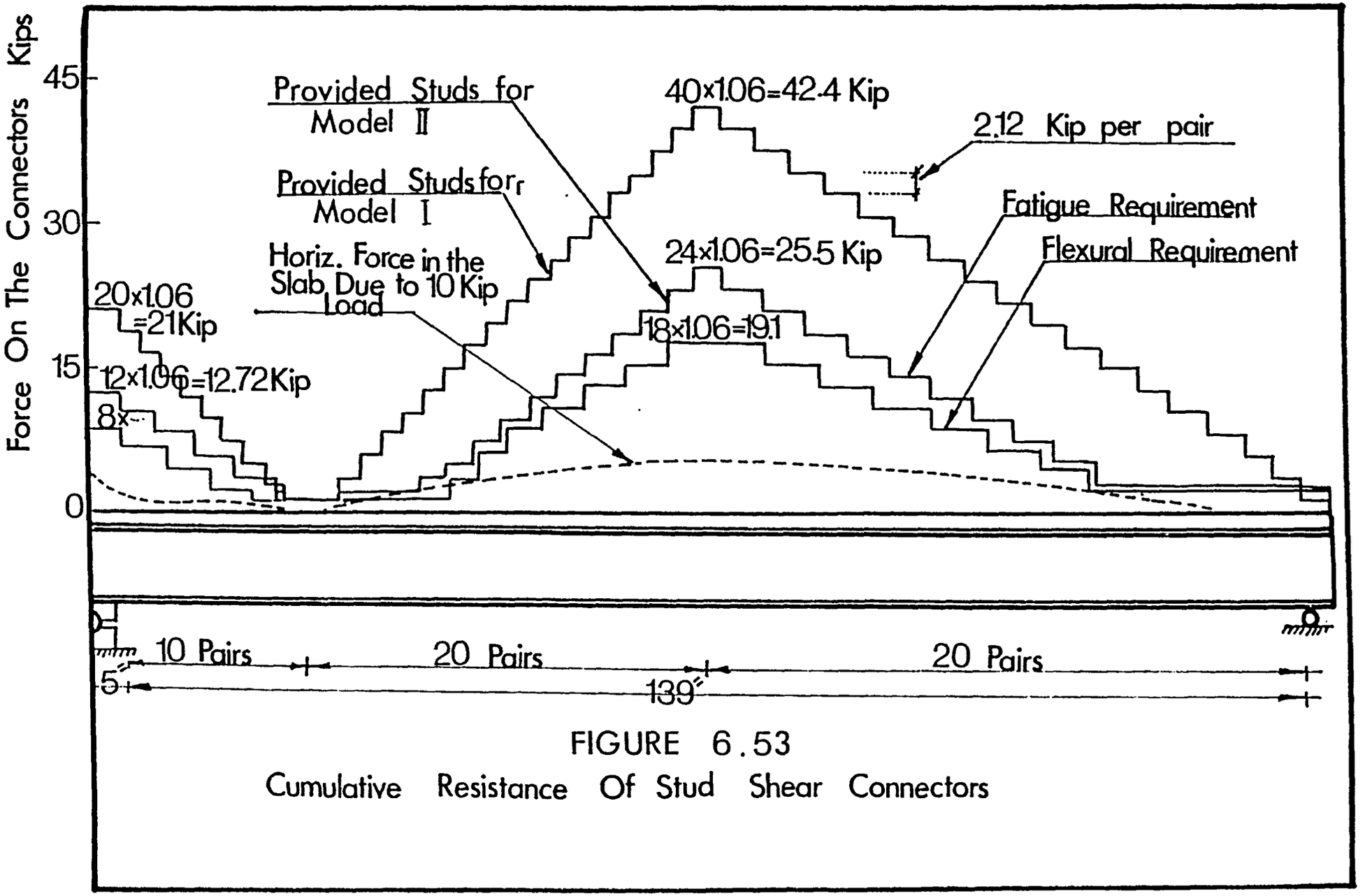

FIGURE 6.53

Cumulative Resistance Of Stud Shear Connectors

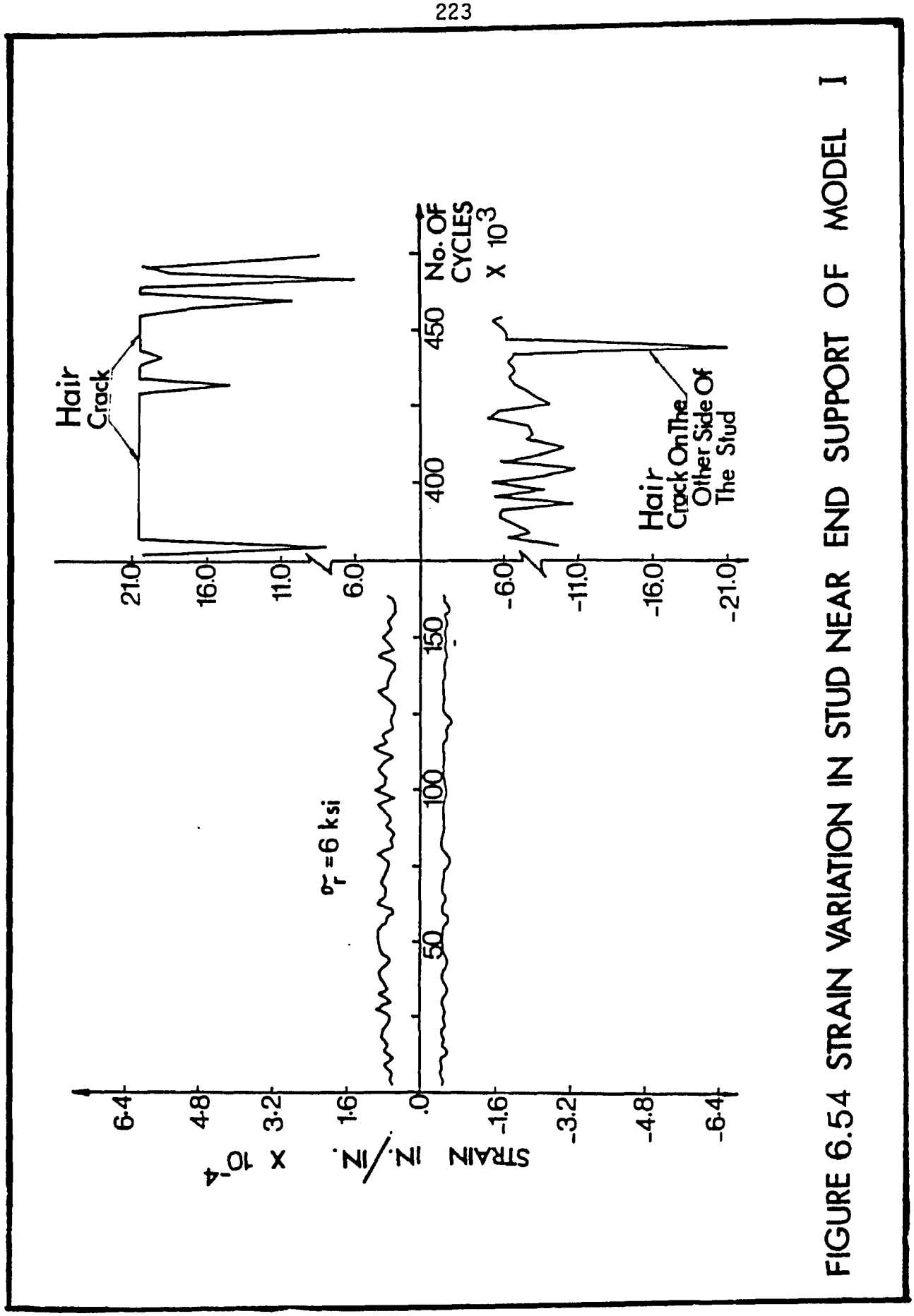

FIGURE 6.54 STRAIN VARIATION IN STUD NEAR END SUPPORT OF MODEL I

the provided shear connectors may have been more than sufficient and that shear connectors fatigue requirements are adequate.

It should be mentioned that the steel bolts holding the moving mass to the top plate of the actuator was fatigued after 50,000 cycles. However, this was repaired by means of super high-strength 1-1/2 inch bolts. At the end of the fatigue test it was decided to repair the fatigued model and re-examine its dynamic characteristics. The repair was achieved by welding 3/8 inch thick plates, one to the exterior side of the web and one on the bottom flange, as shown in Figure 6.55. Bridge model I was retested under dynamic load, and results indicate that the bridge model regained its first natural frequency, but did not achieve the same damping ratio.

6.8.2 Bridge Model II and Comparison with Bridge Model I

As mentioned before, bridge model II had a portion of its concrete deck prestressed in the vicinity of the intermediate support; the fatigue failure of this model was characterized by the initiation of a visual crack that propagated under repeated application of resonance load until eventually the effective stiffness could no longer sustain the load. Two actuators were used to conduct the resonance fatigue test close to the third mode shape, i.e., at the second flexural mode, by exciting the model at the first natural frequency. This was necessary since the third natural frequency was quite high; however, by using two actuators acting simultaneously and in-phase on each span and with the exciting frequency equal or close to the first natural frequency of the model, the fatigue loading would excite the model in the third mode shape, and close to the first natural frequency. The third mode shape, shown in Figure 6.22, was

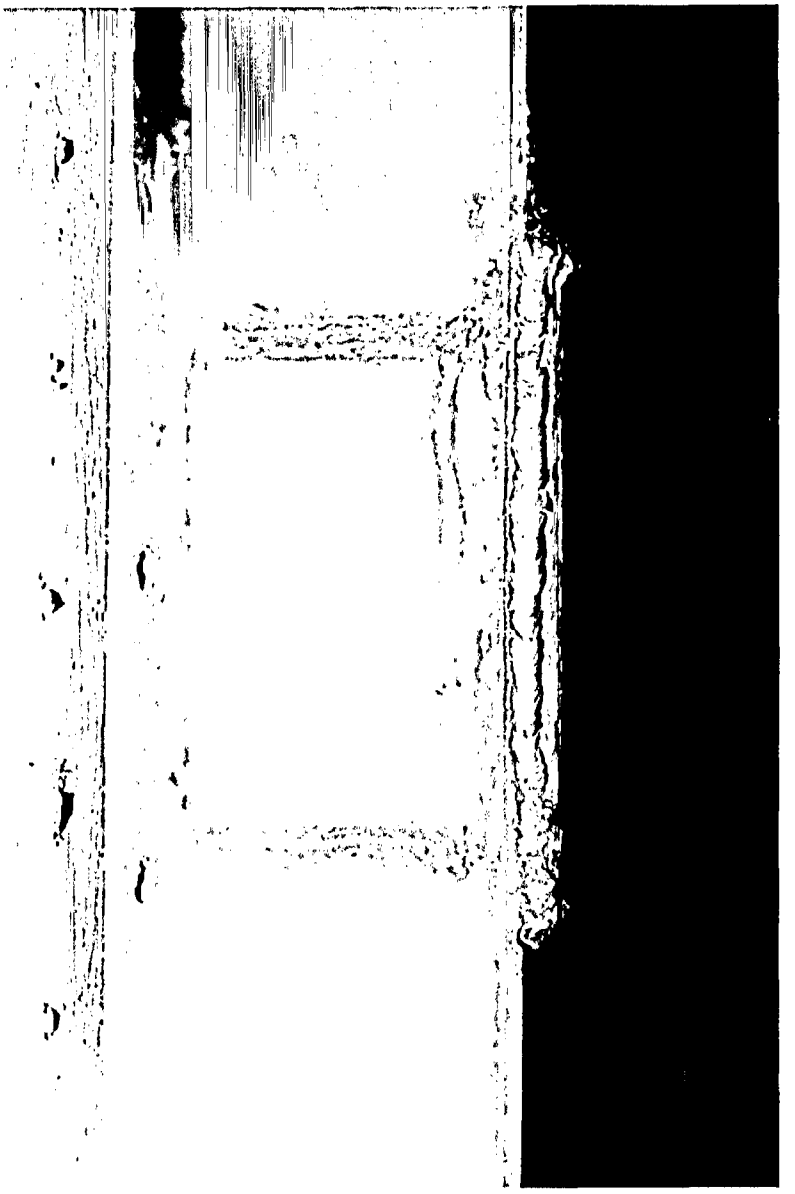

FIGURE 6.55 REPAIR OF FATIGUE CRACKS IN BRIDGE MODEL I

continually producing large negative moment at the intermediate support. This was required to examine the effect of the hogging moment on the prestress force and on the prestressing wires under repeated loads.

Figure 6.56 shows the strain distribution in the bottom flange of the longitudinal steel beams and on top of the prestressed concrete deck at the intermediate support as well as in the top and bottom flanges of the longitudinal steel beams at the mid-span before casting the non-prestressed concrete portions. The strain distribution at the intermediate support indicated that high compressive strains in the concrete deck developed as a result of the prestressing force; this force also had a tendency to displace the steel beams upward, creating positive strain in the top flanges and negative strain in the bottom flanges at the mid-span sections as shown in Figure 6.56.

Figure 6.57 shows the strain variation at the bottom flange of the interior steel beam at the mid-span section. Comparing Figures 6.57 and 6.47 shows that the presence of the prestressed concrete around the intermediate support in bridge model II considerably reduced the stress range in the bottom flange of the interior beam at the mid-span section of bridge model II. The stress range in the top flange of the interior beam at the intermediate support was about 16.50 ksi and no significant changes occurred even at high number of applied fatigue cycles while in bridge model I the stress range significantly increased to 21.24 ksi as shown in Figure 6.52.

A typical strain variation in the transverse direction on the top of the prestressed concrete close to the intermediate support reflected the Poisson's ratio effect on the strain variation in the longitudinal

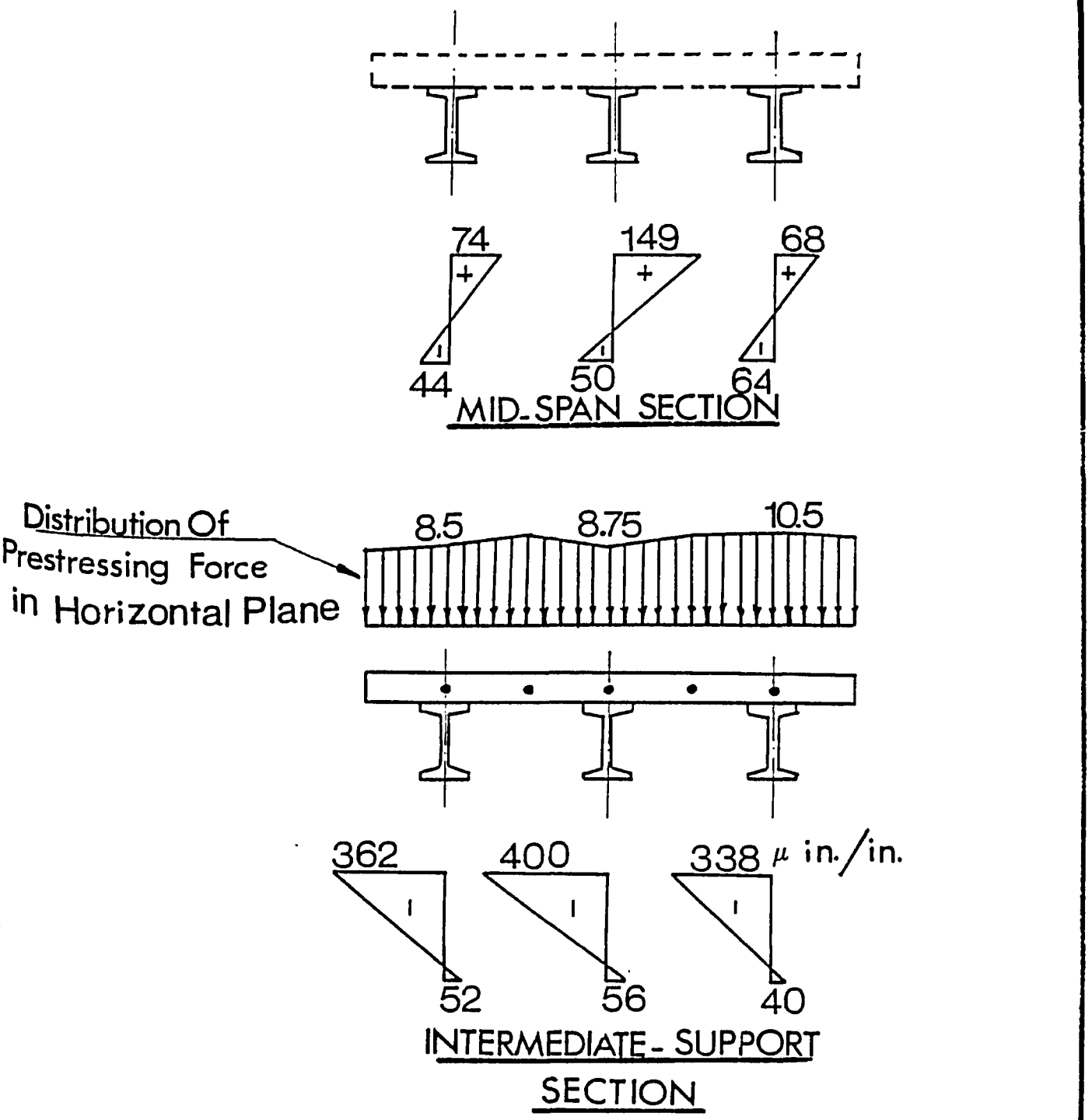

FIGURE 6.56

STRAIN DISTRIBUTION DUE TO PRESTRESSING THE DECK NEAR INTERMEDIATE SUPPORT SECTION OF MODEL II

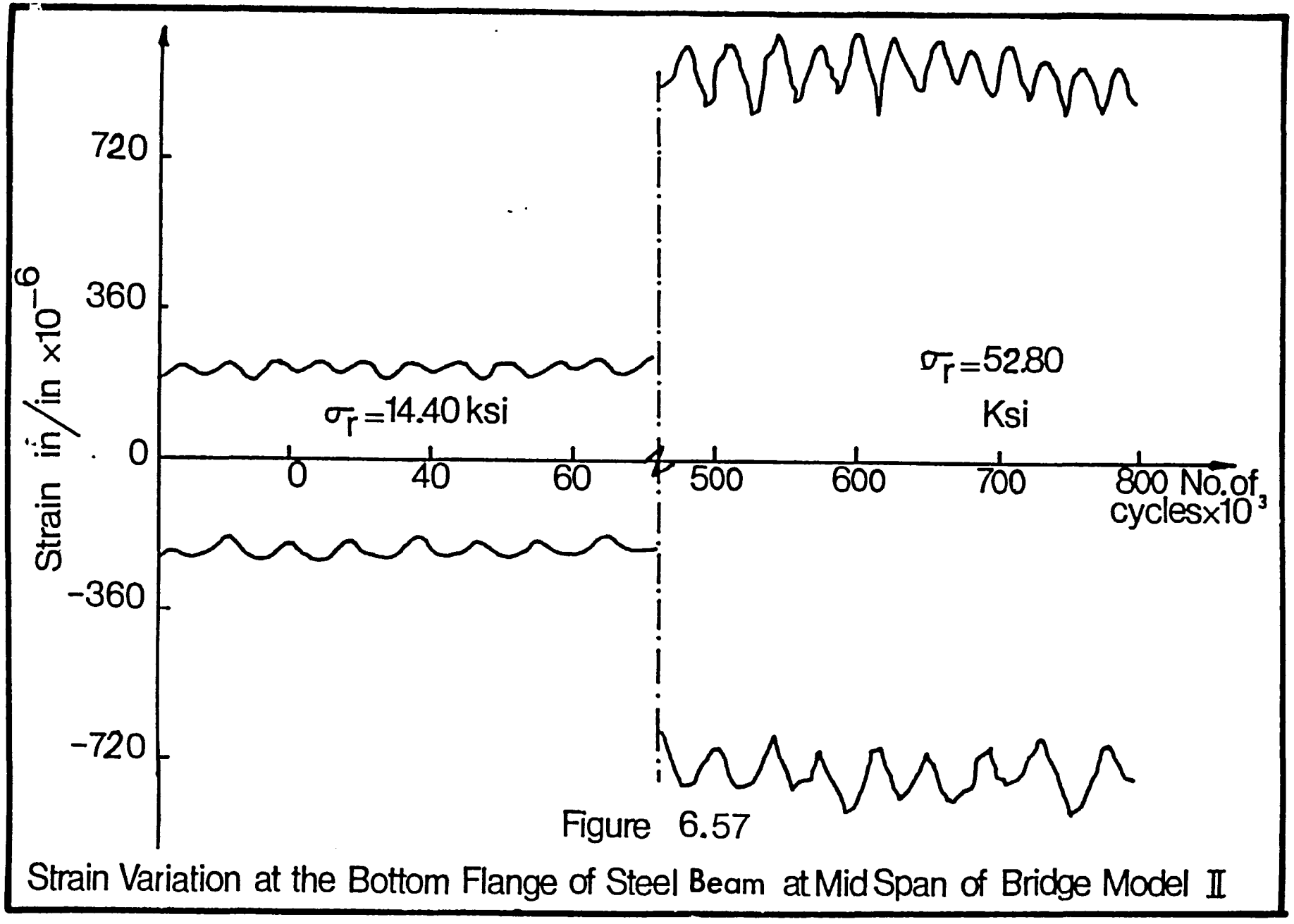

Figure 6.57

Strain Variation at the Bottom Flange of Steel Beam at Mid Span of Bridge Model II

direction, as shown in Figure 6.58. No significant changes were noticed, until about 500,000 cycles when a jump in the transverse strain indicated some transverse cracks had occurred; at about 750,000 cycles the strain became negative strain which indicated more cracks had developed.

The prestressing force created large shear forces on the stud shear connectors located within the prestressed concrete portion. Consequently, this shear force created high tension on one side of the root of the stud; by superimposing this tensile strain on the changes in the stud strain due to the pulsating force resulted in a strain variation corresponding to a small stress range of 4.5 ksi as shown in Figure 6.59. No fatigue failure in the shear connectors, located within the prestressed concrete portion, was monitored throughout the fatigue tests.

Figure 6.60 shows the strain variation in the bonded prestressed wires at the intermediate support. The variation in the strain was small. Consequently, its stress range was relatively small because the stress in the bonded wires did not increase by more than 25% to 38% from its effective prestress value. Therefore, fatigue failure in the wires was unlikely even though the resonance stress was exceeded; the stress range was about 30 ksi at the beginning of the fatigue test, it reached 45 ksi at 800,000 cycles.

At about 800,000 cycles a complete separation between the prestressed and non-prestresed concrete occurred. It started at the top of the connection and went through a 45° inclined plane, as shown in Figure 6.61. It should be mentioned that no visible transverse cracks in the concrete were observed in the negative moment region around the intermediate support from the beginning of the fatigue test up to 800,000 resonant cycles, as

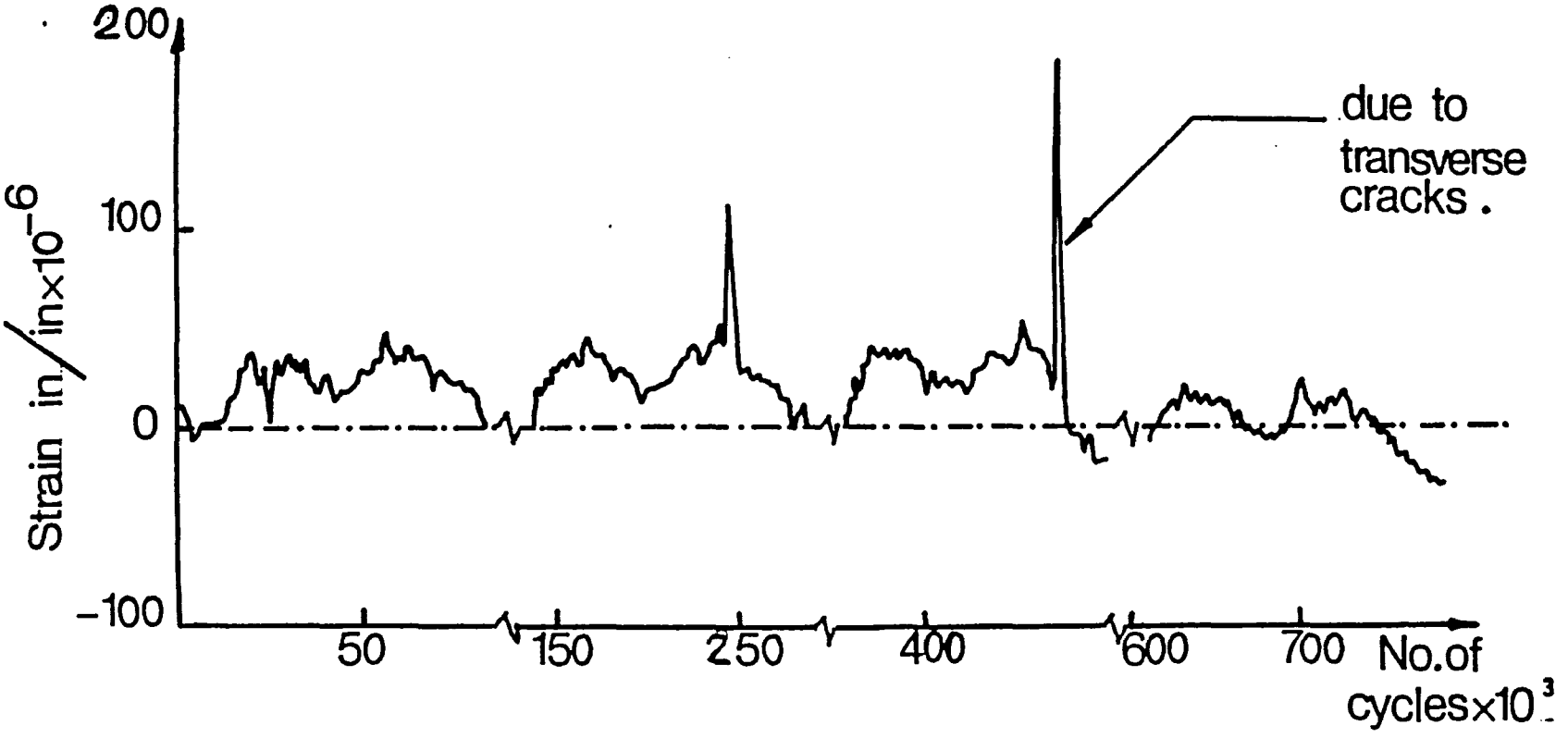

Figure 6.58

Strain Variation in the Transverse Direction on the Top of Presstressed Concrete at the Intermediate Support.

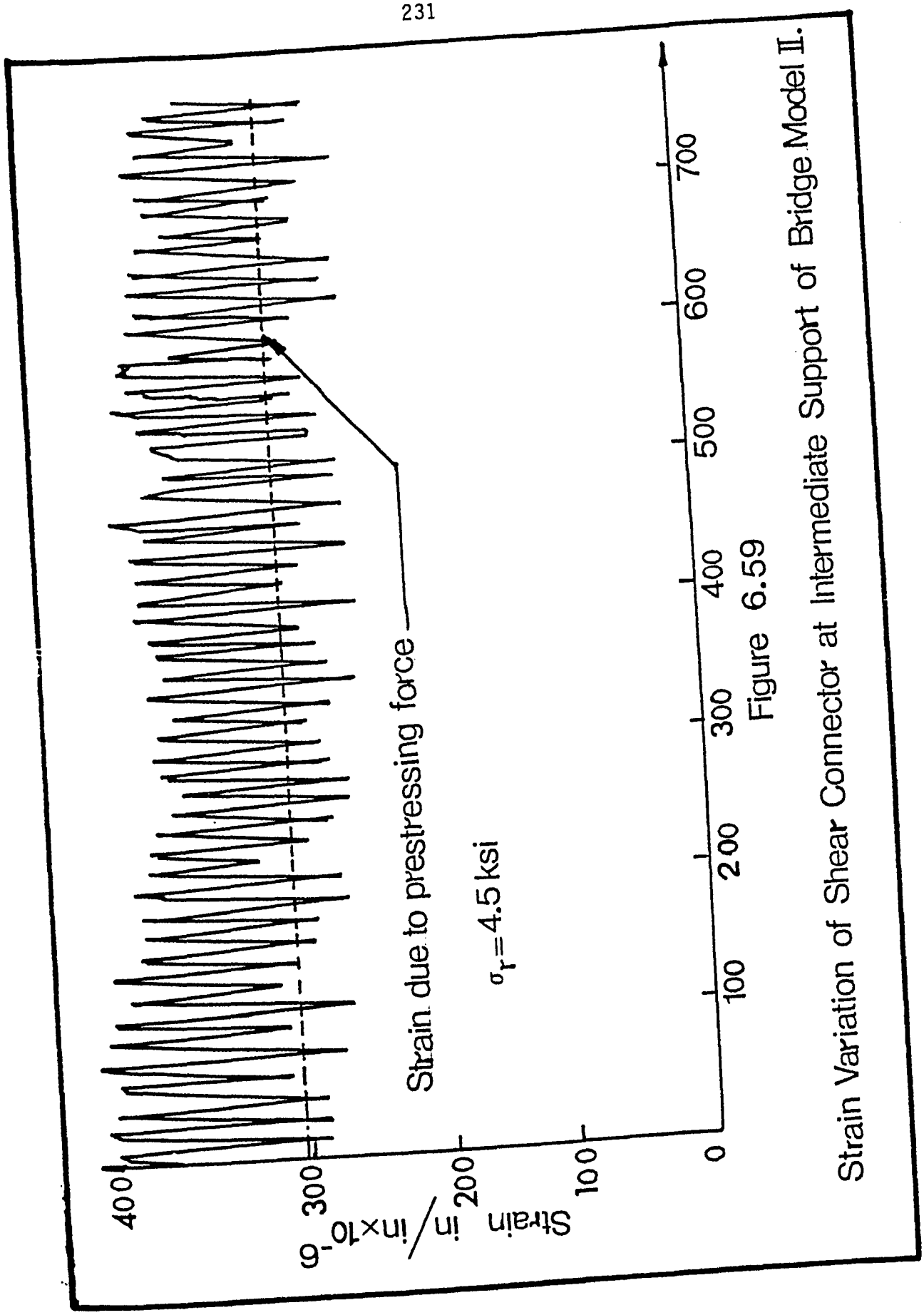

Figure 6.59

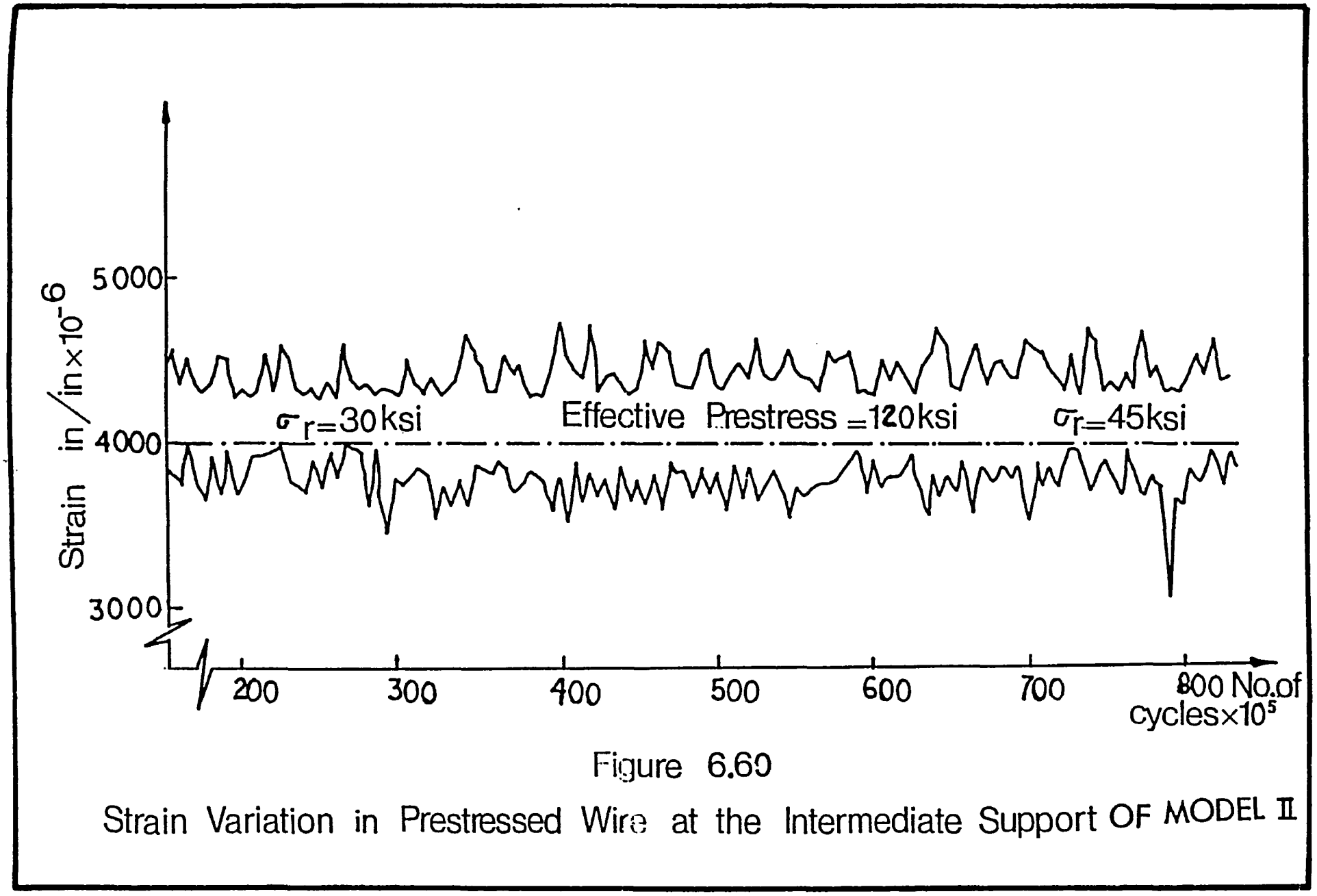

Figure 6.60

Strain Variation in Prestressed Wire at the Intermediate Support OF MODEL II

FIGURE 6.61 SEPARATION BETWEEN PRESTRESSED AND NON-PRESTRESSED CONCRETE PORTIONS ALONG A 45° PLANE AT 800,000 CYCLES

shown in Figure 6.61. On the other hand, bridge model I had a severe transverse cracks around the intermediate support on the top and bottom surfaces of the concrete slab, as shown in Figure 6.62; its bottom concrete cover beam loosened and spalled, as shown in Figure 6.63. At about 850,000 cycles fatigue cracks developed at the top flange of the exterior and middle beams in one span, and in the concrete slab at 6 inches away from the end of the connection between the prestressed and non-prestressed concrete portions, as shown in Figure 6.64. This separation, shown in Figure 6.61, occurred only in one span and not in both spans, although both spans were simultaneously subjected to the same rate of fatigue loadings. The reason for this was a result of removing some of the shear connectors at one end (see page 94) for facilitating the prestressing procedures and replacing them by steel bars, as shown in Figure 6.65. It was noticed that the natural frequency dropped significantly with a dramatic increase in the damping ratio.

Since one span had no fatigue cracks so far, the decision was made to continue the fatigue test. At about 1,100,000 cycles, the bottom flange of the longitudinal steel beams fatigue cracked at the mid-span section underneath the load in the same fatigued span as shown in Figure 6.66.

The dynamic sweep test was conducted after detecting each fatigue crack and the measured first natural frequency was verified by modeling each crack using the finite element computer program SAP IV; the results are given in Table 6.15. The results reveal that the bridge model lost about 36% of its stiffness at the first fatigue crack, shown in Figure 6.64, while at the second fatigue cracks, Figure 6.66, the bridge model lost about 60% of its total stiffness.

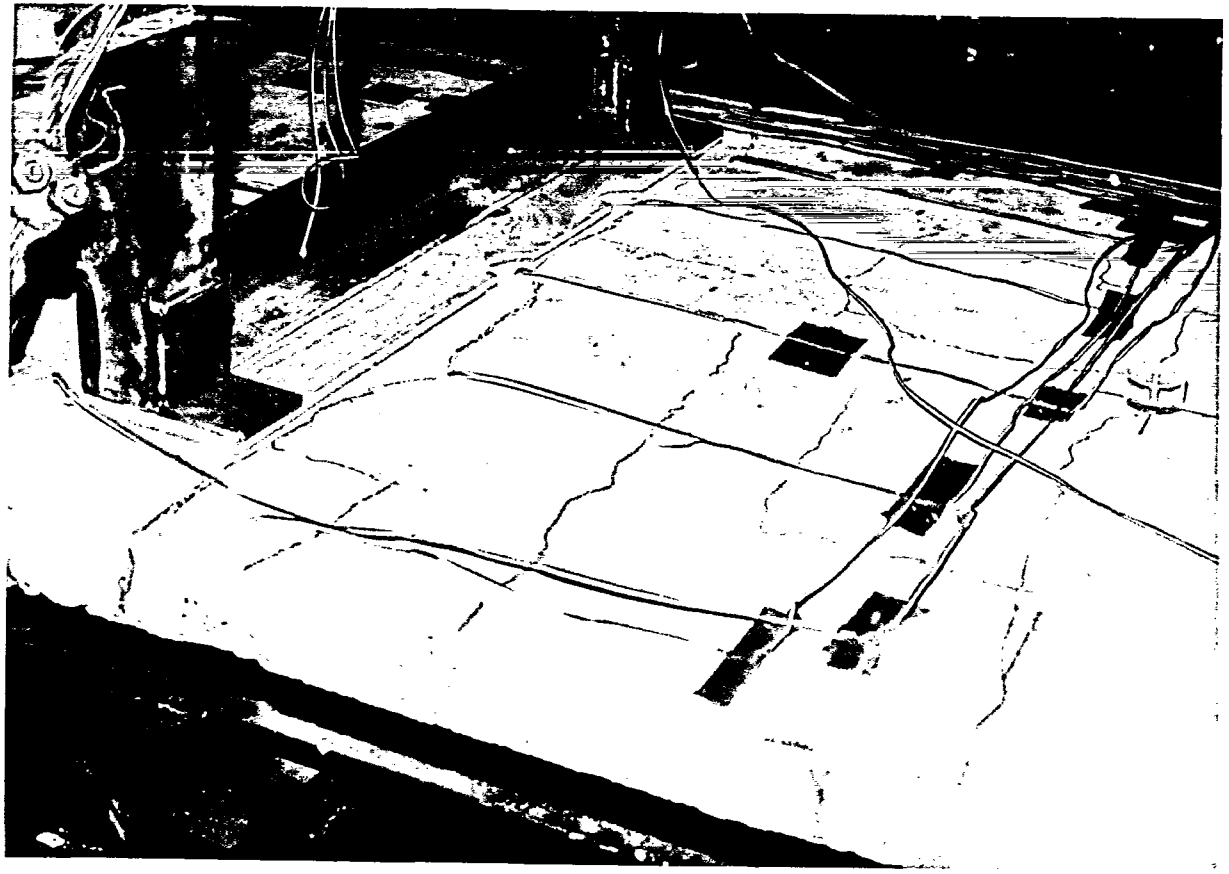

FIGURE 6.62 TRANSVERSE CRACKS IN THE CONCRETE SLAB AROUND THE INTERMEDIATE SUPPORT OF BRIDGE MODEL I

FIGURE 6.63 TRANSVERSE CRACKS AND SPALLING OF CONCRETE COVER IN THE BOTTOM OF THE SLAB AT THE INTERMEDIATE SUPPORT OF BRIDGE MODEL I

FIGURE 6.64 FATIGUE CRACKS IN TOP FLANGES OF EXTERIOR AND MIDDLE BEAMS OF BRIDGE MODEL II AT 840,000 CYCLES

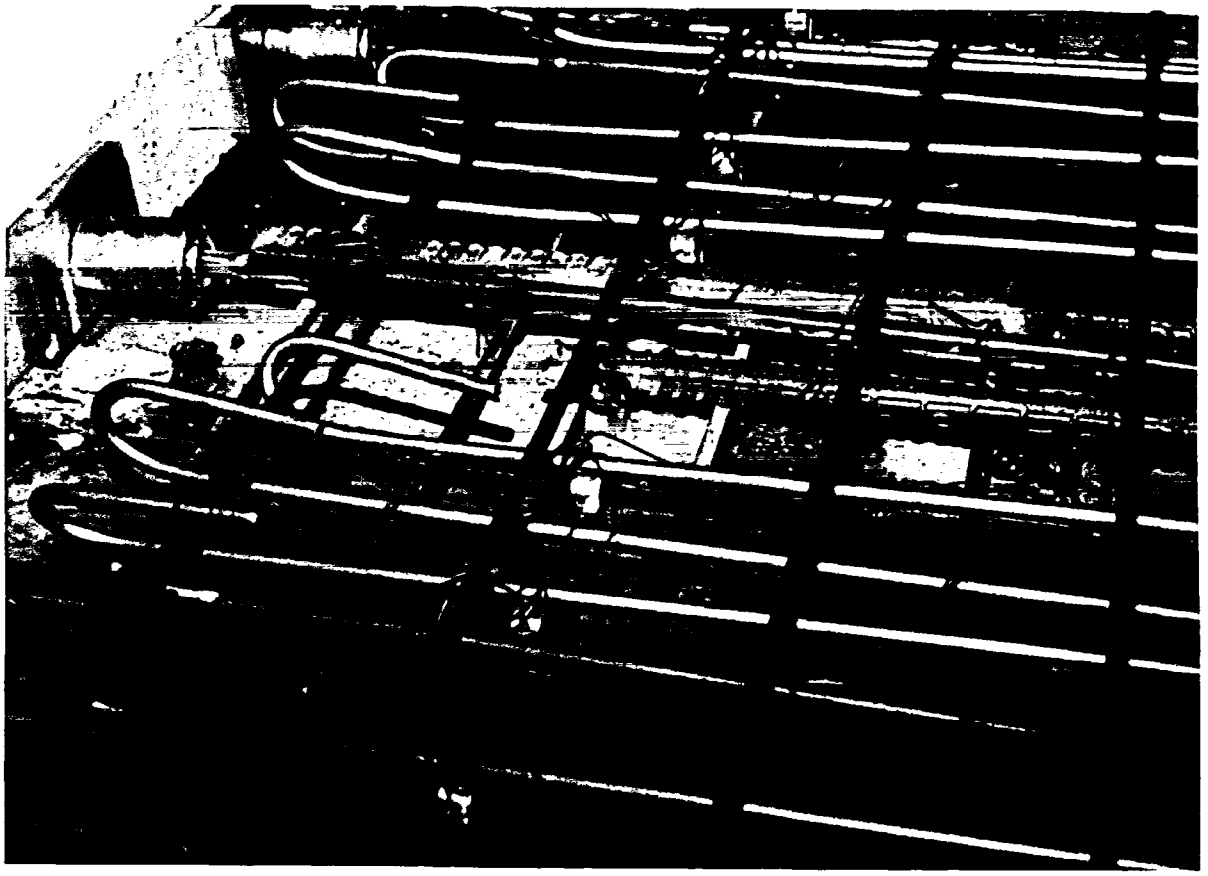

FIGURE 6.65 REPLACING THE STUD SHEAR CONNECTORS BY OTHER MECHANICAL CONNECTOR NEAR ONE SIDE OF THE PRESTRESSED CONCRETE PORTION

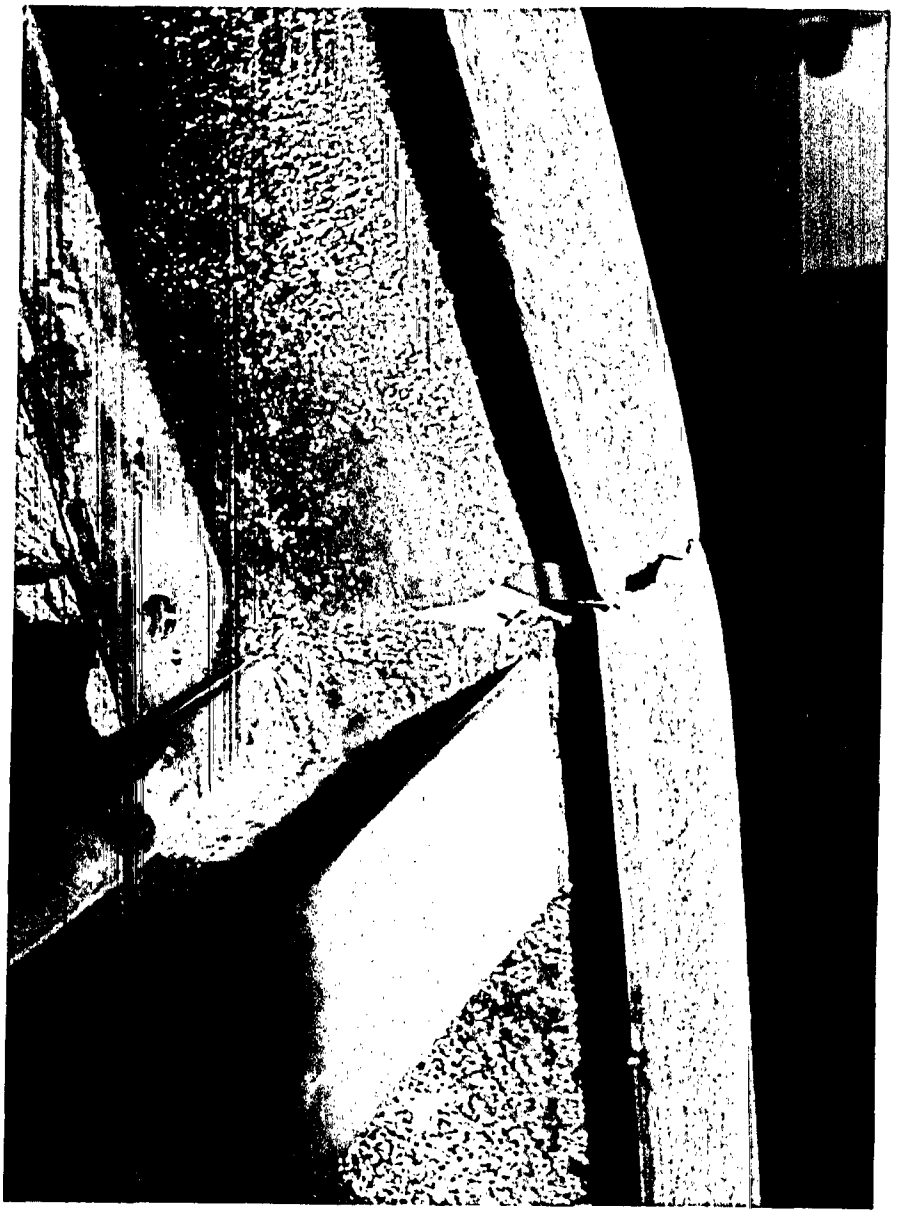

FIGURE 6.66 FATIGUE CRACKS AT MID-SPAN OF BRIDGE MODEL II AT 1,100,000 CYCLES

TABLE 6.15

VARIATION IN THE FIRST NATURAL FREQUENCY
OF BRIDGE MODEL II DUE TO FATIGUE LOADING USING SAP IV

MODE SHAPE NUMBER	NATURAL FREQUENCY C/SEC.					
	BEFORE FATIGUE ZERO CYCLES		CASE I-I* AT 820,000 CYCLES		CASE II-II** AT 1,000,000 CYCLES	
	THEORETICAL	EXPERIMENT	THEORETICAL	EXPERIMENT	THEORETICAL	EXPERIMENT
1	21.1	22	14.8	14	9.6	9

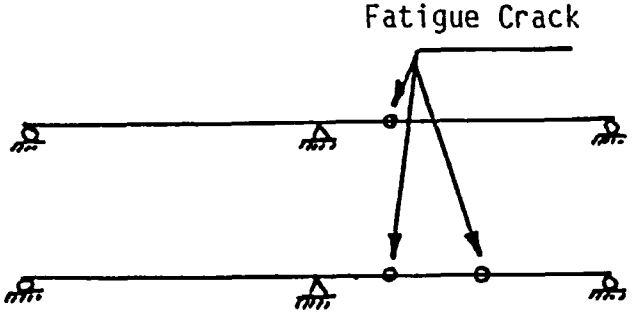

* Case I-I; see Figure 6.64

** Case II-II; see Figure 6.66

It was decided to conduct the ultimate load test without repairing the fatigued span. The reason behind this decision was to compare the ultimate load carrying capacity of repaired model I and the unrepaired model II.

6.9 ULTIMATE LOAD TEST RESULTS

After repairing the fatigue crack in bridge model I, it was tested to failure under a concentrated static load at one mid-span of the middle beam, as shown in Figure 6.67. The collapse load was 56 kips (249 KN) which compares well with the calculated load of 60 kips (267 KN) derived using plastic structural analysis. Such close agreement shows that the hair cracks due to fatigue did not significantly influence the ultimate load carrying capacity of the structure, and the overstressed concrete deck and the diaphragms were still distributing the load adequately in the transverse direction. It was observed that the steel beams at the mid-span had completely yielded and the top reinforcement in the concrete deck had buckled locally, as shown in Figure 6.68. The ultimate load test deflection curve is shown in Figure 6.69. It was observed that the deflection was about 2.0 inches at a load of 40 kips, while at a load of 56 kips the model kept yielding without sustaining any further load.

As mentioned before, bridge model II had only one span completely fatigued. The decision was made to load the two spans simultaneously without repairing the fatigued span. Figure 6.70 shows that the ultimate load carrying capacity for the unfatigued span was about 65 kips, while the fatigued span collapsed at a load of 30 kips. The fatigue cracks in the fatigued span completely opened under the ultimate load, as shown in Figure 6.71. The formation of positive and negative 'plastic' hinges is evident

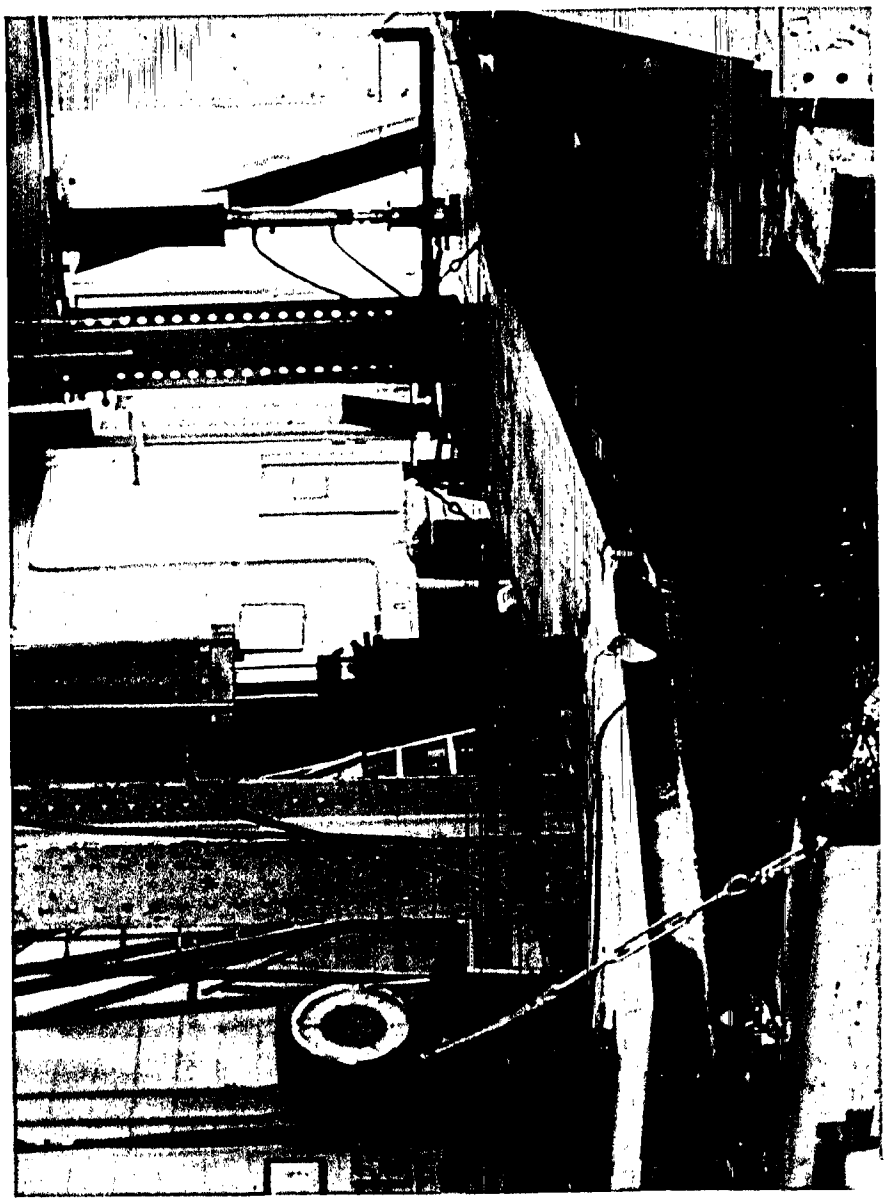

FIGURE 6.67 ULTIMATE LOAD TEST OF BRIDGE MODEL I

FIGURE 6.68 CLOSE-UP OF MID-SPAN 'PLASTIC' HINGE OF BRIDGE MODEL I

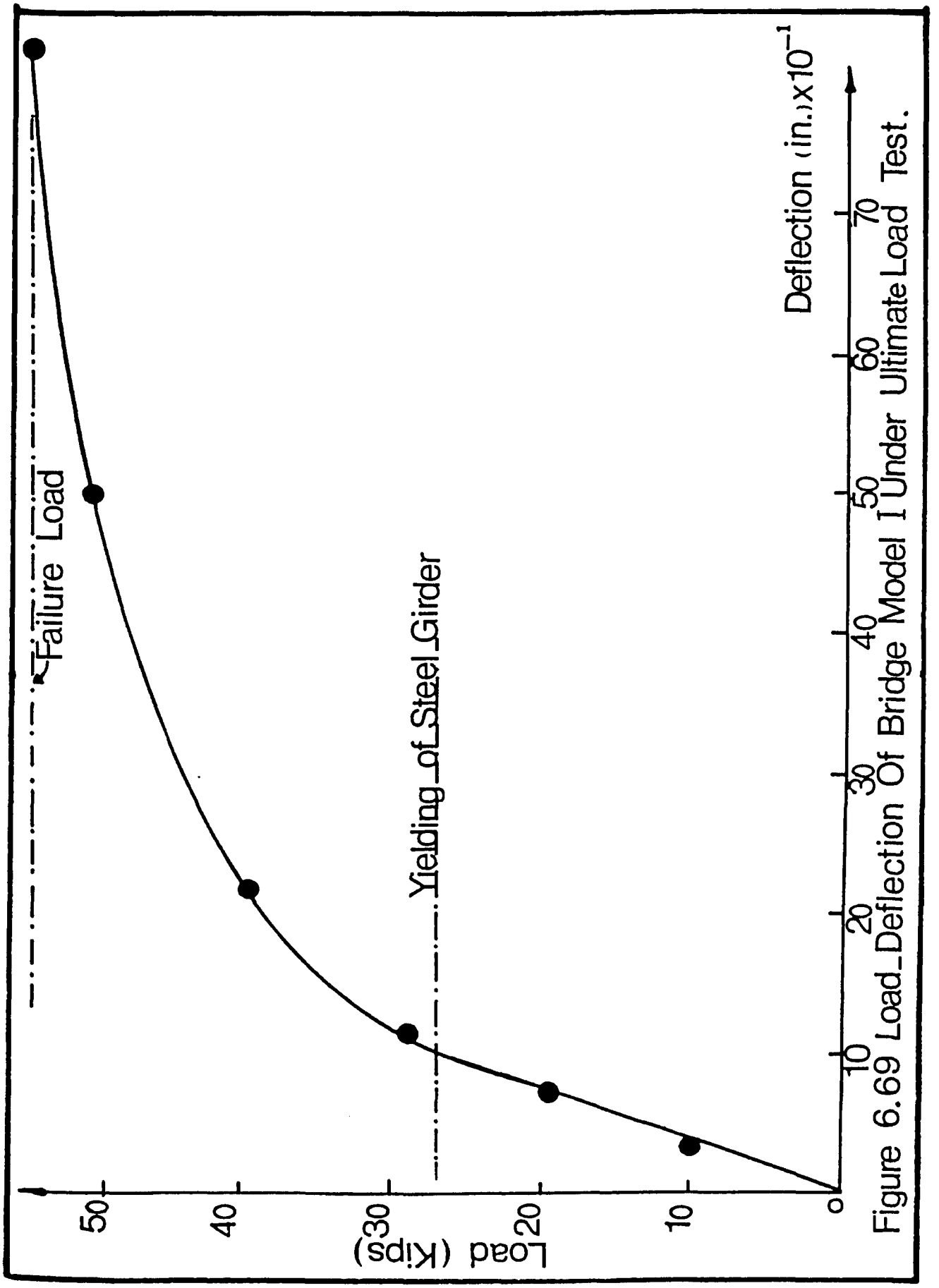

Figure 6.69 Load-Deflection Of Bridge Model I Under Ultimate Load Test.

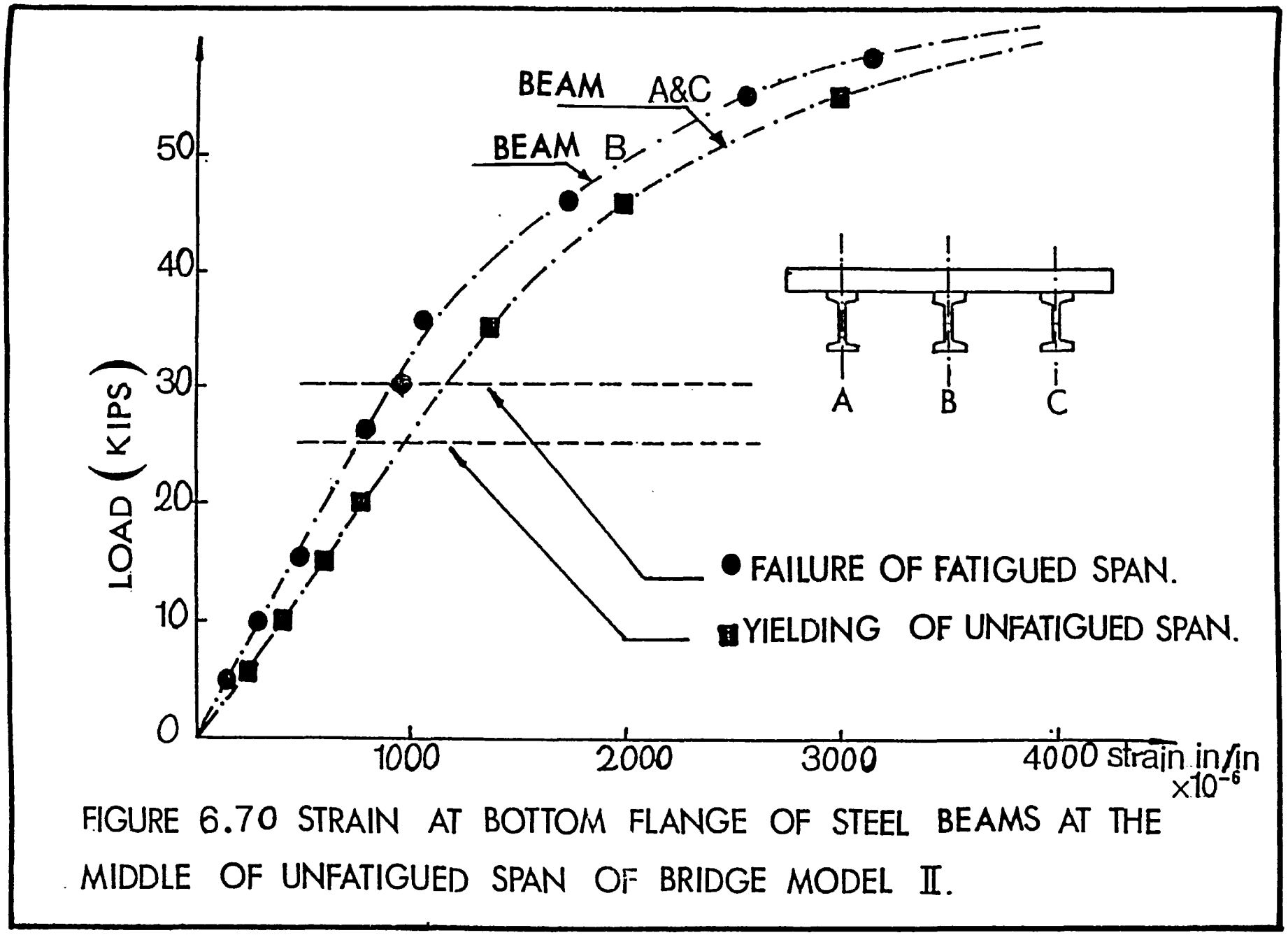

FIGURE 6.70 STRAIN AT BOTTOM FLANGE OF STEEL BEAMS AT THE MIDDLE OF UNFATIGUED SPAN OF BRIDGE MODEL II.

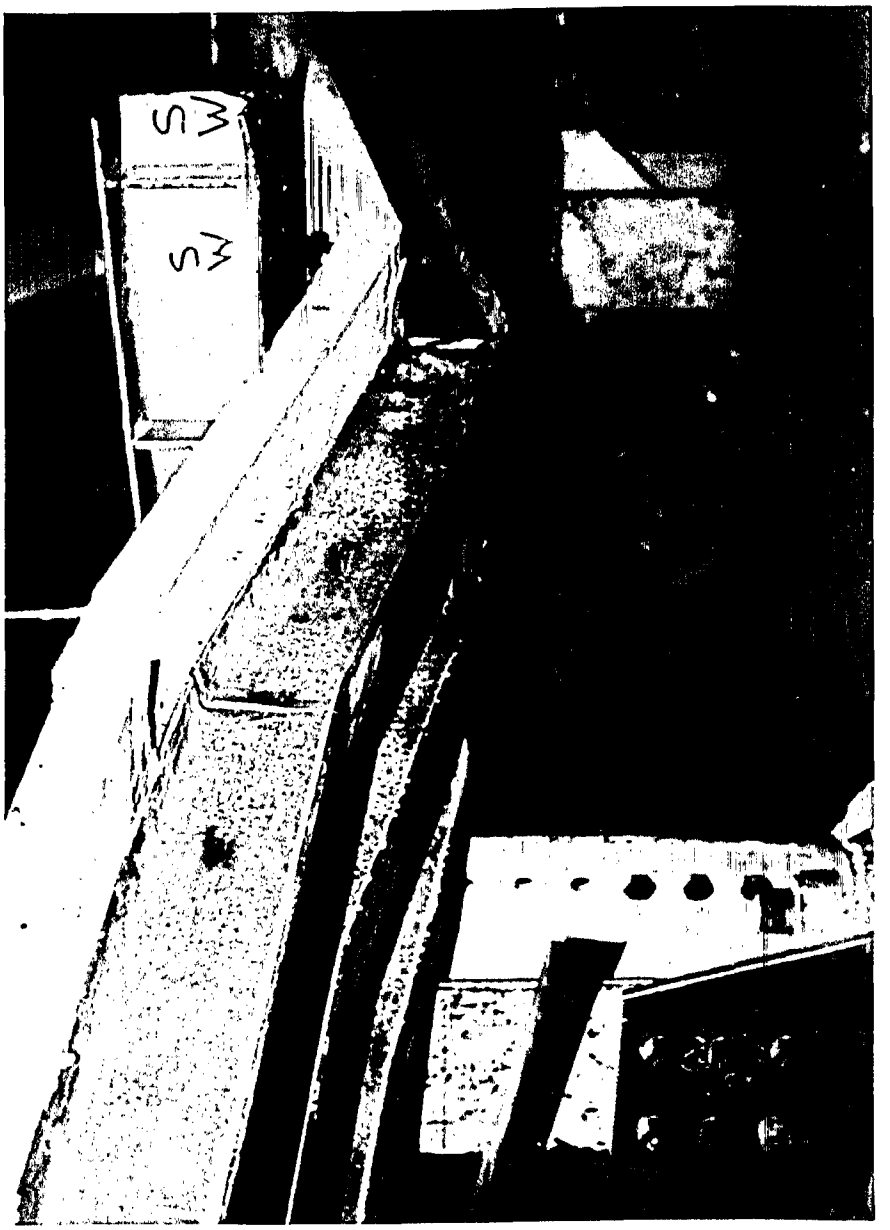

FIGURE 6.71 FATIGUE CRACKS OF BRIDGE MODEL II UNDER ULTIMATE LOAD TEST

in Figure 6.72; a close-up of the formation of the negative 'plastic' hinge is shown in Figure 6.73. Comparing the ultimate load carrying capacity of the two models reveals that bridge model II exhibited a higher load carrying capacity, probably because of the presence of the prestressing steel and perhaps because the fatigued span was acting as a cantilever portion to the unfatigued span, providing additional stiffness in resisting the ultimate load. It should be noted that the slip between the concrete deck slab and the longitudinal steel beams was almost zero in both models even at the ultimate load. In a protype bridge with a prestressed deck in the region of the intermediate pier support, it can be expected that the bridge will have a higher ultimate load carrying capacity because the deck will remain crackless under service loads.

6.10 PARAMETRIC STUDY ON THE SKEW ORTHOTROPIC PLATE

The finite element computer program STRUDL-DYNAL was used to examine the effect of skew angle and aspect ratio on the natural frequencies of a skew orthotropic plate. Figure 6.74 shows the influence of different skew angles with aspect ratio of one on the first four natural frequencies. It can be seen that for small skew angles, increase in the skew angle does not significantly change the first four natural frequencies. However, significant changes in the natural frequency occurs at large skew angles. It was recognized earlier that at larger skew angles such as 60° the number of finite elements should be at least twice the number used for small skew angle in order to accurately calculate the natural frequencies, as shown in Table 6.16.

FIGURE 6.72 ULTIMATE LOAD TEST OF BRIDGE MODEL II

FIGURE 6.73 CLOSE-UP OF NEGATIVE 'PLASTIC' HINGE AT THE INTERMEDIATE SUPPORT OF BRIDGE MODEL II

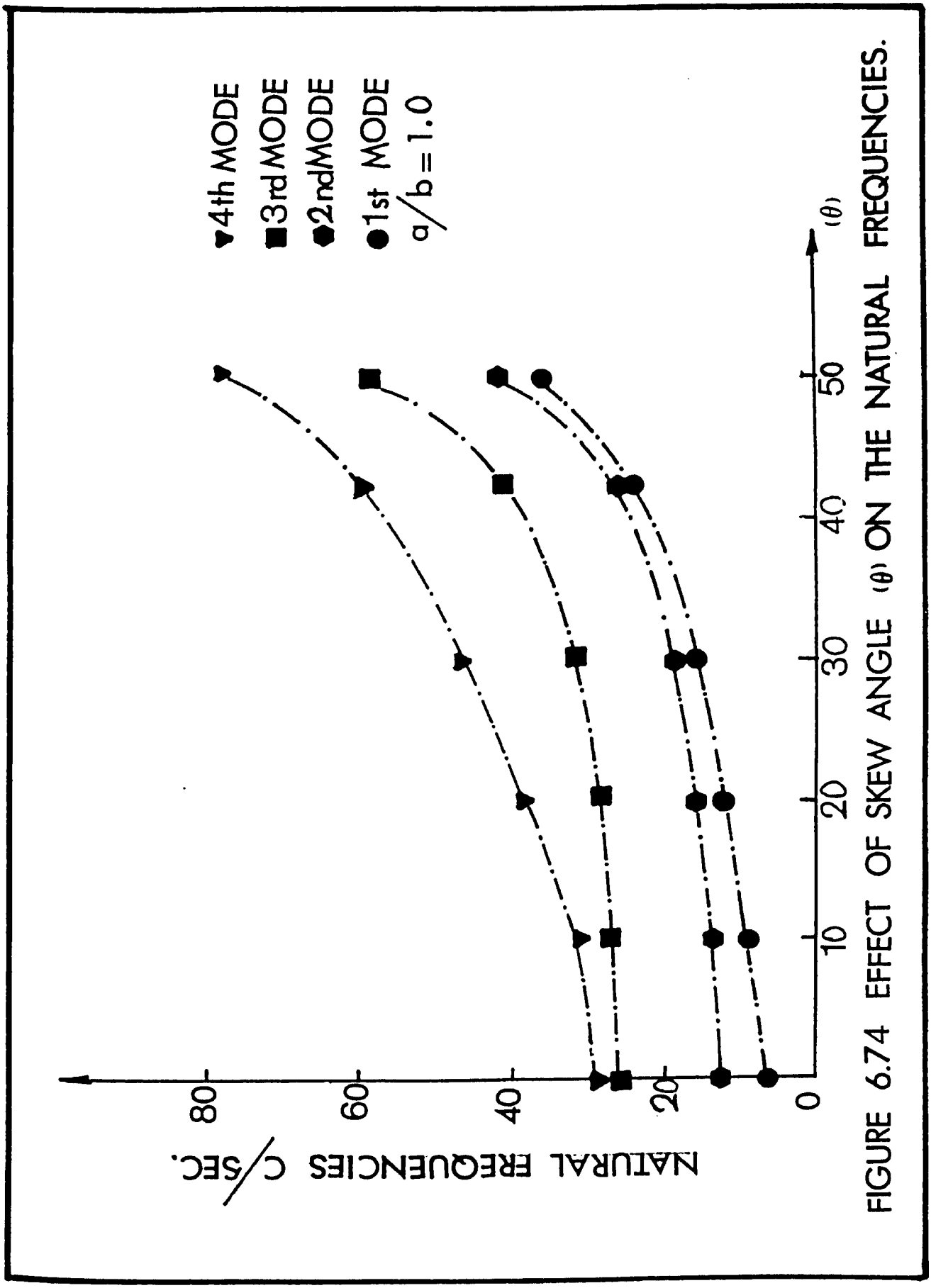

FIGURE 6.74 EFFECT OF SKEW ANGLE (θ) ON THE NATURAL FREQUENCIES.

TABLE 6.16

EFFECT OF SKEW ANGLE ON THE NATURAL FREQUENCIES
OF SKEW ORTHOTROPIC PLATES

(Aspect Ratio = 1.0)

MODE SHAPE NUMBER	NATURAL FREQUENCIES C/SEC.						= SKEW ANGLE
	θ = ZERO	θ = 10°	θ = 20°	θ = 30°	θ = 45°	θ = 60°	
1	7.4	8.8	12.3	16.5	24.8	41.6 (*) 37.6 (**)	
2	12.8	13.5	15.9	19.4	26.1	42.4 38.4	
3	26.9	27.1	28.6	32.0	41.7	69.8 59.9	
4	29.7	32.0	38.6	47.4	60.4	85.3 79.2	

(*) Based on the same number of finite elements used for 0°, 10°, 20°, 30° and 45° skew angle.
(**) Twice the number of the elements.

Figure 6.75 examines the effect of three aspect ratios of 0.5, 1.0 and 2.0 on the first four natural frequencies of a 45° skew orthotropic plate. The results reveal that increasing the aspect ratio has no significant effect on the first natural frequency. However, the reverse is true for the higher mode natural frequencies.

To demonstrate the advantage of using a skew waffle slab rather than a skew solid slab, a comparison study is shown in Table 6.17 between a 45° skew waffle slab and a solid slab having the same amount of weight and the same planform dimensions. The enhancement in the natural frequency by using the skew waffle slab is about 65% compared to that of the skew solid slab. This fact was expected since using a waffle slab, the longitudinal and the transverse rigidities are dramatically increased, which reflects on the dynamic characteristics of the structure. In order to achieve the same goal by using a solid slab, its thickness has to be substantially increased, yielding a non-economic structure.

6.11 PUSH-OUT TEST RESULTS

The design of shear connectors should be based not only on theoretical calculations, but also on results of push-out tests. Therefore, the push-out test under static load aimed to find curves relating the shear load on the specimen to the slip between beam and slab, and to find the maximum load which the stud connector can sustain. The result reveals that the fatigue failure of the connector was quite different from that under static load. Figure 6.76 shows the failure of the stud connector under static load as a result of the yielding of the connector. Strain gage readings on the stud and on the flange close to the stud location, shown in Figure

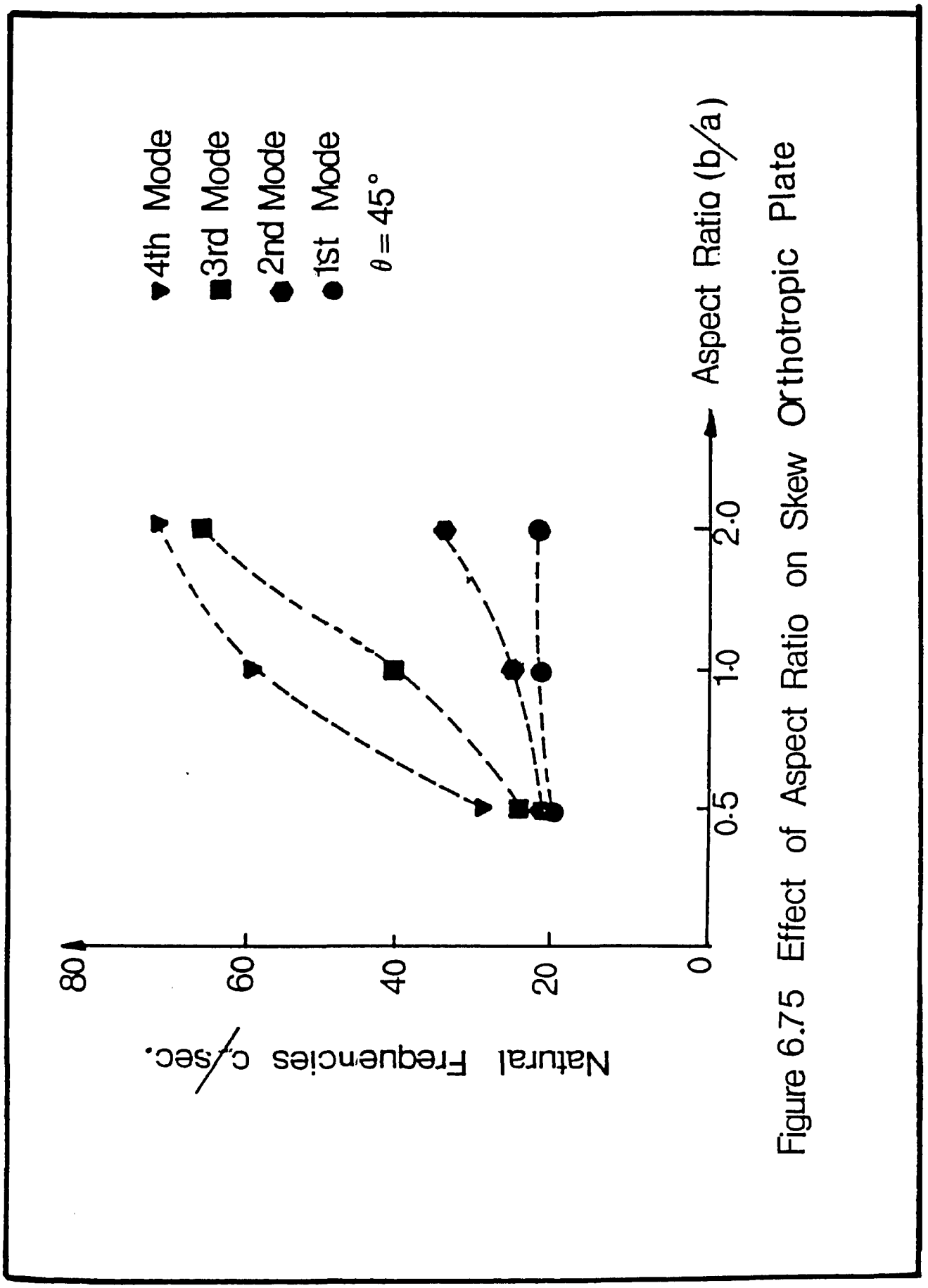

Figure 6.75 Effect of Aspect Ratio on Skew Orthotropic Plate

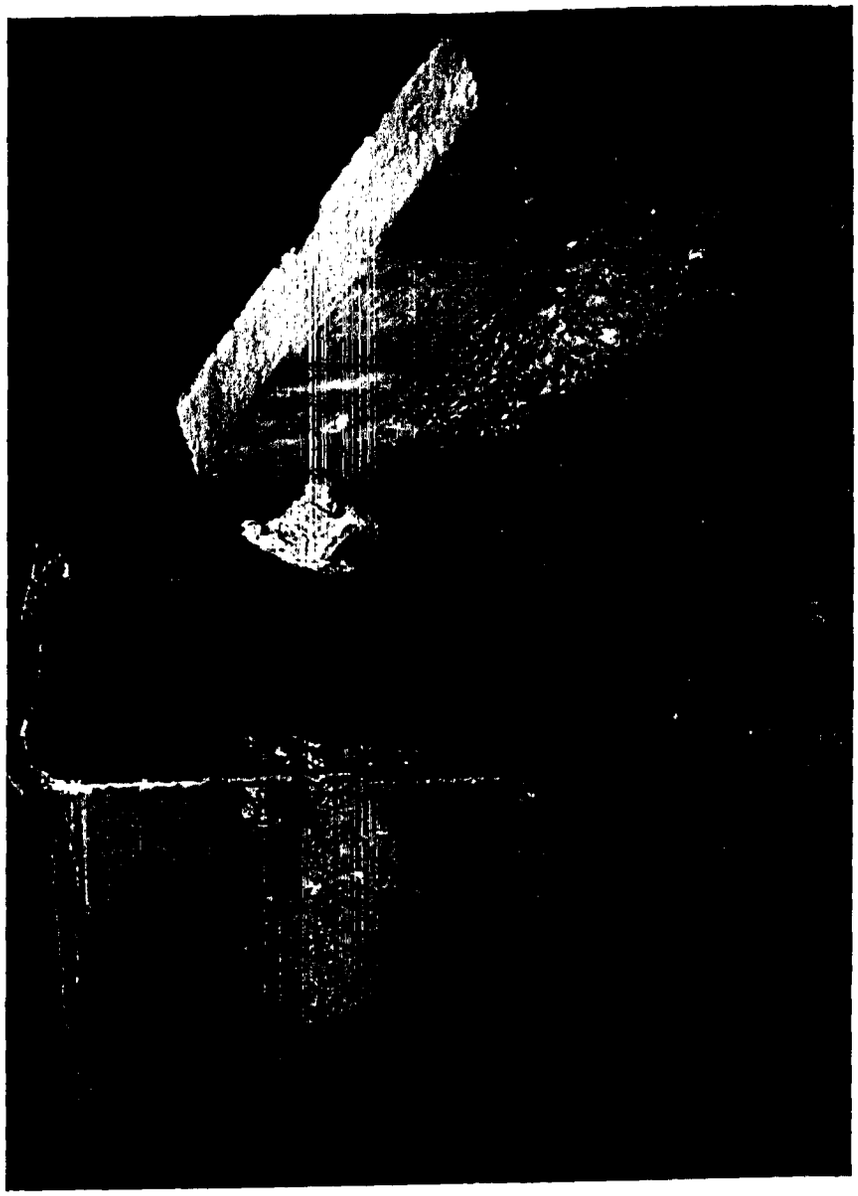

FIGURE 6.76 YIELDING OF STUD SHEAR CONNECTOR UNDER STATIC LOAD

TABLE 6.17

NATURAL FREQUENCIES OF THE SKEW SOLID AND SKEW WAFFLE SLABS HAVING SAME WEIGHT AND SAME PLATEFORM SIZE

MODE NUMBER	NATURAL FREQUENCY C/SEC.		ENHANCEMENT IN THE NATURAL FREQUENCY %
	SOLID SLAB*	WAFFLE SLAB*	
1	15.00	24.70	64%
2	15.8	26.1	65%
3	25.36	41.7	65%
4	36.6	60.4	65%

* Skew angle = 45° and aspect ratio = 1

6.77, confirmed that failure of the specimen occurred due to yielding of the connectors.

A typical load slip curve shown in Figure 6.78 indicated that the initial part of the curve represents the bond between the flange and the slab. The amount of slip significantly increased after the bond was completely destroyed. For example, at a load of 10 kips the slip was 0.001 inch, while at a load of 20 kips the slip became 0.030 inch. The slip increased dramatically once the stud started yielding.

Furthermore, fatigue failure was most likely caused in the weld between the beam and the connector as a result of stress concentration in the weld. Typical fatigue failure of two stud shear connectors is shown in Figure 6.79. It was observed that because of the effect of the pulsating load on the shear connector, the failure occurred at a load less than that obtained during the static push-out test. Therefore, in the design of the two bridge models, special considerations were given to the fatigue requirements of the shear connectors.

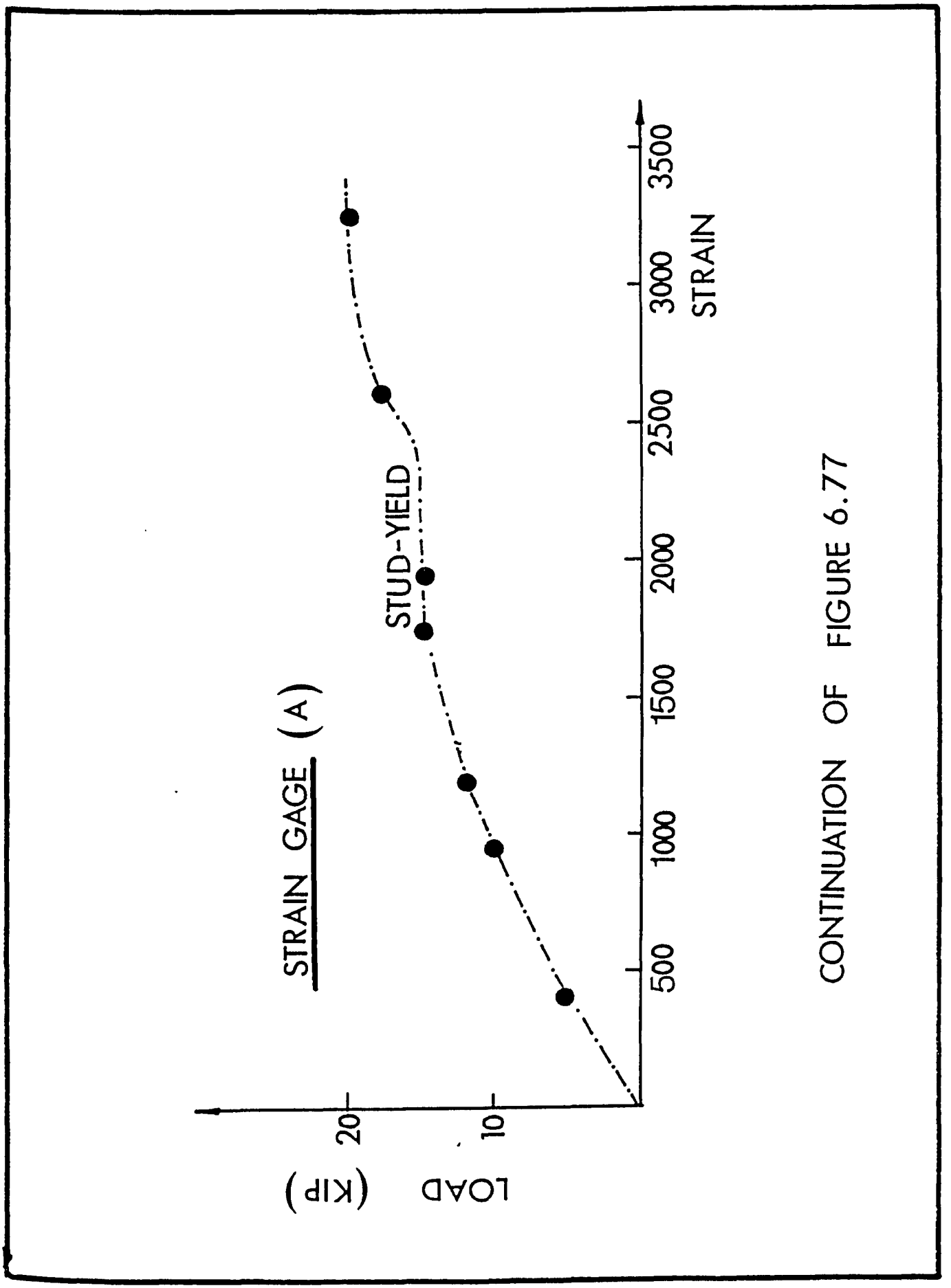

CONTINUATION OF FIGURE 6.77

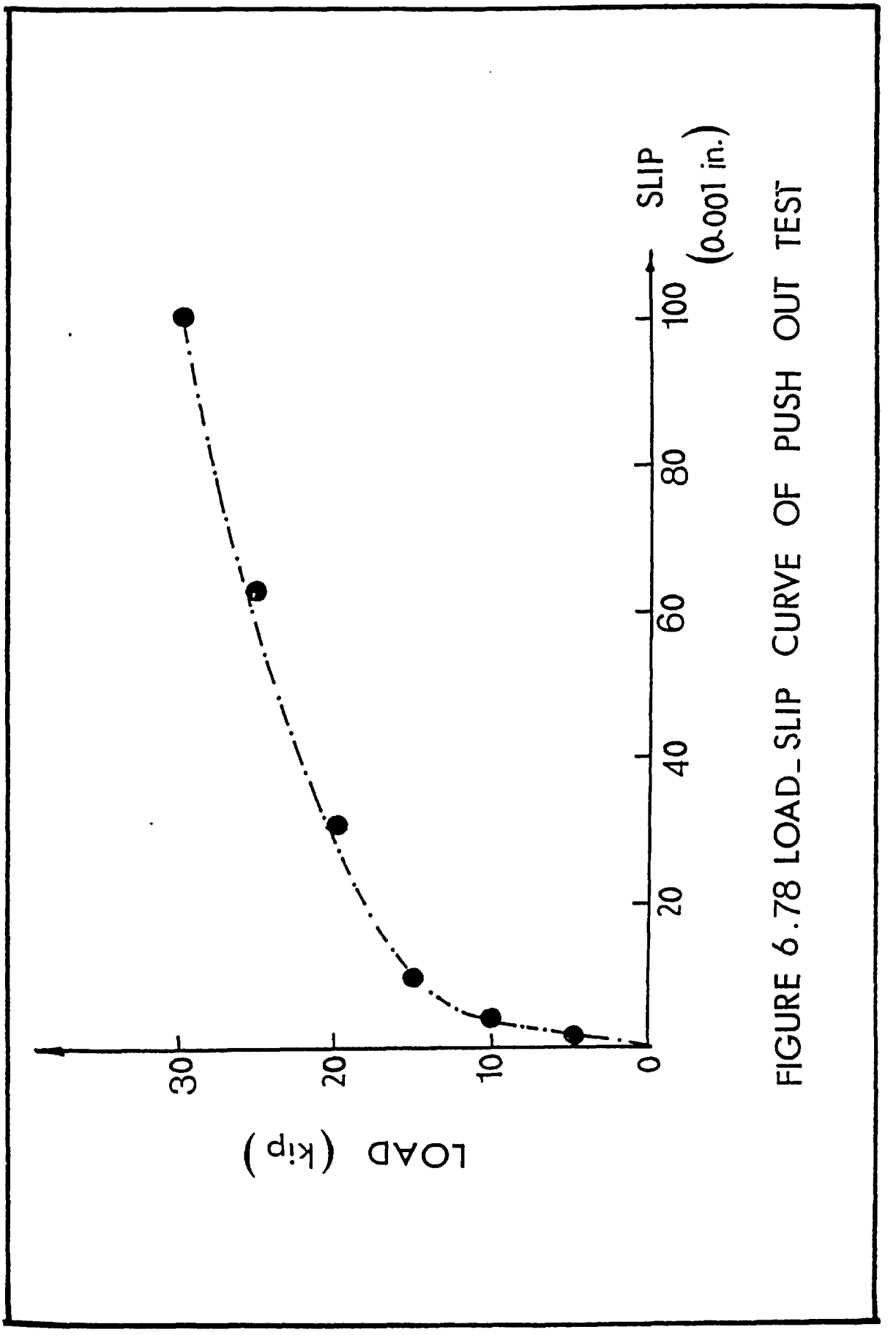

FIGURE 6.78 LOAD_SLIP CURVE OF PUSH OUT TEST

FIGURE 6.79 FATIGUE FAILURE OF STUD SHEAR CONNECTORS UNDER PULSATING LOAD

CHAPTER VII

SUMMARY AND CONCLUSIONS

7.1 SUMMARY

In this investigation, the dynamic response of continuous composite bridges was investigated using the orthotropic plate theory. The analogy in the dynamic response between a continuous prestressed composite bridge and a single-span orthotropic plate with different boundary conditions was explored. The influences of the aspect ratio and rigidity ratio on the natural frequencies were examined and compared to those obtained from beam theory. The theoretical approach was supported by experimental results obtained from tests on two two-span continuous composite bridge models. Fatigue tests were conducted to examine the behavior of the longitudinal steel beams, shear connectors and the prestressed wires at the intermediate support.

A series solution for the free vibration problem of skew waffle slabs using the orthotropic plate theory was presented. A computer program was written to formulate the transcendental frequency equations for symmetric and anti-symmetric mode shapes, from which the associated natural frequencies were found. The theoretical results were verified by finite element computer solution programs such as SAP IV and STRUDL-DYNAL; the theoretical results were also substantiated by experimental results available elsewhere. Parametric studies were carried out to examine the effect of different aspect ratios and skew angles on the natural frequencies of skew orthotropic plates.

The analysis of either the continuous composite bridge or the skew waffle slab leads to the all-important lower natural frequencies which are then compared to the applied transient loads frequency in order to avoid the state of resonance. This derived frequency will be valuable in establishing the dynamic load allowance for use in design practice.

7.2 CONCLUSIONS

The following conclusions are drawn based on the results obtained from the theoretical and experimental studies:

1) Enhancement in the continuous composite bridge natural frequencies can be realized by eliminating the transverse cracks in the negative moment region by means of prestressing the slab in that region of the bridge;

2) One hundred percent composite interaction between the concrete and the steel girders can be achieved in the negative moment region of continuous composite bridges under dynamic and fatigue loading by placing stud shear connectors in the negative moment region and applying prestressing to the deck slab around the negative moment region;

3) Prestressing can be used to effectively decrease the fatigue stress range and consequently the bridge fatigue life as well as the ultimate load carrying capacity will increase;

4) The natural frequencies of a two-span continuous composite bridge are identical to those of a single-span bridge with proper boundary conditions, provided that there is no transverse crack in the negative moment area;

5) Cracking of the concrete deck as well as fatigue cracks in continuous composite bridges can substantially reduce the natural frequencies and thus increase the damping of the structure;

6) Fatigue loading of continuous composite bridges close to their resonance frequencies can cause very rapid increase in the stress range, thus leading to sudden failure of the structure;

7) A fatigue-cracked continuous composite bridge can regain most of its stiffness and ultimate load-carrying capacity when properly repaired. Fatigue-induced hair cracks in the secondary members of the structure have no significant effect on the dynamic response nor on the ultimate load-carrying capacity of the bridge;

8) The good agreement between the series solution of a skew orthotropoic plate and experimental results supports the mathematical derivation and verifies the assumptions made;

9) Skew waffle slabs possess higher natural frequencies than solid skew slabs.

7.3 SUGGESTIONS FOR FUTURE RESEARCH

For future research, the following suggestions are recommended:

1. The series solution of the free vibration problem of skew orthotropic plates needs to be extended to a continuous-span structure, with different boundary conditions;

2. Experimental research needs to be carried out on skew waffle slabs to examine the effect of prestressing and the influence of different rib orientation on the vibration levels of the structure.

APPENDIX A

GOVERNING DIFFERENTIAL EQUATION FOR THE FREE VIBRATION OF A SKEW ORTHOTROPIC PLATE

Refering to Figure 3.6, the transformation of the governing differential equation from the rectangular coordinates into the skew coordinates was done using the following relations:

(1) Relation between (x,y), (u,v) and the skew angle θ

$$u_{,x} = \frac{1}{c}$$

$$u_{,y} = 0$$

$$v_{,x} = -s/c$$

$$v_{,y} = 1$$

(2) Differentiation of the mode shape function of (u,v,t) with respect to x.

$$w_{,x} = w_{,u}\ u_{,x} + w_{,v}\ v_{,x}$$

$$= w_{,u}\ 1/c - w_{,v}\ s/c$$

$$= 1/c\ [w_{,u} - s\ w_{,v}]$$

$$w_{,xy} = 1/c\ [w_{,uu}\ u_{,y} + w_{,uv}\ v_{,y} - sw_{,vu}\ u_{,y} - sw_{,vv}\ v_{,y}]$$

$$= 1/c\ [w_{,uv} - sw_{,vv}]$$

$$w_{,xyy} = 1/c\ [w_{,uuv}\ v_{,y} + w_{,uvv}\ v_{,y} - sw_{,uvv}\ u_{,y} - sw_{,vvv}\ v_{,y}]$$

$$= 1/c\ [w_{,uvv} - sw_{,vvv}]$$

$$w_{,xx} = 1/c\ w_{,u}\ u_{,xx} + u_{,x}\ [w_{,uu}\ u_{,x} + w_{,uv}\ v_{,x}]$$

$$+ 1/c\ w_{,v}\ v_{,xx} + v_{,x}\ [w_{,vu}\ u_{,x} + w_{,vv}\ v_{,x}]$$

$$= 1/c\ [w_{,uu}\quad 1/c - s/c\ w_{,uv}]$$

$$- s/c\ [w_{,vu}\quad 1/c - s/c\ w_{,vv}]$$

$$= 1/c^2\ [w_{,uu} - 2sw_{,uv} + s^2 w_{,vv}]$$

$$w_{,xxx} = 1/c^2\ [w_{,uuu}\quad u_{,x} + w_{,uuv}\quad v_{,x}]$$

$$- \frac{2s}{c^2}\ [w_{,uuv}\quad u_{,x} + w_{,uvv}\quad v_{,x}]$$

$$+ \frac{s^2}{c^2}\ [w_{,vvu}\quad u_{,x} + w_{,vvv}\quad v_{,x}]$$

$$= \frac{1}{c^2}\ [\frac{1}{c}\ w_{,uuu} - \frac{s}{c}\ w_{,uuv}]$$

$$- \frac{2s}{c^2}\ [\frac{1}{c}\ w_{,uuv} - \frac{s}{c}\ w_{,uvv}]$$

$$+ \frac{s^2}{c^2}\ [\frac{1}{c}\ w_{,uvv} - \frac{s}{c}\ w_{,vvv}]$$

$$= \frac{1}{c^3}\ [w_{,uuu} - 3sw_{,uuv} + 3s^2 w_{,uvv} - s^3 w_{,vvv}]$$

$$w_{,xxxx} = \frac{1}{c^3}\ [w_{,uuuu}\quad u_{,x} + w_{,uuuv}\quad v_{,x}$$

$$- 3sw_{,uuuv}\quad u_{,x} - 3sw_{,uuvv}\quad v_{,x}$$

$$+ 3s^2 w_{,uuvv}\quad u_{,x} + 3s^2 w_{,uvvv}\quad v_{,x}$$

$$- s^3 w_{,uvvv}\quad u_{,x} - s^3 w_{,vvvv}\quad v_{,x}]$$

$$= \frac{1}{c^3}\ [\frac{1}{c}\ w_{,uuuu} - \frac{s}{c}\ w_{,uuuv}$$

$$- \frac{3s}{c}\ w_{,uuuv} + \frac{3s^2}{c}\ w_{,uuvv}$$

$$+ \frac{3s^2}{c} w_{,uuvv} - \frac{3s^3}{c} w_{,uvvv}$$

$$- \frac{s^3}{c} w_{,uvvv} + \frac{s^4}{c} w_{,vvvv}]$$

$$= \frac{1}{c^4} [w_{,uuuu} - 4sw_{,uuuv} + 6s^2 w_{,uuvv} - 4s^3 w_{,uvvv} + s^4 w_{,vvvv}]$$

(3) Differentiation of the mode shape function of (u,v,t) with respect to y.

$$w_{,y} = w_{,u} \quad u_{,y} + w_{,v} \quad v_{,y}$$

$$= w_{,v}$$

$$w_{,yyyy} = w_{,vvvv}$$

(4) Differentiation of the mode shape function of (u,v,t) with respect to x and y.

$$w_{,xxy} = \frac{1}{c^2} [w_{,uuu} \quad u_{,y} + w_{,uuv} \quad v_{,y}$$

$$- 2sw_{,uuv} \quad u_{,y} - 2sw_{,uvv} \quad v_{,y}$$

$$+ s^2 w_{,uvv} \quad u_{,y} + s^2 w_{,vvv} \quad v_{,y}]$$

$$w_{,xxyy} = \frac{1}{c^2} [w_{,uuv} - 2sw_{,uvv} + s^2 w_{,vvv}]$$

$$= \frac{1}{c^2} [w_{,uuuv} \quad u_{,y} + w_{,uuvv} \quad v_{,y}$$

$$- 2sw_{,uuuv} \quad u_{,y} - 2sw_{,uvvv} \quad v_{,y}$$

$$+ s^2 w_{,uvvv} \quad u_{,y} + s^2 w_{,vvv} \quad v_{,y}]$$

$$= \frac{1}{c^2} [w_{,uuvv} - 2s w_{,uvvv} + s^2 w_{,vvvv}]$$

Finally, Equation 3.2.6 becomes

$$D_x \quad \frac{1}{c^4} [w_{,uuuu} - 4s w_{,uuuv} + 6s^2 w_{,uuvv} - 4s^3 w_{,uvvv} + s^4 w_{,vvvv}]$$

$$+ 2H \frac{1}{c^2} [w_{,uuvv} - 2s w_{,uvvv} + s^2 w_{,vvvv}]$$

$$+ D_y \quad w_{,vvvv} = -\bar{m} h_1 w_{,tt}$$

$$D_x w_{,uuuu} - 4s D_x w_{,uuuv} + [6s D_x^2 + 2Hc^2] w_{,uuvv}$$

$$- 4[s^3 D_x + Hsc^2] w_{,uvvv} + [D_x s^4 + 2Hs^2 c^2 + D_y c^4] w_{,vvvv}$$

$$= \bar{m} h_1 c^4 w_{,tt}$$

The above equation represents the free vibration governing differential equation of a skew orthotropic plate, given by Equation 3.3.2.

APPENDIX B

EVALUATION OF THE DEFINITE INTEGRALS FOR FOURIER SERIES

The derivation of each of the following definite integrals is very lengthy. However, only the final result is given below. It should be noted that the value of each definite integral is a function of the frequency as well as the elastic properties of the plate.

$$a_{oo} = \frac{1}{2a} \int_{-a}^{a} H_o(u)\, du$$

$$a_{om} = \frac{1}{a} \int_{-a}^{a} H_o(u) \cos \alpha_m u\, du$$

$$b_{om} = \frac{1}{a} \int_{-a}^{a} H_n(u) \sin \alpha_m u\, du$$

$$a_{no} = \frac{1}{2a} \int_{-a}^{a} H_n(u)\, du$$

$$a_{nm} = \frac{1}{a} \int_{-a}^{a} H_n(u) \cos \alpha_m u\, du$$

$$b_{nm} = \frac{1}{a} \int_{-a}^{a} H_n(u) \sin \alpha_m u\, du$$

a_{oo}, a_{om}, b_{om}, a_{no}, a_{nm} and b_{nm} are function of the following definite integrals:

$$I_{j1} = \frac{1}{a} \int_{-a}^{a} \sinh u_{1n} \cos u_{2n} \sin \alpha_m u\, du = -T_{a1} (S_{a1} A_{8n} + S_{a2} A_{7n})$$

$$I_{j2} = \frac{1}{a} \int_{-a}^{a} \cosh u_{1n} \sin u_{2n} \sin \alpha_m u\, du = T_{a1} (S_{a1} A_{7n} - S_{a2} A_{8n})$$

$$I_{j3} = \frac{1}{a} \int_{-a}^{a} \sinh u_{1n} \cos u_{3n} \sin \alpha_m u\, du = -T_{b1} (S_{b1} B_{8n} + S_{b2} B_{7n})$$

$$I_{j4} = \frac{1}{a} \int_{-a}^{a} \cosh u_{1n} \sin u_{3n} \sin \alpha_m u\, du = T_{b1} (S_{b1} B_{7n} - S_{b2} B_{8n})$$

$$I_{j5} = \frac{1}{b}\int_{-b}^{b} \sinh w_{1n} \cos w_{2n} \sin \beta_m v \; dv = -S_{x1}\,(u_{x1}A_{4n} + u_{x2}A_{3n})$$

$$I_{j6} = \frac{1}{b}\int_{-b}^{b} \cosh w_{1n} \sin w_{2n} \sin \beta_m v \; dv = S_{x1}\,(u_{x1}A_{3n} - u_{x2}A_{4n})$$

$$I_{j7} = \frac{1}{b}\int_{-b}^{b} \sinh \bar{w}_{1n} \cos w_{3n} \sin \beta_m v \; dv = -S_{y1}\,(u_{y1}B_{4n} + u_{y2}B_{3n})$$

$$I_{j8} = \frac{1}{b}\int_{-b}^{b} \cosh \bar{w}_{1n} \cos w_{3n} \sin \beta_m v \; dv = S_{y1}\,(u_{y1}B_{3n} - u_{y2}B_{4n})$$

$$I_{k1} = \frac{1}{a}\int_{-a}^{a} \cosh u_{1n} \cos u_{2n} \cos \alpha_m u \; du = T_{a2}\,(S_{a3}A_{7n} + S_{a4}A_{8n})$$

$$I_{k2} = \frac{1}{a}\int_{-a}^{a} \sinh u_{1n} \sin u_{2n} \cos \alpha_m u \; du = T_{a2}\,(S_{a3}A_{8n} - S_{a4}A_{7n})$$

$$I_{k3} = \frac{1}{a}\int_{-a}^{a} \cosh u_{1n} \cos u_{3n} \cos \alpha_m u \; du = T_{b1}\,(S_{b3}B_{7n} + S_{b4}B_{8n})$$

$$I_{k4} = \frac{1}{a}\int_{-a}^{a} \sinh u_{1n} \sin u_{3n} \cos \alpha_m u \; du = T_{b2}\,(S_{b3}B_{8n} - S_{b4}B_{7n})$$

$$I_{k5} = \frac{1}{b}\int_{-b}^{b} \cosh w_{1n} \cos w_{2n} \cos \beta_m v \; dv = S_{x2}\,(u_{x3}A_{3n} + u_{x4}A_{4n})$$

$$I_{k6} = \frac{1}{b}\int_{-b}^{b} \sinh w_{1n} \sin w_{2n} \cos \beta_m v \; dv = S_{x2}\,(u_{x3}A_{4n} - u_{x4}A_{3n})$$

$$I_{k7} = \frac{1}{b}\int_{-b}^{b} \cosh \bar{w}_{1n} \cos w_{3n} \cos \beta_m v \; dv = S_{y2}\,(u_{y3}B_{3n} + u_{y4}B_{4n})$$

$$I_{k8} = \frac{1}{b}\int_{-b}^{b} \sinh \bar{w}_{1n} \sin w_{3n} \cos \beta_m v \; dv = S_{y2}\,(u_{y3}B_{4n} - u_{y4}B_{3n})$$

$$J_{1m} = \frac{1}{a}\int_{-a}^{a} \frac{u^2}{a^2} \cos\alpha_n u \, du = \frac{1}{b}\int_{-b}^{b} \frac{v^2}{b^2} \cos \beta_n v \, dv = (-1)^n \frac{4}{n^2\pi^2}$$

$$J_{3m} = \frac{1}{a}\int_{-a}^{a} \frac{u^4}{a^4} \cos \alpha_n u \, du = \frac{1}{b}\int_{-b}^{b} \frac{v^4}{b^4} \cos \beta_n v \, dv = 2J_{1m}\left(1 - \frac{6}{n^2\pi^2}\right)$$

$$J_{5m} = \frac{1}{a}\int_{-a}^{a} \frac{u}{a} \sin \alpha_n u \, du = \frac{1}{b}\int_{-b}^{b} \frac{v}{b} \sin \beta_n v \, dv = -\frac{n\pi}{2} J_{1m}$$

$$J_{7m} = \frac{1}{a}\int_{-a}^{a} \frac{u^3}{a^3} \sin \alpha_n \, u \, du = \frac{1}{b}\int_{-b}^{b} \frac{v^3}{b^3} \sin \beta_n v \, dv = -\frac{n\pi}{4} J_{3m}$$

$$K_{1n} = \frac{1}{2a}\int_{-a}^{a} \cosh u_{1n} \cos u_{2n} \, du = \frac{z_1}{a\beta_n}(K_1A_{7n} + K_2A_{8n})$$

$$K_{2n} = \frac{1}{2a}\int_{-a}^{a} \sinh u_{1n} \sin u_{2n} du = \frac{z_1}{a\beta_n}(K_1A_{8n} - K_2A_{7n})$$

$$K_{3n} = \frac{1}{2a}\int_{-a}^{a} \cosh u_{1n} \cos u_{3n} du = \frac{y_1}{a\beta_n}(K_1B_{7n} + K_3B_{8n})$$

$$K_{4n} = \frac{1}{2a}\int_{-a}^{a} \sinh u_{1n} \sin u_{3n} du = \frac{y_1}{a\beta_n}(K_1B_{8n} + K_3B_{7n})$$

$$K_{5n} = \frac{1}{2b}\int_{-b}^{b} \cosh v_{1n} \cos v_{2n} dv = \frac{1}{b\alpha_n}(K_1A_{3n} + K_2A_{4n})$$

$$K_{6n} = \frac{1}{2b}\int_{-b}^{b} \sinh v_{1n} \sin v_{2n} dv = \frac{1}{b\alpha_n}(K_1A_{4n} - K_2A_{3n})$$

$$K_{7n} = \frac{1}{2b}\int_{-b}^{b} \cosh \bar{w}_{1n} \cos v_{3n} dv = \frac{1}{b\alpha_n}(K_1B_{3n} + K_3B_{4n})$$

$$K_{8n} = \frac{1}{2b}\int_{-b}^{b} \sinh \bar{w}_{1n} \sin v_{3n} dv = \frac{1}{b\alpha_n}(K_1 B_{4n} - K_3 B_{3n})$$

APPENDIX C

FAST FOURIER TRANSFORM COMPUTER PROGRAM TO TRANSFER THE MEASURED DATA FROM TIME DOMAIN TO FREQUENCY DOMAIN

```
//X005W JOB (R040,CJK,10,20),GRACE,CLASS=A,REGION=700K
//   EXEC  ZETAPLOT
//FORT.SYSIN  DD  *
      DIMENSION X(28000),Y(28000),XN(28000),Z(28000),F(28000)
      CALL PLTIDZ('NINA GRACE       ','R040,CJK  ')
      READ 2,(X(J),J=1,7832)
   2  FORMAT(11F7.0)
      N=0
      K=0
      DO 3 J=1,7832
      IF (ABS (X(J)).GT. 2.0)GO TO 51
       GO TO 3
  51  IF(ABS(X(J)).LT. 2000.)GO TO 4
      GO TO 3
   4   K=K+1
      N=N+1
      XN(N)=X(J)
   3  CONTINUE
      DO 1 I=1,K
      Y(I)=0.0
   1  CONTINUE
      FN=N/1.0
      FM=ALOG(FN)/ALOG(2.0)
      M=FM
       N=2**M
       NPTS=N
      DELTAT=1./350.
      ISIGN=-1
      CALL FFT (XN,Y,N,M,ISIGN,DELTAT,Z,F)
      CALL ZPLOT2(F,Z,NPTS,-1.0,160.0,10.0,0.0,1.0,-1000.0,500.,0
     1,-1,0)
       CALL PLTEND(40.0)
       STOP
       END
         SUBROUTINE FFT (XN,Y,N,M,ISIGN,DELTAT,Z,F)
      REAL XN(28000),Y(28000),Z(28000),F(5000)
C        X REAL PART &Y IMAG. PART
C        TOTAL NO. OF INPUT DATA
         NV2=N/2
         NM1=N-1
         J=1
         DO 7 I=1,NM1
         IF(I.GE.J)GO TO 5
         T=XN(J)
         XN(J)=XN(I)
         XN(I)=T
         T=Y(J)
         Y(J)=Y(I)
         Y(I)=T
   5     K=NV2
   6     IF(K.GE.J)GO TO 7
         J=J-K
         K=K/2
          GO TO 6
   7     J=J+K
         PI2=ISIGN*ATAN(1.)*8.
         DO 20 L =1,M
         LE =2**L
         LE1=LE/2
         SCL=PI2/LE
         DO 20 J=1,LE1
         ARG=(J-1)*SCL
         C=COS(ARG)
         S=SIN(ARG)
         DO 20 I=J,N,LE
         IP=I+LE1
         T1=XN(IP)*C+Y(IP)*S
         T2=Y(IP)*C-XN(IP)*S
         XN(IP)=XN(I)-T1
         Y(IP)=Y(I)-T2
         XN(I)=XN(I)+T1
  20     Y(I)=Y(I)+T2
         DO 25 I=1,N
         Z(I)=(SQRT(XN(I)**2+Y(I)**2))*DELTAT
         F(I)=I/(N*DELTAT)
  25       CONTINUE
         RETURN
         END
/*
//GO.SYSIN  DD  *
```

APPENDIX D

MEGADAC 2000 DATA ACQUISITION

MEGADAC 2000 DATA ACQUISITION

This Appendix describes the procedure that was used to record and to store on tape the data from different sensors such as accelerometers, LVDTs, DCDTs and dynamic strain gages. Furthermore, after the data is stored, it needs to be transmitted to a wylbur file on the University of Windsor IBM 4031 through an IBM personal computer.

D.1 Recording and Storing of Data

The Megadac manual explains this procedure in general terms. However, the following procedures were used throughout this research:

D.1.1 Mode Table

This table enabled the author to establish a certain profile for communication with the data acquisition by assigning the following values for different mode entry:

MODE ENTRY	VALUE	DESCRIPTION
0	1	CR only transmitted
1	1	No line feed E chord
2	0	Full duplex mode
3	0	Status reporting enabled
4	0	XON/XOFF Protocol in effect
5	0	One-up number sent
6	0	No delay after CR
7	11	Number of entries transmitted
8	0	Wait for I/O to complete
9	1	High resolution
10	1	Signed data
11	0	19.2K baud rate
12	0	Even parity
13	1	Monitor channel 1
14	2	Monitor channel 2

15	3	Monitor channel 3
16	0	Transmitted by computer
17	0	Normal error recovery
18	0	Do not rewind
19	0	One tape drive
20	0	No auto restart
21	0	No IEEE
22	0	No IEEE parallel port
23	0	Cassette format

D.1.2 Base Entries

The following 18 base entries in Scan Table were initialized by the author which contained the directions to be followed by the Megadac for processing the input-output channels throughout the dynamic tests:

MODE ENTRY	VALUE	DESCRIPTION
0	64	Number of Scan entries
1	500	Samples/seconds
2	0	Samples/second
3	0	Internal clock
4	1	Tape mark inserted
5	1	Auto-balance enabled
6	0	No table expansion
7	1	Brust scan mode
8	0	Start storing immediately (*)
9	0	Stop storing immediately (*)
10	0	Do not repeat the recording cycle
11	1	Monitor Scan Entry #1
12	2	Monitor Scan Entry #2
13	3	Monitor Scan Entry #3
14	0	To be used for fatigue test (*)
15	0	To be used for fatigue test (*)
16	0	To be used for fatigue test (*)
17	0	To be used for fatigue test (*)
18	10	To be used for fatigue test (*)

(*) will be changed for fatigue tests.

D.1.3 Scan Entries

This table of Scan Entries gave a mapping information of each channel for extraction of data samples; each scan entry contained a high and low

limit which were used for starting and stopping the recording process during the fatigue tests only. Also, it contained an appropriate gain value and an auto-balance value that was applied to each channel. The gain value was different according to the type of sensors and basically, it depended on the output voltage from the sensors. For example, the following Scan Entry was assigned to the peizoelectric accelerometer during the dynamic test:

001 00000 00000 00008 00000

and during the fatigue test is was

001 000200 002000 00008 0000

D.2 TRANSMITTING DATA FROM MEGADAC TO IBM PC

After all the data were successfully stored on the Megadac tape, it required transmission to an IBM-PC disk file. The RS-232C cable was connected from the Megadac's RS-232 port to the IBM port labelled COM2, and the RS-232 cable was connected from a modem, attached to Wylbur, to the IBM port labelled COM1.

The Asynch Comm System Disk contained programs such as KOUNT and AUTO2 which were developed by Mr. G. Monforton, a student in the Electrical Engineering Department. The 'KOUNT' programs was used first to transmit the data from the tape to IBM-PC fisk file. A list of this program is given below.

```
10 OPEN "COM2:19200,E,7,2,RS,CS,DS,CD" AS #1
20 PRINT #1, "CO2"
30 LINE INPUT #1,A$
```

```
40 LINE INPUT #1,A$
50 INPUT "DISK FILENAME (FILENAME.EXT)";FI$
60 OPEN FI$ FOR OUTPUT AS #2
70 INPUT "Enter transmit command (X[nnn[C]]):",X$
75 INPUT "Number of iterations";NIT
80 PRINT #1,X$
90 LINE INPUT #1,A$
100 PRINT A$,LOF(1)
110 IF LEFT$(A$,1)<>"#" THEN PRINT #2,A$
120 WHILE NOT EOF(!)
125 I=I+1
130 IF LOF(1)<5000 AND X=0 THEN PRINT #1,CHR$(19):X=1
150 IF X=1 AND LOF(1)<13000 THEN X=0:PRINT #1,CHR$(17)
160 LINE INPUT #1.A$
170 PRINT A$,LOF(1)
180 IF LEFT$(A$,1)<>"#" THEN PRINT #2,A$
190 WEND
195 IF I<4 THEN I=0:KOUNT=KOUNT+1:IF KOUNT<NIT GOTO 200 ELSE GOTO 8
200 END
```

D.3 Transmitting Data from IBM-PC to IBM 4031

After having the data on an IBM-PC disk file, it was transmitted to the main computer at the University of Windsor by using the computer program called Auto2.

This final transmission of the data was important to obtain a computer trace plot for all of the time histories of each accelerometer and to conduct the data reduction using the Fast Fourier Transform.

APPENDIX E

LIST OF COMPUTER PROGRAM

FOR THE FREE VIBRATION OF A SKEW ORTHOTROPIC PLATE

```
//SKEW1 JOB 1,'SKEW',CLASS=C
// EXEC WATFIV
//GO.SYSIN DD *
$JOB   WATFIV  ROLOFA3 GRACE
C
C
C
```

```
      DIMENSION CD(44,44),IR(44),IC(44),AP(15)
      N=1
      NSS=5
      NS=8+NSS+4
      JS=NS
      NST1=NSS
      NST2=JS
      PI=3.141592
      PI9=90./PI
      READ (5,3) Z
    3 FORMAT (1X,F3.1)
      WRITE (6,4) Z
    4 FORMAT (45X,'Z=',F3.1)
      READ (5,5) A,B,SA,DX,DY,D1,D2,DXY,DYX,EI,GJ,NNN
    6 FORMAT (///,41X,'THE BRIDGE IS FLEXURALLY STRONG AND TOSIONALLY
     1WEAK',//,61X,'INPUT DATA ',/////,57X,'PROPERTIES OF THE BRIDGE'
     2,//,51X,'HALF-WIDTH OF THE BRIDGE ',2X,F10.2,/,51X,'HALF SPAN
     3OF THE BRIDGE',3X,F10.2,/,51X,'SKEW ANGLE',10X,F10.2,/,51X,'DX'
     4,15X,E10.2,/,51X,'DY',15X,E10.2,/,51X,'D1',10X,E10.2,/,51X,'D2'
     5,15X,E10.2,/,51X,'DXY',17X,E10.2,/,51X,'DYX',17X,E10.2,/,51X,
     6'EI',15X,E10.2,/,51X,'GJ',E10.2)
    5 FORMAT (1X,F8.2,1X,F8.2,1X,F8.2,1X,E9.1,1X,E9.1,1X,E9.2,/,1X,E9.1
     1,1X,E9.1,1X,E9.1,1X,F4.2,1X,F4.2,1X,I4)
      WRITE (6,6) A,B,SA,DX,DY,D1,D2,DXY,DYX,EI,GJ
      H=(D1+D2+DXY+DYX)/2.0
      READ (5,7) ROW
    7 FORMAT (1X,E9.1)
      WRITE (6,8) ROW
    8 FORMAT (5X,'MASS PER UNIT AREA ,ROW =',E10.2)
      PK=H**2-DX*DY
      PRINT700 ,PK,H
700   FORMAT (15X,E35.20,5X,E18.5)
      IF (PK) 9,12,13
   13 WRITE (6,14)
   14 FORMAT (20X,'THE BRIDGE IS TORISONALLY STIFF AND FLEXURALLY
     1WEAK')
      GO TO 29
   12 WRITE (6,15)
   15 FORMAT (25X,'THE BRIDGE IS ISOTROPIC')
      GO TO 29
C
C
C
```

```
C
C
C     ***************************************************************
C     ***************************************************************
C                          COMPUTE THE MATRIX
C
C
C
C                                  ******************
C                                   ****************
C                                    **************
      CALL COFF1(CO,DETA,N,M,IR,IC)
  132   FORMAT (1X,E7.3)
   40 CONTINUE
      IA=NC
      MA=NC
      DO 803 J=1,NC
      DO 803 K=1,NC
  803   CO(J,K)=CO(J,K)/1.0E7
      CALL MINVRS (CO,IA,MA,DETA,IER,IR,IC)
      IF (DETA) 18,19,18
   19 WRITE (6,22) OMGA,DETA
   22 FORMAT (40X,'THE FIRST NATURAL FREQUENCY IS =',E9.1,/,40X,
     1'DET=',E7.1)
      GO TO 29
   18 CONTINUE
      WRITE (6,23) OMGA,DETA
   23 FORMAT (3X,'OMGA',E20.4,2X,'DET',E10.5)
   20 CONTINUE
   29 STOP
      END
C
C
C
C     ***************************************************************
C     ***************************************************************
      SUBROUTINE CONST (N,ROW)
      REAL K3,K4,K5
      COMMON A,PI,SA,C,S,TN,C4,AA,AA3,AA4,Z,C2,C3,ST,SF,T,PK,
     1RS,JSYMM,OMGA,DXOM,R7A,NNC
      COMMON /BLO/ B,DX,DY,DXY,DYX,D1,D2,EI,GJ,H
      COMMON /BL1/ P,K3,K4,K5,BB,BB3,BB4,X2,Y2,A1,A2,A3,A4,B1,
     1B2,B3,B4,SCA,SCB,SCC,SCD,S1(3),S2(3),S3(3)
      COMMON /BL2/ R1,R2,R3,R4,R5,R6,R7,R8,R9,R10,R11,R12,R1K3,
     1X22,X23,X24,Y22,Y23,Y24,A5,A6,A7,A8,A9,A10,A11,A12,A13,A14
     2,A15
     3,A16,A17,A18,A19,A20,A21,A22,A23,A24,AG,A5,A6,A7,A8,A9,A10,
     4A11,A12,A13,A14,A15,A16,A17,A18,A19,A20,A21,A22,A23,A24
      P=A/B
      THETA=SA*PI/180.0
      C=COS(THETA)
      S=SIN(THETA)
      C2=C*C
      C3=C2*C
      C4=C2*C2
      ST=S*S
      SF=ST*ST
      SCC=4.0*S*DX
      SCA=(3.0*ST*DX+C2*H)*2.0
      SCD=(ST*DX+C2*H)*4.0*S
      SCB=SF*DX+2.0*ST*C2*H+C4*DY
      AA=A*A
      AA3=AA*A
      AA4=AA*AA
      BB=B*B
      BB3=BB*B
      BB4=BB*BB
      CONTINUE
      RN=N
      RNP=RN*PI
      ST=RNP/B
      AN2=AA*BB
      B1=B/2.0
      BN4=AN2*BB
      R04 =2.0*10.**7
      OMGA=OMGA*OMGA
      DXOM=(2.0*PI*(16.)/ 1
      A1Y=(((DX*DY)-DXY)
      A1=(
```

```
      X2=1.0/(PKK3+PKK4)
      Y2=1.0/(PKK3+PKK5)
      X22=X2*X2
      X23=X22*X2
      X24=X23*X2
      Y22=Y2*Y2
      Y23=Y22*Y2
      Y24=Y23*Y2
      DD=D1+DXY+DYX
      TN=S/C
      DXT=DX*TN**2
      B1=S*(2.0*DXT+2.0*D2+DXY+DYX)
      B2=-(ST*(DXT+2.0*H1+C2*DY)
      B3=DX/C3
      B4=-3.0*S*B3
      B5=(3.0*DXT+DD)/C
      B6=-S*(DXT+DD)/C
      B7=DX/C
      B8=-2.0*S*B7
      B9=(ST+D1*C2/DX)*B7
      B10=-S*GJ
      B11=-TN
      B12=1.0/C
      R1K3=R1*K3
      R1K4=R1*K4
      R1K5=R1*K5
      A1=2.0*K3*K4
      A2=(PKK3-PKK4)
      A3=K3*(PKK3-3.0*PKK4)
      A4=K4*(3.0*PKK3-PKK4)
      A5=-E1*(A2*A2-A1*A1)*X24
      A6=2.0*E1*A1*A2*X24
      A7=-R1K4-R2
      A8=-X2*(R1*K4-R2*X2*A2)
      A9=-X2*(R1K3+R2*X2*A1)
      A10=R3*A3-R4*A1-R5*K3
      A11=-R3*A4-R4*A2+R5*K4+R6
      A12=-X2*(R4*K3+R5*X2*A1-R6*X22*A3)
      A13=(R3+R4*X2*K4-R5*X22*A2-R6*X23*A4)
      A14=(R7*A2-R8*K4-R9)
      A15=-R7*A1-R8*K3
      A16=GJ*K4+R10
      A17=-R7-R3*X2*K4+R9*X22*A2
      A18=-X2*(R8*K3+R9*X2*A1)
      A19=-X22*(A1*GJ-R10*X2*A3)
      A20=-X22*(A2*GJ+R10*X2*A4)
      A21=K3*GJ
      TNK4=TN*K4
      TNK5=TN*K5
      CK3=K3/C
      CK4=K4/C
      CK5=K5/C
      A21=-TN*K3
      A22=TNK4+R12
      A23=CK5*X2
      A24=TN-CK4*X2
      B1=2.0*K3*K5
      B2=PKK3-PKK5
      B3=K5*(PKK3-3.0*PKK5)
      B4=K5*(3.0*PKK3-PKK5)
      B5=-E1*(A22*A2-A21*A1)*Y24
      B6=2.0*E1*Y24*A21*A2
      B7=(R1K5-R2)
      B8=(R1K5+R2*Y2*A2)*Y2
      B9=(R1K5-R2*Y2*A1)*Y2
      B10=R3+R3*R4*A1-R5*K3
      B11=-R5*A4+R4*A2+R5*K5-R6
      B12=-Y2*(R4*K3-R5*Y2*A1-R6*Y2*A3)
      B13=-R3-R4*Y2-R5*(R5*Y22*A3-R6*Y23*A4
      B14=(R7*A2-R8*K5-R9
      B15=-R7*A1-R8*K3
```

```
      R13=Y2*(1.-K3-RY*Y2*(1.)
      B10=Y2*(GJ*B1+R10*Y2*B3)
      B20=Y2*(GJ*B2-R10*Y2*B4)
      CI=1./C
      B22=TNK5*CI
      R23=CK3*Y2
      R24=-TN-CK4*Y2
      DX=SCC/DX
      S1(1)=-DX/C2
      S2(1)=-2.*S*S1(1)
      S3(1)=-DX*D1
      S1(2)=-D2/C2
      S2(2)=-2.*S*S1(2)
      S3(2)=-D2*TN**2-DY
      S1(3)=0.
      S2(3)=DXY/C
      S3(3)=-S*S2(3)
      A26=TN-CK4
      A27=A21*X2
      A28=-CI+TNK4*X2
      B26=-TN-CK5
      B27=A21*Y2
      B28=CI+TNK5*Y2
      R26=R6/DR*C
      R7A=R7/AA
      CI=1./C
    1 CONTINUE
      RETURN
      END
C
C
C
C
C
C
C     ****************************************************************
C     ****************************************************************
C
      SUBROUTINE COFF1 (CD,DETA,N,M,IR,IC)
C     ********** MATRIX FOR SYMMETRICAL MODE *********:
C                ****************************
C     WHICH REPRESENTS THE COFFICIENT OF THE 4(2N+1) EQUATIONS
C     CORRESPONDING TO THE N HARMONICS.
C
C
C     ****************************************************************
      REAL K1N,K2N,K3N,K4N,K5N,K6N,K7N,K8N,L1N,L2N,L3N,L4N,L5N,
     1L6N,L7N,L8N,I1N,I3N,I5N,I7N,K3,K4,K5
      COMMON /A/ PI,SR,C,S,TN,C4,AA,AA3,AA4,Z,C2,C3,ST,SF,T,PK,NS,JS,
     1MM,OMGA,DXOM,R7A,NHC
      COMMON /BLO/ B,DX,DY,DXY,DYX,D1,D2,EI,GJ,H
      COMMON /BL1/ P,K3,K4,K5,B3,B33,B34,X2,Y2,A1,A2,A3,A4,B1,B2,B3,
     1B4,SCH,SC3,SCC,SCB,S1(3),S2(3),S3(3)
      COMMON /BL2/ R1,R2,R3,R4,R5,R6,R7,R8,R9,R10,R11,R12,R13,X22,X23,
     1X24,Y22,Y23,Y24,A5,A6,A7,A8,A9,A10,A11,A12,A13,A14,A15,A16,A17,
     2A18,A19,A20,A21,A22,A23,A24,B6,B5,B6,B7,B8,B9,B10,B11,B12,B13,
     3B14,B15,B16,B17,B18,B19,B20,B21,B22,B23,B24
      COMMON /BL3/ NH,NC,JC,NH2,NH3,NH4,NH5,NH6,NH7,NH8,NH9,N10,N11,
     1N12,N13,N14,N15,N16,N81,N82,N83,NE4,N85,N86,N87
      DIMENSION CD(NC,JC),IR(NC),IC(JC)
      DIMENSION W1(8),BJ(8),BJ(8)
      DO 901 K=1,NS
      DO 901 J=1,NS
  901 CD(K,J)=0.0
      CALL CONST (N,ROP)
      R23=3.*(R32/B3
      S11A=R11/A
      R12=R12/A
      CD(N81,N81)=1.0
      CD(N81,N82)=0.333333333
      CD(N81,N83)=1.0
      CD(N82,NC)=T*AA4/(6.*3.-1
      CD(N8,NC)=T4.*A(R3*T**1.3)/2.)
      CD(N,N82)=0.5*/
      CD(     )=.*
      C      )=
```

```
      CALL CONST (N,KOUT)
      RAP=RAD*PI
      ANP=RAP/A
      BNP=RAP/B
      AN2=AN**2
      OA1=ON*AN
      OA2=ON*AN2
      OA3=OA2*AN
      OA4=OA2*AN2
      BN2=BN**2
      BN3=BN2*BN
      BN4=BN2*BN2
      OB1=ON*BN
      OB2=ON*BN2
      ANA=AN*A
      BNB=BN*B
      XAN=X2*ANA
      YBN=Y2*BNB
      RR1=K4*XAN
      RR2=K4*BNA
      SS1=K5*YAN
      SS2=K5*BNA
      R1N=K3*XAN
      R2N=K3*BNA
      S1N=K3*YAN
      K1N=COSH(R1N)*COS(RR1)
      K2N=SINH(R1N)*SIN(RR1)
      K3N=SINH(R1N)*COS(RR1)
      K4N=COSH(R1N)*SIN(RR1)
      K5N=COSH(R2N)*COS(RR2)
      K6N=SINH(R2N)*SIN(RR2)
      K7N=SINH(R2N)*COS(RR2)
      K8N=COSH(R2N)*SIN(RR2)
      L1N=COSH(S1N)*COS(SS1)
      L2N=SINH(S1N)*SIN(SS1)
      L3N=SINH(S1N)*COS(SS1)
      L4N=COSH(S1N)*SIN(SS1)
      L5N=COSH(R2N)*COS(SS2)
      L6N=SINH(R2N)*SIN(SS2)
      L7N=SINH(R2N)*COS(SS2)
      L8N=COSH(R2N)*SIN(SS2)
      SIN=1.0-3.0/RNP/RNP
      I5N=-2.0/RNP*ON
      I1N=I5N*ISN/ON
      I3N=2.*I1N*R1N
      I7N=I5N*R1N
      ONAX=ONA/X2
      ONAY=ONA/Y2
      W1(1)=(K3*K7N+K4*K8N)/ONAX
      W1(3)=(K3*K8N-K4*K7N)/ONAX
      W1(5)=(K5*L7N+K5*L8N)/BNAY
      W1(4)=(K3*L3N-K5*L7N)/BNAY
      W1(2)=(K3*K3N+K4*K4N)/ANB
      W1(6)=(K3*K4N-K4*K3N)/ANB
      W1(7)=(K3*L3N+K5*L4N)/ANB
      W1(8)=(K3*L4N-K5*L3N)/ANB
      NNN=N1+N
      NN2N=NN2+N
      NN3N=NN3+N
      NN4N=NN4+N
      NN5N=NN5+N
      NN6N=NN6+N
      NN7N=NN7+N
      NN8N=NN8+N
      N1N=-(I+1)
      C1(N,1)=ON3*(-I5N*K5N+I1N*K7N+N11*K8N)
      C1(N,NNN)=ON3*(I1N*K8N-N11*K7N+N11*K5N)
      C1(N,NN2N)=ON3*(I1N*L5N+I3N*L7N+N11*L8N)
      C1(N,NN3N)=ON3*(I1N*L8N-I3N*L7N+N11*L5N)
      C1(NNN,N)=ON3*(N11*K5N-N11*K7N+I5N*K8N)
      C1(NNN,NNN)=ON3*(N11*K8N+N11*K7N+I5N*K5N)
      C1(NNN,NN2N)=ON3*(-N11*L5N+N11*L7N+I5N*L8N)
      C1(NNN,NN3N)=ON3*(-N11*L8N+N11*L7N+I5N*L5N)
```

```
      CD(NH2N,NH1N)=AN2*(A15*K3N+A16*L3N+B15*K4N+B16*L4N)
      CD(NH2N,NH2N)=AN2*(A16*L3N+B16*K4N+B15*L4N)
      CD(NH2N,NH3N)=AN2*(-B15*L3N+B16*L4N-A15*K3N-A16*K4N)
      CD(NH3N,N)=AN2*(A16*EN*K3N+A6*DN*K4N+A15*K3N-A16*K4N)
      CD(NH3N,NH1N)=AN2*(-A6*A0*K3N+A16*K3N+A16*K3N+B16*K4N+B15*K4N)
      CD(NH3N,NH2N)=AN2*(-A16*A0*L3N-A6*A0*L4N-B15*L3N+B16*L4N)
      CD(NH3N,NH3N)=AN2*(A6*A0*L3N-A16*A0*L4N-B16*L3N-B15*L4N)
      CD(NH3N,NC)=-24.0*R10*I3N/BB3
      CD(NC,NH4N)=DA4*(A5*W1(5)+A6*W1(6))
      CD(NC,NH5N)=DA4*(-A6*W1(5)+A5*W1(6))
      CD(NC,NH6N)=DA4*(B5*W1(7)+B6*W1(8))
      CD(NC,NH7N)=DA4*(-B6*W1(7)+B5*W1(8))
      CD(NH4N,NH4N)=K1N
      CD(NH4N,NH5N)=K2N
      CD(NH4N,NH6N)=L1N
      CD(NH4N,NH7N)=L2N
      CD(NH4N,NB2)=I1N
      CD(NH4N,NC)=I*I3N*DA4/BB4
      CD(NH5N,NH4N)=-K4N
      CD(NH5N,NH5N)=K3N
      CD(NH5N,NH6N)=L4N
      CD(NH5N,NH7N)=-L3N
      CD(NH7N,NC)=-R9*I1N/BB*12.*I
      CD(NHON,NH4N)=AN2*(A8*K1N+A9*K2N)
      CD(NHON,NH5N)=AN2*(-A9*K1N+A8*K2N)
      CD(NH6N,NH6N)=AN2*(B8*L1N+B9*L2N)
      CD(NH6N,NH7N)=AN2*(-B9*L1N+B8*L2N)
      CD(NH7N,NH4N)=AN2*(-A9*K4N+A9*K3N)
      CD(NH7N,NH5N)=AN2*(A7*K4N+A8*K3N)
      CD(NH7N,NH6N)=AN2*(B8*L4N-B9*L3N)
      CD(NH7N,NH7N)=AN2*(-B9*L4N-B8*L3N)
      CD(N82,NH4N)=DA2*(A17*W1(5)+A18*W1(6))
      CD(N82,NH5N)=DA2*(-A18*W1(5)+A17*W1(6))
      CD(N82,NH6N)=DA2*(B17*W1(7)+B18*W1(8))
      CD(N82,NH7N)=DA2*(-B18*W1(7)+B17*W1(8))
      CD(N81,N)=DN*W1(1)
      CD(N81,NHN)=DN*W1(2)
      CD(N81,NH2N)=DN*W1(3)
      CD(N81,NH3N)=DN*W1(4)
      CD(N83,N)=DB2*(A7*W1(1)-R1K3*W1(2))
      CD(N83,NHN)=DB2*(R1K3*W1(1)+A7*W1(2))
      CD(N83,NH2N)=DB2*(B7*W1(3)+R1K3*W1(4))
      CD(N83,NH3N)=DB2*(-R1K3*W1(3)+B7*W1(4))
      BNA2=BN2*DN
      BNX2=BNA2/X22
      BNY2=BNA2/Y22
      BNX=BNA2/X2
      BNY=BNA2/Y2
      ANB2=ANB*DNB
      ANX2=ANB2*X22
      ANY2=ANB2*Y22
      ANX=ANB2*X2
      ANY=ANB2*Y2
      A2AX=A2*ANX2
      A2AY=A2*ANY2
      A2BN=A2*BNA2
      B2BN=B2*BNA2
      TA1=A1*BNA2
      TB1=B1*BNA2
      TX1=ANX2*A1
      TY1=ANY2*B1
        PRINT 249 ,N,NHN,NH2N,NH3N,NH4N,NH5N
  249   FORMAT (5X,'N',6I5)
   14 DN=1.
      DO 24 N=1,NH
      DN=-DN
      CALL CONST (N,ROW)
      RN=N
      RNPI2=RN*PI
      RN22=RNPI2**2
      RN24=RN22*RN22
      SAA=2.0/(BNA2*(HNX2+2.0*A2*RN22)+RN24)
      SBA=2.0/(ANA2*(ANY2+2.0*A2*RN22)+RN24)
      SXA=2.0/(ANX2*(ANB2+2.0*A2*RN22)+RN24)
      SYA=2.0/(ANY2*(ANB2+2.0*B2*RN22)+RN24)
      SB1=SYA*RNPI2*DN
      SA1=SXA*RNPI2*DN
      SX1=SAA*RNPI2*DN
      SY1=SBA*RNPI2*DN
```

```
      SA2=SAA*AAA+UA
      SB2=SBA*AAA+UA
      SX2=CA*AAA+UA
      SY2=SYA*AAA+UA
      TA2=AAA*RM22
      TB2=ABA*RM22
      TX2=AXA*RM22
      TY2=AYA*RM22
      TA3=K3*(AAX+RM22)
      TA4=K4*(AAX-RM22)
      TB3=K3*(ABX+RM22)
      TB4=K5*(ABY-RM22)
      TX3=(AAX+RM22)*K3*X2
      TX4=(AAX-RM22)*K4*X2
      TY3=(ABY+RM22)*K3*Y2
      TY4=(ABY-RM22)*K5*Y2
      AJ(1)=SA2*(TA3*K7N+TB4*K5N)
      AJ(2)=SA2*(-TA4*K7N+TA3*K8N)
      AJ(3)=SB2*(TB3*L7N+TB4*L8N)
      AJ(4)=SB2*(-TB4*L7N+TB3*L8N)
      AJ(5)=SX2*(TX3*K5N+TX4*K4N)
      AJ(6)=SX2*(-TX4*K3N+TX3*K4N)
      AJ(7)=SY2*(TY3*L3N+TY4*L4N)
      AJ(8)=SY2*(-TY4*L3N+TY3*L4N)
      BJ(1)=SA1*(-TA2*K7N-TA1*K8N)
      AJ(2)=SA1*(TA1*K7N-TA2*K8N)
      BJ(3)=SB1*(-TB2*L7N-TB1*L8N)
      BJ(4)=SB1*(TB1*L7N-TB2*L8N)
      BJ(5)=SX1*(-TX2*K3N-TX1*K4N)
      BJ(6)=SX1*(TX1*K3N-TX2*K4N)
      BJ(7)=SY1*(-TY2*L3N-TY1*L4N)
      BJ(8)=SY1*(TY1*L3N-TY2*L4N)
   17 NNM=NN+M
      NN2M=NN2+M
      NN3M=NN3+M
      NN4M=NN4+M
      NN5M=NN5+M
      NN6M=NN6+M
      NN7M=NN7+M
      NN8M=NN2+M
      CO(N,NN4M)=OA4*(A5*AJ(5)+A6*AJ(6))
      CO(N,NN5M)=OA4*(-A6*AJ(5)+A5*AJ(6))
      CO(N,NN6M)=OA4*(B5*AJ(7)+B6*AJ(8))
      CO(N,NN7M)=OA4*(-B6*AJ(7)+B5*AJ(8))
      CO(NNN,NN4M)=OA3*(A12*AJ(5)+A13*AJ(6))
      CO(NNN,NN5M)=OA3*(-A13*BJ(5)+A12*BJ(6))
      CO(NNN,NN6M)=OA3*(B12*AJ(7)+B13*AJ(8))
      CO(NNN,NN7M)=OA3*(-B13*BJ(7)+B12*BJ(8))
      CO(NN2N,NN4M)=OA2*(A17*AJ(5)+A18*AJ(6))
      CO(NN2N,NN5M)=OA2*(-A18*AJ(5)+A17*AJ(6))
      CO(NN2N,NN6M)=OA2*(B17*AJ(7)+B18*AJ(8))
      CO(NN2N,NN7M)=OA2*(-B18*AJ(7)+B17*AJ(8))
      CO(NN3N,NN4M)=OA3*(A19*BJ(5)+A20*BJ(6))
      CO(NN3N,NN5M)=OA3*(-A20*BJ(5)+A19*BJ(6))
      CO(NN3N,NN6M)=OA3*(B19*BJ(7)+B20*BJ(8))
      CO(NN3N,NN7M)=OA3*(-B20*BJ(7)+B19*BJ(8))
      CO(NN4N,M)=ON*AJ(1)
      CO(NN4N,NNN)=ON*AJ(2)
      CO(NN4N,NN2M)=ON*AJ(3)
      CO(NN4N,NN3M)=ON*AJ(4)
      CO(NN6N,M)=OB2*(A7*AJ(1)-B1K3*AJ(2))
      CO(NN6N,NNM)=OB2*(B1K3*AJ(1)+A7*AJ(2))
      CO(NN6N,NN2M)=OB2*(B7*AJ(3)+B1K3*AJ(4))
      CO(NN6N,NN3M)=OB2*(-B1K3*AJ(3)+B7*AJ(4))
   24 CONTINUE
      RETURN
      END
C
C
C
C
C
C*****************************************************************
C*****************************************************************
C
C
      SUBROUTINE JUTIS (CO,M,IA,IB,,,IX,IY)
C*****V.I.S.S.  MATRIX FOR JET-BY-JET
```

```
C     WHICH REPRESENTS THE COEFFICIENT OF THE ALGEBRAIC EQUATIONS
C     CORRESPONDING TO THE N HARMONIC.
C
C
C     ******************************************************
      REAL K1N,K2N,K3N,K4N,K5N,K6N,K7N,K8N,L1N,L2N,L3N,L4N,L5N,
     1L6N,L7N,L8N,I1N,I2N,I5N,I7N,K3,K4,K5
      COMMON /AL1/ A,PI,SA,C,S,TN,C4,AA,AA3,AA4,Z,C2,C3,ST,SF,T,PK,NS,JS,
     1ONH,OMGA,DXOM,R7A,NHC
      COMMON /AL0/ B,DX,DY,DXY,DYX,B1,B2,EI,GJ,H
      COMMON /AL7/ P,K3,K4,K5,BB,BB3,BB4,X2,Y2,A1,A2,A3,A4,B1,B2,B3,
     1C4,SCA,SC3,SCC,SCD,S1(3),S2(3),S3(3)
      /COMMON /AL2/ R1,R2,R3,R4,R5,R6,R7,R8,R9,R10,R11,R12,R1K3,X22,X23,
     1X24,Y22,Y23,Y24,A5,A6,A7,A8,A9,A10,A11,A12,A13,A14,A15,A16,A17,
     2A18,A19,A20,A21,A22,A23,A24,B5,B6,B7,B8,B9,B10,B11,B12,B13,
     3B14,B15,B16,B17,B18,B19,B20,B21,B22,B23,B24
      COMMON /AL5/ NH,NC,JC,NH2,NH3,NH4,NH5,NH6,NH7,NH8,NH9,N10,N11,
     1N12,N13,N14,N15,N16,N81,N82,N83,N84,N85,N86,N87
      DIMENSION CD(NC,JC),TR(NC),IC(JC)
      DIMENSION W1(3),AJ(8),AJI(8)
       DO 901 K=1,N5
       DO 901 J=1,N5
  901 CD(K,J)=0.0
      CALL CONST (N,ROW)
      R2B=2.0*B2/BB
      R11A=R11/A
      R12B=R12/B
      CD(N81,N811)=0.0
      CD(N81,N821)=1.000000000
      CD(N81,N831)=0.0
      CD(N81,NC)=1.0
      CD(NC,NC)=6*R6/BB3
      CD(NC,N831)=6.*R3/AA3
      CD(N82,N821)=0.0
      CD(N82,N831)=6.*R7A
      CD(N82,NC)=6.0*R10/BB3
      CD(N83,N831)=0.0
      CD(N83,NC)=3.0*R2B
      ON=1.0
      DO 24 N=1,NH
      ON=-ON
      CALL CONST (N,ROW)
      RN=N
      RNP=RN*PI
      AN=RNP/A
      BN=RNP/B
      AN2=AN**2
      OA1=ON*AN
      OA2=ON*AN2
      OA3=OA2*AN
      OA4=OA2*AN2
      BN2=BN**2
      OB3=BN2*BN
      OB4=BN2*BN2
      OB1=ON*BN
      OB2=ON*BN2
      ANB=AN*B
      BNA=BN*A
      XAN=X2*ANB
      YAN=Y2*BNA
      RR1=K4*XAN
      RI2=K4*BNA
      SS1=K5*YAN
      SS2=K5*BNA
      R1N=K3*XAN
      R2N=K3*BNA
      S1N=K3*YAN
       K1N=COSH(R1N)*COS(RR1)
       K2N=SINH(R1N)*SIN(RR1)
       K3N=SINH(R1N)*COS(RR1)
       K4N=COSH(R1N)*SIN(RR1)
       K5N=COSH(R2N)*COS(RR2)
       K6N=SINH(R2N)*SIN(RR2)
       K7N=SINH(R2N)*COS(RR2)
       K8N=COSH(R2N)*SIN(RR2)
       L1N=COS(S1N)*COS(SS1)
       L2N=SIN(S1N)*SIN(SS1)
       L3N=SIN(S1N)*COS(SS1)
       L4N=COS(S1N)*SIN(SS1)
```

```
      L5N=COSH(R3N)*SIN(S5)
      L6N=SINH(R3N)*SIN(S5)
      L7N=SINH(R2N)*COS(S5)
      L8N=COSH(R2N)*SIN(S5)
      RIN=1.0-6.0/RNP/RNP
      ISN=-2.0/RNP*DN
      I1N=ISN*ISN/DN
      I5N=2.0*I1N*RIN
      I7N=ISN*RIN
      BNAX=BNA/X2
      BNAY=BNA/Y2
      W1(1)=(K3*K7N+K4*K8N)/BNAX
      W1(2)=(K3*K8N-K4*K7N)/BNAX
      W1(3)=(K3*L7N+K5*L8N)/BNAY
      W1(4)=(K3*L8N-K5*L7N)/BNAY
      W1(5)=(K3*K5N+K4*K4N)/ANB
      W1(6)=(K3*K4N-K4*K3N)/ANB
      W1(7)=(K3*L3N+K5*L4N)/ANB
      W1(8)=(K3*L4N-K5*L3N)/ANB
      NRN=NR+1
      NH2N=NH2+N
      NH3N=NH3+N
      NH4N=NH4+N
      NH5N=NH5+N
      NH6N=NH6+N
      NH7N=NH7+N
      NH8N=NH8+N
      EID2=EI*EI
      CO(N,N)=BN3*(-EIB*K6N+A11*K7N-A10*K8N)
      CO(N,NHN)=BN3*(EIB*K5N+A10*K7N+A11*K6N)
      CO(N,NH2N)=BN3*(EIB*L6N-B11*L7N+B10*L8N)
      CO(N,NH3N)=BN3*(-EIB*L5N-B10*L7N-B11*L8N)
      CO(NHN,N)=BN3*(A10*K5N+A11*K6N+EIB*K7N)
      CO(NHN,NHN)=BN3*(-A11*K5N+A10*K6N+EIB*K8N)
      CO(NHN,NH2N)=BN3*(B10*L5N+B11*L6N+EIB*L7N)
      CO(NHN,NH3N)=BN3*(-B11*L5N+B10*L6N+EIB*L8N)
      CO(NHN,NC)=0.0
      CO(NH2N,N)=BN2*(A15*K5N-A14*K6N+AG*BN*K5N+A16*BN*K7N)
      CO(NH2N,NHN)=BN2*(A14*K5N+A15*K6N+A16*BN*K8N+AG*BN*K7N)
      CO(NH2N,NH2N)=BN2*(-B15*L5N+B14*L6N+AG*BN*L8N-B16*BN*L7N)
      CO(NH2N,NH3N)=BN2*(-B14*L5N-B15*L6N-B16*BN*L8N+AG*BN*L7N)
      CO(NH3N,N)=BN2*(A16*BN*K6N-AG*BN*K5N+A14*K7N+A15*K8N)
      CO(NH3N,NHN)=BN2*(+AG*BN*K6N-A16*BN*K5N-A15*K7N+A14*K8N)
      CO(NH3N,NH2N)=BN2*(+B16*BN*L6N+AG*BN*L5N+B14*L7N+B15*L8N)
      CO(NH3N,NH3N)=BN2*(-AG*BN*L6N-B16*BN*L5N-B15*L7N+B14*L8N)
      CO(NH3N,NC)=0.0
      CO(NC,NH4N)=DA3*(A12*W1(5)+A13*W1(6))
      CO(NC,NH5N)=DA3*(-A13*W1(5)+A12*W1(6))
      CO(NC,NH6N)=DA3*(B12*W1(7)+B13*W1(8))
      CO(NC,NH7N)=DA3*(-B13*W1(7)+B12*W1(8))
      CO(NH4N,NH4N)=-K2N
      CO(NH5N,NH5N)=K1N
      CO(NH4N,NH6N)=L2N
      CO(NH4N,NH7N)=-L1N
      CO(NH4N,NB1)=I5N
      CO(NH4N,NB3)=I7N
      CO(NH5N,NH4N)=K3N
      CO(NH5N,NH5N)=K4N
      CO(NH5N,NH6N)=L3N
      CO(NH5N,NH7N)=L4N
      CO(NH2N,NC)=6.*AR9*ISN/(B**2)
      CO(NH5N,NH4N)=AN2*(A9*K1N-A8*K2N)
      CO(NH6N,NH5N)=AN2*(A8*K1N+A9*K2N)
      CO(NH6N,NH6N)=AN2*(-B9*L1N+B8*L2N)
      CO(NH5N,NH7N)=AN2*(-B8*L1N-B9*L2N)
      CO(NH7N,NH4N)=AN2*(A8*K3N+A9*K4N)
      CO(NH7N,NH5N)=AN2*(-A9*K3N+A8*K4N)
      CO(NH7N,NH6N)=AN2*(B8*L3N+B9*L4N)
      CO(NH7N,NH7N)=AN2*(-B9*L3N+B8*L4N)
      CO(N82,NH4N)=DA3*(A19*W1(5)+A20*W1(6))
      CO(N82,NH5N)=DA3*(-A20*W1(5)+A19*W1(6))
      CO(N82,NH6N)=DA3*(B19*W1(7)+B20*W1(8))
      CO(N82,NH7N)=DA3*(-B20*W1(7)+B19*W1(8))
      CO(N81,N)=0.0
      CO(N81,NHN)=0.0
      CO(N81,NH2N)=0.0
      CO(N81,NH3N)=0.0
```

```
      802.          EPINL3=RNH3N1*2.0
      803.          BNX2=ANA2*QA
      804.          BNX2=BNA2/X22
      805.          BNY2=ANA2/Y22
      806.          ANX=ANA2/X2
      807.          ANY=ANA2/Y2
      808.          ANB2=ANB*ANB
      809.          BNX2=BNB2*X22
      810.          ANY2=ANB2*Y22
      811.          ANX=ANB2*X2
      812.          ANY=ANB2*Y2
      813.          A2AX=A2*ANX2
      814.          A2AY=A2*ANY2
      815.          A2BN=A2*ANB2
      816.          B2BN=B2*BNA2
      817.          TA1=A1*BNA2
      818.          TB1=B1*BNA2
      819.          TX1=ANX2*A1
      820.          TY1=ANY2*B1
      821.          PRINT 249,N,NHH,NH2N,NH3N,NH4N,NH5N
      822.      249 FORMAT(5X,'N',6I5)
      823.       14 OM=1.0
      824.          DO 24 M=1,NH
      825.          OM=-OM
      826.          CALL CONST (M,ROM)
      827.          RM=M
      828.          RMP2=RM*PI
      829.          RM22=RMP2**2
      830.          RM24=RM22*RM22
      831.          SAA=2.0/(BNA2*(BNX2+2.0*A2*RM22)+RM24)
      832.          SBA=2.0/(BNA2*(BNY2+2.0*B2*RM22)+RM24)
      833.          SXA=2.0/(ANX2*(ANB2+2.0*A2*RM22)+RM24)
      834.          SYA=2.0/(ANY2*(ANB2+2.0*B2*RM22)+RM24)
      835.          SA1=SAA*RMP2*OM
      836.          SB1=SBA*RMP2*OM
      837.          SX1=SXA*RMP2*OM
      838.          SY1=SYA*RMP2*OM
      839.          SA2=SAA*BNA*OM
      840.          SB2=SBA*BNA*OM
      841.          SX2=SAA*ANB*OM
      842.          SY2=SYA*ANB*OM
      843.          TA2=A2BN+RM22
      844.          TB2=B2BN+RM22
      845.          TX2=A2AX+RM22
      846.          TY2=A2AY+RM22
      847.          TA3=K3*(BNA+RM22)
      848.          TA4=K4*(BNA-RM22)
      849.          TB3=K3*(BNY+RM22)
      850.          TB4=K5*(BNY-RM22)
      851.          TX3=(ANX+RM22)*K3*X2
      852.          TX4=(ANX-RM22)*K4*X2
      853.          TY3=(ANY+RM22)*K3*Y2
      854.          TY4=(ANY-RM22)*K5*Y2
      855.          AJ(1)=SA2*(TA3*K7N+TA4*K8N)
      856.          AJ(2)=SA2*(-TA4*K7N+TA3*K8N)
      857.          AJ(3)=SB2*(TB3*L7N+TB4*L8N)
      858.          AJ(4)=SB2*(-TB4*L7N+TB3*L8N)
      859.          AJ(5)=SX2*(TX3*K3N+TX4*K4N)
      860.          AJ(6)=SX2*(-TX4*K3N+TX3*K4N)
      861.          AJ(7)=SY2*(TY3*L3N+TY4*L4N)
      862.          AJ(8)=SY2*(-TY4*L3N+TY3*L4N)
      863.          BJ(1)=SA1*(-TA2*K7N-TA1*K8N)
      864.          BJ(2)=SA1*(TA1*K7N-TA2*K8N)
      865.          BJ(3)=SB1*(-TB2*L7N-TB1*L8N)
      866.          BJ(4)=SB1*(TB1*L7N-TB2*L8N)
      867.          BJ(5)=SX1*(-TX2*K3N-TX1*K4N)
      868.          BJ(6)=SX1*(TX1*K3N-TX2*K4N)
      869.          BJ(7)=SY1*(-TY2*L3N-TY1*L4N)
      870.          BJ(8)=SY1*(TY1*L3N-TY2*L4N)
      871.       17 NH1=NH+1
      872.          NH2N=NH2+1
      873.          NH3N=NH3+1
      874.          NH4N=NH4+1
      875.          NH5N=NH5+1
      876.          NH6N=NH6+1
      877.          NH7N=NH7+1
      878.          NH8N=NH8+1
      879.          CJ(1,1)=AJ(1)*(AJ(1)*CJ(1,1)+AJ(2)*CJ(2,1)+BJ(1)*CJ(3,1)+BJ(2)*CJ(4,1)+AJ(3)*CJ(5,1)+AJ(4)*CJ(6,1)+AJ(5)*CJ(7,1)+AJ(6)*CJ(8,1))
      880.          CJ(2,1)=AJ(2)*(-AJ(1)*CJ(1,1)+AJ(2)*CJ(2,1)-BJ(2)*CJ(3,1)+BJ(1)*CJ(4,1)-AJ(4)*CJ(5,1)+AJ(3)*CJ(6,1)-AJ(6)*CJ(7,1)+AJ(5)*CJ(8,1))
```

```
C881.           CDI(9,NH2N)=DA2*(-B5*AJ(5)+B6*AJ(6))
C882.           CDI(NH2,NH3N)=DA3*(A12*AJ(5)+A13*AJ(6))
C883.           CDI(NH2,NH4N)=DA3*(A12*AJ(5)+A13*AJ(6))
C884.           CDI(NH2,NH5N)=DA3*(-A13*AJ(5)+A12*AJ(6))
C885.           CDI(NH2,NH6N)=DA3*(A12*AJ(7)+A13*AJ(8))
C886.           CDI(NH2,NH7N)=DA3*(-A13*AJ(7)+A12*AJ(8))
C887.           CDI(NH3N,NH4N)=DA2*(A17*AJ(5)+A18*AJ(6))
C888.           CDI(NH3N,NH5N)=DA2*(-A18*AJ(5)+A17*AJ(6))
C889.           CDI(NH2N,NH6N)=DA2*(B17*BJ(7)+B18*BJ(8))
C890.           CDI(NH2N,NH7N)=DA2*(-B18*BJ(7)+B17*BJ(8))
C891.           CDI(NH3N,NH4N)=DA3*(A19*AJ(5)+A20*AJ(6))
C892.           CDI(NH3N,NH5N)=DA3*(-A20*AJ(5)+A19*AJ(6))
C893.           CDI(NH3N,NH6N)=DA3*(B19*AJ(7)+B20*AJ(8))
C894.           CDI(NH3N,NH7N)=DA3*(-B20*AJ(7)+B19*AJ(8))
C895.           CDI(NH4N,M)=DN*BJ(1)
C896.           CDI(NH4N,NH1M)=DN*BJ(2)
C897.           CDI(NH4N,NH2M)=DN*BJ(3)
C898.           CDI(NH4N,NH3M)=DN*BJ(4)
C899.           CDI(NH6N,M)=DB2*(A7*BJ(1)-R1K3*BJ(2))
C900.           CDI(NH6N,NH1M)=DB2*(R1K3*BJ(1)+A7*BJ(2))
C901.           CDI(NH6N,NH2M)=DB2*(B7*BJ(3)+R1K3*BJ(4))
C902.           CDI(NH6N,NH3M)=DB2*(-R1K3*BJ(3)+B7*BJ(4))
C903.        24 CONTINUE
C904.           RETURN
C905.           END
C906.  $ENTRY
C907.    9.0
C908.    00066.00 00066.00 00045.00 011.4E+06 011.4E+06 01.16E+06
C909.    001.16E+06 001.4E+06 001.4E+06 0.00 0.00 0005
C910.    49.0E-06
C911.  $IBSYS
C912.  $STOP
C913.  //
```



```
WW          WW  FFFFFFFFFFFF   AAAAAAAAAA   3333333333   0000000   555555555555   444   9999999999
 WW        WW   FFFFFFFFFFFF  AAAAAAAAAAAA 3333333333   0000000   555555555555  4444  99999999999
  WW      WW    FF           AA    AA  33      33 00   00 00   00 55          44 44  99    99
   WW    WW     FF           AA    AA        33 00   00 00   00 55          44  44  99    99
    WW  WW      FF          AA      AA       33 00   00 00   00 55         44   44  99    99
     WWWW       FFFFFFFF    AAAAAAAAAAAA     3333 00   00 00   00 555555555 44444444444 999999999999
      WW        FFFFFFFF    AAAAAAAAAAAA     3333 00   00 00   00 555555555 44444444444 999999999999
      WW        FF          AA      AA       33 00   00 00   00 55          44          99
      WW        FF          AA      AA       33 00   00 00   00 55          44          99
      WW        FF          AA      AA 33    33 00   00 00   00 55          44  99      99
      WW        FF          AA      AA 33333333333  000000000  5555555555555 44  9999999999
      WW        FF          AA      AA  3333333333   0000000   5555555555    44  9999999999

7777777777777   00000000   7777777777777  3333333333                    FFFFFFFFFFFF   AAAAAAAAAA   33333333333
7777777777777   00000000   7777777777777  3333333333333                 FFFFFFFFFFFF  AAAAAAAAAAAA 333333333333
77          77  00    00   77          77  33      33                   FF           AA    AA  33      33
77          77  00    00   77          77          33                   FF           AA    AA          33
77          77  00    00   77          77          33                   FF           AA    AA          33
77          77  00    00   77          77          33                   FFFFFFFF     AAAAAAAAAAAA      3333
77          77  00    00   77          77          33                   FFFFFFFF     AAAAAAAAAAAA      3333
77          77  00    00   77          77          33                   FF           AA    AA          33
77          77  00    00   77          77          33                   FF           AA    AA          33
77          77  00    00   77          77 33       33                   FF           AA    AA  33      33
77          77  00    00   77          77 333333333333                  FF           AA    AA  333333333333
77          77  00    00   77          77  3333333333                   FF           AA    AA   3333333333

ND   WYLBUR   JOB 7073  WFA30549  F63                    INIT F63 14:15:57 PM 07 AUG 69  PRINTER1 SYS CPU=  .013 7075          END
ND   WYLBUR   JOB 7077  WFA30549  F63                    INIT F63 14:15:57 PM 07 AUG 69  PRINTER1 SYS CPU=  .013 7077          END
ND   WYLBUR   JOB 7073  WFA30549  F63                    INIT F63 14:15:57 PM 07 AUG 69  PRINTER1 SYS CPU=  .013 7073          END
```

APPENDIX F

TYPICAL OUTPUT OF SAP IV

FOR THE NATURAL FREQUENCIES AND ASSOCIATED MODE SHAPES

OF A SKEW ORTHOTROPIC PLATE

PRINT OF FREQUENCIES

MODE NUMBER	CIRCULAR FREQUENCY (RAD/SEC)	FREQUENCY (CYCLES/SEC)	PERIOD (SEC)	TOLERANCE
1	0.1466D 03	0.2334D 02	0.4284D-01	0.4214D-16
2	0.1502D 03	0.2391D 02	0.4182D-01	0.8346D-15
3	0.3312D 03	0.5271D 02	0.1897D-01	0.9287D-15
4	0.5369D 03	0.8545D 02	0.1170D-01	0.6066D-13
5	0.7003D 03	0.1115D 03	0.8972D-02	0.2712D-10
6	0.7814D 03	0.1244D 03	0.8041D-02	0.3740D-10
7	0.8604D 03	0.1369D 03	0.7302D-02	0.7220D-08
8	0.1183D 04	0.1883D 03	0.5283D-02	0.7758D-05
9	0.1246D 04	0.1983D 03	0.5043D-02	0.7571D-06

PRINT OF EIGENVECTORS

NODE DISPLACEMENTS/ROTATIONS

NODE NUMBER	EIGEN-VECTOR	X-TRANSLATION	Y-TRANSLATION	Z-TRANSLATION	X-ROTATION	Y-ROTATION	Z-ROTATION
195	1	0.0	0.0	0.0	0.0	0.218986D-01	0.0
	2	0.0	0.0	0.0	0.0	-0.398710-01	0.0
	3	0.0	0.0	0.0	0.0	-0.675400-01	0.0
	4	0.0	0.0	0.0	0.0	-0.929150-01	0.0
	5	0.0	0.0	0.0	0.0	-0.625200-01	0.0
	6	0.0	0.0	0.0	0.0	-0.516060-01	0.0
	7	0.0	0.0	0.0	0.0	0.134620 00	0.0
	8	0.0	0.0	0.0	0.0	0.185150 00	0.0
	9	0.0	0.0	0.0	0.0	-0.741740-02	0.0
194	1	0.0	0.0	0.0	0.0	0.216490-01	0.0
	2	0.0	0.0	0.0	0.0	-0.372230-01	0.0
	3	0.0	0.0	0.0	0.0	-0.636050-01	0.0
	4	0.0	0.0	0.0	0.0	-0.853240-01	0.0
	5	0.0	0.0	0.0	0.0	-0.459330-01	0.0
	6	0.0	0.0	0.0	0.0	-0.472410-01	0.0
	7	0.0	0.0	0.0	0.0	0.116780 00	0.0
	8	0.0	0.0	0.0	0.0	0.154150 00	0.0
	9	0.0	0.0	0.0	0.0	-0.253740-02	0.0
193	1	0.0	0.0	0.0	0.0	0.212870-01	0.0
	2	0.0	0.0	0.0	0.0	-0.355710-01	0.0
	3	0.0	0.0	0.0	0.0	-0.574080-01	0.0
	4	0.0	0.0	0.0	0.0	-0.781300-01	0.0
	5	0.0	0.0	0.0	0.0	-0.359070-01	0.0
	6	0.0	0.0	0.0	0.0	-0.419140-01	0.0
	7	0.0	0.0	0.0	0.0	0.913770-01	0.0
	8	0.0	0.0	0.0	0.0	0.111410 00	0.0
	9	0.0	0.0	0.0	0.0	0.279440-02	0.0
192	1	0.0	0.0	0.0	0.0	[illegible]	0.0
	2	0.0	0.0	0.0	0.0	-0.331270-01	0.0
	3	0.0	0.0	0.0	0.0	[illegible]	0.0
	4	0.0	0.0	0.0	0.0	-0.660370-01	0.0
	5	0.0	0.0	0.0	0.0	-0.[illegible]-01	0.0

University of Windsor

University of Windsor

University of Windsor

University of Windsor

University of Windsor

University of Windsor

University of Windsor

University of Windsor

University of Windsor

University of Windsor

University of Windsor

23	1	0.0	0.0	0.1[illegible] 00	-0.[illegible]-02	-0.[illegible]-01	0.0
	2	0.0	0.0	0.[illegible]-01	-0.[illegible]-02	-0.[illegible]-02	0.0
	3	0.0	0.0	0.[illegible] 00	0.[illegible]-02	-0.[illegible]-01	0.0
	4	0.0	0.0	-0.[illegible]-01	0.[illegible]-02	0.[illegible]-02	0.0
	5	0.0	0.0	-0.[illegible] 00	-0.[illegible]-02	0.[illegible]-01	0.0
	6	0.0	0.0	-0.[illegible] 00	0.[illegible]-02	0.[illegible]-01	0.0
	7	0.0	0.0	-0.[illegible]-01	0.[illegible]-01	0.[illegible]-02	0.0
	8	0.0	0.0	-0.[illegible] 00	-0.[illegible]-02	0.[illegible]-01	0.0
	9	0.0	0.0	0.[illegible]-01	0.[illegible]-01	-0.[illegible]-02	0.0
22	1	0.0	0.0	0.121660 00	-0.511420-04	-0.140180-01	0.0
	2	0.0	0.0	0.814120-01	-0.351510-02	-0.121030-01	0.0
	3	0.0	0.0	0.792910-01	0.559420-02	-0.119130-01	0.0
	4	0.0	0.0	-0.542100-01	0.551710-03	0.879450-02	0.0
	5	0.0	0.0	-0.[illegible] 00	-0.322420-02	0.440920-01	0.0
	6	0.0	0.0	-0.229630 00	-0.352540-03	0.326900-01	0.0
	7	0.0	0.0	-0.192010 00	0.113760-01	0.278130-01	0.0
	8	0.0	0.0	-0.156500 00	-0.151220-01	0.229020-01	0.0
	9	0.0	0.0	-0.156660 00	0.205200-01	0.227590-01	0.0
21	1	0.0	0.0	0.122650 00	-0.[illegible]-03	-0.182140-01	0.0
	2	0.0	0.0	0.112140 00	-0.321210-02	-0.166650-01	0.0
	3	0.0	0.0	0.182530-01	0.734770-02	-0.285570-02	0.0
	4	0.0	0.0	-0.394670-01	-0.360060-02	0.670720-02	0.0
	5	0.0	0.0	-0.266960 00	-0.557590-02	0.382600-01	0.0
	6	0.0	0.0	-0.215270 00	-0.232040-02	0.299920-01	0.0
	7	0.0	0.0	-0.265510 00	0.461230-02	0.389070-01	0.0
	8	0.0	0.0	-0.818560-03	-0.177550-01	-0.347850-03	0.0
	9	0.0	0.0	-0.312810 00	0.128900-01	0.443260-01	0.0
20	1	0.0	0.0	0.[illegible] 00	-0.[illegible]-02	-0.[illegible]-01	0.0
	2	0.0	0.0	0.140190 00	-0.293060-02	-0.208300-01	0.0
	3	0.0	0.0	-0.535640-01	0.824660-02	0.782330-02	0.0
	4	0.0	0.0	0.140390-01	-0.763660-02	-0.117980-02	0.0
	5	0.0	0.0	-0.203000 00	-0.[illegible]-02	0.291530-01	0.0
	6	0.0	0.0	-0.192900 00	-0.[illegible]-02	0.263470-01	0.0
	7	0.0	0.0	-0.263360 00	-0.[illegible]-02	0.[illegible]-01	0.0
	8	0.0	0.0	0.136670 00	-0.[illegible]-01	-0.[illegible]-01	0.0
	9	0.0	0.0	-0.[illegible] 00	0.[illegible]-02	0.[illegible]-01	0.0
19	1	0.0	0.0	0.128600 00	-0.[illegible]-03	-0.[illegible]-01	0.0
	2	0.0	0.0	0.[illegible] 00	-0.[illegible]-02	-0.[illegible]-01	0.0
	3	0.0	0.0	-0.[illegible] 00	-0.[illegible]-02	0.[illegible]-01	0.0
	4	0.0	0.0	0.[illegible] 00	-0.[illegible]-01	-0.[illegible]-01	0.0
	5	0.0	0.0	-0.[illegible] 00	-0.[illegible]-01	0.[illegible]-01	0.0
	6	0.0	0.0	-0.[illegible] 00	-0.[illegible]-03	0.[illegible]-01	0.0
	7	0.0	0.0	-0.[illegible] 00	-0.[illegible]-01	0.[illegible]-01	0.0
	8	0.0	0.0	0.[illegible] 00	0.[illegible]-02	-0.[illegible]-01	0.0
	9	0.0	0.0	-0.[illegible] 00	-0.[illegible]-02	0.[illegible]-01	0.0
18	1	0.0	0.0	0.[illegible] 00	-0.[illegible]-03	-0.[illegible]-01	0.0
	2	0.0	0.0	0.[illegible] 00	-0.[illegible]-02	-0.[illegible]-01	0.0
	3	0.0	0.0	-0.[illegible] 00	0.[illegible]-02	0.[illegible]-01	0.0
	4	0.0	0.0	0.[illegible] 00	-0.[illegible]-01	-0.[illegible]-01	0.0
	5	0.0	0.0	-0.[illegible]-01	-0.[illegible]-01	0.[illegible]-02	0.0
	6	0.0	0.0	-0.[illegible] 00	0.[illegible]-02	0.[illegible]-01	0.0
	7	0.0	0.0	-0.[illegible]-02	-0.[illegible]-01	0.[illegible]-02	0.0
	8	0.0	0.0	0.[illegible]-01	0.[illegible]-01	-0.[illegible]-01	0.0
	9	0.0	0.0	-0.[illegible] 00	-0.[illegible]-02	0.[illegible]-01	0.0
17	1	0.0	0.0	0.[illegible] 00	-0.[illegible]-03	-0.[illegible]-01	0.0
	2	0.0	0.0	0.[illegible] 00	-0.[illegible]-02	-0.[illegible]-01	0.0
	3	0.0	0.0	-0.[illegible] 00	0.[illegible]-02	0.[illegible]-01	0.0
	4	0.0	0.0	0.[illegible] 00	-0.[illegible]-01	-0.[illegible]-01	0.0
	5	0.0	0.0	0.[illegible]-01	-0.[illegible]-01	-0.[illegible]-01	0.0
	6	0.0	0.0	-0.[illegible] 00	0.[illegible]-02	0.[illegible]-01	0.0
	7	0.0	0.0	0.[illegible] 00	-0.[illegible]-01	-0.[illegible]-01	0.0
	8	0.0	0.0	-0.[illegible] 00	0.[illegible]-01	-0.[illegible]-01	0.0
	9	0.0	0.0	-0.[illegible] 00	-0.[illegible]-01	0.[illegible]-01	0.0
16	1	0.0	0.0	-0.[illegible] 00	-0.[illegible]-01	-0.[illegible]-01	0.0
	2	0.0	0.0	0.[illegible] 00	-0.[illegible]-02	-0.[illegible]-01	0.0
	3	0.0	0.0	-0.[illegible] 00	0.[illegible]-02	0.[illegible]-01	0.0
	4	0.0	0.0	0.[illegible] 00	-0.[illegible]-01	-0.[illegible]-01	0.0
	5	0.0	0.0	0.178020 00	-0.971660-02	-0.263270-01	0.0

	15	1	0.0		0.141170 00	-0.[illegible]	[illegible]
		2	0.0		0.[illegible] 00	-0.[illegible]	[illegible]
		3	0.0	0.0	-0.[illegible] 00	0.[illegible]	[illegible]
		4	0.0	0.0	0.[illegible] 00	-0.[illegible]	[illegible]
		5	0.0	0.0	0.[illegible] 00	-0.[illegible]	[illegible]
		6	0.0	0.0	-0.[illegible] 00	0.[illegible]	[illegible]
		7	0.0	0.0	0.[illegible] 00	-0.[illegible]	[illegible]
		8	0.0	0.0	-0.784070 00	0.[illegible] 00	0.0
		9	0.0	0.0	-0.[illegible]	-0.[illegible]	0.0
	14	1	0.0	0.0	0.[illegible] 00	-0.[illegible]	0.0
		2	0.0	0.0	0.[illegible] 00	-0.[illegible]	0.0
		3	0.0	0.0	-0.[illegible] 00	0.[illegible]	0.0
		4	0.0	0.0	0.[illegible] 00	-0.[illegible]	0.0
		5	0.0	0.0	0.[illegible] 00	-0.[illegible]	0.0
		6	0.0	0.0	-0.[illegible] 00	0.[illegible]	0.0
		7	0.0	0.0	0.[illegible] 00	-0.[illegible]	0.0
		8	0.0	0.0	-0.104720 01	0.[illegible]	0.0
		9	0.0	0.0	0.604770-02	-0.[illegible]	0.0
	13	1	-0.[illegible]	0.0	0.0	0.0	-0.[illegible]	0.0
		2	0.[illegible]	0.0	0.0	0.0	0.[illegible]	0.0
		3	-0.[illegible]	0.0	0.0	0.0	-0.[illegible]	0.0
		4	-0.[illegible]	0.0	0.0	0.0	-0.[illegible]	0.0
		5	-0.[illegible]	0.0	0.0	0.0	0.[illegible]	0.0
		6	-0.[illegible]	0.0	0.0	0.0	-0.[illegible]	0.0
		7	-0.[illegible]	0.0	0.0	0.0	-0.[illegible]	0.0
		8	0.[illegible]	0.0	0.0	0.0	0.[illegible]	0.0
		9	-0.[illegible]	0.0	0.0	0.0	-0.[illegible]	0.0
	12	1	0.[illegible]	0.0	0.0	0.0	-0.[illegible]	0.0
		2	-0.[illegible]	0.0	0.0	0.0	0.[illegible]	0.0
		3	0.[illegible]	0.0	0.0	0.0	-0.[illegible]	0.0
		4	0.[illegible]	0.0	0.0	0.0	-0.[illegible]	0.0
		5	0.[illegible]	0.0	0.0	0.0	0.[illegible]	0.0
		6	0.[illegible]	0.0	0.0	0.0	0.[illegible]	0.0
		7	-0.[illegible]	0.0	0.0	0.0	0.[illegible]	0.0
		8	0.[illegible]	0.0	0.0	0.0	0.[illegible]	0.0
		9	0.[illegible]	0.0	0.0	0.0	-0.[illegible]	0.0
	11	1	-0.[illegible]	0.0	0.0	0.0	-0.[illegible]	0.0
		2	0.[illegible]	0.0	0.0	0.0	-0.[illegible]	0.0
		3	-0.[illegible]	0.0	0.0	0.0	-0.[illegible]	0.0
		4	-0.[illegible]	0.0	0.0	0.0	0.[illegible]	0.0
		5	-0.[illegible]	0.0	0.0	0.0	0.[illegible]	0.0
		6	-0.[illegible]	0.0	0.0	0.0	0.[illegible]	0.0
		7	0.[illegible]	0.0	0.0	0.0	0.[illegible]	0.0
		8	0.[illegible]	0.0	0.0	0.0	0.[illegible]	0.0
		9	-0.[illegible]	0.0	0.0	0.0	-0.[illegible]	0.0
	10	1	0.[illegible]	0.0	0.0	0.0	-0.[illegible]	0.0
		2	-0.[illegible]	0.0	0.0	0.0	-0.[illegible]	0.0
		3	0.[illegible]	0.0	0.0	0.0	-0.[illegible]	0.0
		4	0.[illegible]	0.0	0.0	0.0	0.[illegible]	0.0
		5	0.[illegible]	0.0	0.0	0.0	0.[illegible]	0.0
		6	0.[illegible]	0.0	0.0	0.0	0.[illegible]	0.0
		7	-0.[illegible]	0.0	0.0	0.0	0.[illegible]	0.0
		8	-0.[illegible]	0.0	0.0	0.0	0.[illegible]	0.0
		9	0.[illegible]	0.0	0.0	0.0	0.[illegible]	0.0
	9	1	-0.[illegible]	0.0	0.0	0.0	-0.[illegible]	0.0
		2	0.[illegible]	0.0	0.0	0.0	-0.[illegible]	0.0
		3	-0.[illegible]	0.0	0.0	0.0	-0.[illegible]	0.0
		4	-0.[illegible]	0.0	0.0	0.0	0.[illegible]	0.0
		5	-0.[illegible]	0.0	0.0	0.0	0.[illegible]	0.0
		6	-0.[illegible]	0.0	0.0	0.0	0.[illegible]	0.0
		7	0.[illegible]	0.0	0.0	0.0	0.[illegible]	0.0
		8	0.[illegible]	0.0	0.0	0.0	0.[illegible]	0.0
		9	-0.[illegible]	0.0	0.0	0.0	0.[illegible]	0.0
	8	1	0.[illegible]	0.0	0.0	0.0	-0.[illegible]	0.0
		2	-0.[illegible]	0.0	0.0	0.0	-0.[illegible]	0.0
		3	0.[illegible]	0.0	0.0	0.0	0.[illegible]	0.0
		4	0.[illegible]	0.0	0.0	0.0	0.[illegible]	0.0
		5	0.[illegible]	0.0	0.0	0.0	0.[illegible]	0.0

EIGENSOLUTION TIME LOG

APPENDIX G

TYPICAL INPUT AND OUTPUT OF STRUDL-DYNAL FOR SKEW A ORTHOTROPIC PLATE

```
STRUDL 'NABIL' 'SKEW SLAB BRIDGE'
*****************************************************************
*                                                               *
*   MCAUTO STRUDL                          RELEASE 5.0   OCT 1984 *
*   MCAUTO STRUDL INTERACTIVE GRAPHICS     RELEASE 4.0            *
*   MCAUTO STRUDL BATCH GRAPHICS           RELEASE 2.0            *
*   MCAUTO STRUDL DYNAL                    RELEASE 7.0            *
*   MCAUTO STRUDL DESIGN GROUP             RELEASE 2.0            *
*   MCAUTO STRUDL RECON                    RELEASE 2.0            *
*   MCAUTO STRUDL NONLINEAR                RELEASE 2.0            *
*   MCAUTO STRUDL TOWER                    RELEASE 2.0            *
*   MCAUTO STRUDL DANOS                    RELEASE 3.0            *
*                                                               *
*                                                               *
*                    TIME 15:04:47,  8/23/85                    *
*                                                               *
*                  DATA POOL SIZE   30640 BYTES                 *
*                                                               *
*****************************************************************


TYPE SPACE FRAME

UNITS INCHES CYCLES SECONDS KIP DEGREE

JOINT COORDINATES

1 0.0 0.0 0.0

2 15.554 15.554 0.0

3 31.108 31.108

4 46.662 46.662

5 62.216 62.216

6 77.7 77.77
```

8 22.0 0.0
9 37.554 15.554
10 53.108 31.108
11 68.662 46.662
12 84.216 62.216

13 99.77 77.77
14 115.324 93.324
15 44.0 0.0
16 59.554 15.554
17 75.108 31.108
18 90.662 46.662
19 106.216 62.216
20 121.77 77.77
21 137.324 93.324
22 66.000 0.0
23 81.554 15.554
24 97.108 31.108
25 112.662 46.662
26 128.216 62.216
27 143.770 77.77
28 159.324 93.324
29 88.00 0.0
30 103.554 15.554
31 119.108 31.108

7 14 13 20 21

8 13 12 19 20

9 12 11 18 19

10 11 10 17 18

11 10 9 16 17

12 9 8 15 16

13 16 15 22 23

14 17 16 23 24

15 18 17 24 25

16 19 18 25 26

17 20 19 26 27

18 21 20 27 28

19 28 27 34 35

20 27 26 33 34

21 26 25 32 33

22 25 24 31 32

23 24 23 30 31

24 23 22 29 30

25 30 29 36 37

26 31 30 37 38

27 32 31 38 39

28 33 32 39 40

29 34 33 40 41

30 35 34 41 42

```
   33 150.216 62.216
   34 165.77 77.77
   35 181.324 93.324
   36 110.00 0.0
   37 125.554 15.554
```



```
   38 141.108 31.108
   39 156.662 46.662
   40 172.216 62.216
   41 187.770 77.77
   42 203.324 93.324
   43 132.00 0.0
   44 147.554 15.554
   45 163.108 31.108
   46 178.662 46.662
   47 194.216 62.216
   48 209.77 77.77
   49 225.324 93.324
   SUPPORT 1 TO 7  43 TO 49
   ELEMENT INCIDENCE
   1 2 1 8 9
   2 3 2 9 10
   3 4 3 10 11
   4 5 4 11 12
   5 6 5 12 13
```

32 41 40 47 48

33 40 39 46 47

34 39 38 45 46

35 38 37 44 45

36 37 36 43 44

PLOT FORMAT ORIANTATION STANDARD

PLOT PLANE XY THROUGH 11

23-AUG-1985 15:07

_OSA1:[ENGR]GRACE.DAT;1

HORIZONTAL SCALE 20.0000 UNITS PER INCH

VERTICAL SCALE 20.0000 UNITS PER INCH

ORIENTATION

X
*
*
*
*
*****Y

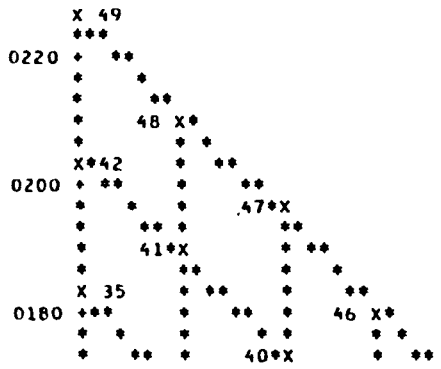

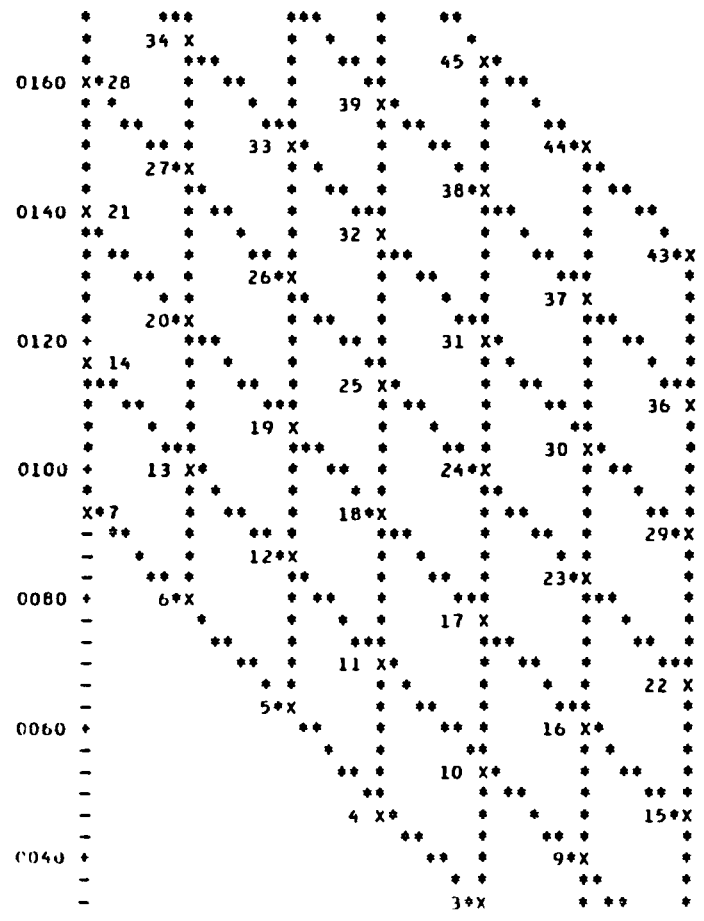

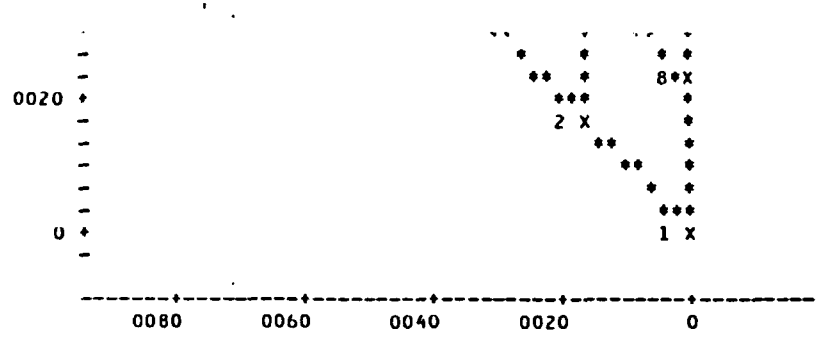


```
ELEMENT PROPERTIES
1 TO 36 TYPE 'PBSQ2' THI 3.4
CONSTANTS
DENSITY 0.20 ALL
E 3600.0 ALL
G 1565.0 ALL
POISSON 0.15 ALL
UNITS CYCLES
JOINT RELEASES
1 TO 7 MOM Y TH1 45.0
43 TO 49 MOM Y TH1 45.0
INERTIA OF JOINTS LUMPED
ASSEMBLE FOR DYNAMICS OMIT REDUCE BAND
```

BEFORE RESEQUENCING

MAXIMUM BANDWIDTH EQUALS 9 JOINTS

PROFILE EQUALS 385 JOINTS

ORIGINAL JOINT SEQUENCE (FREE AND RELEASED JOINTS)

1	2	3	4	5	6	7	8	9	10
11	12	13	14	15	16	17	18	19	20
21	22	23	24	25	26	27	28	29	30
31	32	33	34	35	36	37	38	39	40
41	42	43	44	45	46	47	48	49	

AFTER RESEQUENCING

MAXIMUM BANDWIDTH EQUALS 9 JOINTS

PROFILE EQUALS 385 JOINTS

JOINT ORDER AFTER RESEQUENCING (FREE AND RELEASED JOINTS)

1	2	3	4	5	6	7	8	9	10
11	12	13	14	15	16	17	18	19	20
21	22	23	24	25	26	27	28	29	30
31	32	33	34	35	36	37	38	39	40
41	42	43	44	45	46	47	48	49	

```
INDEPEN DEGREE OF FREEDOM JOINT
8 TO 42 DISP Z
CONDENSE DYNAMIC MATRICES
```

CONDENSATION CORRESPONDENCE TABLE
INDEPENDENT COORDINATES

JOINT ID	XT	YT	ZT	XR	YR	ZR	JOINT ID	XT	YT	ZT	XR	YR	ZR
8			1				9			2			
10			3				11			4			
12			5				13			6			
14			7				15			8			
16			9				17			10			
18			11				19			12			
20			13				21			14			
22			15				23			16			
24			17				25			18			
26			19				27			20			
28			21				29			22			
30			23				31			24			
32			25				33			26			
34			27				35			28			
36			29				37			30			
38			31				39			32			
40			33				41			34			
42			35										

CONDENSATION CORRESPONDENCE TABLE
DEPENDENT COORDINATES

JOINT ID	XT	YT	ZT	XR	YR	ZR	JOINT ID	XT	YT	ZT	XR	YR	ZR

1				1		2				2		
3				3		4				4		
5				5		6				6		
7				7		8	8	9	10	11	12	
9	13	14	15	16	17	10	18	19	20	21	22	
11	23	24	25	26	27	12	28	29	30	31	32	
13	33	34	35	36	37	14	38	39	40	41	42	
15	43	44	45	46	47	16	48	49	50	51	52	
17	53	54	55	56	57	18	58	59	60	61	62	
19	63	64	65	66	67	20	68	69	70	71	72	
21	73	74	75	76	77	22	78	79	80	81	82	

JOINT ID	XT	YT	ZT	XR	YR	ZR	JOINT ID	XT	YT	ZT	XR	YR	ZR
23	83	84		85	86	87	24	88	89		90	91	92
25	93	94		95	96	97	26	98	99		100	101	102
27	103	104		105	106	107	28	108	109		110	111	112
29	113	114		115	116	117	30	118	119		120	121	122
31	123	124		125	126	127	32	128	129		130	131	132
33	133	134		135	136	137	34	138	139		140	141	142
35	143	144		145	146	147	36	148	149		150	151	152
37	153	154		155	156	157	38	158	159		160	161	162
39	163	164		165	166	167	40	168	169		170	171	172
41	173	174		175	176	177	42	178	179		180	181	182
43					183		44					184	
45					185		46					186	
47					187		48					188	
49					189								

UNITS CYCLES SECONDS

MODAL ANALYSIS HOW 5

**** STRUDL MESSAGE - ALL EIGENVALUES ARE COMPUTED.
EIGENVECTORS COMPUTED FOR FIRST 5 EIGENVALUES

****
RESULTS OF LATEST ANALYSIS
****

PROBLEM - NABIL TITLE - SKEW SLAB BRIDGE

ACTIVE UNITS INCH KIPS CYC. FAHR SEC. LBM

EIGENVALUES

MODE	EIGENVALUE	FREQUENCY	PERIOD
1	0.613146E+03	0.247618E+02	0.403848E-01
2	0.678898E+03	0.260557E+02	0.383794E-01
3	0.173902E+04	0.417016E+02	0.239799E-01
4	0.364407E+04	0.603661E+02	0.165656E-01
5	0.509647E+04	0.713896E+02	0.140076E-01
6	0.591189E+04	0.768888E+02	0.130058E-01
7	0.838497E+04	0.915695E+02	0.109207E-01
8	0.101383E+05	0.100689E+03	0.993156E-02
9	0.136498E+05	0.116832E+03	0.855928E-02
10	0.171297E+05	0.130881E+03	0.764055E-02
11	0.220062E+05	0.148345E+03	0.674105E-02
12	0.226318E+05	0.150439E+03	0.664722E-02
13	0.252742E+05	0.158979E+03	0.629015E-02
14	0.293495E+05	0.171317E+03	0.583713E-02
15	0.349257E+05	0.186884E+03	0.535091E-02
16	0.374389E+05	0.193491E+03	0.516819E-02
17	0.414236E+05	0.203528E+03	0.491333E-02
18	0.514092E+05	0.226736E+03	0.441042E-02
19	0.527682E+05	0.229713E+03	0.435325E-02
20	0.579837E+05	0.240798E+03	0.415286E-02
21	0.627515E+05	0.250502E+03	0.399198E-02
22	0.666672E+05	0.258200E+03	0.387297E-02
23	0.743738E+05	0.272715E+03	0.366684E-02

25	0.835729E+05	0.289090E+03	0.345913E-02
26	0.851035E+05	0.291725E+03	0.342789E-02
27	0.907398E+05	0.301230E+03	0.331972E-02
28	0.938352E+05	0.306325E+03	0.326450E-02
29	0.112461E+06	0.335353E+03	0.298194E-02
30	0.112997E+06	0.336151E+03	0.297485E-02
31	0.119090E+06	0.345094E+03	0.289776E-02
32	0.128024E+06	0.357805E+03	0.279482E-02
33	0.138070E+06	0.371577E+03	0.269123E-02
34	0.150022E+06	0.387326E+03	0.258180E-02
35	0.156186E+06	0.395204E+03	0.253034E-02

LIST DYNAMIC NORMALIZED MODES 5 BY JOINT ALL

****
RESULTS OF LATEST ANALYSIS
****

PROBLEM - NABIL TITLE - SKEW SLAB BRIDGE

ACTIVE UNITS INCH KIPS CYC. FAHR SEC. LBM

NORMALIZED EIGENVECTORS

MODE 1 MAXIMUM VALUE (IN INTERNAL UNITS) IS -4.362455E-01 AT JOINT 29 IN DIRECTION DISP Z

JOINT		DISPLACEMENT			ROTATION		
		X DISP.	Y DISP.	Z DISP.	X ROT.	Y ROT.	Z ROT.
1	GLOBAL	0.0000000	0.0000000	0.0000000	0.0000000	-0.0004489	0.0000000
2	GLOBAL	0.0000000	0.0000000	0.0000000	0.0000000	-0.0009567	0.0000000
3	GLOBAL	0.0000000	0.0000000	0.0000000	0.0000000	-0.0013929	0.0000000
4	GLOBAL	0.0000000	0.0000000	0.0000000	0.0000000	-0.0014611	0.0000000
5	GLOBAL	0.0000000	0.0000000	0.0000000	0.0000000	-0.0013271	0.0000000
6	GLOBAL	0.0000000	0.0000000	0.0000000	0.0000000	-0.0010248	0.0000000
7	GLOBAL	0.0000000	0.0000000	0.0000000	0.0000000	-0.0035484	0.0000000
8	GLOBAL	0.0000000	0.0000000	0.1341274	-0.0010935	-0.0019142	0.0000000
9	GLOBAL	0.0000000	0.0000000	0.2051122	-0.0020069	-0.0023560	0.0000000
10	GLOBAL	0.0000000	0.0000000	0.2289370	-0.0024738	-0.0022557	0.0000000
11	GLOBAL	0.0000000	0.0000000	0.2141957	-0.0024106	-0.0019355	0.0000000
12	GLOBAL	0.0000000	0.0000000	0.2000232	-0.0020956	-0.0019159	0.0000000
13	GLOBAL	0.0000000	0.0000000	0.2595682	-0.0018446	-0.0031326	0.0000000
14	GLOBAL	0.0000000	0.0000000	0.5793134	0.0000315	-0.0044088	0.0000000
15	GLOBAL	0.0000000	0.0000000	0.5204008	-0.0021598	-0.0033994	0.0000000
16	GLOBAL	0.0000000	0.0000000	0.5792282	-0.0026294	-0.0027190	0.0000000
17	GLOBAL	0.0000000	0.0000000	0.5395411	-0.0025662	-0.0019089	0.0000000
18	GLOBAL	0.0000000					

20	GLOBAL	0.0000000	0.0000000	0.6885368	0.0004756	-0.0025117	0.0000000
21	GLOBAL	0.0000000	0.0000000	0.9973981	0.0019357	-0.0013525	0.0000000
22	GLOBAL	0.0000000	0.0000000	0.9296590	-0.0026920	-0.0021766	0.0000000
23	GLOBAL	0.0000000	0.0000000	0.8220967	-0.0021686	-0.0005715	0.0000000
24	GLOBAL	0.0000000	0.0000000	0.6646527	-0.0012131	0.0001902	0.0000000
25	GLOBAL	0.0000000	0.0000000	0.5943004	-0.0000021	0.0000035	0.0000000
26	GLOBAL	0.0000000	0.0000000	0.6636025	0.0012076	-0.0001854	0.0000000
27	GLOBAL	0.0000000	0.0000000	0.8201500	0.0021612	0.0005718	0.0000000
28	GLOBAL	0.0000000	0.0000000	0.9271765	0.0026836	0.0021712	0.0000000
29	GLOBAL	0.0000000	0.0000000	1.0000000	-0.0019436	0.0013565	0.0000000
30	GLOBAL	0.0000000	0.0000000	0.6898974	-0.0004811	0.0025196	0.0000000

JOINT		DISPLACEMENT			ROTATION		
		X DISP.	Y DISP.	Z DISP.	X ROT.	Y ROT.	Z ROT.
31	GLOBAL	0.0000000	0.0000000	0.5004438	0.0010494	0.0020909	0.0000000
32	GLOBAL	0.0000000	0.0000000	0.4760798	0.0019582	0.0016170	0.0000000
33	GLOBAL	0.0000000	0.0000000	0.5383360	0.0025595	0.0019061	0.0000000
34	GLOBAL	0.0000000	0.0000000	0.5777455	0.0026218	0.0027125	0.0000000
35	GLOBAL	0.0000000	0.0000000	0.5189824	0.0021535	0.0033903	0.0000000
36	GLOBAL	0.0000000	0.0000000	0.5808172	-0.0000358	0.0044199	0.0000000
37	GLOBAL	0.0000000	0.0000000	0.2598387	0.0018411	0.0031394	0.0000000
38	GLOBAL	0.0000000	0.0000000	0.1994605	0.0020950	0.0019174	0.0000000
39	GLOBAL	0.0000000	0.0000000	0.2137047	0.0024051	0.0019307	0.0000000
40	GLOBAL	0.0000000	0.0000000	0.2283725	0.0024674	0.0022504	0.0000000
41	GLOBAL	0.0000000	0.0000000	0.2045643	0.0020014	0.0023499	0.0000000
42	GLOBAL	0.0000000	0.0000000	0.1337534	0.0010904	0.0019089	0.0000000
43	GLOBAL	0.0000000	0.0000000	0.0000000	0.0000000	0.0035588	0.0000000
44	GLOBAL	0.0000000	0.0000000	0.0000000	0.0000000	0.0010293	0.0000000
45	GLOBAL	0.0000000	0.0000000	0.0000000	0.0000000	0.0013225	0.0000000
46	GLOBAL	0.0000000	0.0000000	0.0000000	0.0000000	0.0014580	0.0000000
47	GLOBAL	0.0000000	0.0000000	0.0000000	0.0000000	0.0013892	0.0000000
48	GLOBAL	0.0000000	0.0000000	0.0000000	0.0000000	0.0009541	0.0000000
49	GLOBAL	0.0000000	0.0000000	0.0000000	0.0000000	0.0004476	0.0000000

MODE 2 MAXIMUM VALUE (IN INTERNAL UNITS) IS -5.249441E-01 AT JOINT 21 IN DIRECTION DISP Z

JOINT		DISPLACEMENT			ROTATION		
		X DISP.	Y DISP.	Z DISP.	X ROT.	Y ROT.	Z ROT.
1	GLOBAL	0.0000000	0.0000000	0.0000000	0.0000000	0.0005531	0.0000000
2	GLOBAL	0.0000000	0.0000000	0.0000000	0.0000000	0.0011141	0.0000000
3	GLOBAL	0.0000000	0.0000000	0.0000000	0.0000000	0.0014906	0.0000000
4	GLOBAL	0.0000000	0.0000000	0.0000000	0.0000000	0.0013221	0.0000000
5	GLOBAL	0.0000000	0.0000000	0.0000000	0.0000000	0.0007702	0.0000000
6	GLOBAL	0.0000000	0.0000000	0.0000000	0.0000000	0.0002989	0.0000000
7	GLOBAL	0.0000000	0.0000000	0.0000000	0.0000000	-0.0029835	0.0000000

9	GLOBAL	0.0000000	0.0000000	-0.2237696	0.0022957	0.0024717	0.0000000
10	GLOBAL	0.0000000	0.0000000	-0.2195177	0.0025991	0.0019622	0.0000000
11	GLOBAL	0.0000000	0.0000000	-0.1507479	0.0021228	0.0009956	0.0000000
12	GLOBAL	0.0000000	0.0000000	-0.0430389	0.0011359	-0.0002483	0.0000000
13	GLOBAL	0.0000000	0.0000000	0.1259483	0.0000786	-0.0024011	0.0000000
14	GLOBAL	0.0000000	0.0000000	0.5451343	0.0013385	-0.0044633	0.0000000
15	GLOBAL	0.0000000	0.0000000	-0.5797123	0.0025949	0.0035991	0.0000000
16	GLOBAL	0.0000000	0.0000000	-0.5852216	0.0031083	0.0023780	0.0000000
17	GLOBAL	0.0000000	0.0000000	-0.4350099	0.0029135	0.0008288	0.0000000
18	GLOBAL	0.0000000	0.0000000	-0.1880378	0.0021476	-0.0006411	0.0000000
19	GLOBAL	0.0000000	0.0000000	0.1212436	0.0015310	-0.0020037	0.0000000

JOINT		DISPLACEMENT			ROTATION		
		X DISP.	Y DISP.	Z DISP.	X ROT.	Y ROT.	Z ROT.
20	GLOBAL	0.0000000	0.0000000	0.5229210	0.0019751	-0.0028684	0.0000000
21	GLOBAL	0.0000000	0.0000000	1.0000000	0.0030336	-0.0018291	0.0000000
22	GLOBAL	0.0000000	0.0000000	-0.9841622	0.0034258	0.0019071	0.0000000
23	GLOBAL	0.0000000	0.0000000	-0.7442301	0.0030587	-0.0002373	0.0000000
24	GLOBAL	0.0000000	0.0000000	-0.3833370	0.0024498	-0.0015027	0.0000000
25	GLOBAL	0.0000000	0.0000000	0.0004106	0.0021416	-0.0018250	0.0000000
26	GLOBAL	0.0000000	0.0000000	0.3843906	0.0024531	-0.0015039	0.0000000
27	GLOBAL	0.0000000	0.0000000	0.7457683	0.0030639	-0.0002371	0.0000000
28	GLOBAL	0.0000000	0.0000000	0.9860590	0.0034319	0.0019110	0.0000000
29	GLOBAL	0.0000000	0.0000000	-0.9980409	0.0030287	-0.0018258	0.0000000
30	GLOBAL	0.0000000	0.0000000	-0.5217424	0.0019730	-0.0028630	0.0000000
31	GLOBAL	0.0000000	0.0000000	-0.1205767	0.0015325	-0.0019997	0.0000000
32	GLOBAL	0.0000000	0.0000000	0.1887108	0.0021517	-0.0006391	0.0000000
33	GLOBAL	0.0000000	0.0000000	0.4359642	0.0029190	0.0008314	0.0000000
34	GLOBAL	0.0000000	0.0000000	0.5863768	0.0031140	0.0023830	0.0000000
35	GLOBAL	0.0000000	0.0000000	0.5808136	0.0025997	0.0036061	0.0000000
36	GLOBAL	0.0000000	0.0000000	-0.5440601	0.0013368	-0.0044543	0.0000000
37	GLOBAL	0.0000000	0.0000000	-0.1256703	0.0000807	-0.0023941	0.0000000
38	GLOBAL	0.0000000	0.0000000	0.0432390	0.0011393	-0.0002464	0.0000000
39	GLOBAL	0.0000000	0.0000000	0.1511011	0.0021272	0.0009982	0.0000000
40	GLOBAL	0.0000000	0.0000000	0.2199621	0.0026041	0.0019663	0.0000000
41	GLOBAL	0.0000000	0.0000000	0.2241992	0.0023000	0.0024765	0.0000000
42	GLOBAL	0.0000000	0.0000000	0.1566413	0.0013132	0.0021933	0.0000000
43	GLOBAL	0.0000000	0.0000000	0.0000000	0.0000000	-0.0029791	0.0000000
44	GLOBAL	0.0000000	0.0000000	0.0000000	0.0000000	0.0002935	0.0000000
45	GLOBAL	0.0000000	0.0000000	0.0000000	0.0000000	0.0007729	0.0000000
46	GLOBAL	0.0000000	0.0000000	0.0000000	0.0000000	0.0013249	0.0000000
47	GLOBAL	0.0000000	0.0000000	0.0000000	0.0000000	0.0014935	0.0000000
48	GLOBAL	0.0000000	0.0000000	0.0000000	0.0000000	0.0011162	0.0000000
49	GLOBAL	0.0000000	0.0000000	0.0000000	0.0000000	0.0005541	0.0000000

MODE 3 MAXIMUM VALUE (IN INTERNAL UNITS) IS -5.139022E-01 AT JOINT 22 IN DIRECTION DISP Z

JOINT		DISPLACEMENT			ROTATION		
		X DISP.	Y DISP.	Z DISP.	X ROT.	Y ROT.	Z ROT.
1	GLOBAL	0.0000000	0.0000000	0.0000000	0.0000000	-0.0013104	0.0000000
2	GLOBAL	0.0000000	0.0000000	0.0000000	0.0000000	-0.0020741	0.0000000
3	GLOBAL	0.0000000	0.0000000	0.0000000	0.0000000	-0.0018380	0.0000000
4	GLOBAL	0.0000000	0.0000000	0.0000000	0.0000000	-0.0002365	0.0000000
5	GLOBAL	0.0000000	0.0000000	0.0000000	0.0000000	0.0016027	0.0000000
6	GLOBAL	0.0000000	0.0000000	0.0000000	0.0000000	0.0025969	0.0000000
7	GLOBAL	0.0000000	0.0000000	0.0000000	0.0000000	0.0006154	0.0000000
8	GLOBAL	0.0000000	0.0000000	0.2884207	-0.0026912	-0.0036225	0.0000000

JOINT		DISPLACEMENT			ROTATION		
		X DISP.	Y DISP.	Z DISP.	X ROT.	Y ROT.	Z ROT.
9	GLOBAL	0.0000000	0.0000000	0.3057021	-0.0037625	-0.0026167	0.0000000
10	GLOBAL	0.0000000	0.0000000	0.1315865	-0.0027913	-0.0000210	0.0000000
11	GLOBAL	0.0000000	0.0000000	-0.1309723	-0.0001243	0.0024731	0.0000000
12	GLOBAL	0.0000000	0.0000000	-0.3101279	0.0025675	0.0032594	0.0000000
13	GLOBAL	0.0000000	0.0000000	-0.2674580	0.0036604	0.0014519	0.0000000
14	GLOBAL	0.0000000	0.0000000	0.1245852	0.0042386	-0.0023716	0.0000000
15	GLOBAL	0.0000000	0.0000000	0.8334723	-0.0047458	-0.0034710	0.0000000
16	GLOBAL	0.0000000	0.0000000	0.4984599	-0.0047904	0.0003022	0.0000000
17	GLOBAL	0.0000000	0.0000000	-0.0870962	-0.0030519	0.0031239	0.0000000
18	GLOBAL	0.0000000	0.0000000	-0.5793295	0.0000256	0.0035001	0.0000000
19	GLOBAL	0.0000000	0.0000000	-0.6626256	0.0029100	0.0012918	0.0000000
20	GLOBAL	0.0000000	0.0000000	-0.2317030	0.0046125	-0.0021350	0.0000000
21	GLOBAL	0.0000000	0.0000000	0.5962937	0.0055927	-0.0041055	0.0000000
22	GLOBAL	0.0000000	0.0000000	1.0000000	-0.0059407	0.0012091	0.0000000
23	GLOBAL	0.0000000	0.0000000	0.2038440	-0.0051510	0.0035670	0.0000000
24	GLOBAL	0.0000000	0.0000000	-0.5403695	-0.0031361	0.0028180	0.0000000
25	GLOBAL	0.0000000	0.0000000	-0.8424065	-0.0000024	-0.0000034	0.0000000
26	GLOBAL	0.0000000	0.0000000	-0.5403123	0.0031322	-0.0028209	0.0000000
27	GLOBAL	0.0000000	0.0000000	0.2036778	0.0051480	-0.0035666	0.0000000
28	GLOBAL	0.0000000	0.0000000	0.9994804	0.0059377	-0.0012084	0.0000000
29	GLOBAL	0.0000000	0.0000000	0.5966490	-0.0055944	0.0041072	0.0000000
30	GLOBAL	0.0000000	0.0000000	-0.2314576	-0.0046130	0.0021337	0.0000000
31	GLOBAL	0.0000000	0.0000000	-0.6620234	-0.0029110	-0.0012981	0.0000000
32	GLOBAL	0.0000000	0.0000000	-0.5786968	-0.0000315	-0.0035018	0.0000000
33	GLOBAL	0.0000000	0.0000000	-0.0869436	0.0030485	-0.0031223	0.0000000
34	GLOBAL	0.0000000	0.0000000	0.4982091	0.0047877	-0.0003019	0.0000000
35	GLOBAL	0.0000000	0.0000000	0.8330252	0.0047432	0.0034693	0.0000000
36	GLOBAL	0.0000000	0.0000000	0.1247228	-0.0042361	0.0023730	0.0000000
37	GLOBAL	0.0000000	0.0000000	-0.2669165	-0.0036537	-0.0014552	0.0000000
38	GLOBAL	0.0000000	0.0000000	-0.3089695	-0.0025719	-0.0032592	0.0000000
39	GLOBAL	0.0000000	0.0000000	-0.1306916	0.0001240	-0.0024675	0.0000000
40	GLOBAL	0.0000000	0.0000000	0.1315392	0.0027897	0.0000215	0.0000000
41	GLOBAL	0.0000000	0.0000000	0.3055386	0.0037604	0.0026154	0.0000000
42	GLOBAL	0.0000000	0.0000000	0.2884207	-0.0026912	-0.0036225	0.0000000

44	GLOBAL	0.0000000	0.0000000	0.0000000	0.0000000	-0.0025969	0.0000000
45	GLOBAL	0.0000000	0.0000000	0.0000000	0.0000000	-0.0015957	0.0000000
46	GLOBAL	0.0000000	0.0000000	0.0000000	0.0000000	0.0002357	0.0000000
47	GLOBAL	0.0000000	0.0000000	0.0000000	0.0000000	0.0018371	0.0000000
48	GLOBAL	0.0000000	0.0000000	0.0000000	0.0000000	0.0020730	0.0000000
49	GLOBAL	0.0000000	0.0000000	0.0000000	0.0000000	0.0013096	0.0000000

MODE 4 MAXIMUM VALUE (IN INTERNAL UNITS) IS 6.565287E-01 AT JOINT 35 IN DIRECTION DISP Z

JOINT		DISPLACEMENT			ROTATION		
		X DISP.	Y DISP.	Z DISP.	X ROT.	Y ROT.	Z ROT.

JOINT		DISPLACEMENT			ROTATION		
		X DISP.	Y DISP.	Z DISP.	X ROT.	Y ROT.	Z ROT.
1	GLOBAL	0.0000000	0.0000000	0.0000000	0.0000000	0.0024484	0.0000000
2	GLOBAL	0.0000000	0.0000000	0.0000000	0.0000000	0.0032473	0.0000000
3	GLOBAL	0.0000000	0.0000000	0.0000000	0.0000000	0.0022198	0.0000000
4	GLOBAL	0.0000000	0.0000000	0.0000000	0.0000000	-0.0000965	0.0000000
5	GLOBAL	0.0000000	0.0000000	0.0000000	0.0000000	-0.0009739	0.0000000
6	GLOBAL	0.0000000	0.0000000	0.0000000	0.0000000	0.0000727	0.0000000
7	GLOBAL	0.0000000	0.0000000	0.0000000	0.0000000	0.0036863	0.0000000
8	GLOBAL	0.0000000	0.0000000	-0.4441501	0.0044119	0.0049631	0.0000000
9	GLOBAL	0.0000000	0.0000000	-0.3865919	0.0050389	0.0024761	0.0000000
10	GLOBAL	0.0000000	0.0000000	-0.1057527	0.0026663	-0.0007907	0.0000000
11	GLOBAL	0.0000000	0.0000000	0.1063649	-0.0006531	-0.0015286	0.0000000
12	GLOBAL	0.0000000	0.0000000	0.0403083	-0.0015081	0.0005752	0.0000000
13	GLOBAL	0.0000000	0.0000000	-0.2028449	0.0004405	0.0031246	0.0000000
14	GLOBAL	0.0000000	0.0000000	-0.4605951	0.0001672	0.0019911	0.0000000
15	GLOBAL	0.0000000	0.0000000	-0.9997525	0.0060960	0.0016702	0.0000000
16	GLOBAL	0.0000000	0.0000000	-0.3882183	0.0042726	-0.0028489	0.0000000
17	GLOBAL	0.0000000	0.0000000	0.1846015	0.0006886	-0.0029816	0.0000000
18	GLOBAL	0.0000000	0.0000000	0.2167386	-0.0023799	0.0003014	0.0000000
19	GLOBAL	0.0000000	0.0000000	-0.2103966	-0.0022588	0.0026402	0.0000000
20	GLOBAL	0.0000000	0.0000000	-0.5127647	-0.0002636	0.0005314	0.0000000
21	GLOBAL	0.0000000	0.0000000	-0.2071430	0.0014264	-0.0053994	0.0000000
22	GLOBAL	0.0000000	0.0000000	-0.6742787	0.0047763	-0.0059875	0.0000000
23	GLOBAL	0.0000000	0.0000000	0.1946001	0.0017592	-0.0046310	0.0000000
24	GLOBAL	0.0000000	0.0000000	0.4235371	-0.0017189	-0.0000273	0.0000000
25	GLOBAL	0.0000000	0.0000000	-0.0000318	-0.0035051	0.0023818	0.0000000
26	GLOBAL	0.0000000	0.0000000	-0.4236227	-0.0017192	-0.0000273	0.0000000
27	GLOBAL	0.0000000	0.0000000	-0.1946362	0.0017595	-0.0046321	0.0000000
28	GLOBAL	0.0000000	0.0000000	0.6744435	0.0047774	-0.0059890	0.0000000
29	GLOBAL	0.0000000	0.0000000	0.2070822	0.0014264	-0.0053979	0.0000000
30	GLOBAL	0.0000000	0.0000000	0.5126650	-0.0002634	0.0005311	0.0000000
31	GLOBAL	0.0000000	0.0000000	0.2103725	-0.0022594	0.0026394	0.0000000
32	GLOBAL	0.0000000	0.0000000	-0.2167846	-0.0023804	0.0003013	0.0000000
33	GLOBAL	0.0000000	0.0000000	-0.1946374	0.0006988	-0.0029822	0.0000000

BIBLIOGRAPHY

1. Ayre, R.S., Ford, G. and Jacobsen, L.S., "Transverse Vibration of a Two-Span Beam Under Action of a Moving Constant Force," The ASME, Journal of Applied Mechanics, March 1950, pp. 1-12.

2. Baldwin, J.W., Jr., Salane, H.J. and Duffield, R.C., "Fatigue Test of a Three-Span Composite Highway Bridge," Department of Civil Engineering, University of Missouri-Columbia, Columbia, Missouri, June 1978.

3. Barton, M.V., "Vibration of Rectangular and Skew Cantilever Plates," Journal of Applied Mechanics, June 1951.

4. Barton, M.V., "Vibration of Rectangular and Skew Plates Representing Idealized Missile Fins," Defense Research Laboratory, The University of Texas, DRL-222, CM-570, December 1949.

5. Bathe, K.J., Wilson, E.L. and Paterson, F.E., "A Structural Analysis Program for Static and Dynamic Response of Linear System," (SAP IV), Report #EERC 72-11, April 1974.

6. Billing, J.R., "Estimation of the Natural Frequencies of Continuous Multi-Span Bridges," Report No. RR219, Research and Development Division, Ministry of Transportation and Communications, Downsview, Ontario, Canada, January, 1979.

7. Campbell, T.I. and Siu, W.H., "Computation of Natural Frequencies of Skewed Slabs Using Equivalent Rectangular Slab Concept," Canadian Journal of Civil Engineering, Vol. 7, 1980, pp. 384-388.

8. Chladni, E.F.F., "Entdeckungen uber die Theorie des Klanges," Leipzig, 1787.

9. Csagoly P.F., Campbell, T.I. and Agarwall, A.C., "Bridge Vibration Study," RR181, Ministry of Transportation and Communications, Ontario, 1972, 30 pp.

10. Culver, C. and Coston, R., "Tests of Composite Beams with Stud Shear Connectors," Journal of Structural Division, Proceeding of ASCE, Vol. 87, No. ST1, February 1961.

11. Dalley, J.W. and Ripperger, E.A., "Experimental Values of Natural Frequencies for Skew and Rectangular Cantilever Plates," Defense Research Laboratory, The University of Texas, DRL-231, CF-1354, December, 1949.

12. Daniels, J. H. and Fisher, J.W., "Fatigue Behavior of Continuous Composite Beams," Department of Civil Engineering, Lehigh University, Bethlehem, Pennsylvania, Fritz Engineering Laboratory, Report No. 324.1, December 1966.

13. Dickinson, S.M., "The Flexural Vibration of Rectangular Orthotropic Plates," Journal of Applied Mechanics, ASME, March 1969, pp. 101-106.

14. Dickinson, S.M. and Warburton, G.B., "Natural Frequencies of Plate Systems Using the Edge Effect Method," Journal of Mechanical Engineering Science, Vol. 9, New York, 1967, pp. 318-324.

15. Dill, E.A. and Pister, K.S., "Vibration of Rectangular Plates and Plate Systems," Proceeding of Third National Congress of Applied Mechanics, ASME, 1958, pp. 122-132.

16. Elishakoff, I. and Sternberg, A., "Eigenfrequencies of Continuous Plates with Arbitrary Number of Equal Spans," Transaction of ASME, Journal of Applied Mechanics, Vol. 46, September 1979, pp. 656-662.

17. El-Sebakhy, I.S.A., "Behavior of Reinforced and Prestressed Waffle Slabs," Thesis presented to the University of Windsor, Windsor, Ontario, Canada, in Partial Fulfillment of the Requirements for the Degree of Master of Science in 1979.

18. El-Sebakhy, I.S.A., "Elastic and Ultimate Behavior of Waffle Slab Structures," Dissertation presented to the University of Windsor, Windsor, Ontario, Canada, in Partial Fulfillment of the Requirements for the Degree of Ph.D. in 1982.

19. El-Sebakhy, I.S.A. Grace, N.F. and Kennedy, J.B., "Behavior of Prestressed Rectangular and Skew Waffle Slabs Under Dynamic, Fatigue and Ultimate Loads," Under Preparation.

20. Fisher, J.W. and Viest, I.M., "Fatigue Life of Bridge Beams Subjected to Controlled Truck Traffic," International Association for Bridge and Structural Engineering, Rio de Janeiro, 1964.

21. Grace, N.F., "Effect of Prestressing the Deck in Continuous Bridge of Composite Construction," Thesis presented to the University of Windsor, Windsor, Ontario, Canada, in partial fulfillment of the requirements for the Degree of Master of Science, in 1981.

22. Grace, N.F. and Kennedy, J.B., "Dynamic Analysis of Orthotropic Plate Structures," Journal of Engineering Mechanics, ASCE, Vol. 111, No. 8, August, 1985. Paper No. 19922.

23. Grace, N.F. and Kennedy, J.B., "Dynamic-Fatigue Response of Continuous Composite Bridges,: Proceedings of Japan-U.S. Seminar on Composite Construction, Seattle, Washington, July 18-21, 1984.

24. Grace, N.F. and Kennedy, J.B., "Free Vibration of a Continuous Composite Bridge," Submitted for the Annual Conference of the Canadian Society of Civil Engineering, 1986.

25. Gupta, D.S., "Orthotropic Continuous Skew Plates," Dissertation Presented to the University of Windsor, Windsor, Canada, in Partial Fulfillment of the Requirement for the Degree of Ph.D. in 1974.

26. Gupta, D.S.R. and Kennedy, J.B., "Continuous Skew Orthogonal Plate Structures," Journal of the Structural Division, ASCE, Vol. 104, No. ST2, Paper 13566, February 1978, pp. 313-328.

27. Hearman, R.F.S., "The Frequency of Flexural Vibration of Rectangular Orthotropic Plates with Clamped or Supported Edges," Journal of Applied Mechanics, ASME, December, 1959, pp. 537-540.

28. Hearman, R.F.S., "On the Transverse Vibrations of Rectangular Orthotropic Plates," Journal of Applied Mechanics, Transaction of the ASME, June 1959.

29. Hoffman, W.H., Huffington, N.J. and Magness, L.S., "A Study of Orthogonal Stiffened Plates," Transaction of the ASCE, Journal of Applied Mechanics, Sept. 1956, pp. 343-350.

30. Housner, G.M. and Hudson, D.E., "Applied Mechanics - Dynamics," Van Nostrand, 1950.

31. Huang, T., "Dynamic Response of Three-Span Continuous Highway Bridges," Dissertation Presented to the University of Illinois, in Partial Fulfillment of the Requirement for the Degree of Ph.D., 1969.

32. Huang, T., "Vibration of Bridges," Shock and Vibration Digest, Vol. 8, No. 3, March 1976, pp. 61-76.

33. Huffington, N.J. and Hoppmann, I.I., "On the Transverse Vibrations of Rectangular Orthotropic Plates," Proceedings of the ASME, Series E, 1959, pp. 389-395.

34. Inglis, C.E., "A Mathematical Treatise on Vibrations in Railway Bridges," Cambridge University Press, London, 1934.

35. Kanazaw, T and Kawai, T. "On the Lateral Vibration of Anisotropic Rectangular Plates," Proceeding Second Japan National Congress for Applied Mechanics (1952), p. 333.

36. Kennedy, J.B. and Grace, N.F., "Prestressed Decks in Continuous Composite Bridges," ASCE J. of the Structural Division, Vol. 108 No. ST11, 1982, pp. 2394-2410.

37. Kennedy, J.B. and Grace, N.F., "Load Distribution in Continuous Composite Bridges," Canadian Journal of Civil Engineering, Vol. 10, No. 3, 1983, pp. 384-395.

38. Kennedy, J.B. and Bakht, B., "Feasibility of Waffle Slabs for Bridges," Canadian Journal of Civil Engineering, Vol. 10, No. 4, 1983, pp. 627-638.

39. Kennedy, J.B. and Iyengar, K.J., "Rigidities of Non-orthogonally Shaped Waffle Slabs," Journal of Structural Division, Proceedings of ASCE, Vol. 108, No ST10, October 1982.

40. King, J.P.C., Holowka, M., Dorton, R.A. and Agarwal, A.C., "Test Results from the Conestogo River Bridge," Bridge Engineering Volume 2, Proceeding of a Conference Conducted by the Transportation Research Board, September 25-27, 1978.

41. King, D.C., Slutter, R.G. and Driscoll, G.C., "Fatigue Strength of 1/2-Inch Diameter Stud Shear Connectors," Highway Research Record No. 103, Highway Research Board, 1965, pp. 78-106.

42. Kirk, C.L., "Vibration Characteristics of Stiffened Plates," Journal of Mechanical Engineering Science, Vol. 2, No. 3, 1960, pp. 242-253.

43. Laura, P.A. and Smith, G.A., "Vibration of Rib Stiffened Plates Carrying Concentrated Masses," Journal of the Acoustical Society of America, Vol. 43, 1968, p. 332-385.

44. Leckie, F.A., "Application of Transfer Matrices to Plate Vibration," Ingenieur-Archiv, Vol. 32, No. 2, 1963, pp. 100-111.

45. Leissa, A.W., "The Free Vibration of Rectangular Plates," Journal of Sound and Vibration, Vol. 3, No. 31, 1973, pp. 257-293.

46. Long, B.R., "Vibration of Eccentrically Stiffened Plates," The Shock and Vibration Bulletin, Bulletin 33, Part 1, August 1968, pp. 45-53.

47. Maeda, Y. and Kajikawa, Y., "Fatigue Strength of Steel Plates with a Stud Shear Connector for Application to Continuous Composite Beams," International Association for Bridge and Structural Engineering, Published by the Secretariat of IABSE in Zurich, Amsterdam, May 8-13, 1972.

48. Mahalingam, S., "Vibrations of Stiffened Rectangular Plate," Journal of the Royal Aeronautical Society, Vol. 67, 1963, pp. 305-307.

49. Mise, K. and Kunii, S., "A Theory for Forced Vibration of a Railway Bridge Under the Action of Moving Loads," Journal of Mechanics and Applied Mathematics, Vol. 9, 1956, p. 195.

50. Naruoka, M. and Yonezawa, H., "A Study on the Period of the Free Lateral Vibration of the Beam Bridge by the Theory of Orthotropic Rectangular Plate," Ingenieur-Archiv, Vol. 26, 1958, pp. 20-29.

51. Ng, S.F. and Kilkarni, G.G., "On the Transverse Free Vibration of Beam-Slab Type Highway Bridges," Journal of Sound and Vibration, Vol. 3, No. 21, 1972, pp. 249-261.

52. Olsen, A.R., "Design and Test Results of a Composite Model," A Thesis Submitted to the University of Missouri-Columbia in Partial Fulfillment of the Requirements for the Degree of Master of Science in Civil Engineering, December 1971.

53. "Ontario Highway Bridge Design Code," Ministry of Transportation and Communications, Ontario, 1982.

54. Ritz, W., "Theorie der Transversal-Schwingungen einer Quardratischen Platte mit Freien Randern," Annalen der Physik 28, 1909, pp. 737-786.

55. Salane, H. J., Duffield, R.C., McBean, R.P. and Baldwin, J.W. Jr., "An Investigation of the Behavior of a Three-Span Composite Highway Bridge," College of Engineering, University of Missouri-Columbia, Columbia, Missouri, 1978.

56. Skipp, B.O., "Vibration in Civil Engineering," Proceeding of a Symposium Organized by British National Section of the International Association for Earthquake Engineering, Imperial College of Science and Technology, London, April, 1965.

57. Slutter, R.G. and Fisher, J.W., "A Proposed Procedure for the Design of Shear Connectors in Composite Beams," Fritz Engineerieng Laboratory Report No. 316.4, March 1966.

58. "Standard Specifications for Highway Bridges," American Association of State Highway and Transportation Officials, 1983.

59. The Structural Design Language Engineering User's Manual, 'STRUDL DYNAL, PLOTS and DANOS,' Release 6.7, McDonnell Douglas Automation Company, 1985.

60. Sundara, R.I. and Tagadish, K.S., "Vibration of Rectangular Orthotropic Plates," Applied Scientific Research, Section A, Vol. 13, 1964, pp. 37-42.

61. Thorkildsen, R.L. and Hoppman, W.H., "Effect of Rotatory Inertia on the Frequencies of Vibration of Stiffened Plates," Transaction of the ASME, Journal of Applied Mechanics, Vol. 26, 1959, pp. 298-300.

62. Timoshenko, S.P. and Krieger, W., "Theory of Plates and Shells," McGraw-Hill, 1959.

63. Timoshenko, S.P., "On the Forced Vibration of Bridges," Philosophical Magazine, Vol. 43, 1922, p. 1018.

64. Timoshenko, S.P., "Vibration Problems in Engineering," D. Van Nostrand Company, Inc., New York, 1937.

65. Toprac, A.A., "Fatigue Strength of 3/4-Inch Stud Shear Connectors," Highway Research Record 103, pp. 53-77, 1965.

66. Troitsky, M.S., "Stiffened Plates, Bending, Stability and Vibrations," Elsevier Scientific Publishing Company, 1976.

67. Ungar, G.E., "Free Oscillations of Edge-Connected Simply Supported Plate Systems," Journal of Engineering for Industry, Transactions of the ASME, November, 1961, pp. 434-440.

68. Ungar, E.E., "Maximum Stresses in Beams and Plates Vibrating at Resonance," Journal of Engineering for Industry, Transaction of the ASME, February 1962, pp. 149-156.

69. Veletsos, A.S. and Newmark, N.M., "Natural Frequencies of Continuous Plates," Journal of Applied Mechanics, ASME Transactions, Series E, Vol. 23, 1956, pp. 97-102.

70. "Vibration Testing-Instrumentation and Data Analysis," ASME/DED Vibration Conference, Washington, D.C., September 1975.

71. Voigt, W., "Lechrubuch der Kristallphysik," B.G. Tuebuer, Berlin, 1910, pp. 675-698.

72. Warburton, G.B., "The Vibration of Rectangular Plates," Proceedings of the Institute of Mechanical Engineering, Series A, Vol. 168, 1954, pp. 371-384.

73. Willis, R., "Appendix, Report of the Commissioners Appointed to Inquire into the Application of Iron and Railway Structures," Stationary Office, London, 1849.

74. Yamada, Y. and Veletsos, A.S., "Free Vibration of Simple Span I-Beam Bridges," Eighth Progress Report, Part B, Highway Bridge Impact Investigation, University of Illinois, 1958.

VITA AUCTORIS

Nabil Fouad Fanouse Grace

1952 Born on 23rd of July in Port-Said, Egypt.

1970 Matriculated from Tanta High School, Tanta, Egypt.

1975 Graduated with Bachelor of Science (Honour) in Civil Engineering, from Cairo University, Cairo, Egypt.

1976 Joined as a part-time Designer Engineer in a consulting firm for Civil Engineering under the direction of Dr. M. Hanna.

1979 Enrolled in a Master's program in Civil Engineering Department, University of Windsor, Canada.

1981 Graduated with Master of Applied Science, University of Windsor.

1981 Enrolled for Doctoral Studies in Civil Engineering at the University of Windsor, Canada.

1985 Engineer II in the Department of Advanced Technology, Giffels Associates, Southfield, Michigan, U.S.A.

1985 Professional Engineer Examinations Parts I and II were taken for registration in Michigan State, U.S.A.

1986 Registered as a member of the American Society of Civil Engineering.

1986 Engineer III in the Department of Advanced Technology, Giffels Associates, Southfield, Michigan, U.S.A.

1986 Registered as a Professional Engineer for the State of Michigan under number 32044.